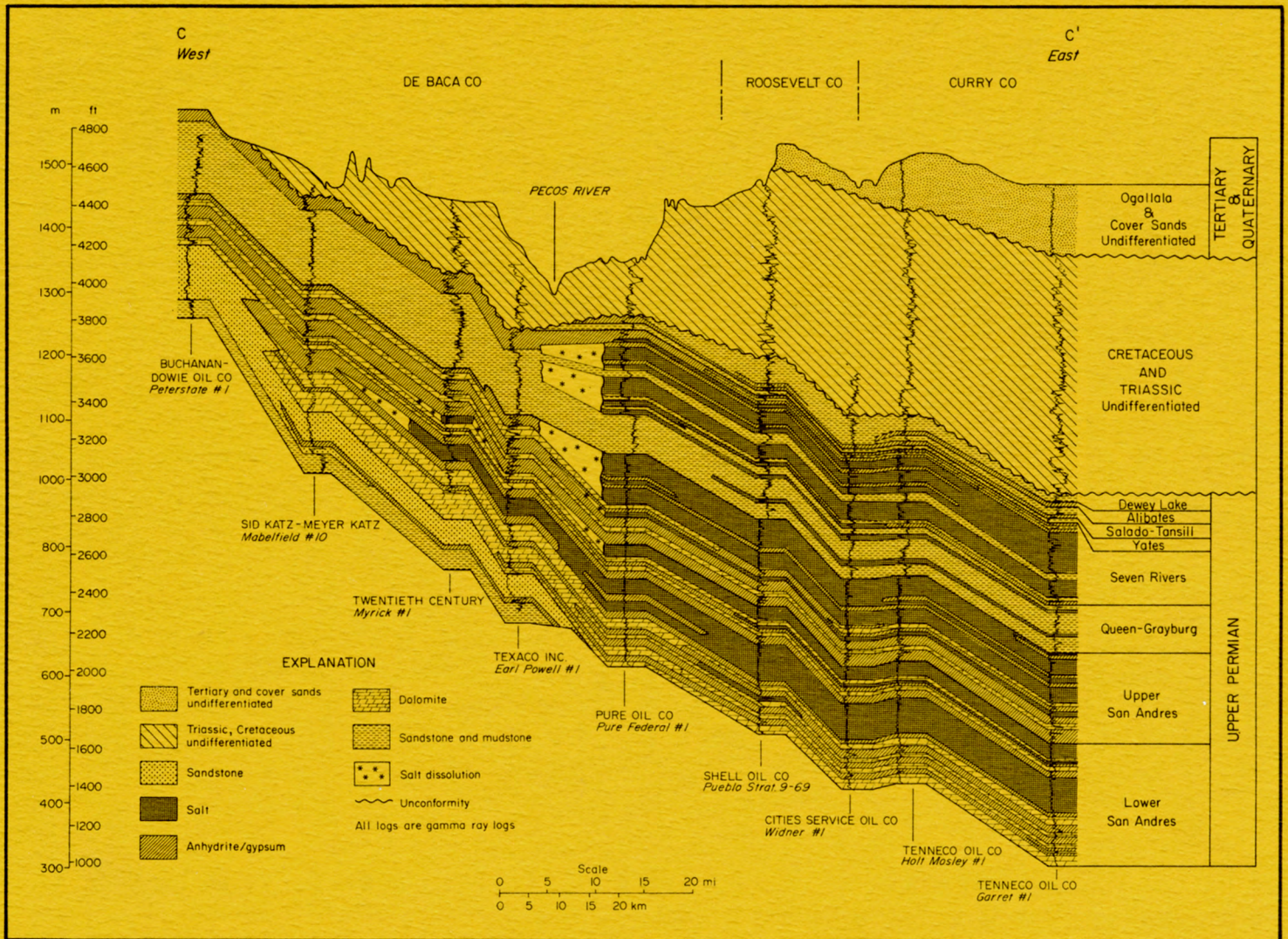


1982

# Geology and Geohydrology of the Palo Duro Basin, Texas Panhandle

## A Report on the Progress of Nuclear Waste Isolation Feasibility Studies (1981)



T. C. Gustavson, R. L. Bassett, R. Budnik, R. J. Finley, A. G. Goldstein, J. H. McGowen, E. Roedder, S. C. Ruppel, R. W. Baumgardner, Jr., M. E. Bentley, S. P. Dutton, G. E. Fogg, S. D. Hovorka, D. A. McGookey, P. J. Ramondetta, W. W. Simpkins, D. Smith, D. A. Smith, E. A. Duncan, J. A. Griffin, R. M. Merritt, and E. R. Naiman

Bureau of Economic Geology  
W. L. Fisher, Director



The University of Texas at Austin  
Austin, Texas 78712

Geological Circular 82-7

GEOLOGY AND GEOHYDROLOGY OF THE PALO DURO BASIN, TEXAS PANHANDLE

A Report on the Progress of Nuclear Waste Isolation Feasibility Studies (1981)

Annual Report

for period October 1, 1980 - September 30, 1981

by

T. C. Gustavson, R. L. Bassett, R. Budnik, R. J. Finley, A. G. Goldstein,  
J. H. McGowen, E. Roedder, S. C. Ruppel, R. W. Baumgardner, Jr.,  
M. E. Bentley, S. P. Dutton, G. E. Fogg, S. D. Hovorka,  
D. A. McGookey, P. J. Ramondetta, W. W. Simpkins,  
D. Smith, D. A. Smith, E. A. Duncan,  
J. A. Griffin, R. M. Merritt,  
and E. R. Naiman

Prepared for the  
U.S. Department of Energy  
Office of Nuclear Waste Isolation  
under contract no. DE-AC97-80ET46615

Bureau of Economic Geology  
W. L. Fisher, Director  
The University of Texas at Austin  
University Station, P.O. Box X  
Austin, Texas 78712

1982

## CONTENTS

|   |     |
|---|-----|
| Purpose and Scope, by Research Staff . . . . .  | 1   |
| Palo Duro and Dalhart Basin Studies -- A Summary of Fourth-Year<br>Research Activities, by Research Staff . . . . .   | 3   |
| Regional and Plate Tectonic Setting of the Palo Duro Basin,<br>by A. G. Goldstein . . . . .   | 6   |
| Quantitative Analysis of Regional Bouguer Gravity Data,<br>by A. G. Goldstein . . . . .   | 11  |
| Brittle Deformation Associated with Salt Dissolution, Palo Duro Basin,<br>by A. G. Goldstein . . . . .  | 18  |
| Structural Influence on Deposition and Deformation at the Northwest Margin<br>of the Palo Duro Basin, by D. A. McGookey and A. G. Goldstein . . . . .             | 28  |
| Regional Stratigraphic Framework of the Texas Panhandle,<br>by R. Budnik and D. Smith . . . . .   | 38  |
| Depositional History and Reservoir Quality of Granite Wash, by S. P. Dutton . . . . .   | 87  |
| Petrographic Summary of Permian Rocks from the DOE/Gruy Federal No. 1 Grabbe<br>Well, Swisher County, by S. D. Hovorka, E. R. Naiman, and J. H. McGowen . . . . . | 91  |
| Possible Permian Diurnal Periodicity in NaCl Precipitation, Palo Duro Basin, Texas,<br>by E. Roedder . . . . .  | 101 |
| Use of Geophysical Well Logs for the Determination of Mud and Anhydrite<br>Content in Bedded Salt, by P. J. Ramondetta and R. M. Merritt . . . . .                | 105 |
| Trapping Mechanisms of Oil in the San Andres Formation, Northern Shelf of the<br>Midland Basin, by P. J. Ramondetta . . . . .                                     | 109 |
| Permeability of Wolfcamp Carbonates, by R. L. Bassett, D. A. Smith, and<br>M. E. Bentley . . . . .  | 123 |
| Preliminary Modeling of Ground-Water Flow near Salt Dissolution<br>Zones, Texas Panhandle, by W. W. Simpkins and G. E. Fogg . . . . .                             | 130 |
| Regional Salinity and Chemical Composition of Waters in Deep Aquifers in the<br>Palo Duro Basin, by R. L. Bassett and E. A. Duncan . . . . .                      | 138 |
| AQ/SALT: Calibration of a Brine Model, by R. L. Bassett and J. A. Griffin . . . . .   | 146 |
| Geochemistry and Mass Transfer in Brines from Permian Wolfcamp Carbonates<br>in the Palo Duro, Dalhart, and Anadarko Basins, by R. L. Bassett . . . . .           | 153 |
| Stream Incision and Scarp Retreat Rates Based on Volcanic Ash Date from the<br>Seymour Formation, by W. W. Simpkins and R. W. Baumgardner, Jr. . . . .            | 160 |

|   |      |
|---|------|
| Geomorphic Studies of Representative Drainage Basins,<br>by R. W. Baumgardner, Jr. . . . .  | .164 |
| Erosion Process Studies in the Texas Panhandle -- Analysis of a Two-Year<br>Data Record, by W. W. Simpkins, T. C. Gustavson, and R. J. Finley . . . . . | .168 |
| Structural Control of Major Drainage Elements Surrounding the Southern<br>High Plains, by T. C. Gustavson . . . . .                                     | .176 |
| Determination of Salt Purity Using Gamma-Ray Logs: San Andres Formation,<br>Palo Duro Basin, by S. C. Ruppel and P. J. Ramondetta. . . . .              | .183 |
| Acknowledgments . . . . .   | .200 |
| References . . . . .  | .201 |

## ILLUSTRATIONS

### Figures

|   |    |
|---|----|
| 1. Organizational structure of the West Texas Waste Isolation Program<br>(FY 1981). . . . .   | 2  |
| 2. Map of late Paleozoic structural elements . . . . .  | 9  |
| 3. Sedimentation curves for the Palo Duro, Anadarko, and Dalhart Basins . . . . .   | 10 |
| 4. Bouguer anomaly map of the Texas Panhandle . . . . .   | 13 |
| 5. Structure-contour map on top of crystalline basement, Texas Panhandle . . . . .  | 14 |
| 6. Gravity model A-A' . . . . .   | 15 |
| 7. Gravity calculated from the model compared to gravity observed<br>along A-A' . . . . .   | 16 |
| 8. Salt dissolution zones and location of Caprock Canyons State Park and<br>Randall County well. . . . .                                  | 21 |
| 9. Schematic stratigraphic column for the Caprock Canyons State Park area<br>showing zones of characteristic brittle deformation. . . . . | 22 |
| 10. Inclined and horizontal veins in Caprock Canyons State Park . . . . .   | 23 |
| 11. Close-up view of inclined fibrous gypsum veins, showing medial scar and<br>vertical vein fibers . . . . .                             | 23 |

|  |    |
|--|----|
| 12. Undeformed gypsum vein filling part of preexisting normal fault in Quartermaster Formation . . . . . | 24 |
| 13. Minor thrust fault cutting Quartermaster Formation . . . . .   | 24 |
| 14. Hackle fringe on systematic joint . . . . .  | 25 |
| 15. Wallner lines on nonsystematic joints in the Quartermaster Formation . . . . .                       | 25 |
| 16. Photograph of a part of the Randall County core . . . . .  | 26 |
| 17. Conceptual model of brittle deformation above dissolution zones . . . . .                            | 27 |
| 18. Structure map on top of basement showing major structural features of study area . . . . .           | 30 |
| 19. Sedimentation rate graphs for four wells in Potter and Oldham Counties, Texas . . . . .              | 31 |
| 20. Isopach map of Wolfcamp Series showing positions of shelf margins . . . . .                          | 32 |
| 21. Isopach map of interval from the top of Wichita Group to the top of Tubb Formation . . . . .         | 33 |
| 22. Structure map, top of the Tubb Formation . . . . .   | 34 |
| 23. Salt quality map, San Andres cycle 4 salt, determined from gamma-ray logs . . . . .                  | 35 |
| 24. Cross section showing present configuration of strata across the Amarillo Uplift . . . . .           | 36 |
| 25. Structural elements of the Texas Panhandle and location of study area . . . . .                      | 55 |
| 26. Stratigraphic column and general lithology of the Palo Duro and Dalhart Basins . . . . .             | 56 |
| 27. Precambrian basement terranes . . . . .  | 57 |
| 28. Isopach map of Cambrian (?) sandstone directly overlying Precambrian basement . . . . .              | 58 |
| 29. Isopach map of Lower Ordovician Ellenburger Group . . . . .  | 59 |
| 30. Isopach and series distribution map of Mississippian System . . . . .                                | 60 |
| 31. Structure-contour map on the top of Precambrian basement . . . . .                                   | 61 |
| 32. Facies distribution map of Lower Pennsylvanian System . . . . .                                      | 62 |

|   |    |
|---|----|
| 33. Facies distribution map of Upper Pennsylvanian System . . . . .   | 63 |
| 34. Isopach map of Pennsylvanian System . . . . .   | 64 |
| 35. Isopach map of Permian System . . . . .   | 65 |
| 36. Isopach map of Wolfcamp Series . . . . .  | 66 |
| 37. North-south cross sections B-B' and C-C' through the Red Cave<br>Formation . . . . .  | 67 |
| 38. Composite depositional model for Red Cave carbonate, evaporite, and<br>clastic facies . . . . .   | 68 |
| 39. Isopach map, lower Clear Fork Formation, Texas Panhandle . . . . .  | 69 |
| 40. Facies and environments recorded in Tubb strata of the Palo Duro and<br>Dalhart Basins . . . . .  | 70 |
| 41. Northwest-southeast cross section, Tubb Formation, Palo Duro Basin. . . . .   | 71 |
| 42. Facies maps of evaporite-carbonate units 1, 2, and 3 of the Tubb<br>Formation . . . . .   | 72 |
| 43. North-south facies cross section through Palo Duro and Dalhart Basins<br>showing relationship of environments for the upper Clear Fork and<br>Glorieta Formations . . . . . | 73 |
| 44. Regional north-south cross section G-G' of upper Clear Fork Formation<br>showing generalized lithologic interpretations . . . . .   | 74 |
| 45. Net-salt map of upper Clear Fork Formation. . . . .   | 75 |
| 46. Isopach map of net clastics, Glorieta Formation, Palo Duro Basin and<br>east-central New Mexico . . . . .   | 76 |
| 47. Regional north-south cross section B-B' of the San Andres Formation<br>showing interpretation of lithic composition . . . . .   | 77 |
| 48. Net-salt map, lower part of the San Andres Formation . . . . .  | 78 |
| 49. Net-salt map, upper part of the San Andres Formation . . . . .  | 79 |
| 50. Post-San Andres formations, north-south cross section E-E' . . . . .  | 80 |
| 51. Net salt in Seven Rivers Formation . . . . .  | 81 |
| 52. North-south cross section A-A', Salado, Tansill, and Alibates Formations,<br>Palo Duro Basin . . . . .  | 82 |

|   |     |
|---|-----|
| 53. Net salt, Salado-Tansill Formation . . . . .  | 83  |
| 54. Isopach map, Alibates Formation . . . . .   | 84  |
| 55. Generalized cross section emphasizing relief of pre-Ogallala surface . . . . .  | 85  |
| 56. Isopach map, Ogallala Formation . . . . .   | 86  |
| 57. Granite-wash isolith map of Lower Pennsylvanian to Lower Permian strata<br>in the Texas Panhandle . . . . .   | 88  |
| 58. North-south regional cross section A-A' from the Amarillo Uplift into<br>the Anadarko Basin . . . . .   | 89  |
| 59. North-south regional cross section A-B from the central Palo Duro Basin<br>to the Amarillo Uplift . . . . .   | 90  |
| 60. Plot of quartz-feldspar-rock fragment ratios from 28 samples from the<br>No. 1 Grabbe core . . . . .  | 94  |
| 61. Photomicrograph showing trough crossbeds visible in very fine,<br>subarkosic sandstone . . . . .  | 95  |
| 62. Histogram of grain sizes observed in Permian siliciclastics in the<br>No. 1 Grabbe core . . . . .   | 95  |
| 63. Muddy, very fine sandstone: immature subarkose, showing bimodality . . . . .  | 96  |
| 64. Red clay intraclasts and clay drapes within coarse, muddy<br>siltstone exhibiting disrupted textures . . . . .  | 96  |
| 65. Poikilotopic halite cement filling both intragrain and moldic porosity in<br>silty, dolomitized pellet oosparite . . . . .  | 97  |
| 66. Dolomitized fossiliferous intrasparite containing intraclasts, pellets,<br>and coated skeletal fragments . . . . .  | 97  |
| 67. Chevron structure in halite . . . . .   | 98  |
| 68. Large cubes of halite that disrupted and compressed originally well-laminated<br>red clay and silt during displacive growth of halite cubes in the sediment . . . . . | 99  |
| 69. Well-formed cubes of halite that disturbed initially well-laminated, muddy,<br>coarse siltstone . . . . .   | 99  |
| 70. Contact between silty aphanocrystalline dolomite and displacive anhydrite<br>nodules composed of felted, medium crystalline laths . . . . .                           | 100 |
| 71. Compressed anhydrite nodules elongated parallel to bedding and composed<br>of finely crystalline, bladed anhydrite . . . . .  | 100 |

|   |      |
|---|------|
| 72. Part of two elongated single crystals showing 12 bands . . . . .  | .104 |
| 73. Part of an elongated single crystal showing 14 bands . . . . .  | .104 |
| 74. Detail of salt across one clear septum shown in figure 73 . . . . .   | .104 |
| 75. Histogram of impurities in 1-ft samples of salt core . . . . .  | .107 |
| 76. Compensated neutron porosity correlated with mud content . . . . .  | .107 |
| 77. Gamma-ray intensity correlated with mud content . . . . .   | .108 |
| 78. Bulk density correlated with anhydrite content . . . . .  | .108 |
| 79. Map of the Northern and Northwestern Shelves showing oil fields and<br>oil production within each region . . . . .                | .112 |
| 80. Map of study area showing San Andres oil production, shelf margins,<br>and surface lineaments . . . . .                           | .113 |
| 81. Schematic block diagram of depositional environments during a regressive<br>depositional phase in early San Andres time . . . . . | .114 |
| 82. Plot of porosity versus permeability in the Yellowhouse dolomite . . . . .  | .115 |
| 83. Distribution of lithofacies during early San Andres time . . . . .  | .116 |
| 84. Structure map, top of San Andres Formation . . . . .  | .118 |
| 85. Isopach map, upper San Andres Formation, Yoakum and Terry Counties,<br>Texas . . . . .  | .120 |
| 86. Structure map, top of Yellowhouse dolomite, San Andres Formation,<br>northern Hockley and southern Lamb Counties, Texas . . . . . | .121 |
| 87. North-south cross section of San Andres Formation across Levelland and<br>Slaughter fields, Texas . . . . .                       | .122 |
| 88. Permeability of carbonate rocks in the Permian Wolfcamp Series . . . . .  | .125 |
| 89. Pressure buildup analysis using the Horner method . . . . .   | .126 |
| 90. Frequency distribution of the effective permeability in Wolfcamp<br>carbonates . . . . .  | .127 |
| 91. Map of physiographic units and major streams in the study area,<br>Texas Panhandle . . . . .                                      | .133 |
| 92. Stratigraphic cross section used for ground-water model . . . . .   | .134 |

|  |      |
|--|------|
| 93. Finite-element mesh designed from the cross section shown in figure 92 . . . . .   | .135 |
| 94. Steady-state hydraulic heads and recharge/discharge rates computed by the model . . . . .  | .136 |
| 95. Regional east-west cross section illustrating spatial relations among the major depositional systems in the Palo Duro Basin . . . . .  | .141 |
| 96. Isopach map of granite wash in the deep-basin brine aquifer . . . . .  | .142 |
| 97. Carbonate isoliths for the Wolfcampian-age section of the deep-basin brine aquifer . . . . .   | .143 |
| 98a. Trilinear diagram illustrating the compositional variation of brine samples . . . . .   | .144 |
| 98b. Trilinear diagram illustrating the compositional variation of brine samples . . . . .   | .145 |
| 99. Measured values for the activity of water in solutions with varying electrolyte compositions . . . . .   | .148 |
| 100. Saturation state of brine samples from Wolfcamp carbonate facies as computed with AQ/SALT . . . . .   | .149 |
| 101. Phase diagram for the Na-K-Mg-Cl-SO <sub>4</sub> -H <sub>2</sub> O system at 25°C . . . . .   | .150 |
| 102. Saturation states computed with AQ/SALT and SOLMNEQ for Lower Permian Wolfcamp brines . . . . .   | .156 |
| 103. Saturation state of Lower Permian Wolfcamp brine with respect to dolomite as computed with AQ/SALT and SOLMNEQ . . . . .  | .157 |
| 104. Distribution of CO <sub>2</sub> partial pressure in oil and gas fields in the Palo Duro and Dalhart Basins . . . . .  | .158 |
| 105. Location map showing the P <sub>CO<sub>2</sub></sub> of oil and gas fields in the Palo Duro, Dalhart, and Anadarko Basins and P <sub>CO<sub>2</sub></sub> computed from results obtained from brine in wildcat and production wells . . . . . | .159 |
| 106. Location of type section, Seymour Formation . . . . .   | .162 |
| 107. Stratigraphic column, type section, Seymour Formation . . . . .   | .163 |
| 108. Location of representative drainage basins selected for morphometric study . . . . .  | .165 |
| 109. Morphometric data from the Little Red River Basin . . . . .   | .166 |

|      |  |      |
|------|--|------|
| 110. | Scattergram showing relation between slope angle and net erosion/deposition rate for the Muleshoe station . . . . .  | .171 |
| 111. | Scattergram showing relation between percent vegetative cover and net erosion/deposition rate for the Muleshoe station. . . . .                                      | .172 |
| 112. | Scattergram showing the relation between cumulative rainfall and mean erosion rates for stations in the Texas Panhandle . . . . .                                    | .173 |
| 113. | Zones of salt dissolution in eastern New Mexico and in Texas and Oklahoma Panhandles . . . . .   | .177 |
| 114. | Stratigraphic section illustrating salt dissolution and collapse of strata beneath the Pecos River . . . . .   | .178 |
| 115. | Stratigraphic section illustrating salt dissolution and collapse of strata beneath the Canadian River . . . . .  | .179 |
| 116. | Stratigraphic section illustrating dissolution of Seven Rivers and Salado salts and collapse of overlying strata . . . . .   | .180 |
| 117. | Stratigraphic section illustrating dissolution of Salado Formation salts and collapse of overlying strata . . . . .  | .181 |
| 118. | Evolution of drainage in eastern New Mexico and the Texas Panhandle . . . . .  | .182 |
| 119. | Correlation between gamma-ray log response and mud content in San Andres Formation cycle 4 salt interval, DOE-Gruy Federal Rex White No. 1, Randall County . . . . . | .185 |
| 120. | Correlation between gamma-ray log response and mud content in San Andres Formation cycle 4 salt interval, DOE-Gruy Federal Grabbe No. 1, Swisher County . . . . .    | .186 |
| 121. | Contour map of average gamma-ray (API unit) values for the upper San Andres Formation salt interval . . . . .  | .187 |
| 122. | Contour map of average gamma-ray (API unit) values, cycle 5 salt, lower San Andres Formation . . . . .   | .188 |
| 123. | Contour map of average gamma-ray (API unit) values, cycle 4 salt, lower San Andres Formation . . . . .   | .189 |

## Tables

|   |     |
|---|-----|
| 1. Petroleum exploration wells . . . . .  | 17  |
| 2. Gamma-ray and sample logs used in figure 18 . . . . .  | 37  |
| 3. Hydraulic parameters derived from analysis of drill-stem tests . . . . .   | 128 |
| 4. Permeability of core samples from the Wolfcamp Series . . . . .  | 129 |
| 5. Hydrostratigraphic units and hydraulic conductivities utilized in the<br>ground-water model . . . . .  | 137 |
| 6. Chemical compositions of solutions in equilibrium with phases in the<br>Na-K-Mg-Cl-SO <sub>4</sub> -H <sub>2</sub> O system . . . . .              | 151 |
| 7. Mineral names and chemical formulas. . . . .   | 152 |
| 8. Selected morphometric parameters for representative drainage basins . . . . .  | 167 |
| 9. Mean, maximum, and minimum annual net erosion rates for erosion-monitoring<br>stations in the Texas Panhandle . . . . .                            | 174 |
| 10. Mean, maximum, and minimum annual net erosion rates for assigned slope<br>classes at erosion-monitoring stations in the Texas Panhandle . . . . . | 175 |
| 11. Mean, maximum, and minimum annual net retreat rates for rebar at three<br>erosion-monitoring stations in the Texas Panhandle . . . . .            | 175 |
| 12. Point count data, cycle 4 salt, Gruy Federal, Inc., Rex H. White No. 1,<br>Randall County, Texas . . . . .  | 190 |
| 13. Point count data, cycle 4 salt, Gruy Federal, Inc., Grabbe No. 1,<br>Swisher County, Texas . . . . .  | 195 |

## PURPOSE AND SCOPE

### Research Staff

*Integrated study of the basin structure, tectonic history, rock physics, physical stratigraphy, hydrogeology, geochemistry, natural resources, and geomorphology of the Palo Duro and Dalhart Basins in the Texas Panhandle is part of a national evaluation of ancient salt basins as potential sites for isolation and management of nuclear wastes.*

Since early 1977, the Bureau of Economic Geology has been evaluating several salt-bearing basins within the State of Texas as part of the national nuclear waste repository program. The Bureau, a research unit of The University of Texas at Austin, is conducting a long-term program to gather and interpret all geologic and hydrologic information necessary for description, delineation, and evaluation of salt-bearing and related strata in the Palo Duro and Dalhart Basins of the Texas Panhandle.

The program in fiscal year (FY) 81 was divided into five broad research tasks, which were addressed by a surficial analysis and shallow stratigraphy group, a hydrology and geochemistry group, a basin analysis group, a host-rock analysis group, and a seismicity and tectonic environment group (fig. 1). The surficial analysis and shallow stratigraphy group has collected remotely sensed, surface and subsurface data to describe salt dissolution, surface processes, and rates and styles of geomorphic development. The hydrology and geochemistry group continued analysis of shallow and deep fluid circulation within the basins and rock and fluid geochemistry within the salt-bearing and other stratigraphic units. The basin analysis group characterized the major salt-bearing stratigraphic units within the basins, assessed the potential for generating and trapping hydrocarbons within the basins, and initiated studies of salt quality. Concurrently, the host-rock analysis group continued a study of cores from several drilling sites for analysis of salt and other lithologic units within the cores. The seismicity and tectonic environment group continued studies of regional gravity, deep-basement structure and tectonic development of the basin, and structural controls of sedimentation and analyzed surface fracture systems.

This report, a summary of progress during FY81, presents principal conclusions and reviews methods used and types of data and maps generated. Topical reports, discussing in detail various geological aspects of the Palo Duro and Dalhart Basins, are being published as phases of the study are completed. This research was supported by the U.S. Department of Energy and its predecessor, the Energy Research and Development Administration, under contracts numbered EY-77-S-05-5466 (FY78), DE-AC97-79ET44614 (FY79), and DE-AC97-80ET46615 (FY 80 and FY81).

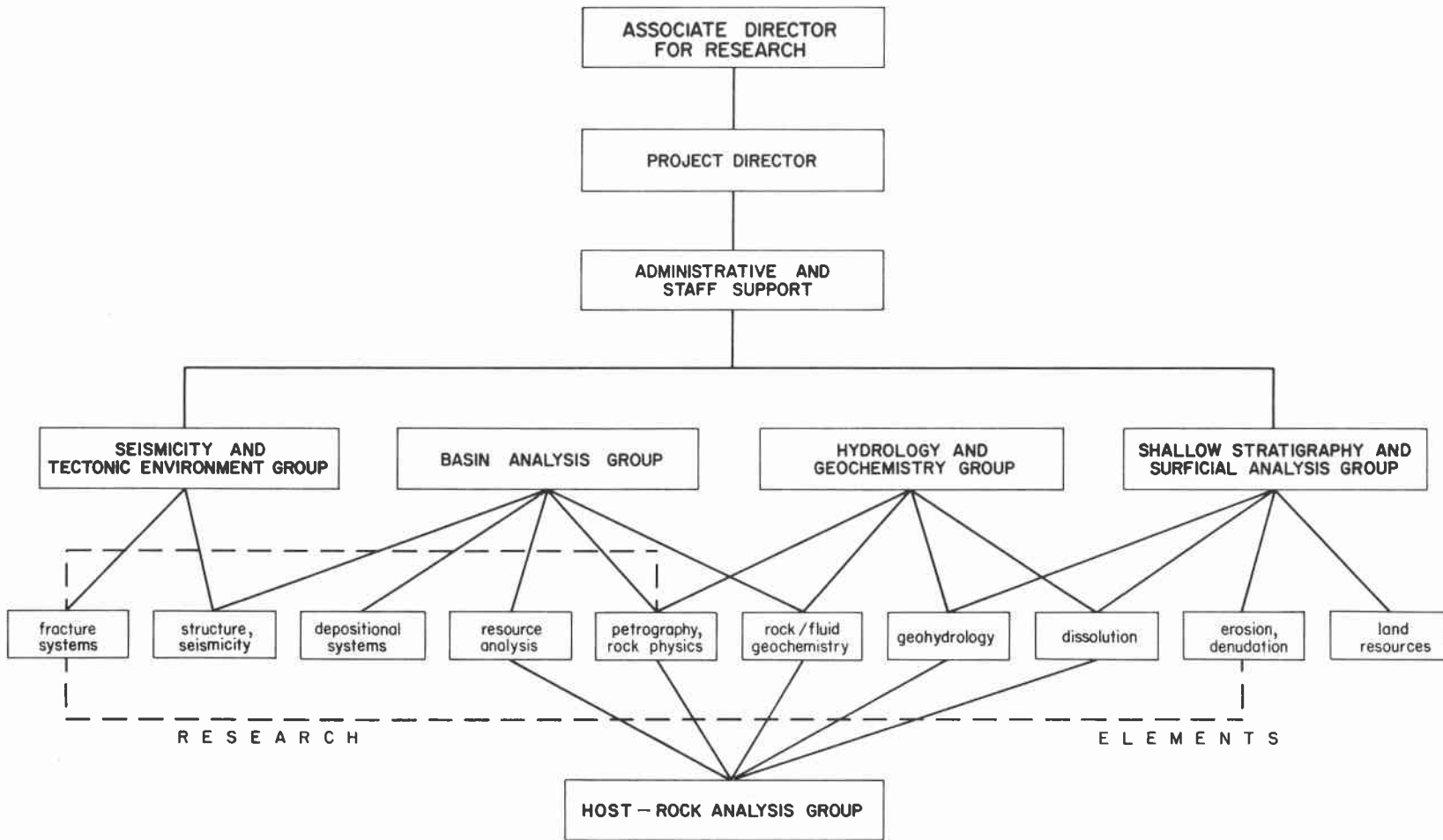


Figure 1. Organizational structure of the West Texas Waste Isolation Program (FY 1981).

## PALO DURO AND DALHART BASIN STUDIES--A SUMMARY OF FOURTH-YEAR RESEARCH ACTIVITIES

### Research Staff

*The fourth year of investigation was highlighted by regional gravity analyses, analysis of structural controls of sedimentation, analyses of the depositional systems and resources of the Dockum Group and Permian and Pennsylvanian granite wash, analyses of hydrocarbon trapping mechanisms in the San Andres Formation, analyses of permeability of Wolfcampian carbonates, geochemical interpretation of deep-basin aquifers, calibration of a brine model, initiation of ground-water-flow modeling, analyses of erosion rates and drainage basin morphometry, analyses of Quaternary salt dissolution, and analyses of the structural controls of stream development.*

The Palo Duro Basin is part of a province in the interior of the North American crustal plate that was deformed in response to late Paleozoic compressive deformation at the continental margin. The deformation within this province was the result of non-collisional orogeny and northward subduction beneath North America. Regional gravity data have been analyzed using two-dimensional modeling techniques and standard stratigraphic cross sections. Results show that the major anomaly associated with the Amarillo Uplift may be due to faulting of the entire crust along a steep fault. Throughout the Palo Duro Basin and especially along the structurally complex northwest margin of the basin, movement along faults has had both obvious and subtle effects on the distribution of lithofacies, variation in thickness of sedimentary units, and post-depositional deformation of strata.

Brittle deformation associated with salt dissolution zones has been identified in the Caprock Canyons State Park, Briscoe County, Texas, and the DOE/Gruy Federal No. 1 Rex White (Randall County) stratigraphic test well. The sequence of structural events suggests a horizontal extension preceding major collapse, as a result of dissolution. In addition, it appears that systematic regional joints predated dissolution collapse and could have been pathways for fluid migration.

Oil and gas fields in Permian and Pennsylvanian granite-wash reservoirs are controlled by both structural and stratigraphic traps. Porosity and permeability are related to the amount and kind of authigenic cements present. Large amounts of oil are trapped in the San Andres Formation in a discontinuous, structurally high and stratigraphically thin belt that rims the deep Midland Basin and overlies older shelf margins. Additional San Andres oil is trapped by a series of steplike, updip, porosity pinch-outs.

The mud and/or anhydrite content of bedded salt of the San Andres Formation, Palo Duro Basin, Texas, can be reliably correlated with gamma-ray intensity, neutron porosity,

bulk density, and interval transit time (sonic log). These methods permit recognition of mud or anhydrite content where cores are unavailable.

Individual halite crystals in Permian salt beds from the Palo Duro Basin show a regular crystalline pattern that may reflect diurnally changing conditions during crystallization. The thickness of halite bands (0.40 to 0.85 mm) may correspond to evaporation of a maximum of 4 to 8 mm of water per day. Banding also suggests very shallow water conditions. These thin, rhythmic alternations appear to be distinct from the well-known, presumably annual, cyclic mineralogy in many saline deposits.

Permeability estimated from analysis of drill-stem-test charts ranges from 0.1 to 260 md in the Permian Wolfcamp carbonates. The range of 1 to 10 md probably represents average permeability of carbonates in the region, except in zones along dolomitized shelf edges, where porosity is extremely high and average permeabilities are consistently higher than 100 md.

Brines in the deep aquifers of the Palo Duro Basin derive their salinity primarily from dissolution of halite in the overlying evaporite section or from evaporites encountered early in the flow path. Brines appear to be near saturation with respect to anhydrite except in regions of active sulfate reduction and generation of  $H_2S$ . Brines in the Wolfcamp carbonates are probably in equilibrium with calcite, given the results of chemical analyses of samples collected during wildcat drilling. Mass transfer computations that correct for  $CO_2$  outgassing indicate that the  $P_{CO_2}$  of Palo Duro brines is remarkably similar to the  $P_{CO_2}$  observed in producing gas fields in the basin.

The AQ/SALT model is a reliable tool for evaluating the reaction state between brines and host rock because it predicts the potential for reaction or the likelihood of equilibrium. Calibration with well-controlled experimental data verifies the algorithms used. A two-dimensional, finite-element ground-water model was constructed in the vertical plane along a stratigraphic cross section of the Tertiary Ogallala Formation, the Triassic Dockum Group, and the Permian sediments in Swisher, Briscoe, Hall, and Childress Counties. Preliminary runs of the model suggest that the salt dissolution process is sustained by (1) downward flow of fresh ground water from the Ogallala aquifer and surface recharge area into the salt dissolution zone, (2) upward movement of resultant brine waters through transmissive dolomite/anhydrite beds of the Blaine Formation, and (3) discharge of the brine to saline springs in topographically low areas.

Thinning of the upper parts of salt strata of the Salado and Clear Fork Formations along their subcrop beneath the High Plains, structural collapse of overlying strata, and surface expression of subsidence as topographic and lake basins suggest, collectively, that

salt dissolution has occurred during the Quaternary. The lake basins contain Pliocene to Early Pleistocene faunas. The Pecos River valley on the western margin, the Canadian River valley on the northern margin, and the Palo Duro Canyon on the northeastern margin of the High Plains all originated as subsidence troughs as a result of dissolution of Permian bedded salts.

The Pleistocene Seymour Formation contains eroded alluvial sediment derived from the Ogallala Formation along the westward-retreating Caprock Escarpment. Volcanic ash deposits within the Seymour in North-Central Texas are Pearlette type "O" (Kansan) (G. Izette, written communication, 1981). Using this age, maximum rates of stream incision and escarpment retreat can be calculated as 0.071-0.091 mm/yr and 19 cm/yr, respectively.

Erosion and climatic data have been collected at five erosion-monitoring localities in the Texas Panhandle for approximately 2 years. Net erosion predominates at four sites; mean annual net erosion rates measured at erosion pins do not differ significantly from site to site. Although previous correlations of erosion rate with degree of slope and nature of vegetation are indicated, linear multivariate analysis of rain, slope, vegetation, and their interactions on erosion rate suggests that erosion rate may be most responsive to a rainfall x-slope interaction term. Morphometric studies are underway to characterize selected drainage basins along the Caprock Escarpment.

## REGIONAL AND PLATE TECTONIC SETTING OF THE PALO DURO BASIN

Arthur G. Goldstein

*The Palo Duro Basin is part of a province in the interior of the North American plate that was deformed in conjunction with late Paleozoic convergent deformation at the continental margin. The deformation within this province was probably the result of non-collisional orogeny and northward subduction beneath North America.*

The Palo Duro Basin is one of several basins that developed over at least 700,000 km<sup>2</sup> of the interior of the North American plate late in the Paleozoic Era. The basins are bounded by blocks of crust that were uplifted, forming a series of mountain ranges; some of these mountains are called the Ancestral Rockies. Figure 2 shows the location of major basins, uplifts, and faults that are elements of the Ancestral Rockies system. West of the Laramide Front, the uplifts are identified on the basis of coarse, arkosic debris eroded from them; stratigraphic analysis of Pennsylvanian sediments allows a reconstruction of basins. East of the Laramide Front, the province has not been modified by Cenozoic deformations, and both the basins and the uplifts have been analyzed using subsurface data.

The following general characteristics can be applied to the province as a whole:

- (1) Deep basins are asymmetric, and their deepest parts lie adjacent to a bounding uplift.
- (2) Deformation was "thick skinned" or basement involved, and uplifts are elongate either west-northwest to east-west or north-south to north-northwest.
- (3) Uplifts are typically bounded on one side by a major fault. In many instances these faults are known to have had early Paleozoic histories and were reactivated during the late Paleozoic. The Paleozoic motion directions are controversial because in only rare instances can they be determined unequivocally. Fault motion has been described as both right- and left-lateral transcurrent high-angle reverse and normal. In southern Oklahoma, some of the faults bounding the Wichita Uplift are low-angle thrusts with dips of approximately 30°S. However, major motions occurred on high-angle reverse faults, and strike-slip components were small.
- (4) Uplifts rose with respect to base level, while basins subsided with respect to base level. Areas that had been the sites of slow marine sedimentation were stripped of their cover and became sources of coarse arkosic debris (granite wash), while basins accumulated large thicknesses of the granite wash as well

as carbonates and shales. For the Palo Duro, Dalhart, and western Anadarko Basins, the history of subsidence was similar (fig. 3). Peak subsidence occurred in Meramecian (Middle Mississippian), Morrowan (Early Pennsylvanian), and Missourian (Middle Pennsylvanian) time.

- (5) The region as a whole continued to subside, the result being that eventually uplifts were buried by Permian marine and terrestrial sediments.
- (6) The timing of deformation, that is, subsidence and uplift, throughout the province was not uniform. In the northeastern part of the province, the final peak of deformation occurred in the Missourian Epoch (late Middle Pennsylvanian), whereas in the southwestern part the final peak was in the Wolfcampian Epoch (Early Permian). However, deformation always occurred simultaneously with "thin-skinned" thrusting and folding in the Ouachita-Marathon orogen.
- (7) No late Paleozoic volcanic or intrusive rocks have been found in the province.

The simultaneity of deformation in the foreland and orogen has been used in the past as evidence of a continental collision (Kluth and Coney, 1981). This model proposes that collision-generated stresses were somehow propagated through the crust to produce the Ancestral Rockies. This model has numerous problems (Goldstein, 1981), the most glaring of which are:

- (1) The absence of this style of foreland deformation throughout the remainder of the Marathon-Ouachita-Appalachian-Caledonian orogen;
- (2) The failure of this model to account for the regional subsidence (one might expect regional uplift for such a model); and
- (3) The lack of any independent evidence of a continental collision along the southern margin of North America.

A non-collisional model better accounts for the observed phenomena. In such a model, northward subduction in the late Paleozoic may have been on a flat Benioff zone; that is, rather than descending into the mantle at dips of 30 to 70 degrees, the subducted oceanic lithosphere could have slid along the base of continental lithosphere at depths of approximately 62.5 mi (100 km). This process is known to be happening along sections of the Andes in Chile and Peru (Barazangi and Isacks, 1976), where it is associated with conspicuous absences of Quaternary volcanic activity and regions of intraplate deformation similar to the Ancestral Rockies. At depths of greater than about 25 mi (40 km), the oceanic lithosphere would undergo an isochemical transformation from basalt and gabbro to eclogite. Eclogites, high-pressure rocks composed of garnet and clinopyroxene, have a

density of  $3.5 \text{ g/cm}^3$ , denser than the  $3.3 \text{ g/cm}^3$  average density of mantle material. Thus, the proposed phase transformation would be expected to cause isostatic subsidence as long as delamination of the subducted slab did not occur. Order-of-magnitude calculations show subduction and transformation of only a 4.4-mi-thick (7-km) slab of oceanic lithosphere would result in approximately 9.4 mi (1.5 km) of isostatic subsidence. Additional regional subsidence would occur because of sediment loading. Basin edges also would subside more than basin centers owing to loading by reverse and thrust faults.

The implication of such a model is that continental collision need never have occurred along the southern margin of North America. This in turn implies the possible existence of a proto-Gulf of Mexico. Similar conclusions have been reached by Keller and Cebull (1973) on the basis of seismic studies of the lower crust, by Garrison and others (1980) on the basis of isotopic and geologic studies in Ciudad Victoria, Mexico, and by Anderson and Schmidt (in press) on the basis of paleogeographic reconstructions of Mexico and Central America.

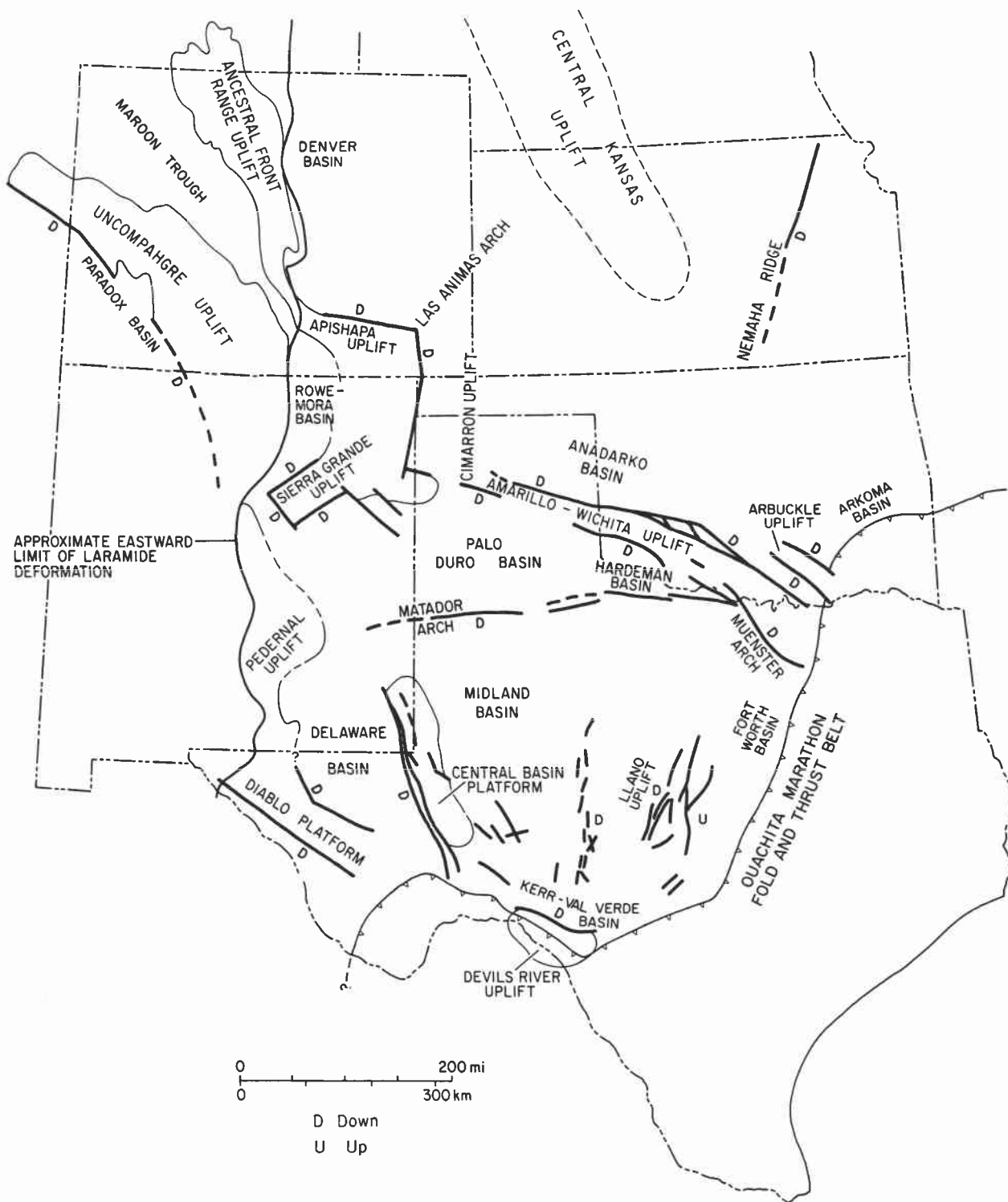


Figure 2. Map of late Paleozoic structural elements showing the Laramide Front and frontal edge of the Ouachita Fold Belt.

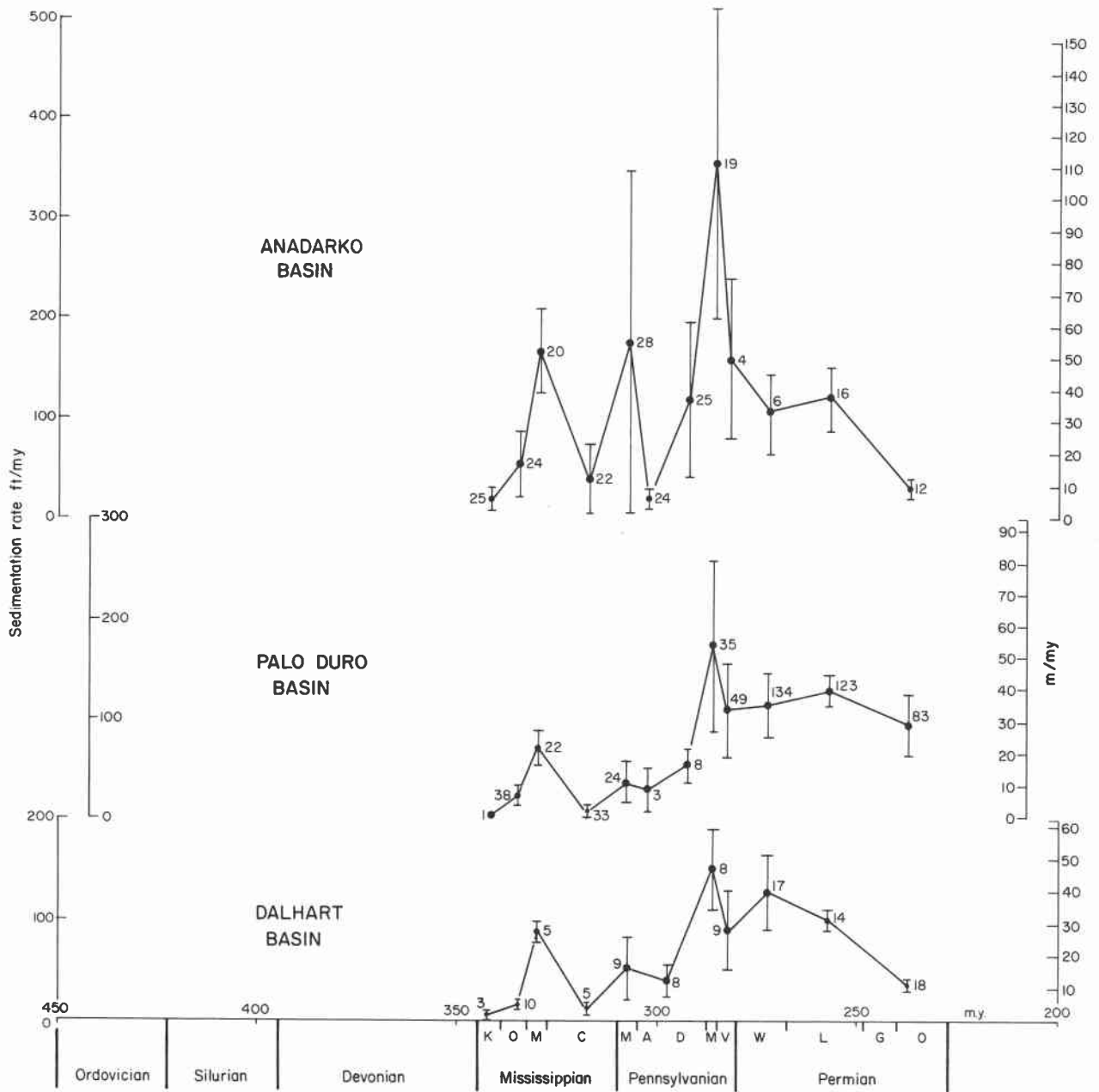


Figure 3. Sedimentation rate curves for the Palo Duro, Anadarko, and Dalhart Basins. Data are derived from analyses of sample logs and show similar subsidence histories. Peak subsidence was in the Meramecian, Morrowan, and Missourian.

## QUANTITATIVE ANALYSIS OF REGIONAL BOUGUER GRAVITY DATA

Arthur G. Goldstein

*Regional gravity data have been analyzed using two-dimensional modeling techniques and standard stratigraphic cross sections. Results show that the major gravity anomaly associated with the Amarillo Uplift may be due to a steep fault cutting the entire crust.*

A Bouguer gravity anomaly is a measure of departure from a perfectly uniform earth. Gradients in Bouguer anomaly values are produced by lateral contrasts in the density of subsurface earth materials. Analysis of these data provides quantitative information about subsurface geology where drill data are too sparse, too shallow, or non-existent. A Bouguer anomaly map of the Palo Duro Basin (fig. 4), prepared by G. R. Keller, incorporates data from numerous public and private sources and has a station density of approximately 1 per 75 km<sup>2</sup>, or an average station spacing of 5 km. Data from these numerous sources have been converted so that they represent departures from a single datum, which is the value of gravity derived from the international gravity formula.

These gravity data have been analyzed quantitatively using the methods of Talwani and others (1959). The Bouguer gravity values that would have been generated over a given two-dimensional density distribution are calculated and compared with observed Bouguer values. When the computed and observed values are coincident, the density distribution is considered to be one possible expression of the distribution of subsurface earth materials. The main limitation of this method is its non-uniqueness: an infinite number of density distributions can give rise to identical Bouguer gravity values. For this study, models of subsurface density distributions have been constrained by cross sections constructed from petroleum exploration wells, density logs, lithology of basement rocks, and measured densities from samples of basement rocks retrieved from deep wells (W. Muehlberger, personal communication, 1981).

The basement structure of the region, displayed in figure 5, can be correlated with the gravity map. The Amarillo Uplift is marked by a major positive gravity anomaly. In the eastern part of the Panhandle, where the structural relief across the northern edge of the Amarillo Uplift is approximately 20,000 ft (6,000 m), the amplitude of this anomaly is approximately 40 mgal; in western Oklahoma, where the structural relief is somewhere between approximately 30,000 ft (9,000 m) and 40,000 ft (12,000 m), the anomaly reaches amplitudes of up to 80 mgal. In north-central Carson County, the amplitude of this anomaly drops sharply to 10 mgal. This location corresponds to the region in which the apparent vertical displacement along the north side of the uplift also drops sharply from

approximately 10,000 ft (3,000 m) to 3,000 ft (900 m). These observations all suggest that the anomaly is produced by structural features, as opposed to being produced by mafic bodies in the upper crust (Powell and Fischer, 1976; Mitchell and Landisman, 1970).

To test quantitatively this hypothesis, a lithologic cross section (A-A' on fig. 4) was constructed using geophysical logs from the petroleum exploration wells identified in figure 4 and listed in table 1. Nearly all the wells penetrate the full section of sedimentary rocks in the basin. This cross section was converted to a density model (fig. 6) by simplifying and assigning densities to lithic units on the basis of analysis of density logs of the Randall and Swisher Counties stratigraphic test wells and of published values for typical lithologies (Dobrin, 1960). The gravitational attraction at points over the model was calculated and compared to the observed values. The model was altered until a good correlation existed between the computed and observed values (fig. 7). For this model, the geometry of the basin fill cannot be greatly altered, and thus most changes were made in the basement. Below the base of the sedimentary section, a crustal profile using the refraction seismic data of Stewart and Pakiser (1962) was added. This shows the base of the crust to be at a depth of 50 km. This crustal structure is disturbed by faults that displace various layers, the most significant of which is the bounding fault of the Amarillo Uplift, shown displacing the Moho discontinuity by approximately 10,000 ft (3 km). Although this does not agree with results obtained by Mitchell and Landisman (1970), it is thought to be realistic. The fault originated in the Late Precambrian-Early Cambrian during an aborted rift of the North American plate (Hoffman and others, 1974). During this rifting, the crust was thinned under the region of the Anadarko Basin, allowing that area to subside much more than surrounding areas, thereby creating the basic framework of the basin. The bounding fault on the north side of the Amarillo Uplift appears to have been the boundary between thinned and non-thinned crust, since south of that fault the crust has never subsided as much as it has north of the fault. Thus, the fault probably penetrates the entire crust.

Additional departures from a uniform crustal section include a  $3.00 \text{ g/cm}^3$  body representing the Swisher diabasic terrain and an adjacent deep prism of  $2.55 \text{ g/cm}^3$  material representing the rhyolitic material of the Panhandle volcanic terrain. The depth to which this prism of rhyolite is shown to extend, approximately 19,500 ft (6.5 km), is much greater than previously postulated. There is no direct evidence of the true depth of the Panhandle volcanic terrain, but the Whittenberg No. 1 Masterson well in east-central Potter County penetrated approximately 3,700 ft (1,110 m) of rhyolite and diabase without reaching the surface upon which it was extruded. The top of the basement

penetrated by that well is now at a depth of approximately 8,700 ft (2.6 km), and the total depth is approximately 12,380 ft (3.7 km), over half the postulated depth of the rhyolite prism.

As mentioned previously, this model is one of an infinite number of possible models. It is, however, supported by subsurface data and must therefore be considered a viable concept of crustal structure in this region.

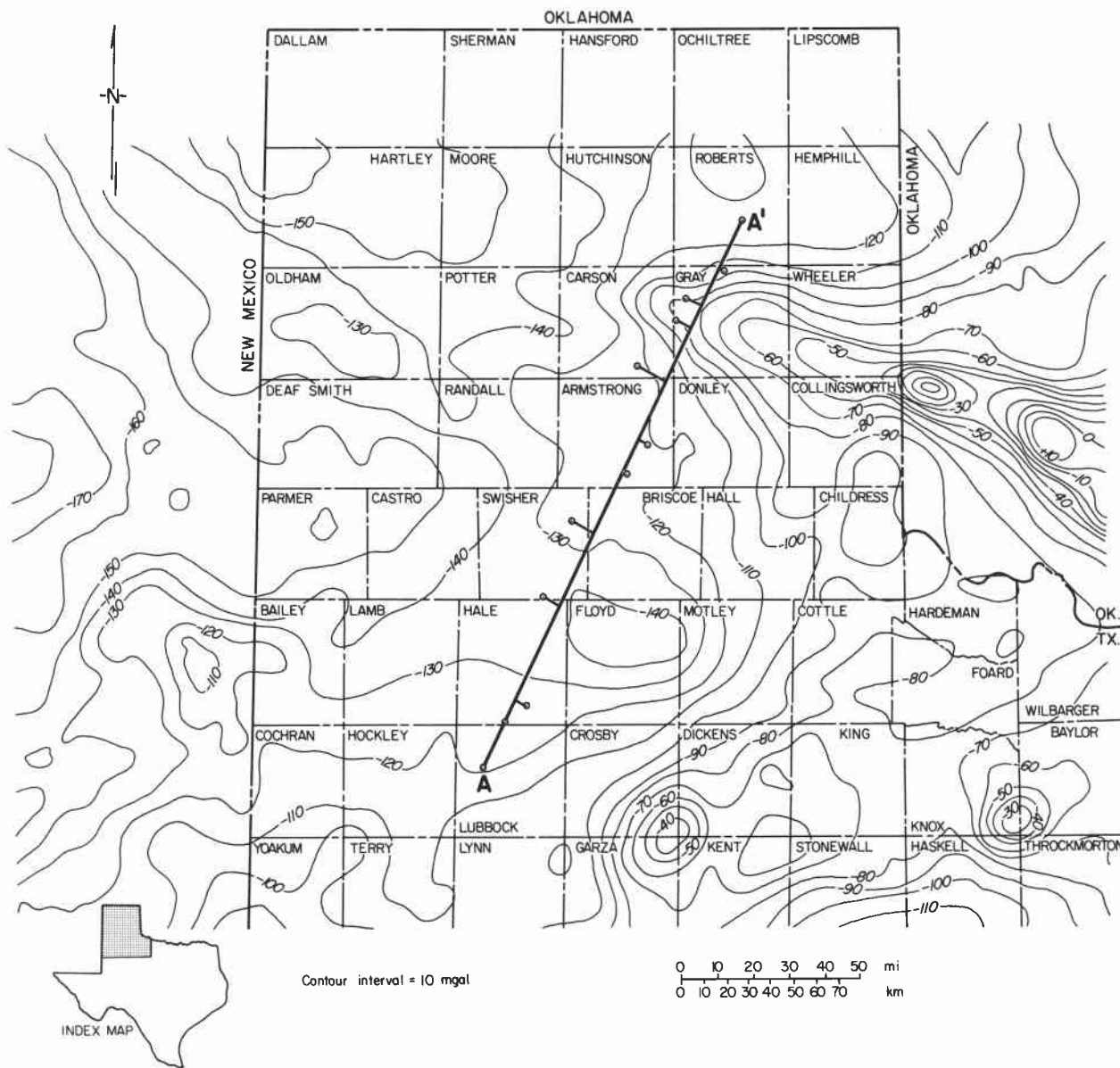


Figure 4. Bouguer anomaly map of the Texas Panhandle and vicinity showing location of wells used to construct a two-dimensional gravity model, A-A'.

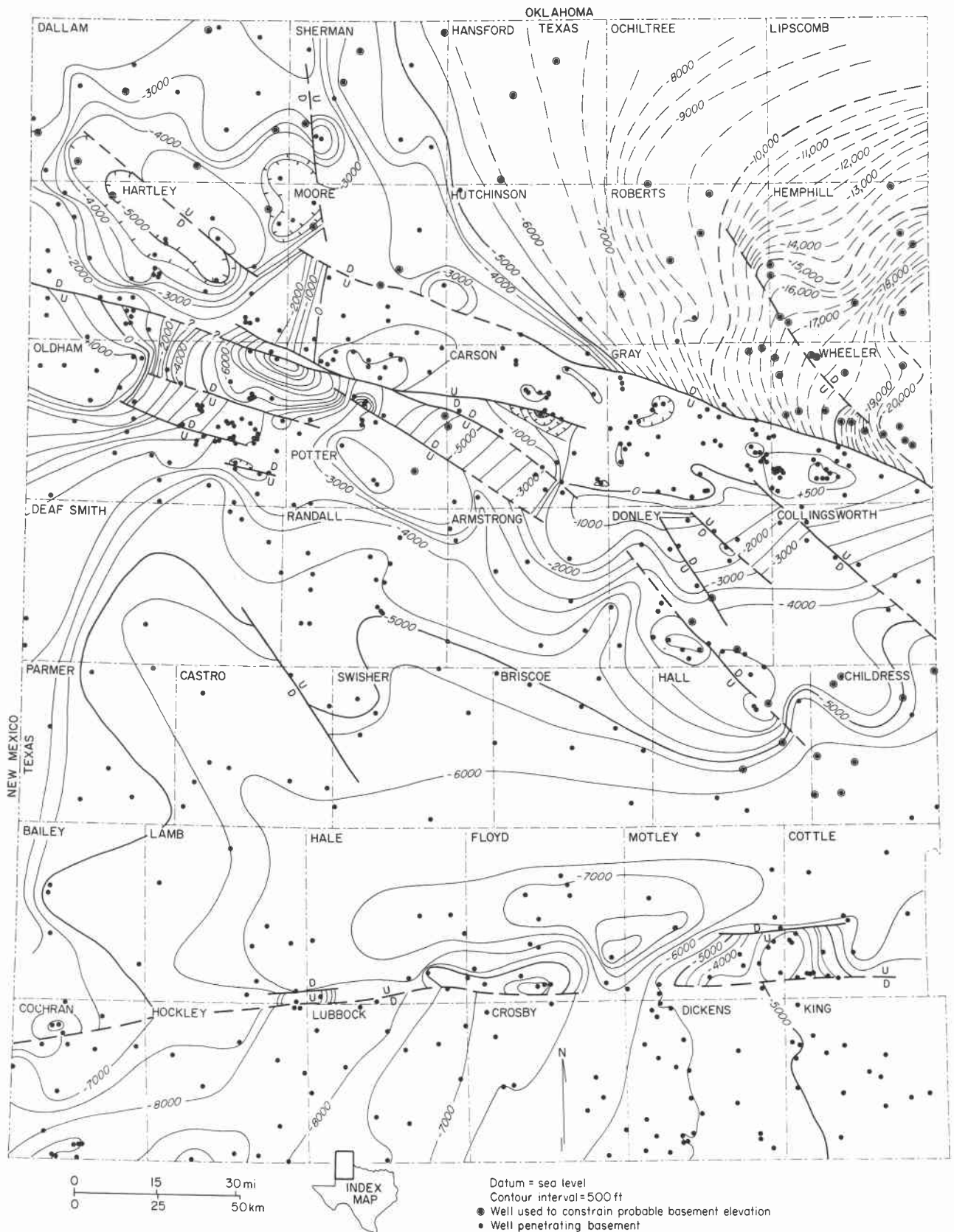


Figure 5. Structure-contour map on top of crystalline basement, Texas Panhandle.

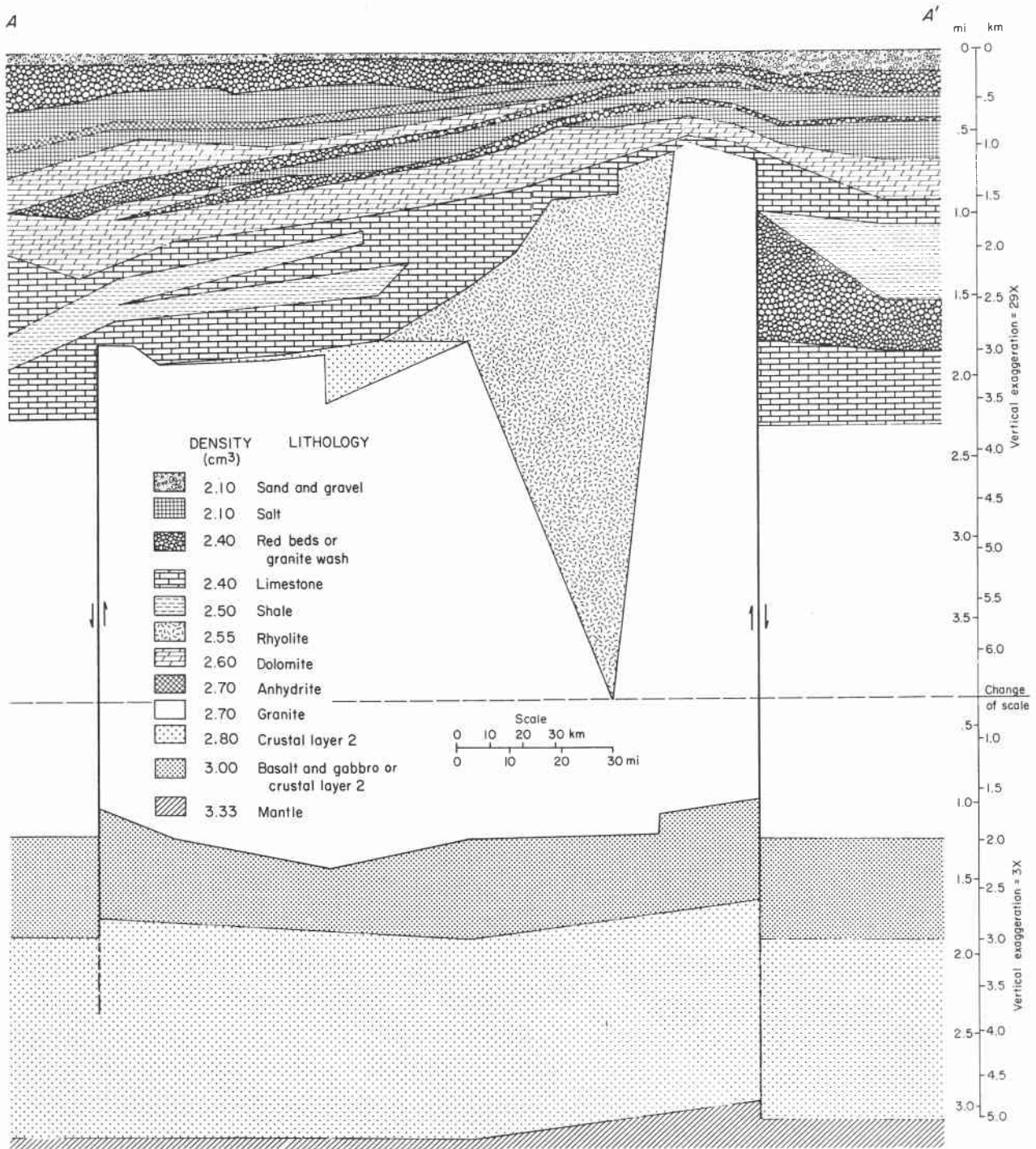


Figure 6. Gravity model A-A'. Note the change in vertical scale required so that the detail of the basin fill, as well as the complete crustal section, can be displayed.

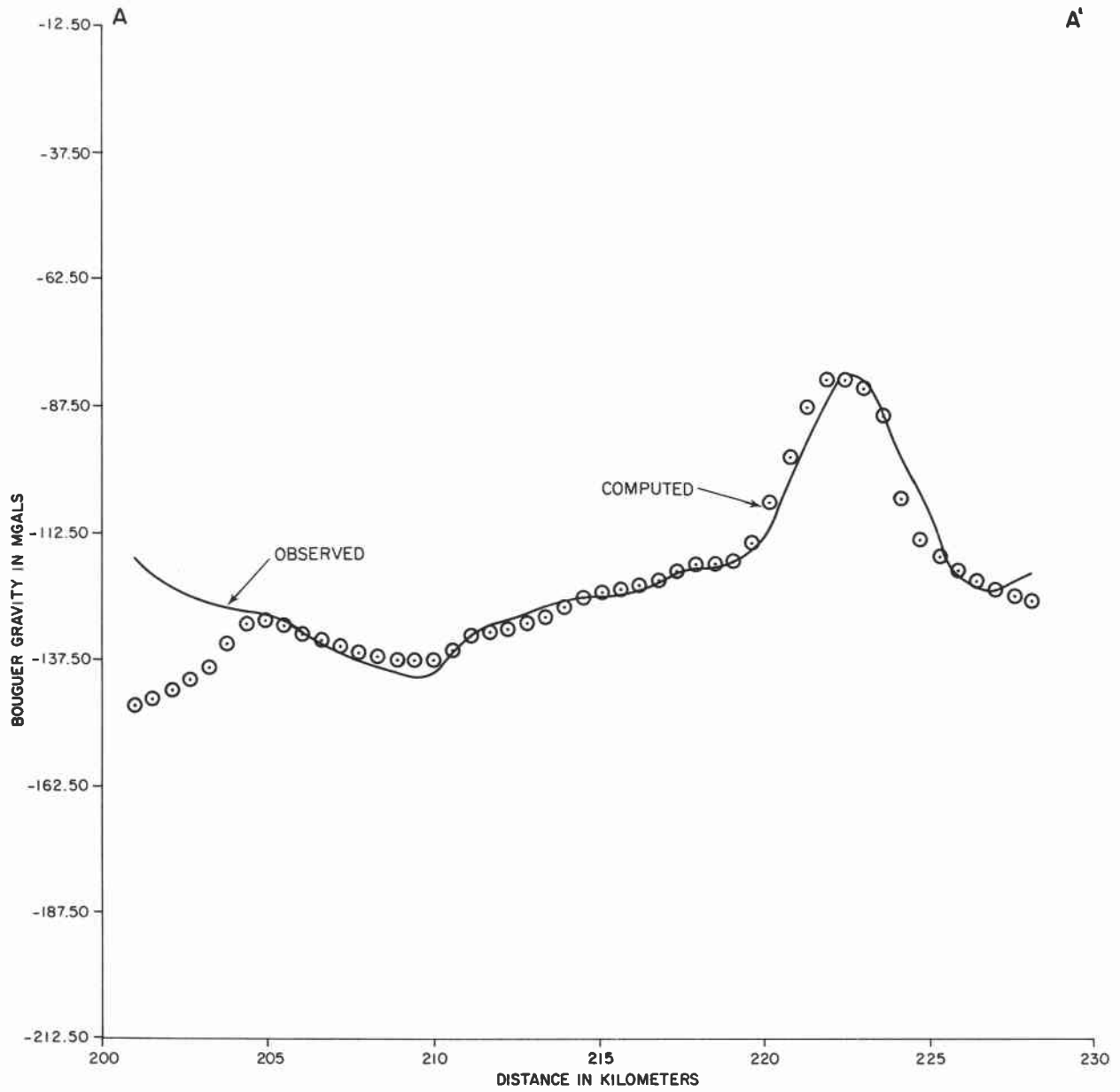


Figure 7. Gravity calculated from the model compared to gravity observed along A-A' (fig. 6).

Table 1. Petroleum exploration wells from which geophysical log data were used to construct figure 4.

| County    | BEG No. | Operator          | Well Name          |
|-----------|---------|-------------------|--------------------|
| Lubbock   | 19      | Bankline          | #1-A Elliott       |
| Hale      | 42      | Honolulu Oil      | #1 Schultz         |
| Hale      | 34      | Humble            | #2 Lutrick         |
| Hale      | 9       | Honolulu Oil      | #1 Clements        |
| Swisher   | 12      | Frankfort Oil     | #1 Sweatt          |
| Swisher   | 6       | Standard Oil      | #1 A. B. Johnson   |
| Armstrong | 21      | H. L. Hunt        | #4 Ritchie         |
| Armstrong | 14      | Massie Hunt Trust | #1 Helms           |
| Armstrong | 8       | Placid Oil        | #1 Matheson        |
| Carson    | 37      | J. M. Huber       | #1 Newton          |
| Gray      | 55      | Cities Service    | #1-C Dauer         |
| Gray      | 38      | Mobil             | #10 Heitholt       |
| Gray      | 6       | Cabot Corp.       | #1 Hobart-Fatheree |
| Roberts   | 33      | Phillips          | #1-C Cowan         |

## BRITTLE DEFORMATION ASSOCIATED WITH SALT DISSOLUTION, PALO DURO BASIN

Arthur G. Goldstein

*Brittle deformation associated with salt dissolution zones has been identified in the Caprock Canyons State Park, Briscoe County, Texas, and in core of the Randall County stratigraphic test well. The sequence of structural events suggests a horizontal extension preceding major collapse. In addition, it appears that systematic regional joints predated dissolution collapse and could have been pathways for fluid migration.*

In areas where salt dissolution has occurred, collapse has caused deformation of overlying strata. Catastrophic collapse has led to the formation of collapse chimneys and to a style of folding best described as chaotic. Large areas of the Texas Panhandle appear to have subsided as much as 400 ft (121 m) while retaining their regional structural and stratigraphic integrity. This integrity is not apparent locally. A suite of brittle deformational structures has been observed that is believed to be a result of dissolution and collapse. Mechanical and geometric analysis of these faults, veins, and fractures indicates the kinds of processes that occur in and adjacent to zones of salt dissolution. Descriptions of brittle structures are from field studies in Caprock Canyons State Park, Hall County, Texas (fig. 8), and from core taken from the DOE/Gruy Federal No. 1 Rex White stratigraphic test well (Randall County, Texas).

In Caprock Canyons State Park, thickly bedded Upper Permian and Triassic red sandstones overlie more thinly bedded Permian sandstones and siltstones interlayered with bedded gypsum (fig. 9). Thinly layered sandstones contain numerous veins of fibrous gypsum (fig. 10) that are bisected by a medial scar (fig. 11). The medial scar is the site of earliest mineralization. Mineral material is added at the vein-wall rock contact, and the fibers indicate the direction of maximum principal extension at the time they were added to the vein.

Two types of veins are present; those parallel to bedding and those cutting the bedding at angles from 30° to 60°. Inclined veins show both normal and reverse displacements (figs. 12 and 13). Nearly all inclined veins display undeformed crystals adjacent to the vein-wall rock contact, an indication that fault movement predated mineralization (fig. 12).

The geometry of vein intersections also indicates that faulting predated mineralization. The mineral fibers of adjacent horizontal and inclined veins merge without a break. Some veins have fibers that have a sinusoidal or "S" shape, which indicates that some motion occurred during vein growth. For the most part, however, vein fibers are straight

and do not deviate from vertical by more than approximately  $10^{\circ}$ . As mentioned previously, the long axis of the mineral fibers parallels the direction of maximum principal extension. Thus, these veins formed through vertical extension. The amount of extension taken up by any one vein shifts laterally as veins intersect.

The most likely cause of the vertical extension recorded by these veins is dissolution of salt followed by collapse or gentle lowering under the influence of gravity. The vertical distribution of veins at Caprock Canyons State Park supports this hypothesis. Intense gypsum veining is stratigraphically confined between massive Upper Permian sandstones and bedded gypsum (fig. 9). The gypsum beds have been traced, in the subsurface, to where they are interbedded with salt. Structureless mudstones exposed between these gypsum beds at the surface most likely represent the insoluble residue from dissolution of that salt.

Although the massive sandstones overlying the zone of intense gypsum veining do not contain any veins or faults, they do show some evidence of deformation that may be related to dissolution and collapse. Two styles of joints are present in these rocks. Systematic joints are vertical, evenly spaced, regularly oriented fractures. Hackle fringes on joint faces are evidence of horizontal propagation under the influence of horizontal extension (fig. 14). This fringe forms because a horizontally propagating fracture attempts to be perpendicular to both the stresses in the bed being fractured and the local stresses at the base or top of the bed. The second style of jointing is nonsystematic: these joints are curved, are irregularly spaced, show no preferred orientation, and truncate against systematic joints, thus postdating them. Many nonsystematic joints have surface markings that indicate vertical propagation directions. The concentric lines in figure 15 form as the fracture breaks across some slight asperity, thus generating compressional seismic waves. These waves interfere constructively and destructively with the fracture front, causing curved, raised ridges that are perpendicular to the propagation direction. Figure 15 illustrates a fracture that propagated from the base of the bed upward; other fractures show the reverse. Nonsystematic fractures never exhibit horizontal propagation directions; they seem to have formed as a result of vertical collapse and related vertical extension.

A zone of veins and faults similar to that in Caprock Canyons State Park has been observed in the core from the Randall County stratigraphic test well (fig. 16). The zone extends from approximately 420 ft to 620 ft (128 to 188 m) and thus is approximately 150 ft (146 m) thicker than the zone observed at outcrop in the park. The sequence of events recorded in the cored zone is similar to that observed in Caprock Canyons:

(1) formation of horizontal stylolites (burial) in carbonate rocks, (2) formation and mineralization of vertical fractures (joints), (3) formation of numerous minor faults, both normal and reverse, and (4) mineralization of bedding planes and faults under vertical extension; some fault motion occurred both during and after mineralization.

This sequence of events is illustrated in figure 17 along with a suggestion of the relationship to salt dissolution. Stage 1 was a normal burial process; it is recorded in nearly every sedimentary rock. Stage 2 was a result of horizontal extension and could have occurred when dissolution began. The region between total salt dissolution and no salt dissolution is an area of horizontal, or parallel-bedding, extension, as simple trigonometry illustrates. Stage 3 marked a highly different stress regime characterized by vertical extension resulting from removal of support from below.

The implications of this model are that (1) since vertical joints apparently predated salt dissolution, they would be available for enhanced ground-water flow and enhanced salt dissolution; therefore, any potential site must be thoroughly investigated for zones of intense joints; (2) the increased fracturing in beds overlying zones of salt dissolution makes them more easily eroded, suggesting a link between location of dissolution fronts and location of the caprock escarpment; and (3) the horizontal stresses generated during Stage 2 could have propagated much farther beyond the dissolution front than is indicated in figure 17. There should be a clear seismologic signature in areas affected by this horizontal extension.

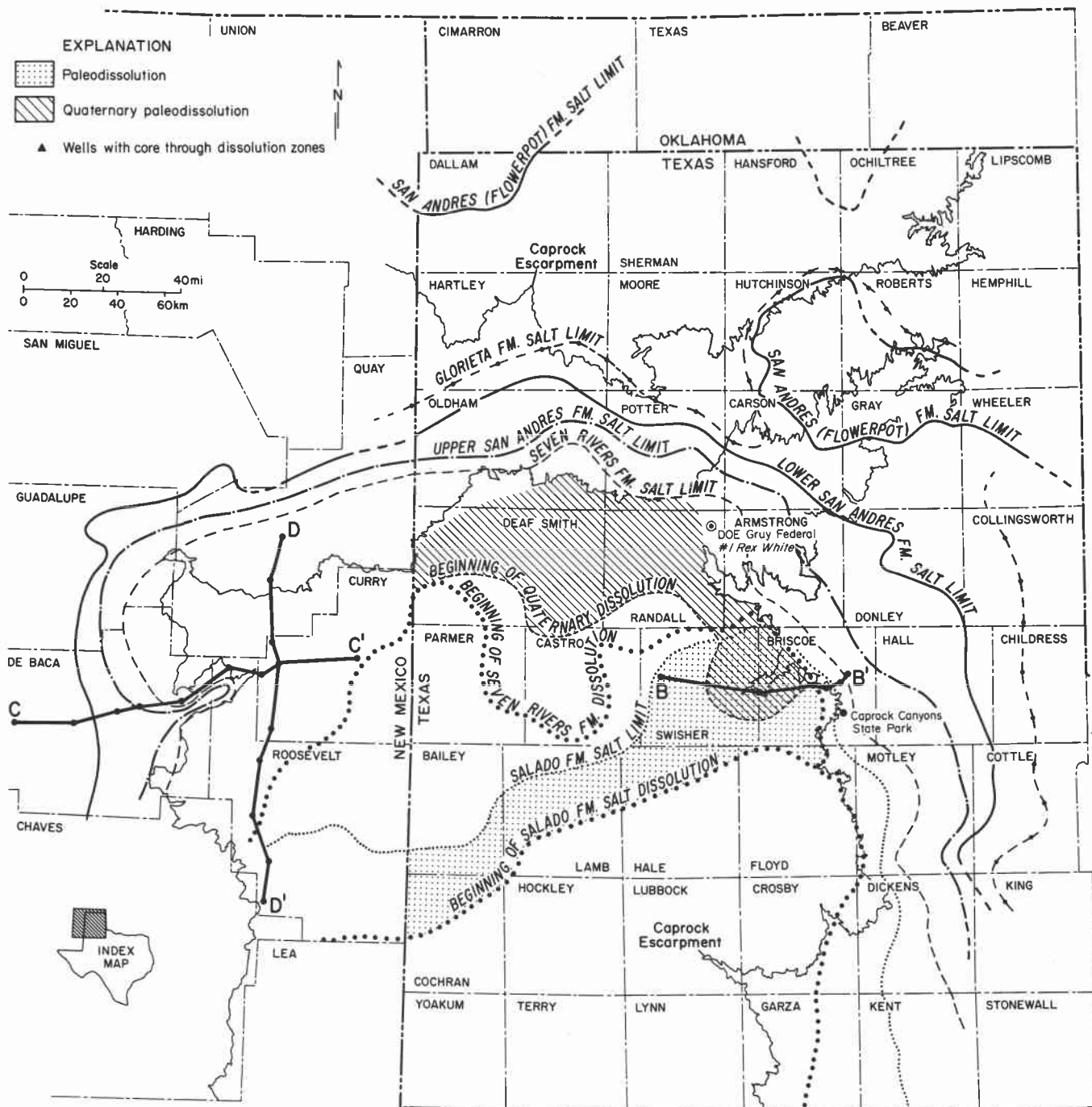


Figure 8. Salt dissolution zones and location of Caprock Canyons State Park and Randall County well.

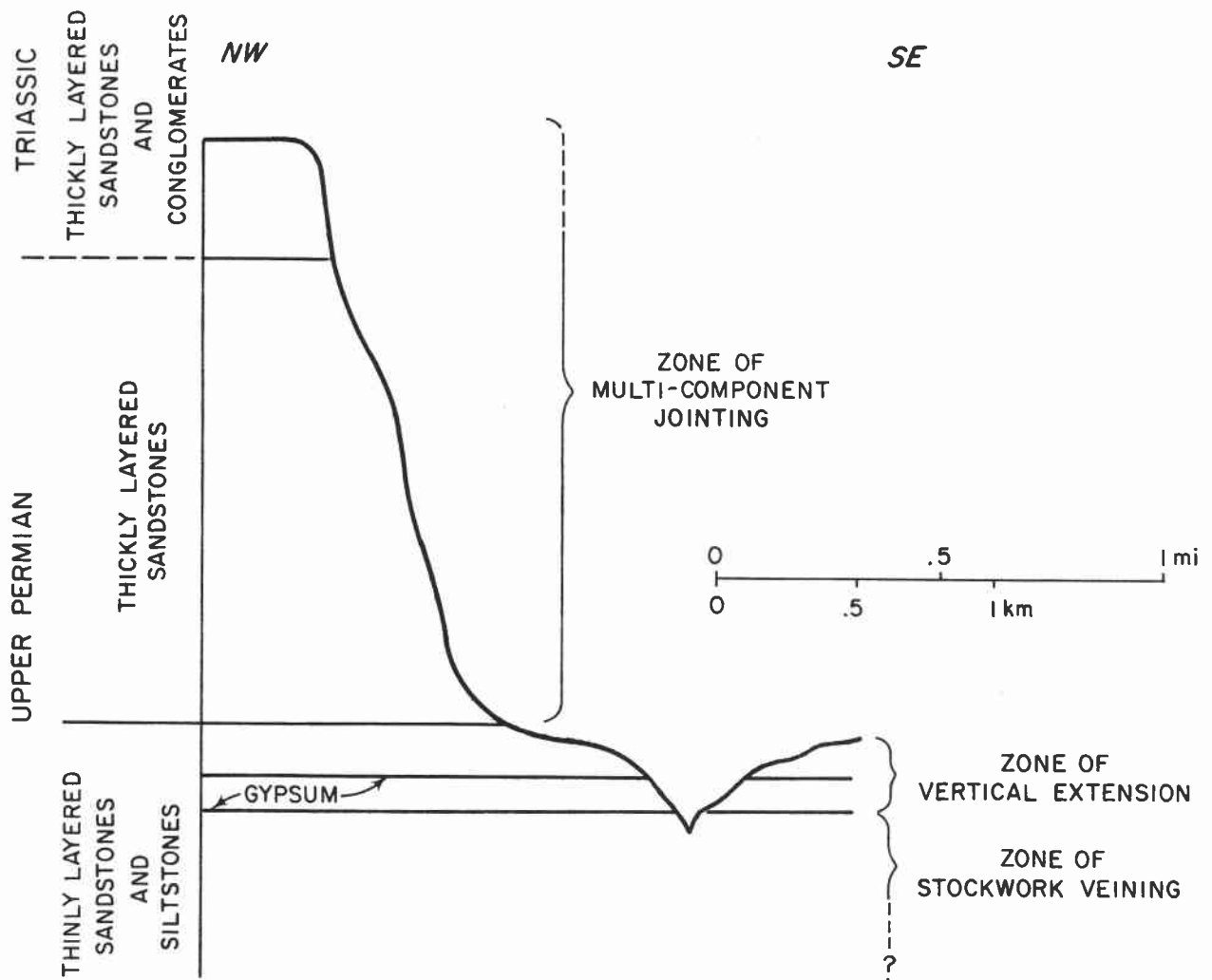


Figure 9. Schematic stratigraphic column for the Caprock Canyons State Park area showing zones of characteristic brittle deformation.

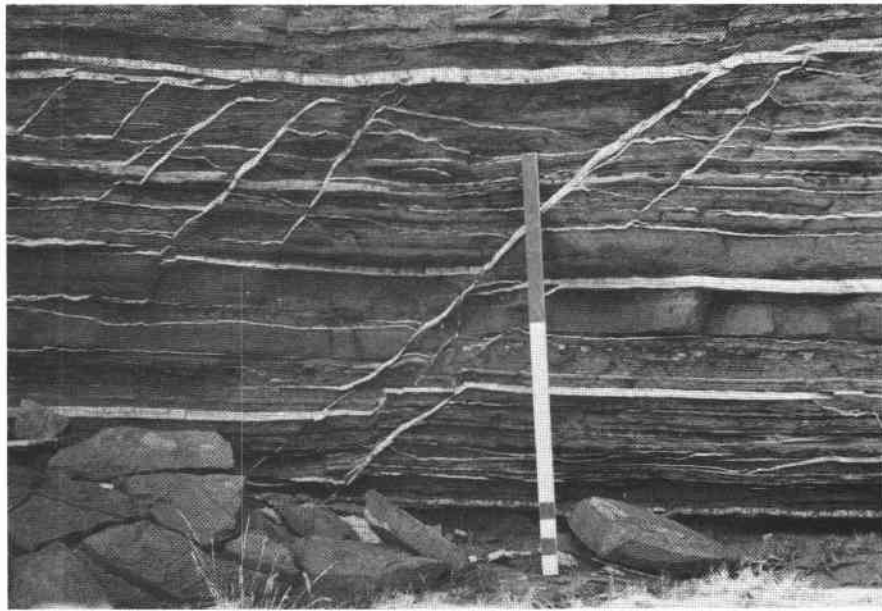


Figure 10. Inclined and horizontal veins in Caprock Canyons State Park. Some inclined veins fill normal faults. Scale is in meters.



Figure 11. Close-up view of inclined fibrous gypsum veins, showing medial scar and vertical vein fibers.

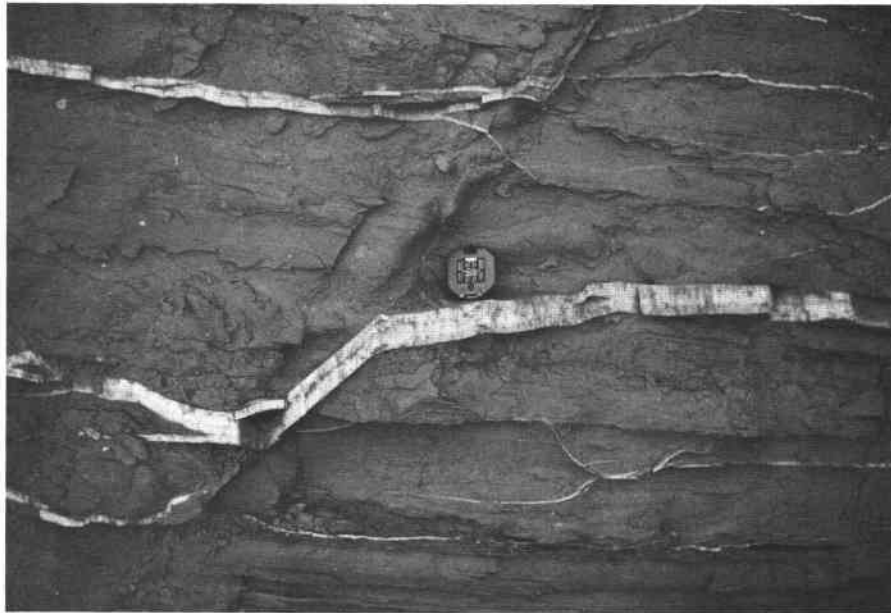


Figure 12. Undeformed gypsum vein filling part of preexisting normal fault in Quartermaster Formation.



Figure 13. Minor thrust fault cutting Quartermaster Formation. Note that the fault postdates vein formation.



Figure 14. Hackle fringe on systematic joint. This arises from slight misalignment of stresses within the bed being fractured and in the surrounding rock mass. Propagation direction was horizontal, from right to left.



Figure 15. Wallner lines on nonsystematic joints in the Quartermaster Formation. Beds are approximately 10 ft (3 m) thick. The Wallner lines show propagation from the base of the beds upward.

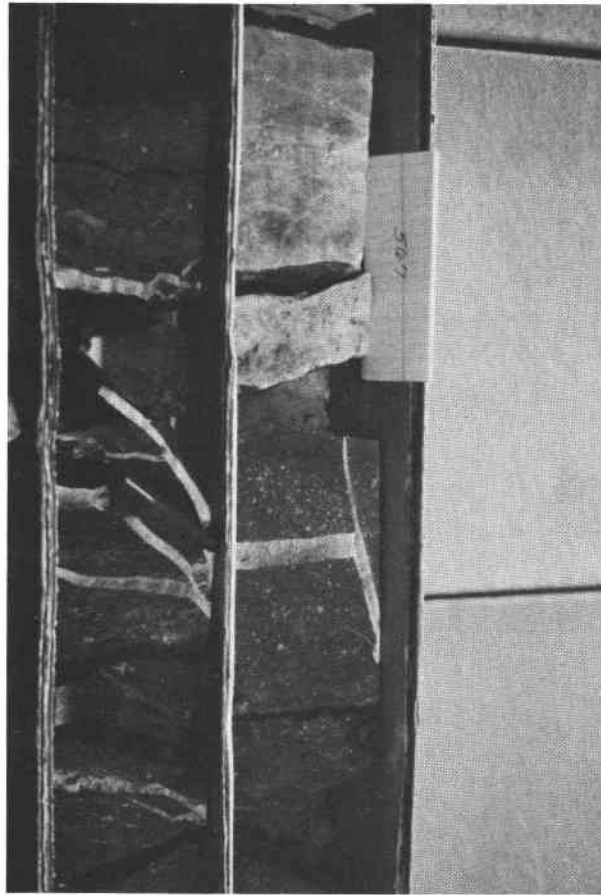


Figure 16. Photograph of a part of the Randall County core. At 567 ft the white mineral is gypsum coating a vertical joint. The gypsum has horizontal extension fibers. Immediately below is a horizontal vein with vertical fibers and some synchronous remineralization of the joint where it departs slightly from vertical.

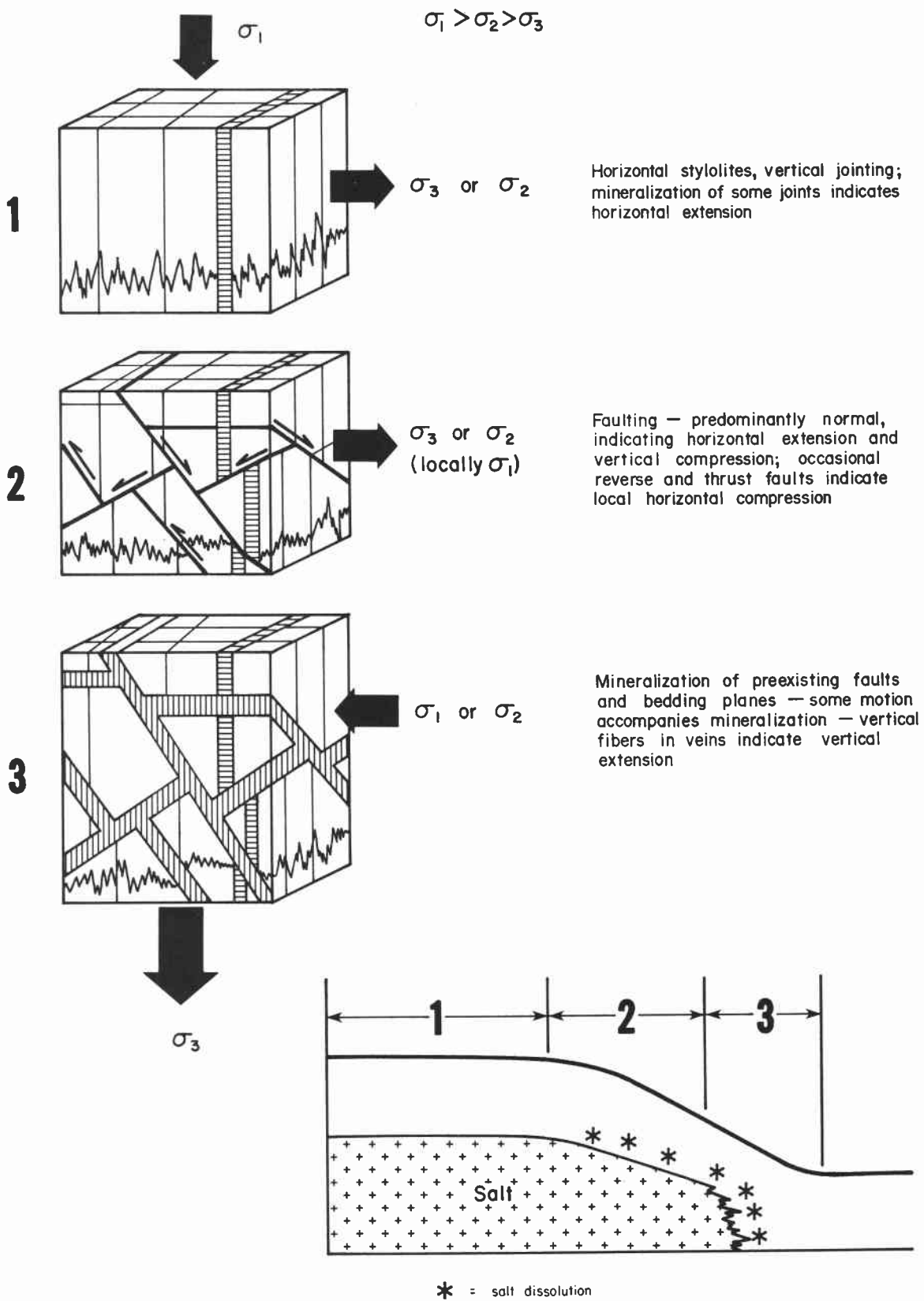


Figure 17. Conceptual model of brittle deformation above dissolution zones. Stage 1 represents normal burial; Stage 2 represents horizontal extension as a precursor to dissolution collapse; and Stage 3 represents collapse.

## STRUCTURAL INFLUENCE ON DEPOSITION AND DEFORMATION AT THE NORTHWEST MARGIN OF THE PALO DURO BASIN

Douglas A. McGookey and Arthur G. Goldstein

*At the structurally complex and variable northwest margin of the Palo Duro Basin, structural controls involving crystalline basement rocks have had both obvious and subtle effects on the distribution of facies and lithologies, thickness of sedimentary units, and post-depositional deformation of strata.*

Structural elements developed on crystalline basement rocks have helped determine the thickness, structure, distribution, and composition of post-Mississippian strata in the Palo Duro Basin. Structural control is well displayed at the northwest margin of the Palo Duro Basin, where adjacent, fault-bounded, and structurally high and low features have been mapped using well and sample log control. Faults may have formed during late Precambrian to early Paleozoic continental rifting (Hoffman and others, 1974), and the same faults were probably reactivated by Pennsylvanian tectonism. Continued movement along the faults because of differential subsidence and tectonic forces has affected successive deposition in both obvious and subtle ways.

At the northwest margin of the Palo Duro Basin in Hartley, Oldham, Moore, and Potter Counties, structural relief on the crystalline basement is reflected in the distribution of facies and post-depositional deformation of superposed strata. Elements present in the four-county area include the western part of the Amarillo Uplift, the northwestern part of the Palo Duro Basin, the Bravo Dome, the southern Dalhart Basin, and a part of the Cimarron Arch (fig. 18). Lower and middle Paleozoic strata are thin or missing in this area. Beginning in Late Mississippian or Early Pennsylvanian time, some parts of the area began to subside and sediment accumulated in these subbasins. Granite wash shed from faulted and uplifted granitic highlands is shown in figure 57. Major fault blocks responded to tectonic forces that formed the basins and uplifts with complex motions that resulted in some blocks subsiding more rapidly than others. This relationship is illustrated in figure 19, which shows sedimentation rates for two wells separated by the Potter County fault. The Oldham 10 well, located on the downthrown side of the fault, exhibits evidence of rapid subsidence during the Middle and Late Pennsylvanian; conversely, the Potter 4 well, on the upthrown side of the fault, was nearly stable with respect to sea level (see fig. 18 and table 2 for names and locations of wells). Thick accumulation of Lower Pennsylvanian sediments at the site of the Potter 80 well indicates that the structural low in the northeast part of Oldham County began to subside in Early Pennsylvanian time. Over the Bush Dome, greater subsidence and sedimentation rates in

Early Permian time are indicated by the Potter 38 well log. These comparative subsidence rates reflect basin history, timing, and fault movement.

In Wolfcampian time, the nature and distribution of shelf edges were controlled, in part, by the locations of basement uplifts (fig. 20). Shelf margins were established at or near sea level around basement highs on which the shelf margin was established by deposition of carbonate banks (Handford, 1980). For example, the trend of an early Wolfcampian shelf margin follows the eastern edge of the Bravo Dome, circles around the Dalhart Basin and the western edge of the Amarillo Uplift, and extends south over the Bush Dome. A later Wolfcampian shelf margin was established around the margin of the Dalhart Basin, and carbonates and clastics filled structurally low areas. The greatest thickness of Middle Wolfcamp sediment is preserved in a fault-bounded structural low in the northeast corner of Oldham County that subsided faster than surrounding areas. Later, during the deposition of the Wichita Group, the shelf margin prograded southward across the Palo Duro Basin.

During deposition of strata between the Wichita Group and Tubb Formation, subsidence diminished as basins were filled with clastic and carbonate deposits. Figure 21, an isopach map of the strata between the top of the Wichita Group and the top of the Tubb Formation, shows that subsiding, structurally low areas contain thick sedimentary units in the Palo Duro and Dalhart Basins; thin units were deposited on the Amarillo Uplift, Bravo Dome, Cimarron Arch, and Bush Dome. Figure 22 is a structure map of the top of the Tubb Formation that shows that post-Tubb subsidence, differential compaction, and deformation continued to alter the top of the originally flat-lying surface. Faults were probably reactivated Pennsylvanian elements.

Reduced differential subsidence and filling of basins led to the formation of extensive, flat-lying sabkha environments by early Clear Fork time. Salt purity (salt versus mud content) was controlled in part by the location of buried basement topography, as illustrated by cycle 4 salt of the San Andres Formation (fig. 23). Contours of the percent of mud in the San Andres salt document a high content of mud over the buried Bush Dome and adjacent to the Amarillo Uplift and Bravo Dome; relatively cleaner salt occupies the structural low in northwest Oldham County. Variations in salt quality may be the result of slight differences in subsidence that allowed slightly different sedimentary environments to exist in areas of dissimilar structural stability. Upper Permian evaporite sediments were deposited across the basin at or near sea level, so more salt accumulated in subsiding areas. Assuming constant input of clastic sediments (probably wind transported) during periods of evaporite deposition, the purest salt would be expected in areas that were both rapidly subsiding and remote from clastic sources.

A cross section (fig. 24) illustrates how subsiding basement and continuous faulting controlled the distribution and thickness of stratigraphic units as well as the post-depositional dissolution of evaporites. Salt dissolution occurred initially and continues preferentially over the structurally highest salt (McGookey, 1981). In the northwest Palo Duro Basin, the structurally highest salt occurs over the Amarillo Uplift. Salt dissolution and erosion resulted in the capture of the Canadian River (Gustavson, this volume), and the process of salt dissolution and erosion continues today. Structural influence on deposition and deformation thus has an important effect on variations in lithology and post-depositional deformation of strata.

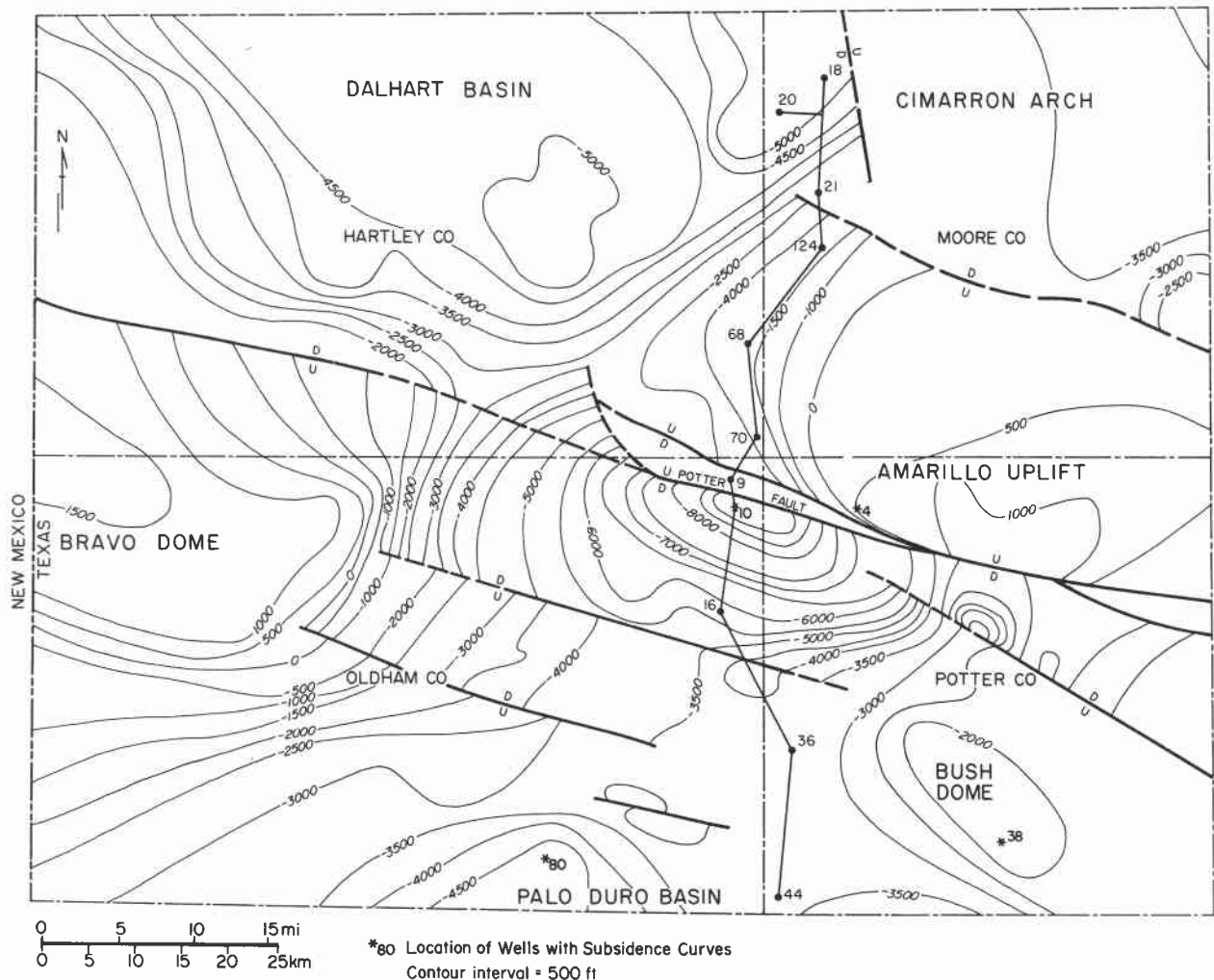


Figure 18. Structure map of top of basement showing major structural features of the study area. Graphs of sedimentation rates at the location of wells indicated are shown on figure 19. Line of section refers to cross section in figure 24. Basement elevation is offset by 8,850 ft, from -9,500 ft to +650 ft across the Potter County fault.

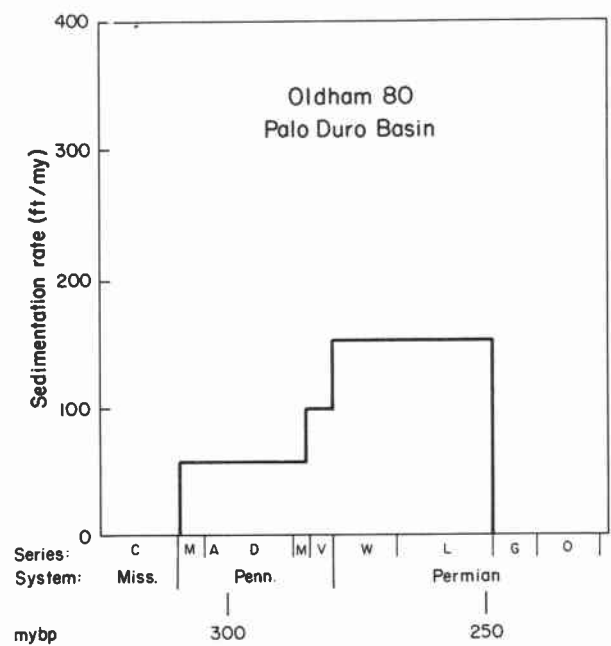
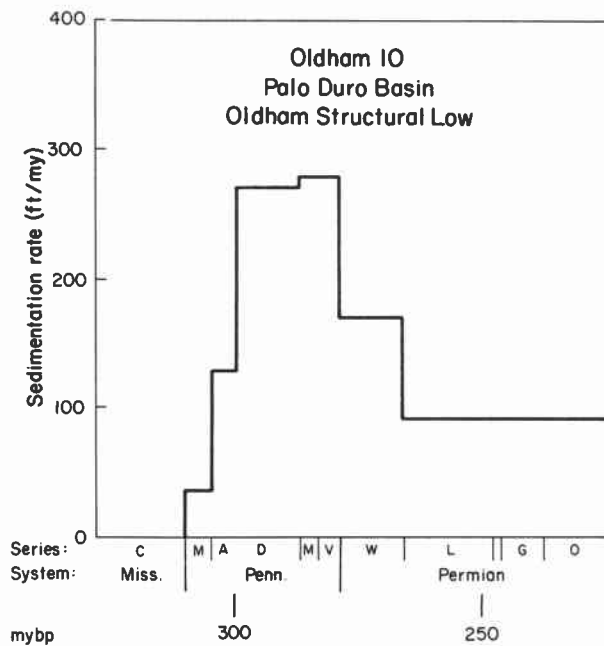
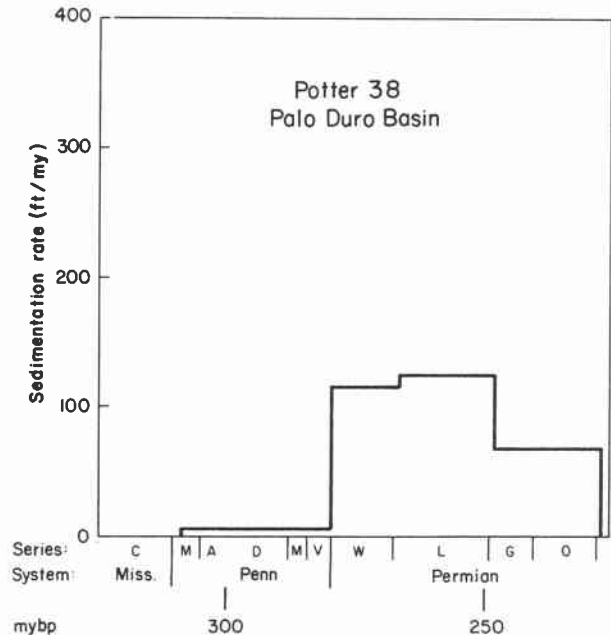
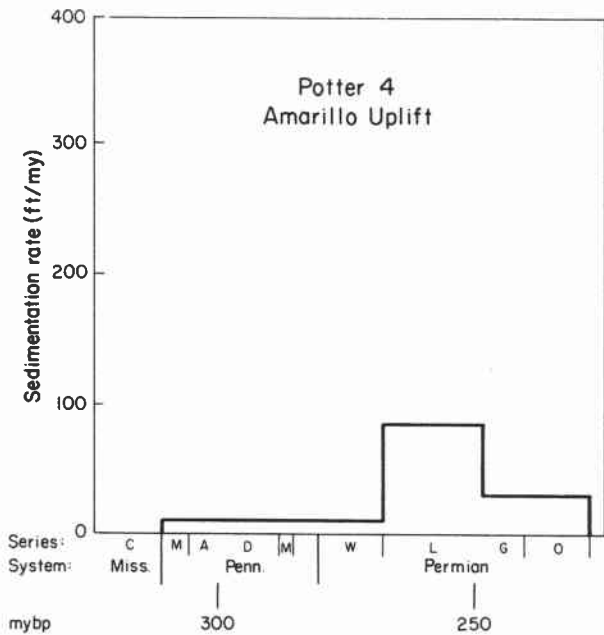


Figure 19. Sedimentation rate graphs for four wells in Potter and Oldham Counties, Texas. Greatest difference in sedimentation rates was between Oldham No. 10 and Potter No. 4 wells, which are on either side of the Potter County fault. Graphs were derived from sample logs.

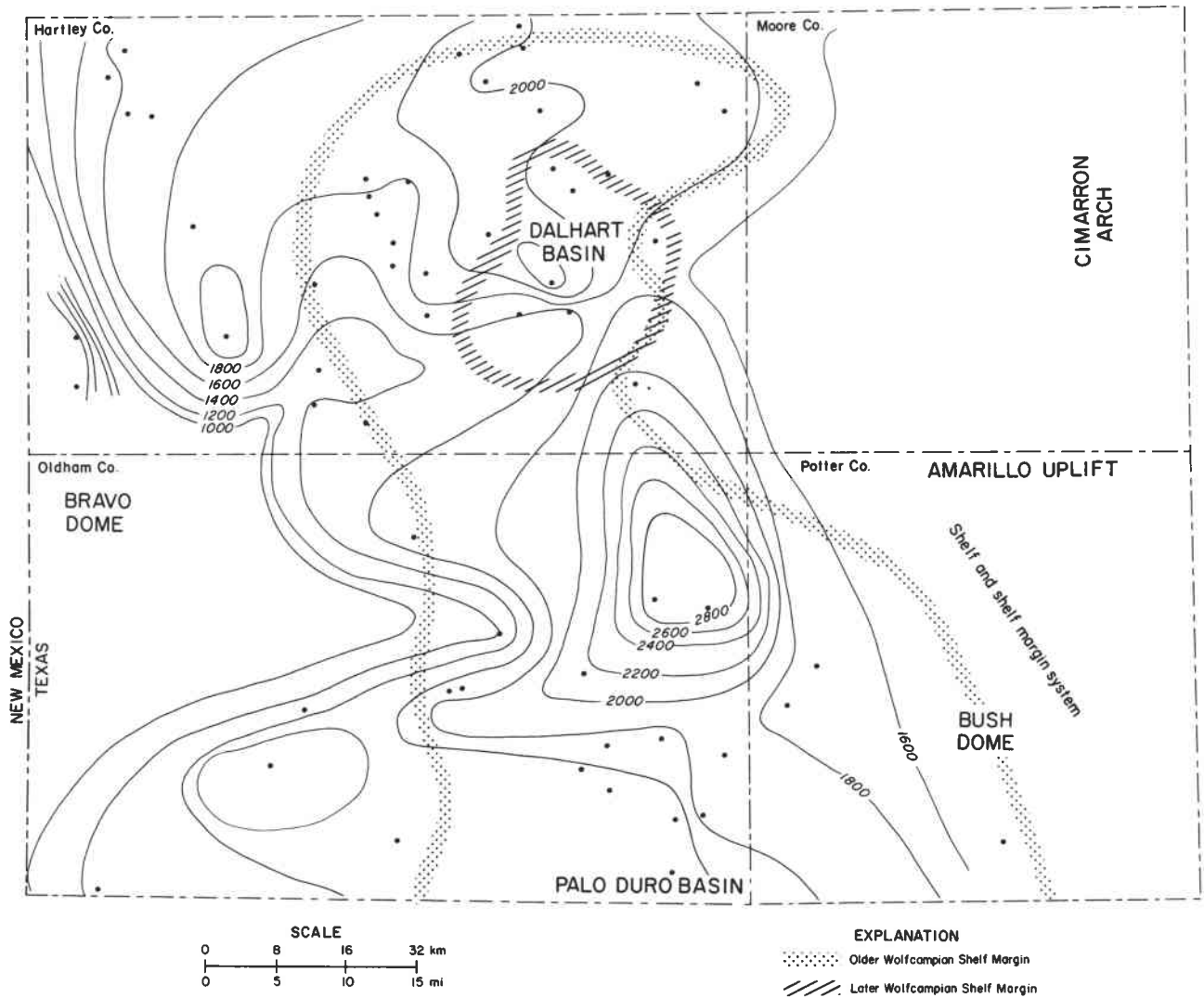


Figure 20. Isopach map of Wolfcamp Series showing positions of shelf margins. Shelf margins generally are developed around structural highs such as the Amarillo Uplift and Bravo Dome (after Handford, 1980).

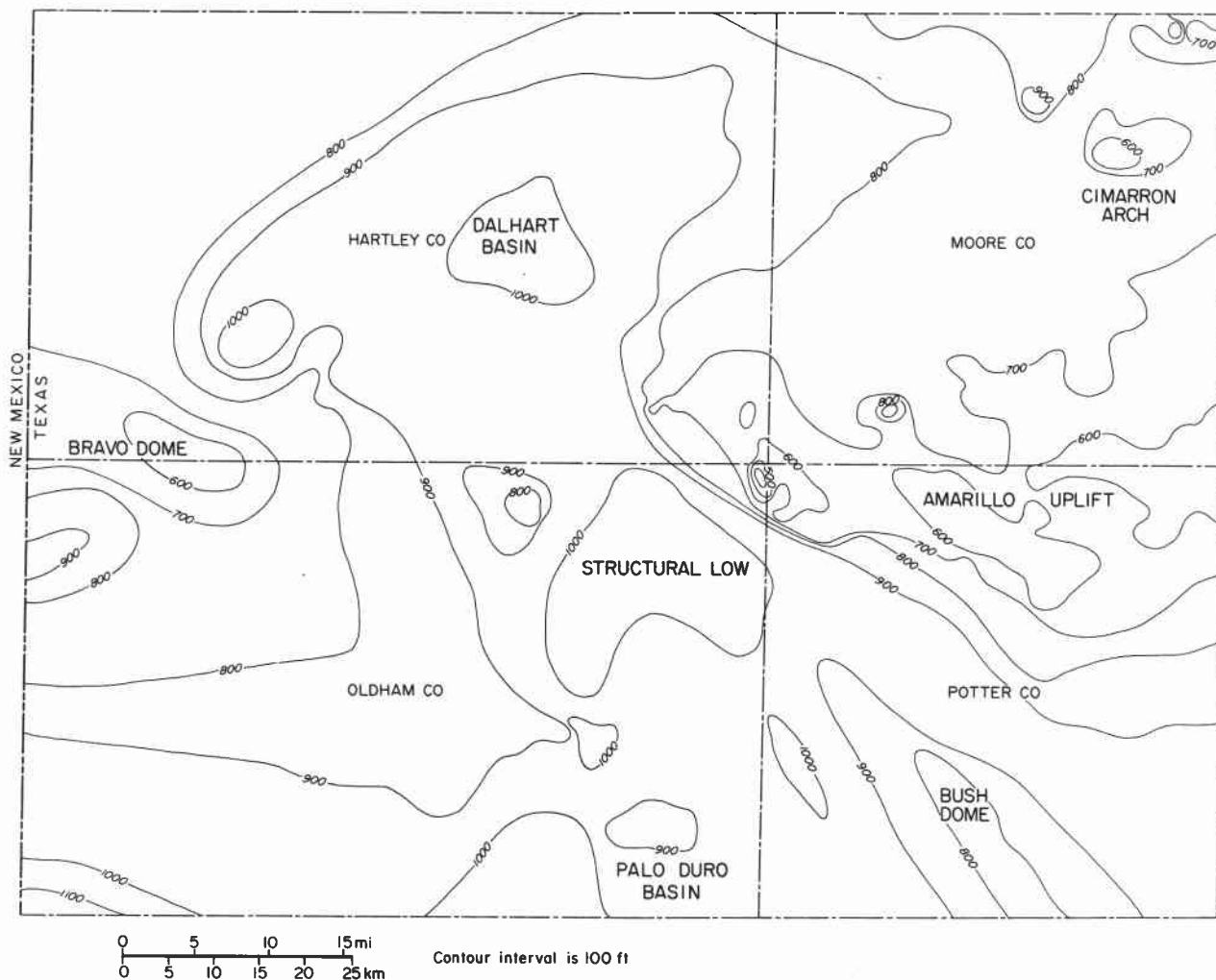


Figure 21. Isopach map of interval from the top of Wichita Group to the top of Tubb Formation. After burial of the Amarillo Uplift by Permian sediments, structural lows continued to subside and preserve relatively more sediments, thus preserving the pattern of earlier deposition.

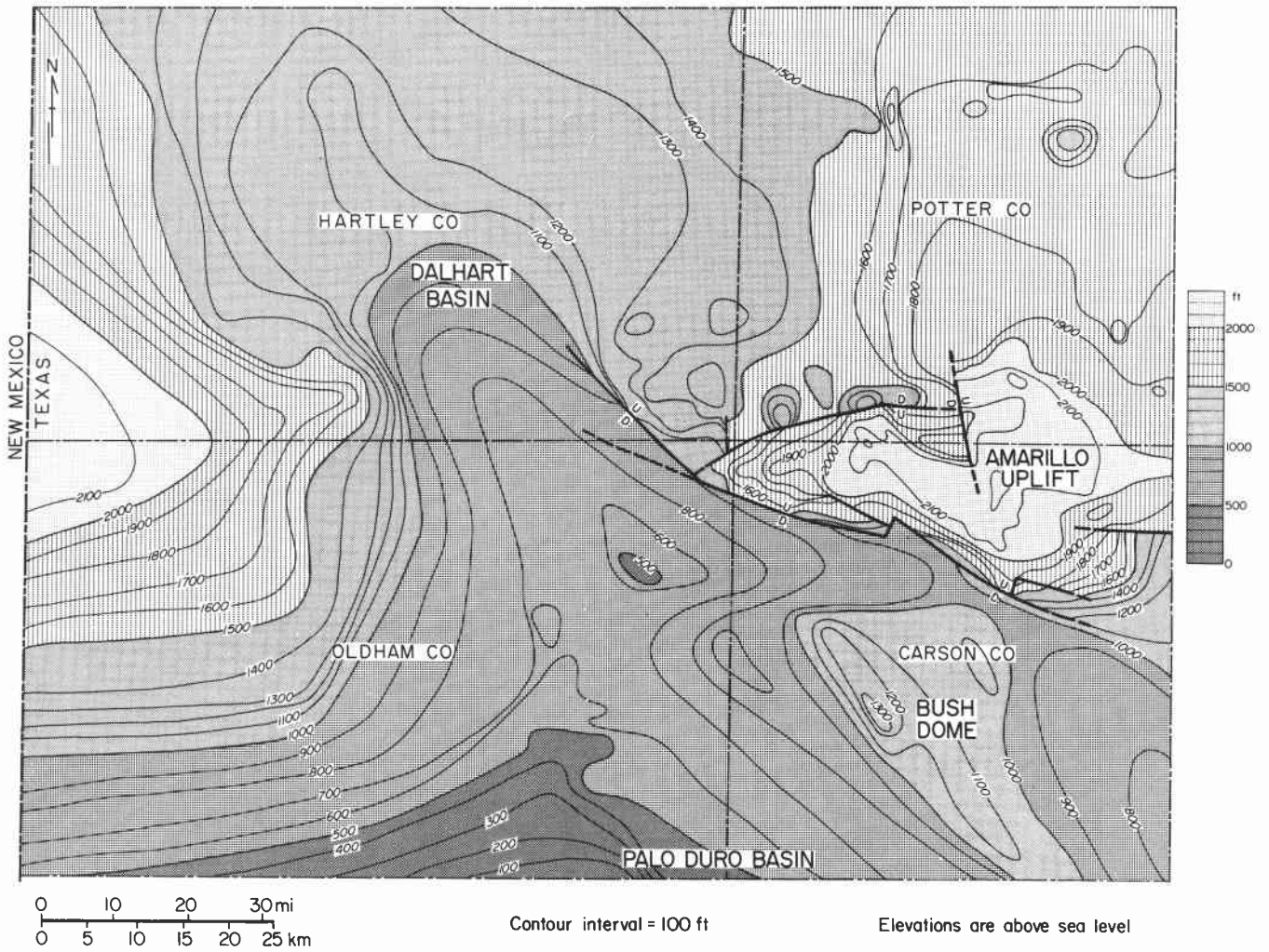


Figure 22. Structure map, top of the Tubb Formation.

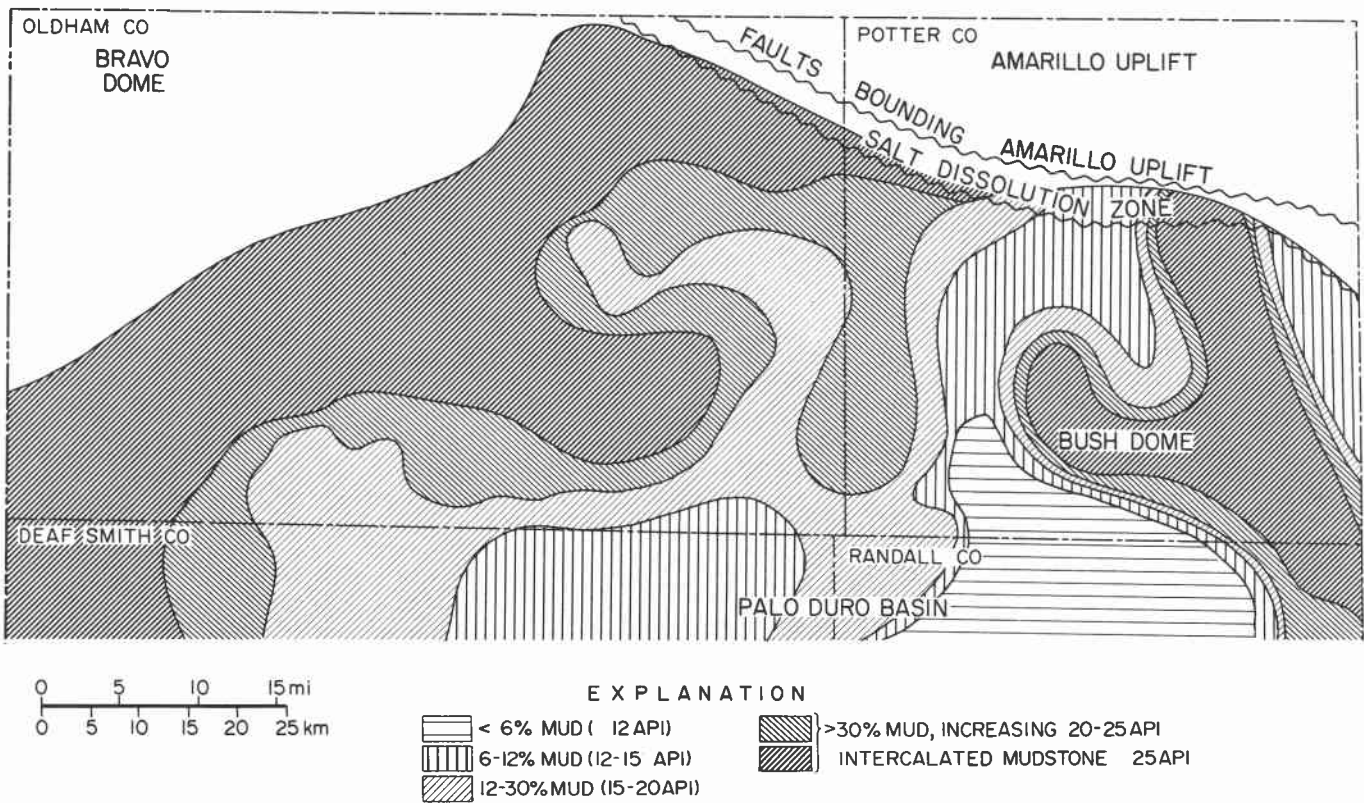


Figure 23. Salt quality map, San Andres cycle 4 salt, determined from analyses of gamma-ray logs. Purest (non-muddy) salts were deposited in areas of subsidence, remote from uplifts and domes (P. J. Ramondetta, personal communication, 1981).

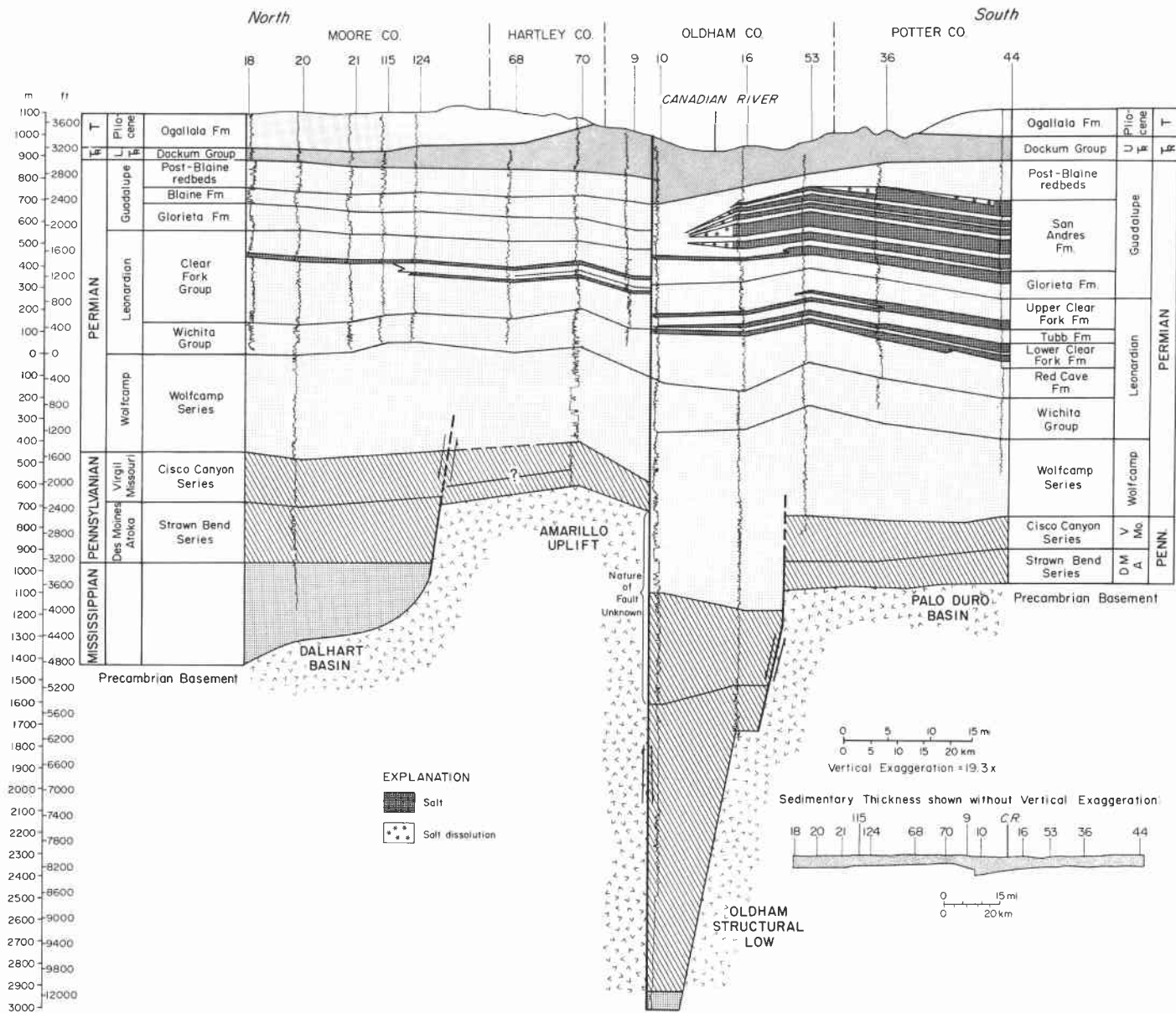


Figure 24. Cross section showing present configuration of strata across the Amarillo Uplift. For line of section, see figure 18.

Table 2. Gamma-ray and sample logs used in figure 18.

|            |  |
|------------|--|
| Hartley 68 | Phillips Petroleum Co., Feltz No. 2              |
| Hartley 70 | Sinclair Oil and Gas Co., Bivins Estate No. 15   |
| Moore 18   | Texas Co., Lacy Meek No. B-1                     |
| Moore 20   | Union Oil of California, W. B. Wooster No. 1-384 |
| Moore 21   | Pioneer Production Corp., Thompson No. 1         |
| Moore 115  | ADA Oil Co., Nevehein No. 1                      |
| Moore 124  | Phillips Petroleum Co., Drury No. 2              |
| Oldham 9   | Pioneer Production Corp., Bivins No. D-13        |
| Oldham 10  | Shell Oil Co., Bivins Ranch No. 1                |
| Oldham 16  | Shell Oil Co., L. S. Ranch B-1                   |
| Oldham 53  | Shell Oil Co., strat. 4-58                       |
| Oldham 80  | Page Petroleum Inc., Scott 1-11                  |
| Potter 4   | Sinclair Oil and Gas Co., Bivins No. 9           |
| Potter 36  | Harrington and Mars, Bush Estate A-1             |
| Potter 38  | Amarillo Oil Co., Lundegreen No. 1               |
| Potter 44  | Humble Oil Co., O.H. Gouldy No. 1                |

## REGIONAL STRATIGRAPHIC FRAMEWORK OF THE TEXAS PANHANDLE

Roy Budnik and Dale Smith

*The Palo Duro and Dalhart Basins were formed as a result of Pennsylvanian tectonic activity. Pennsylvanian rocks are primarily normal marine sediments. The Permian System records large-scale cycles of transgression and regression of restricted shallow marine seas; evaporites were deposited over large supratidal sabkha areas. Post-Permian deposition was primarily in terrestrial environments. The structural and stratigraphic relationships of each system are examined in detail.*

The Texas Panhandle covers approximately 44,000 mi<sup>2</sup> (114,000 km<sup>2</sup>) and includes the Palo Duro Basin and four other cratonic sedimentary basins, each bounded by positive tectonic features (fig. 25). The general geology has been summarized by Roth (1955), Totten (1956), Nicholson (1960), Dutton and others (1979), and Gustavson and others (1980, 1981). Depths of these basins vary considerably; the Dalhart, Hardeman, northern Midland, and Palo Duro Basins are shallow, approximately 10,000 to 12,000 ft (3,000 to 4,000 m) deep, whereas the Anadarko Basin is approximately 30,000 ft (9,000 m) deep. Prominent uplifts, domes, and arches consisting principally of Precambrian igneous and metamorphic rocks intruded by alkaline rocks separate several of the basins in the Texas Panhandle area (fig. 25) (Handford, 1981).

The Palo Duro Basin consists of two temporally separate but spatially overlapping basins. The initial basin formed as a northwestern extension of the Hardeman Basin during the Early Pennsylvanian. It was bounded on the north and northeast by the Amarillo-Wichita Uplift and on the south by the Matador Arch - Red River Uplift. The western limits are defined by a more stable area separating the Palo Duro and Tucumcari Basins. A second basin developed in the Early Permian; it was relatively broad and shallow, with no major nearby sources of sediment. Even so, more than twice the thickness of sediment accumulated during the Permian compared with the Pennsylvanian.

The Palo Duro and Dalhart Basins comprise rocks ranging in age from Precambrian to Holocene. Figure 26 illustrates the stratigraphy and complex nomenclature of the Texas Panhandle area. The remainder of this report deals with each of these stratigraphic units in detail.

### PRECAMBRIAN BASEMENT

The Precambrian basement of the Texas Panhandle consists of a complex of intrusive and extrusive igneous rocks and minor metasediments. Muehlberger and others

(1967), modifying work by Flawn (1956), delineated six basement terranes in the study area (fig. 27).

(1) The Chaves granitic terrane, dated at 1,350 m.y., is the oldest unit in the area. It consists predominantly of granite and underlies the deepest part of the Palo Duro Basin and the northern Midland Basin.

(2) The region north and northwest of the Palo Duro Basin, extending into Oklahoma, Kansas, New Mexico, and Colorado, is underlain by the rather uniform Sierra Grande granite terrane. It consists of biotite granite to granodiorite and yields a consistent date of 1,270 m.y.

(3) The Panhandle volcanic terrane is a thick sequence of rhyolite porphyry and tuff that was extruded as flows and ignimbrites. These extrusives have an average age of 1,140 m.y. and underlie a large section of the Palo Duro and Dalhart Basins.

(4) The buried Amarillo Uplift, Bravo Dome, and the northeastern shelf of the Palo Duro Basin are underlain by 1,140-m.y.-old granites of the Amarillo granite terrane.

(5) Most of what were the deeper parts of the Palo Duro Basin during the Pennsylvanian and Permian are underlain by the Swisher diabasic terrane. Muehlberger and others (1967) thought that this terrane overlies the Panhandle volcanics. The age of the Swisher terrane has been debated. Roth (1960) noted that diabase intruded fossiliferous limestone in a well in Briscoe County. However, Muehlberger and others (1967) reported an age of 1,200 m.y. from diabase in a well in Parmer County.

(6) The eastern part of the Matador Arch and most of the Red River Uplift are underlain by the Tillman metasedimentary group. The age of this biotite-grade meta-graywacke sequence is unknown.

#### PRE-PENNSYLVANIAN SYSTEMS

Rocks of definite Cambrian age are unknown in the Palo Duro area. A basal sandstone that occurs locally on top of the Precambrian is correlated on the bases of lithology and stratigraphic position with the Upper Cambrian Hickory Sandstone of the western Anadarko Basin (Totten, 1956). This basal unit consists of 0 to 200 ft (60 m) of porous, fine- to coarse-grained, quartzose to arkosic, glauconitic sandstone and was probably derived from nearby sources (fig. 28).

Unconformably overlying this basal unit is the Lower Ordovician Ellenburger Group. It consists of coarsely crystalline, gray to buff dolomite, with occasional interbeds of limestone or chert. The unit locally exceeds 1,000 ft (300 m) in thickness but is absent in

the deepest part of the Palo Duro Basin because of erosion in Early Ordovician to Early Mississippian time over the Texas Arch and other, more minor, northwest-trending structures (fig. 29). To the south, in the Midland Basin, and to the north, in the Anadarko Basin, rocks of Early Ordovician to earliest Mississippian (Kinderhookian) age onlap and pinch out against the Texas Arch (Nicholson, 1960).

The Texas Arch was finally submerged during Osage time and was, during the rest of the Mississippian, a shelf area between the deep Midland Basin and the shallower Anadarko Basin. As much as 1,100 ft (350 m) of shelf carbonates were deposited (fig. 30). The lowest part (Osage) consists of light-gray, very cherty limestone and dolomite. The middle part (Meramec) is predominantly light-gray oolitic limestones with some dolomite and chert. In the upper part of the section (Chester), the limestones are light-gray, oolitic, and fossiliferous, with little chert. In the lower Chester, red-brown shales and gray-red sandstones are present (Totten, 1956). The clastics may mark the first phase of mid-Paleozoic deformation in the Panhandle.

In the Palo Duro Basin, the series distribution and isopachous trend of the Mississippian strata (fig. 30) approximately parallel those in the overlying Pennsylvanian (McKee and others, 1975, plate 3-A), which suggests that the basin may have started to develop in the Mississippian. The same relation is absent in the Dalhart Basin, perhaps because it formed somewhat later.

## PENNSYLVANIAN SYSTEM

### Structural Setting

During the latest Mississippian and earliest Pennsylvanian, the relatively stable shelf at the site of the former Texas Arch started to break up along preexisting structural trends (fig. 31). The earliest movement appears to have been a gentle upwarping (Adams, 1962) parallel to and immediately south of the Anadarko Basin (initially formed in the Cambrian; Ham and Wilson, 1967). Mississippian strata were completely eroded in this area; Pennsylvanian rocks lie directly on Precambrian basement (fig. 30). As deformation continued into the Pennsylvanian, north-northwest-trending faults coincident with and parallel to the axis of the former Texas Arch were reactivated. Mississippian rocks were eroded from the highest parts of these fault-bounded blocks (fig. 30). Foster and others (1972) noted a similar relation between the distribution of Mississippian rocks and fault blocks in eastern New Mexico. Also during this time, the east-west-trending Matador

Arch started to rise along the trend of the Tillman metasedimentary belt. The Matador Arch consisted of a series of small, fault-bounded blocks that stood along the southern edge of the Palo Duro and Hardeman Basins.

Once delineated, basin geometry remained relatively stable during the Pennsylvanian and into the Permian. The Amarillo-Wichita Uplift, the Sierra Grande Uplift, and the Oldham Nose were major sediment sources at various times. The Matador Arch and the northwest-trending fault blocks were only minor sources of clastics. More important, they were loci of carbonate sediment accumulation (figs. 32 and 33) throughout the period.

The Palo Duro and Hardeman Basins were essentially one unit during the Pennsylvanian. Sediments thicken southeastward into the Hardeman Basin and onlap and thin south, west, and north onto now-buried structural highs that surround the Palo Duro Basin (fig. 34). The Hardeman Basin was an important sediment conduit for clastics derived from the Wichita Uplift (Dutton, 1980; Erxleben, 1975). More than 4,500 ft (1,500 m) of Pennsylvanian sediments accumulated in the Palo Duro and Hardeman Basins (Adams, 1962). The Dalhart Basin, which received over 2,400 ft (730 m) of sediment during the Pennsylvanian (Dutton, 1980), was connected to the Palo Duro Basin through a saddle between the Amarillo Uplift and the Bravo Dome.

### Stratigraphy

Because Pennsylvanian-age strata do not crop out within the Palo Duro Basin, time-stratigraphic boundaries are used in the subsurface. Formation names, therefore, are not used. Four units are defined: (1) Morrow-Atoka/Bend Series, (2) Desmoines/Strawn Series, (3) Missouri/Canyon Series, and (4) Virgil/Cisco Series (Nicholson, 1960; fig. 26).

During Morrow and Atoka time, the Palo Duro and Dalhart Basins were again inundated by a shallow sea. Coarse clastics, including a limited amount of arkose interbedded with shale, coal, and thin limestone, make up the Bend Series. This unit was deposited and preserved only in the structurally lowest parts of the basins (Frezon and Dixon, 1975; Forgotson and others, 1966).

In the Desmoines, more intense deformation occurred (Adams, 1962; Frezon and Dixon, 1975). The Bravo Dome and the Sierra Grande and Amarillo-Wichita Uplifts became important sediment sources for coarse arkosic sandstone (granite wash), which flooded the Palo Duro, Dalhart, and Hardeman Basins. Movement on the northwest-trending fault blocks also appears to have been greatest at this time (Foster and others,

1975). Most of the granite wash was trapped on the shelves landward of the fault blocks (fig. 32; Dutton, 1980) in the Palo Duro Basin. In the Dalhart Basin as well, granite wash accumulated nearest to the sources west and south of the basin (Dutton, 1980). The higher parts of the fault blocks within the Palo Duro Basin and along the Matador Arch provided areas for the rapid buildup of Strawn limestone (Adams, 1962; fig. 32). With the exception of brief periods of uplift during Missouri time (Frezon and Dixon, 1975), the late Desmoines, Missouri, and Virgil marked a time of apparent stability. Limestone and granite wash depositional rates equaled the subsidence rates in the shallow parts of the basin, while shale and relatively clean sandstone were deposited in the deeper parts (fig. 33).

### Depositional Systems

Three primary depositional systems operated throughout the Pennsylvanian and early Permian (Dutton, 1980; Handford and Dutton, 1980): (1) fan-delta facies of coarse marine and non-marine sandstone, shale, and coal; (2) shelf and shelf-margin facies of limestone with some marine shale; and (3) basin facies of thick shale sequences with thin interbeds of limestone and sandstone (figs. 32 and 33).

The fan deltas consisted of alluvial fans that built out into the marine environments from the Amarillo-Wichita Uplift and other high-relief areas around the basins. Typical deposits include arkosic sandstone (granite wash) laid down in braided-channel, delta-plain, and destructional-bar environments. These interfinger with thin limestone, sandstone, shale, and coal, which record the rapid changes common to this environment (McGowen, 1970). In the Palo Duro Basin, fan deltas reached their maximum development during the Desmoines Epoch.

The Pennsylvanian shelf facies is similar to the underlying Mississippian carbonates. Uniformly thick limestones are interbedded with thin shales. Near areas of active uplifts, the limestones become arkosic and interbedded with units typical of the fan-delta facies. At the shelf margins and fringing the intrabasinal fault blocks, thick buildups of limestone formed. These persisted for as long as carbonate deposition kept pace with subsidence and terrigenous sediment influx.

In the deepest parts of the basins, dark shales and thin, dark limestones were deposited. The only major clastic source was through a high-constructive delta system that built out of the Hardeman Basin during the latest Pennsylvanian or earliest Permian. The system consisted of thick delta-front sandstones and prodelta shales (Handford, 1979).

## PERMIAN SYSTEM

The greatest volume of sediment in the area belongs to the Permian System. The thickness of rocks deposited during this time exceeds 6,500 ft (1,980 m) in the Palo Duro Basin, and 5,000 ft (1,525 m) in the Dalhart Basin (fig. 35). The Permian was a period of gradual subsidence and deposition, predominantly of evaporites and related facies. All four series within the Permian are represented--Wolfcamp, Leonard, Guadalupe, and Ochoa (fig. 26).

### Wolfcamp Series

As was true for the underlying Pennsylvanian, the Wolfcamp was not divided into formations. The Wolfcamp Series is in part lithostratigraphic, but the unit generally correlates with the time-stratigraphic series to the south in the Midland Basin.

The Wolfcamp marks an important change in the Palo Duro Basin. The lower Wolfcamp is made up of clastic and limestone facies that are similar in lithology and distribution to the underlying Pennsylvanian facies (Handford and Dutton, 1980). The upper Wolfcamp, in contrast, consists almost entirely of dolomite that grades upward into Leonard-age dolomite and anhydrite.

The nature of the contact between Pennsylvanian- and Permian-age rocks is a matter of disagreement. Dutton (1980) and Dixon (1967) thought that sedimentation was continuous from the Pennsylvanian into the Permian. Totten (1956) indicated an unconformity at the base of the Wolfcamp in his stratigraphic column, but did not discuss the evidence for it. McKee and others (1975, plate 9-A) showed a large area of the basin where Wolfcamp rocks lie directly on Canyon Series rocks (fig. 33), but, again, there was no discussion of its significance. A West Texas Geological Society cross section (1953) showed an unconformity at the base of the Wolfcamp throughout the Midland and part of the Palo Duro Basins. Silver and Todd (1969), however, placed an unconformity within the Wolfcamp in the same region. Sample logs from wells drilled through the Pennsylvanian-Permian boundary in the Palo Duro Basin show that almost everywhere the basal Wolfcamp consists of terrigenous clastics, which include glauconitic sandstone or shale, occasionally with a limestone conglomerate or, rarely, coal. Whether the overlying rocks are equivalent to the lower or upper Wolfcamp of the Midland Basin is as yet unresolved. In this discussion, the part of the Wolfcamp resembling the Pennsylvanian will be referred to as the lower Wolfcamp, and the part similar to the Leonard will be called the upper Wolfcamp.

The Wolfcamp averages about 1,000 ft (330 m) in thickness (Birsa, 1977), the greatest thickness exceeding 2,000 ft (600 m). The lower Wolfcamp thins against and is locally absent on top of basement highs (Silver and Todd, 1969). The upper Wolfcamp thins over the highs as well, but it is present throughout the basin (Handford and others, 1981). As noted by Birsa (1977), the axis of greatest thickness of the Permian (fig. 35) trends east-west across the southern end of the basin. The Pennsylvanian axis, in contrast, trends northwest-southeast (fig. 34). The Wolfcamp has two axes, which show a transition between the Pennsylvanian and Permian trends (fig. 36).

Depositional patterns in the lower Wolfcamp are similar to those in the Pennsylvanian (Handford, 1980; Handford and Dutton, 1980). Fan deltas periodically built out from the now low-lying Amarillo Uplift. Carbonates built up along the shelf margins, parallel, in large part, to those in the Upper Pennsylvanian.

The center of the basin received primarily mud and relatively clean sand. The high-constructive delta mentioned in the section on the Pennsylvanian may, in fact, be entirely Wolfcampian in age (Handford, 1979). The Hardeman Basin was apparently completely filled by this time.

By the end of the Wolfcamp, all of the uplifts that supplied sediment to the Palo Duro Basin during the Pennsylvanian and earliest Permian were completely submerged (Dixon, 1967). The basin was completely filled with sediment, so that once again the Texas Panhandle was the site of a broad shelf that extended northward into the Midcontinent (Handford and Dutton, 1980; Rascoe, 1962). The shelf margin remained south of the Matador Arch, in the northern Midland Basin, through the remainder of the Permian (Silver and Todd, 1969).

### Leonard Series

#### WICHITA GROUP

The Leonard Series in the Dalhart and Palo Duro Basins is represented by the Wichita and Clear Fork Groups (fig. 26). The Wichita Group, which was named by Sellards (1933) for exposures along the Wichita River and in Wichita County, Texas, is predominantly dolomite and anhydrite in the Palo Duro Basin. In the Dalhart Basin, the Wichita is known by drillers as the "Panhandle lime." The Wichita Group is partly equivalent to rocks of the Sangre de Cristo - Abo Formations in New Mexico and partly equivalent to the Wellington Formation in central Oklahoma (Dixon, 1967; Foster and others, 1972). The average thickness of the Wichita Group in the Palo Duro Basin is 545 ft (166 m); a

maximum thickness of 1,090 ft (332 m) is reached in Floyd County in the Palo Duro Basin (Birsa, 1977). Greatest dolomite thicknesses are in an east-west trend through Floyd, Hale, and Lamb Counties, Texas, along the northern edge of the Matador Arch. Greatest thicknesses of anhydrite are on the eastern and northeastern margins of the Palo Duro Basin.

Strata of the Wichita Group were deposited principally within sabkha and alluvial fan-plain environments (Handford, 1979a). The Wichita sabkha system, which extended throughout the Panhandle area, consisted of an irregular belt of dolomite and anhydrite deposition. Red-bed facies were deposited in alluvial fan plains, and clastic sediments were transported from the northwest (Handford, 1979a). Deposition during Wichita time represents the continued transition that began in the Wolfcamp from the fan-delta, marine shelf, and deep-basin environments of the Pennsylvanian to sabkhas, brine pans, and shallow marine conditions that prevailed during Late Permian time. The Wichita Group is conformably overlain by the Red Cave Formation of the Clear Fork Group and underlain by the Wolfcamp Series (fig. 26).

#### CLEAR FORK GROUP

The Clear Fork Group is divided into five formations on the basis of lithology (Handford and Fredericks, 1980; Presley, 1980a; Handford, 1981); in ascending order, the Clear Fork lithologic units include (1) the Red Cave Formation, (2) the lower Clear Fork Formation, (3) the Tubb Formation, (4) the upper Clear Fork Formation, and (5) the Glorieta Formation. No major unconformities are evident between lithologic units. Handford (1981) also suggested a subdivision of the Clear Fork, based on primary cyclic episodes of deposition, which emphasizes the genetic relationships within the Wichita and the Clear Fork Groups. The genetic facies boundaries are defined on the basis of cyclic carbonate-evaporite facies and red-bed facies repeated during Leonardian time. The genetic facies are (1) Wichita Group - Red Cave Formation, (2) lower Clear Fork - Tubb Formations, and (3) upper Clear Fork - Glorieta Formations.

*Red Cave Formation.*--The Red Cave Formation is the oldest unit of the Clear Fork Group; it is also the oldest of the major red-bed formations in the Dalhart and Palo Duro Basins. The Red Cave Formation consists of southward-thinning, regionally extensive, red to green mudstones and siltstones that coarsen to the northwest into conglomerates and arkoses of the Abo Formation of northeastern New Mexico, and intertongue with anhydrite and dolomite to the south (Handford and Fredericks, 1980). Handford and Fredericks (1980) have subdivided the Red Cave Formation of the Palo Duro Basin into

five members; two carbonate-anhydrite members, referred to as the upper and lower evaporites, are layered between three clastic members that interfinger and pass southward into carbonate facies (fig. 37). The evaporite units occur only in the Palo Duro Basin.

Handford and Fredericks (1980) suggested that the Red Cave Formation was deposited in three depositional systems. Dolomite was probably deposited in an inner-shelf, marine environment. Dolomites of the inner-shelf system are most common in the southern part of the Palo Duro Basin; greatest accumulation, up to 220 ft (67 m), is found in extreme northwestern Lamb County. Lithologies include tan to gray dolomitic mudstone and pellet wackestone. North of the inner-shelf system, a wide sabkha was dominated by deposition of carbonate or terrigenous muds (fig. 38). The carbonate-evaporite sabkha system supplied sediments to form the lower and upper cyclic evaporite members. The sandstone and siltstone facies in the northwestern Panhandle area were deposited by fluvial processes in a wadi-plain environment (Handford and Fredericks, 1980). Clastic members of the Red Cave Formation are cyclical and progradational to the south. Evaporite members were probably deposited as a result of clastic sediment reduction or termination during periods of subsidence (Handford and Fredericks, 1980).

*Lower Clear Fork Formation.*--Within the lower Clear Fork Formation, two depositional cycles are recognized across most of the Panhandle. In the southern Palo Duro Basin, numerous additional small-scale cycles were described by Handford (1981). The larger cycles record periods of regional transgression followed immediately by the development and seaward progradation of a frequently flooded, carbonate tidal flat-sabkha complex. This complex was eventually blanketed by terrigenous clastic facies that terminated the cycle (Handford, 1981). The lower Clear Fork Formation comprises six lithofacies from north to south (fig. 39): (1) red beds, (2) chaotic mudstone-salt, (3) banded to massive salt, (4) laminated to massive anhydrite, (5) nodular anhydrite, and (6) dolomite (Handford, 1981). The lower Clear Fork is thickest in central Palo Duro Basin, where it reaches a maximum thickness of 533 ft (138 m) in southeastern Castro County; it is absent in most of the Dalhart Basin (fig. 39).

*Tubb Formation.*--The lower and upper Clear Fork Formations conformably overlie and underlie the Tubb Formation. The Tubb Formation was subdivided into two major facies by Presley (1981): (1) the siliciclastics, laminated mudstone-siltstone and mudstone deposited in tidal mud flats and (2) the evaporite-carbonate, chaotic mudstone-salt, massive-banded salt, laminated anhydrite, laminated dolomite, and carbonates deposited

from north to south in sabkha-tidal flat-subtidal shelf sequences (fig. 40). Presley (1981) suggested that the Tubb Formation facies represent a progressive southerly shift of environments through time. Deposition was characterized by alternating periods of net clastic and net evaporite-carbonate sedimentation (fig. 41). By late Tubb time, mud-flat sediments were predominant over much of the Palo Duro Basin. In the evaporite-carbonate facies, salt predominates to the north and anhydrite predominates to the south (fig. 42). Carbonates are predominant in the evaporite-carbonate facies in the southern Palo Duro Basin. The siliciclastic facies were deposited from a mud supply from the northwest that decreased southeastward across the Palo Duro Basin (Presley, 1981). Presley (1980b, 1980c) discussed salt deposition and thickness in more detail.

*Upper Clear Fork Formation.*--The upper Clear Fork Formation is the earliest (lowermost) evaporite-carbonate cycle of the youngest genetic facies association within the Clear Fork Group. Presley and McGillis (1982) described the upper Clear Fork Formation of the Palo Duro and Dalhart Basins as comprising four cyclic, offlapping facies from north to south: (1) chaotic mudstone-salt, (2) massive-banded salt, (3) laminated anhydrite, and (4) dolomite. Environments of deposition were inner carbonate shelf, algal flats, salt ponds, and mud-salt flats (fig. 43). Cyclic sedimentation characterizes the entire unit. The basal unit of the upper Clear Fork Formation in the Palo Duro Basin is correlative with the Cimarron Anhydrite in the Dalhart Basin (fig. 44). The upper unit of the upper Clear Fork Formation exhibits a clastic to carbonate facies shift from the Dalhart to the Palo Duro Basin. Salt in the upper Clear Fork is the thickest (up to 350 ft; 107 m) along a trend parallel to the northern edge of the Palo Duro Basin; the southern margin has less than 200 ft (61 m) of net salt (fig. 45). The Dalhart Basin contains up to 125 ft (38 m) of salt (Presley and McGillis, 1981a) (fig. 45). Subsurface salt dissolution has occurred along the Amarillo Uplift, across the Oldham Nose, and on the extreme eastern margin of the Palo Duro Basin.

*Glorieta Formation.*--The Glorieta Formation is the upper unit of the Clear Fork Group in the Palo Duro Basin, where it underlies the San Andres Formation. To the north, in the Dalhart Basin, the Glorieta Formation is overlain by the Blaine Formation of Guadalupian age (fig. 26). The Glorieta Formation represents the last stage (clastic and evaporite dominance of sedimentation) in the upper Clear Fork - Glorieta facies. The Glorieta Formation is predominantly mudstone in two areas: (1) northwest to southeast through Deaf Smith, Castro, and Swisher Counties and (2) west to east through Roosevelt, Bailey, and Lamb Counties (fig. 46) (Presley and McGillis, 1982). Regionally, the Glorieta

Formation is thickest (up to 300 ft; 90 m) along a northeast-southwest linear trend (Presley, 1981b). Presley (1981b) indicated that the clastic facies of the Glorieta Formation were deposited primarily within a continental, eolian environment. Southeast of the Dalhart Basin, the eolian environments grade into salt pans and mudflats (fig. 43). Generally, the clastic facies are thicker where salt deposits thin; net salt thickness parallels net formation thickness. The salt is thickest in the western Palo Duro Basin. In the Dalhart Basin, the Glorieta Formation is primarily a sheet sandstone of an eolian environment (Presley and McGillis, 1982). Presley and McGillis (1981a), McGookey (1981), and Presley (1979b) have presented more detailed discussions of salt deposition, purity, and dissolution.

### Guadalupe-Ochoa Series

#### LOWER GUADALUPE FORMATIONS

*San Andres Formation.*--Characteristic of the San Andres Formation is the lack of significant clastic sediments similar to those of the Clear Fork Group discussed previously. Facies changes from the outcrop to the Midland and Palo Duro Basins are extensive. At the type locality, the San Andres is composed of a thin basal sandstone and massive limestone. In the Midland Basin, the San Andres Formation is dominantly limestone and dolomite, with minor amounts of anhydrite and salt. The San Andres Formation in the Palo Duro Basin is primarily an evaporite sequence containing minor amounts of carbonates and mudstone (fig. 47). Previous work on the San Andres in the Palo Duro Basin includes that of Presley (1979a, 1979b, 1980a, 1981c), Ramondetta (1981), and Presley and Ramondetta (1981). A lower and upper subdivision of the San Andres has been established in the Palo Duro Basin by most geologists.

The lower San Andres Formation is characterized by cyclic deposition with progradation of facies to the south through time (Presley, 1979). A typical cycle consists of four lithologic units; they are, in descending order, (1) a thin shale or shaly carbonate bed, (2) shaly, fossiliferous limestone or dolomite, (3) dolomite, and (4) evaporite (Pitt and Scott, 1981). Five depositional cycles have been suggested for the lower San Andres Formation by Pitt and Scott (1981) and Presley (1979a). Outside of the Palo Duro Basin, in east-central New Mexico and in the Midland Basin, carbonates are dominant in each cycle. However, in all cycles, salt increases and carbonates decrease in thickness updip toward the Palo Duro Basin (fig. 47). Salt also occurs in the middle of the cycles in the Palo Duro Basin, creating numerous second-order cycles. Banded to massive salt becomes

the dominant lithologic unit as a result of these facies changes. Thickest salt in the lower San Andres is in the northern Palo Duro Basin in Oldham, Deaf Smith, Randall, and Armstrong Counties, Texas; maximum net salt thickness is 400 ft (135 m) in Deaf Smith County (Presley, 1981c) (fig. 48). Cycle 4 (fig. 47) contains the thickest salt deposits in the San Andres Formation; maximum net salt is 200 ft (61 m) along a trend northwest to southeast through Oldham, Potter, Randall, and Armstrong Counties. Greatest thickness of salt deposits in cycle 5, 125 ft (38 m), occurs in Deaf Smith County.

The upper San Andres Formation comprises mainly anhydrite and salt in the Palo Duro Basin as well as in east-central New Mexico and in the Midland Basin. Overall regression was the dominant trend during San Andres time (Presley, 1980a); this regressive trend is emphasized by thick evaporites in the upper San Andres Formation. Upper San Andres salt is thickest in west-central Palo Duro Basin in Deaf Smith, Parmer, and Castro Counties; maximum net salt thickness is 300 ft (92 m) in eastern Parmer and western Castro Counties (Presley, 1981c) (fig. 49). Salt dissolution has occurred along the northern Palo Duro Basin margin in Oldham, Potter, and Carson Counties; along the eastern margin in Armstrong, Donley, Hall, Briscoe, and Motley Counties; and along the western margin in Quay County, New Mexico.

In the west and central parts of the Palo Duro Basin, the San Andres Formation is underlain by the Glorieta Formation and overlain by the Artesia Group (Dixon, 1967; Johnson, 1978; Gustavson and others, 1980). The San Andres Formation is equivalent to the Blaine Formation in the eastern Palo Duro Basin and in the Dalhart Basin (Johnson, 1978; Presley, 1980) (fig. 26).

*Blaine Formation.*--The Blaine Formation overlies the Glorieta Formation in the Dalhart Basin and in the eastern Palo Duro Basin. In the eastern and northern Panhandle area, the Blaine Formation is probably temporally equivalent to the San Andres Formation (Dixon, 1967): the transition occurs at the zone where the dissolution has removed salt from the Blaine. The Blaine Formation does not exist west of the Texas Panhandle. Anhydrite is the dominant rock type; dolomite, salt, and red mudstone are minor facies variations. The lack of significant clastic deposition suggests supratidal or inner-shelf deposition and relatively stable tectonic conditions. No significant salt deposits occur in the Blaine Formation in the Dalhart or Palo Duro Basins.

#### UPPER GUADALUPE - OCHOAN FORMATIONS

In the Dalhart and Palo Duro Basins, the Artesia Group includes upper Permian rocks that lie between the San Andres - Blaine Formations and the overlying Alibates and

Dewey Lake Formations (fig. 26). The name "Artesia Group," formerly the Chalk Bluff Formation of New Mexico, is used for areas south of the Amarillo Uplift. North of the Amarillo Uplift, the Artesia Group is equivalent to the Whitehorse Group and the Cloud Chief Formation.

Five units have been defined by Tait and others (1962) for the Artesia Group (fig. 26). They are, in ascending order, the Grayburg, Queen, Seven Rivers, Yates, and Tansill Formations. Above the Tansill Formation in the Midland Basin is the Salado Formation. The boundary between the Tansill and Salado Formations is not clearly evident or defined in the Palo Duro Basin. For this reason, both will be considered as one unit in this report. Rocks overlying the Tansill Formation are regarded by Jones (1956) to be of the Ochoa Series. Because the Tansill-Salado Formation is considered as one unit, the Guadalupe-Ochoa boundary is not important here.

*Queen/Grayburg Formations.*--The Grayburg and Queen Formations are considered here as one unit because no distinct mappable boundary exists between the base of the Grayburg and the top of the Queen in the Texas Panhandle. At the type locality, the Grayburg is primarily dolomite; however, in the Palo Duro Basin, the Grayburg is a red mudstone with minor amounts of evaporites. The Queen Formation, at the type locality near Queen, New Mexico, is dominantly a red sandstone with interbedded dolomite. In Eddy County the Queen Formation is known as the "Artesia red sand" (Jones, 1953). No significant salt deposits are found in the Queen/Grayburg Formations in the Texas Panhandle.

*Seven Rivers Formation.*--In the Palo Duro Basin, mudstone-dominant beds inter-finger near the southern margin with massive salt beds (Presley, 1980a). In the Midland Basin, the Seven Rivers is predominantly salt (Jones, 1953). Presley (1980a) subdivided the Seven Rivers in the Palo Duro Basin into upper and lower units (fig. 50). The upper unit is predominantly massive salt in the southern part of the basin; the lower unit is mostly red mudstone with thin massive salt beds. Salt in the Seven Rivers terminates at the dissolution zone (fig. 51). North and northeast of the dissolution zone the Seven Rivers Formation is a red mudstone. Presley (1979a, 1979b, 1980a, 1980c) and Gustavson and others (1980) discussed Seven Rivers salt and salt dissolution. The Seven Rivers Formation - Yates Formation boundary is transitional (Presley, 1979b).

*Yates Formation.*--In the Palo Duro Basin, the Yates Formation is composed of siltstone and mudstone; no significant salt deposits exist. The Yates is conformably overlain by the Tansill-Salado Formations.

*Tansill-Salado Formations.*--The Tansill-Salado Formations are the youngest salt-bearing rocks of the Palo Duro Basin. In the southern Palo Duro Basin, the Tansill-Salado Formations are primarily salt, but grade northward into red beds (fig. 52); in the Dalhart Basin the boundaries are transitional and difficult to determine. Massive salt is relatively clastic-free. Clastic units are mudstones and siltstones interbedded with salt in the southern Palo Duro Basin. North of the salt dissolution zone (fig. 53), the Tansill-Salado Formations comprise undifferentiated red beds and gypsum and have been described by McGillis and Presley (1981c) as collapse breccia (fig. 52). Depositional environments include brine pans (massive salt) to salt-mud flats (chaotic mudstone-salt) to supratidal salt-mud flats (clastics). The Tansill-Salado Formations represent a regressive cycle (McGillis and Presley, 1981c). After the Tansill-Salado Formations were deposited, transgression of the area resulted in the deposition of the Alibates Formation. McGillis and Presley (1981a, 1981b) presented detailed discussions on salt deposition and dissolution.

#### OCHOAN FORMATIONS

*Rustler and Alibates Formations.*--The Alibates Formation is primarily composed of anhydrite and dolomite with minor amounts of gypsum and red beds. Lithofacies were described by McGillis and Presley (1981a) as laminated dolomite, laminated anhydrite and gypsum, and laminated anhydrite and dolomite. Anhydrite and gypsum are the prevailing lithology in central and southern Palo Duro Basin. In the Dalhart Basin and northern Palo Duro Basin, dolomite is predominant (fig. 54) (McGillis and Presley, 1981a). The Alibates Formation was deposited on low-energy, relatively clastic-free, intertidal to supratidal flats. A minor transgression-regression cycle developed during deposition of the Alibates (McGillis and Presley, 1981a). The Alibates is equivalent to the upper part of the Rustler Formation in the Midland Basin and southeast New Mexico (Dixon, 1967) and may be correlative with the base of the Doxey Shale in the Anadarko Basin (Johnson, 1978).

*Dewey Lake Formation.*--The Dewey Lake Formation conformably overlies the Alibates Formation in the Palo Duro Basin. In parts of the northern Palo Duro Basin and the Dalhart Basin the Dewey Lake Formation is eroded away. In the Anadarko Basin, the Dewey Lake Formation is correlative with the Doxey Shale, which is referred to as the "Quartermaster Formation" in outcrop in much of the Texas Panhandle (Johnson, 1978). The Dewey Lake Formation is a clastic red-bed sequence with a maximum thickness of 200 ft (61 m) in the central Palo Duro Basin (Johnson, 1978). Unconformably overlying the Dewey Lake Formation is the Dockum Group of Triassic age.

## TRIASSIC SYSTEM

The Triassic System is represented in the Palo Duro Basin by the Dockum Group of Late Triassic age. Brand (1956) subdivided the Dockum Group into three formations; they are, in ascending order, the (1) Tecovas Formation, (2) Trujillo Formation, and (3) Chinle Formation. The Tecovas Formation, named by Gould (1905) for exposures on Tecovas Creek, Potter County, Texas, lies unconformably on the Permian strata. In general, the Tecovas Formation may be considered the shaly member of the Dockum Group. Overlying the Tecovas Formation is the Trujillo Formation, named by Gould (1905) for exposures on Trujillo Creek, Oldham County, Texas. The Trujillo Formation is the sand member of the Dockum Group. In the Palo Duro Basin and the northern Texas Panhandle, the Chinle Formation is absent.

The Dockum Group is composed of terrigenous clastic red beds, mudstones, siltstones to conglomerates, and minor facies of dolomite and chert. Directions of transport of sediments are primarily from the west, south, and east. Transport from at least three directions (McGowen and others, 1979) suggests uplift of peripheral areas and/or subsidence of the basin during Triassic time (Brand, 1956). The increase of clastics in the Trujillo Formation, as compared to the shaly Tecovas Formation, suggests an unstable tectonic environment during late Dockum time (Brand, 1956).

The Dockum Group records the major climatic changes from the arid sabkha environments of the Permian to the humid continental environments of the Triassic (McGowen and others, 1979). In this regard the Dockum Group depositional setting is more similar to that of the pre-Permian strata than to that of the Permian strata. The fluvial depositional systems of the Dockum Group created abrupt facies changes both vertically and laterally, providing a wide diversity of depositional features (McGowen and others, 1979). Evidence of a humid continental depositional environment includes fan deltas, lacustrine deposits, lobate deltas, meander stream deposits, forest beds, point bars, fresh-water fossils, and absence of evaporites.

## JURASSIC SYSTEM

Jurassic strata occur in the subsurface of the Dalhart Basin in western Dallam and northwestern Hartley Counties. Lithologies include calcareous sands and shales and minor amounts of limestone.

## CRETACEOUS SYSTEM

Strata of the Cretaceous System occur only in isolated remnants in the Dalhart and Palo Duro Basins east of the main Cretaceous deposits in New Mexico. Outcrops of Cretaceous age strata in New Mexico are gray, marine deposits of several formations (Pitt and Scott, 1981). In the Texas Panhandle the Cretaceous outcrops have been identified by Barnes and Eifler (1967, 1968, 1969, 1970) and by Barnes and others, (1974 and 1978). The Cretaceous subsurface in the Texas Panhandle has not been adequately studied because of lack of subsurface data, and therefore tends to be distinguishable only in contrast to the red beds of the Permian and Triassic.

## TERTIARY SYSTEM

### NEOGENE SERIES

*Ogallala Formation.*--The Ogallala Formation of Neogene age forms a gently sloping plateau on the surface of the High Plains. The relatively flat topographic relief of the High Plains is developed on the resistant capping layer of soil caliche that occurs in the upper Ogallala Formation. Significant water resources are found in the Ogallala. Deposition of the Ogallala Formation resulted from eroded clastic sediments from the Rocky Mountains transported to the Panhandle area by fluvial processes and deposited in large alluvial fans. Seni (1980) described these fans as three overlapping fan lobes deposited in sequence from north to south across the Panhandle, the oldest lobe being in the northern Panhandle area (fig. 55). Thickness of the Ogallala Formation varies owing to relief on the pre-Ogallala surface; the maximum thickness of 800 ft (250 m) is in Carson County (Seni, 1980) (fig. 56). Factors affecting this surface include dissolution of Permian salts, Triassic high areas, erosion, pre-Ogallala steplike pattern of outcrop, and fluvial depositional features (Frye and Leonard, 1964; Seni, 1980). Distribution of the Ogallala Formation in the Dalhart and Palo Duro Basins is primarily dependent on post-Ogallala surface erosion and on retreat of the Eastern Caprock Escarpment.

*Blanco Beds.*--Overlying the Ogallala Formation are the Blanco beds of early Pleistocene age. The age of the Blanco beds has been determined from analyses of stratigraphic relations and vertebrate fauna. In the High Plains, the Blanco beds consist of light-gray calcareous sands, clay, bentonite, nonmarine limestone, and diatomite (Brand, 1953). East of the escarpment, the Blanco is a high terrace and includes coarse gravels and Ogallala material. Thickness of the Blanco beds ranges from 56 to 74 ft (17 to

23 m) (Evans and Meade, 1944). According to Evans and Meade (1944), the Blanco beds are lacustrine sediments deposited in broad shallow basins during a relatively humid period. However, work by Frye and Leonard (1957) indicated a semiarid climate and fluvial deposition.

## QUATERNARY SYSTEM

### PLEISTOCENE SERIES

*Tule Formation.*--A middle Pleistocene age for the Tule Formation has been determined on the basis of abundant vertebrate fauna and the occurrence of the Pearlette volcanic ash deposits. The Tule Formation consists of well-bedded, gray, unconsolidated sands, nonmarine limestone, bentonite, silts, and locally present coarse gravel. The Tule Formation records deposition during a more humid period of lower average annual temperatures than in Blanco time (Frye and Leonard, 1957). Work by Evans and Meade (1944) suggested that the Tule Formation was deposited within a large basin located in Briscoe and Swisher Counties. An average thickness of 70 or 80 ft (21 or 24 m) was found by Evans and Meade (1944) in Briscoe County. Characteristic of lacustrine deposits, finer sands and silts occur in the Tule Formation in the main areas of deposition, and coarse sands and gravel lie along the margins.

*"Cover Sands".*--The "cover sands" of the Palo Duro Basin area overlap unconformably both the Blanco and Tule Formations and in places directly overlie the Ogallala Formation. Composed of eolian and sheet-wash deposits, the "cover sands" record a climatic change from the Tule conditions to a more arid environment barren of fossils (Frye and Leonard, 1957). The "cover sands" are poorly sorted and reflect a local source; red sands of the "cover sands" may be reworked Triassic and Permian red beds.

*Tahoka Formation.*--The Tahoka Formation represents late Pleistocene of the Palo Duro Basin. The last humid cycle of the Pleistocene is recorded by the Tahoka, which is commonly found in playas in the High Plains. The Tahoka consists of fine- to medium-grained sand and silt, nonmarine limestone, and calcareous and gypsiferous clays (Brand, 1953). The Tahoka contains vertebrate fossils that date the unit as late Pleistocene. Shallow undrained basins or lakes are the depositional environment (Frye and Leonard, 1957), and thickness of the Tahoka ranges from 15 to 80 ft (5 to 24 m) (Jones, 1953).

## HOLOCENE SERIES

During the Holocene Epoch, the semiarid climate of the Palo Duro Basin area has resulted in wind erosion of the Tahoka "cover sands," leading to formation of deflation surfaces, dunes, and playa fills. Stock raising and agriculture have contributed, at least locally, to deflation and dune activity. Also occurring during the Holocene were gully erosion and sheet-wash, which resulted in alluvial deposits of ephemeral streams and terraces along river channels.

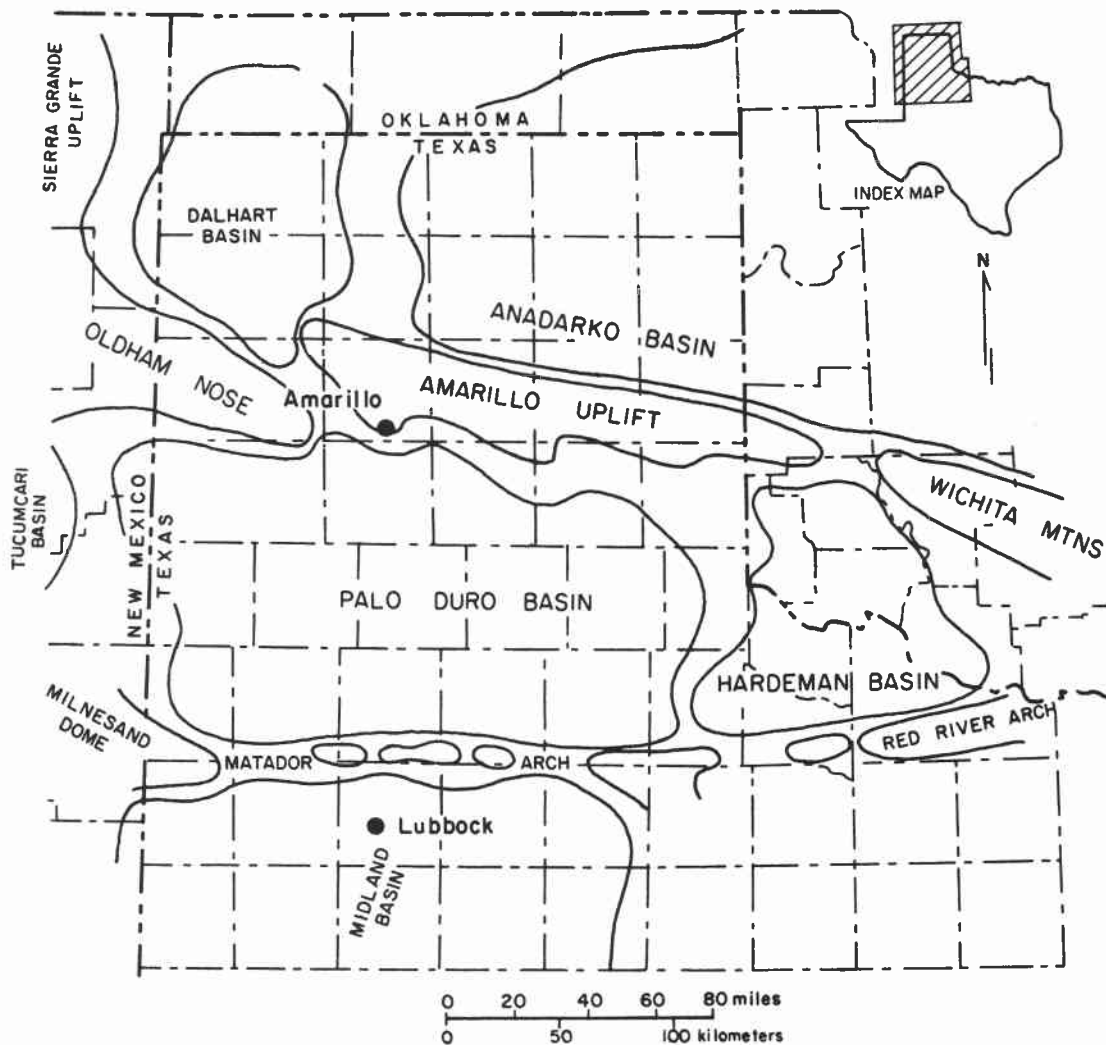


Figure 25. Structural elements of the Texas Panhandle and location of study area (after Nicholson, 1960).

| SYSTEM        | SERIES      | GROUP       | Palo Duro Basin                                     | Dalhart Basin  | General Lithology and depositional setting                             |  |
|---------------|-------------|-------------|---|--|--|--|
|               |             |             | FORMATION   | FORMATION  |  |  |
| QUATERNARY    | HOLOCENE    |             | alluvium, dune sand Playa                           | alluvium, dune sand Playa  |  |  |
|               | PLEISTOCENE |             | Tahoka<br>"cover sands"<br>Tule / "Playa"<br>Blanco | "cover sands"<br>"Playa"   | Lacustrine clastics and windblown deposits                             |  |
| TERTIARY      | NEOGENE     |             | Ogallala  | Ogallala   | Fluvial and lacustrine clastics  |  |
| CRETACEOUS    |             |             | undifferentiated                                    | undifferentiated   | Marine shales and limestone  |  |
| TRIASSIC      |             | DOCKUM      |   |  | Fluvial-deltaic and lacustrine clastics                                |  |
| PERMIAN       | OCHOA       |             | Dewey Lake  | Dewey Lake   | Sabkha salt, anhydrite, red beds, and peritidal dolomite               |  |
|               |             |             | Alibates  | Alibates  |  |  |
|               | GUADALUPE   | ARTESIA     |   | Salado/Tansill   |  | Artesia Group undifferentiated         |
|               |             |             |   | Yates  |  |  |
|               |             |             |   | Seven Rivers   |  |  |
|               |             |             |   | Queen/Grayburg   |  |  |
|               |             |             |   | San Andres   |  |  |
|               | LEONARD     | CLEAR FORK  |   | Glorieta   |  | Glorieta                               |
|               |             |             |   | Upper Clear Fork   |  | Clear Fork                             |
|               |             |             |   | Tubb   |  | undifferentiated Tubb-Wichita Red Beds |
|               |             |             |   | Lower Clear Fork   |  |  |
|               |             |             |   | Red Cave   |  |  |
|               |             | WICHITA     |   |  |  |  |
|               |             | WOLFCAMP    |   |  |  |  |
| PENNSYLVANIAN |             |             | ?   | ?  | Shelf and shelf-margin carbonate, basinal shale, and deltaic sandstone |  |
|               | VIRGIL      | CISCO       |   |  |  |  |
|               | MISSOURI    | CANYON      |   |  |  |  |
|               | DES MOINES  | STRAWN      |   |  |  |  |
|               | ATOKA       | BEND        |   |  |  |  |
| MORROW        |             |             |   |  |  |  |
| MISSISSIPPIAN | CHESTER     |             |   |  | Shelf carbonate and chert  |  |
|               | MERAMEC     |             |   |  |  |  |
|               | OSAGE       |             |   |  |  |  |
| ORDOVICIAN    |             | ELLENBURGER |   |  | Shelf dolomite   |  |
| CAMBRIAN ?    |             |             |   |  | Shallow marine (?) sandstone   |  |
| PRECAMBRIAN   |             |             |   |  | Igneous and metamorphic  |  |

Figure 26. Stratigraphic column and general lithology of the Palo Duro and Dalhart Basins. After Handford and Dutton (1980).

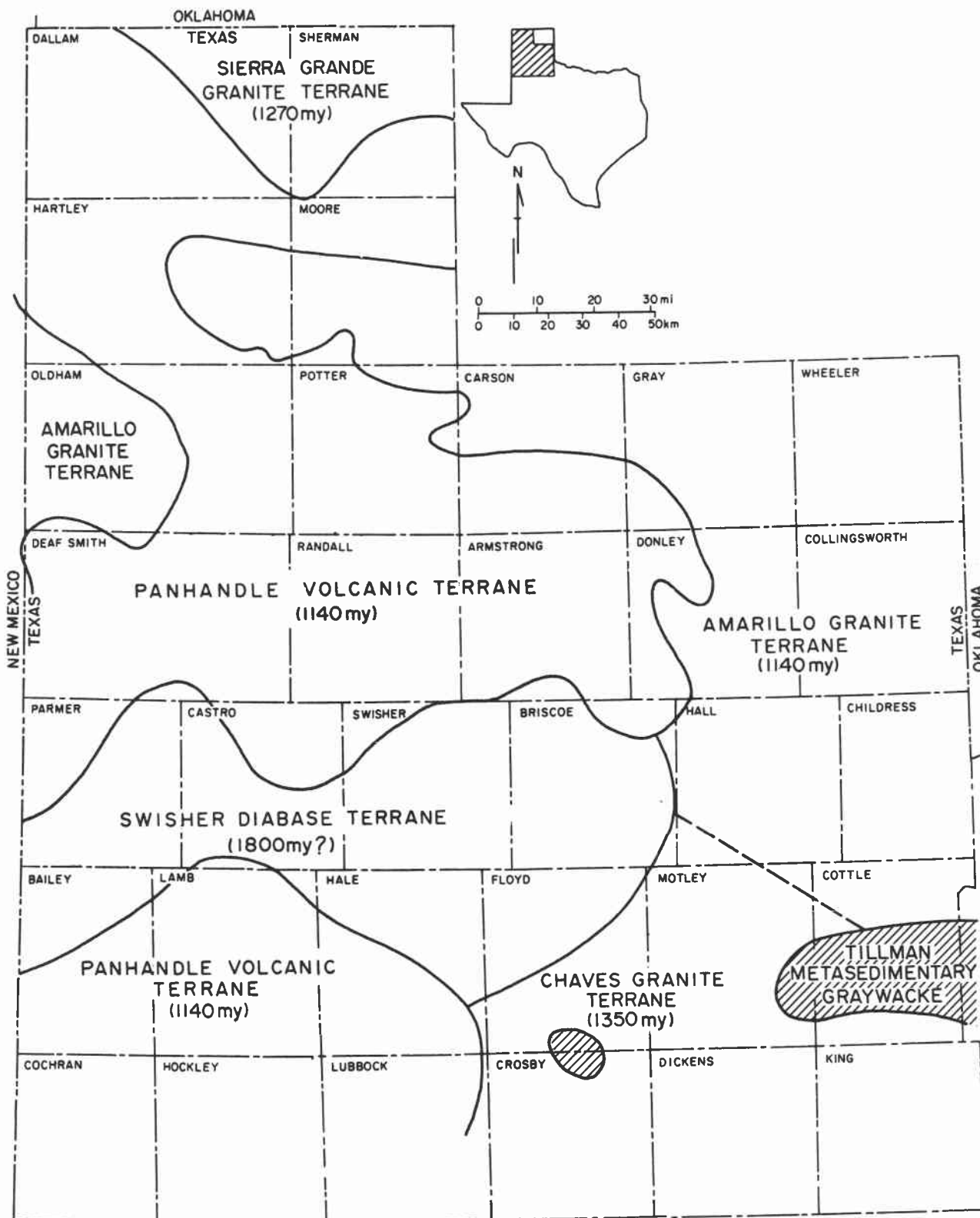


Figure 27. Precambrian basement terranes (Muehlberger and others, 1967).

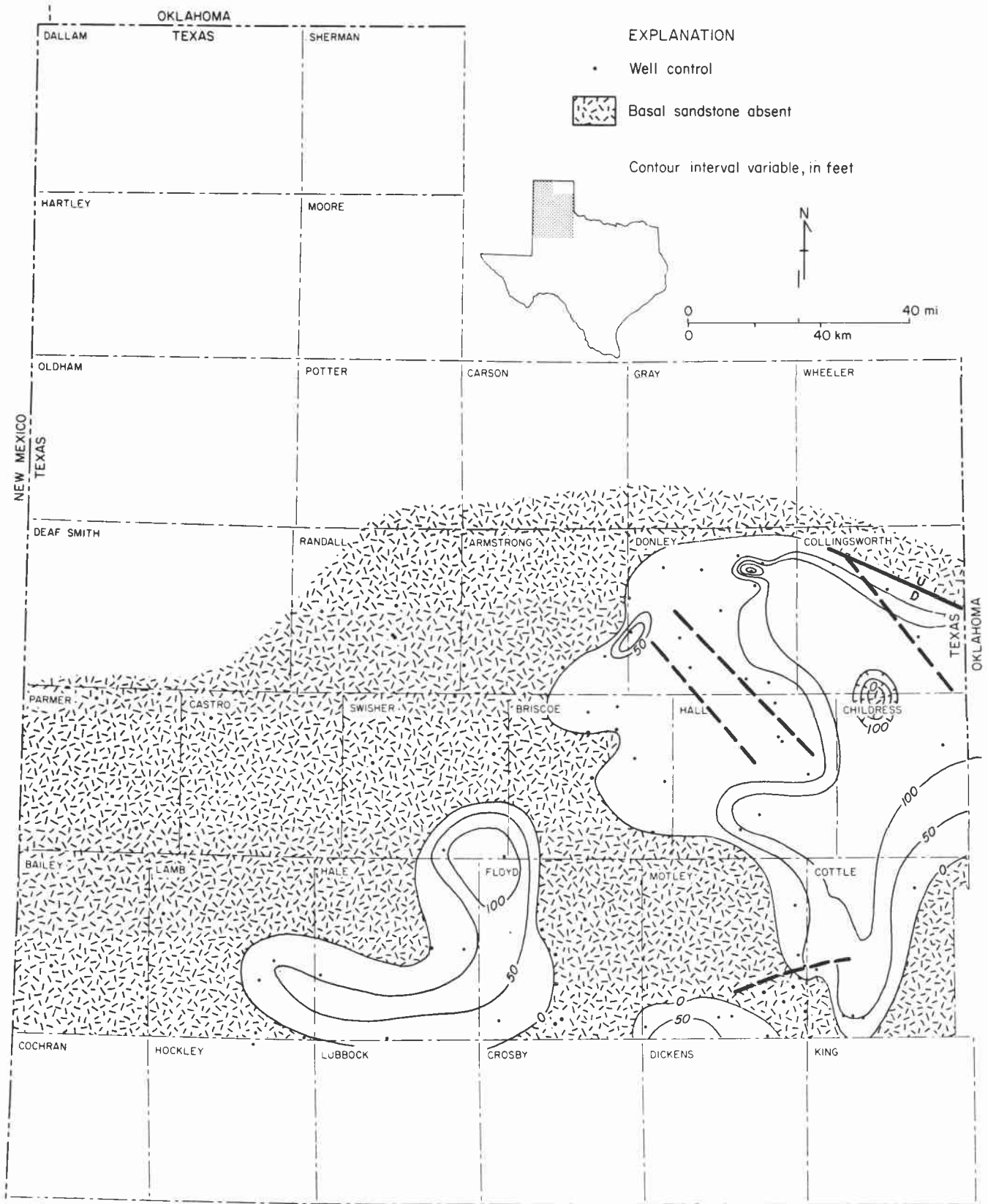


Figure 28. Isopach map of Cambrian (?) sandstone directly overlying Precambrian basement. After Dutton (1980).

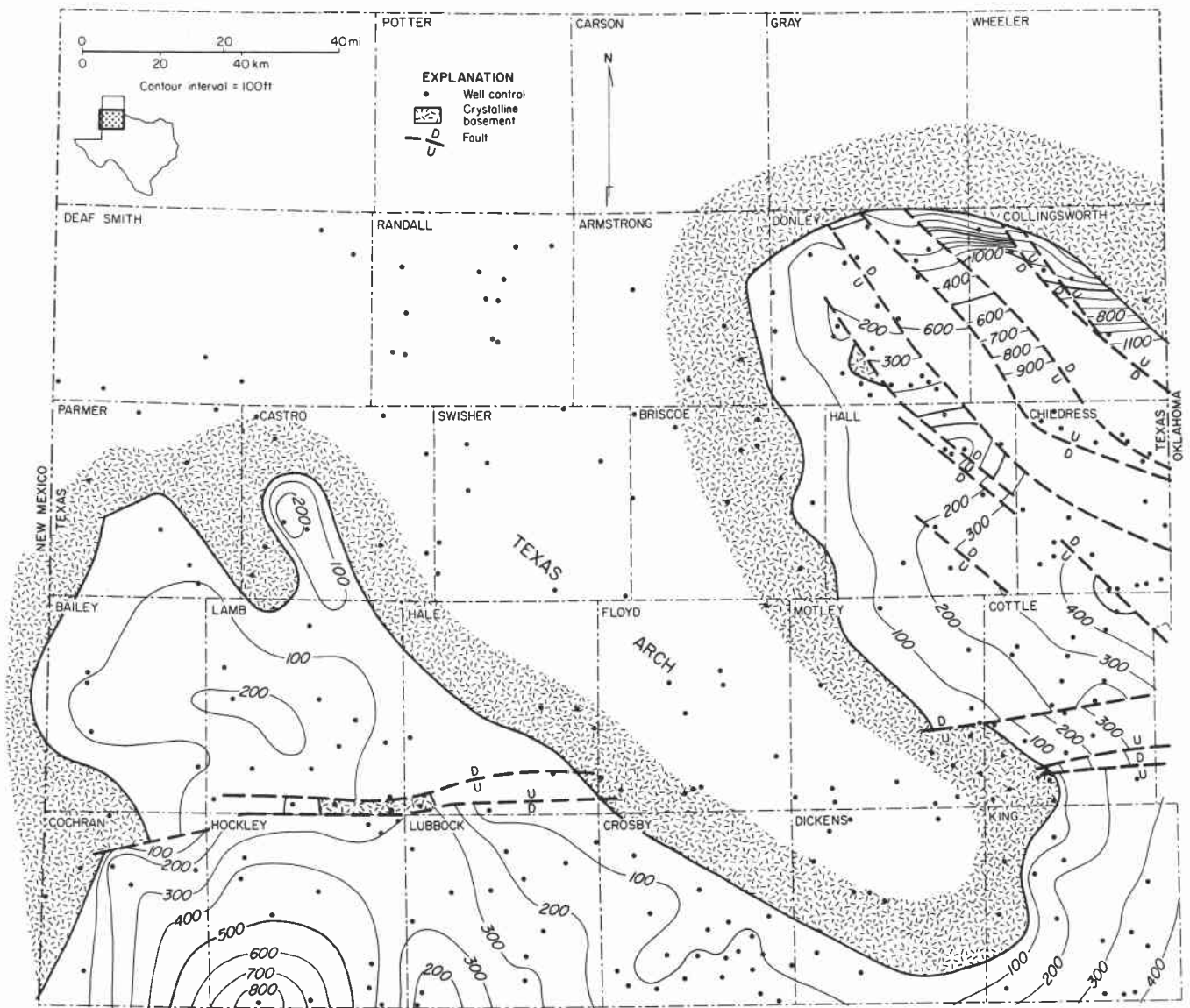


Figure 29. Isopach map of Lower Ordovician Ellenburger Group. After Dutton and others (1982).

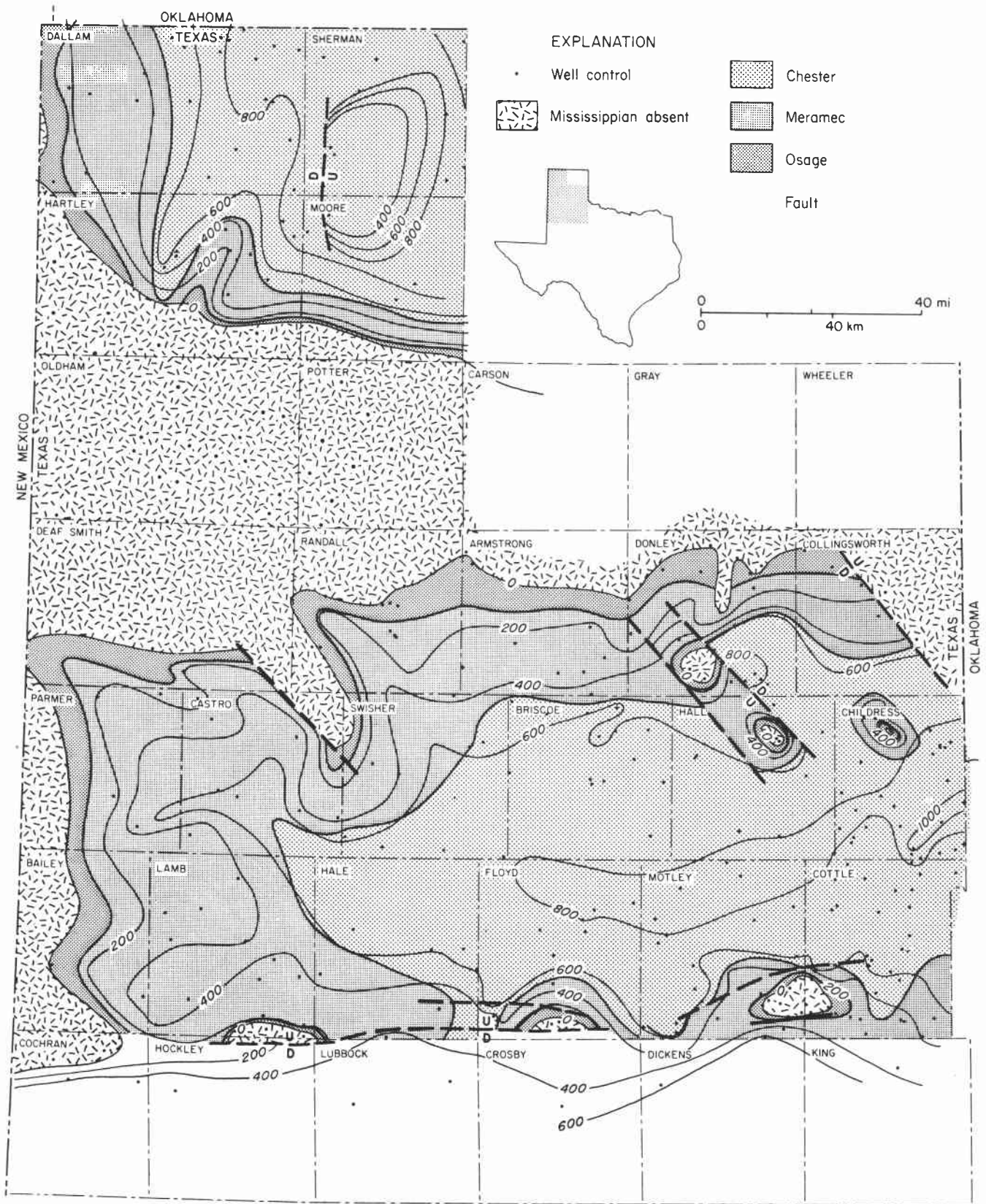


Figure 30. Isopach and series distribution map of Mississippian System. After Dutton (1980) and Nicholson (1960).

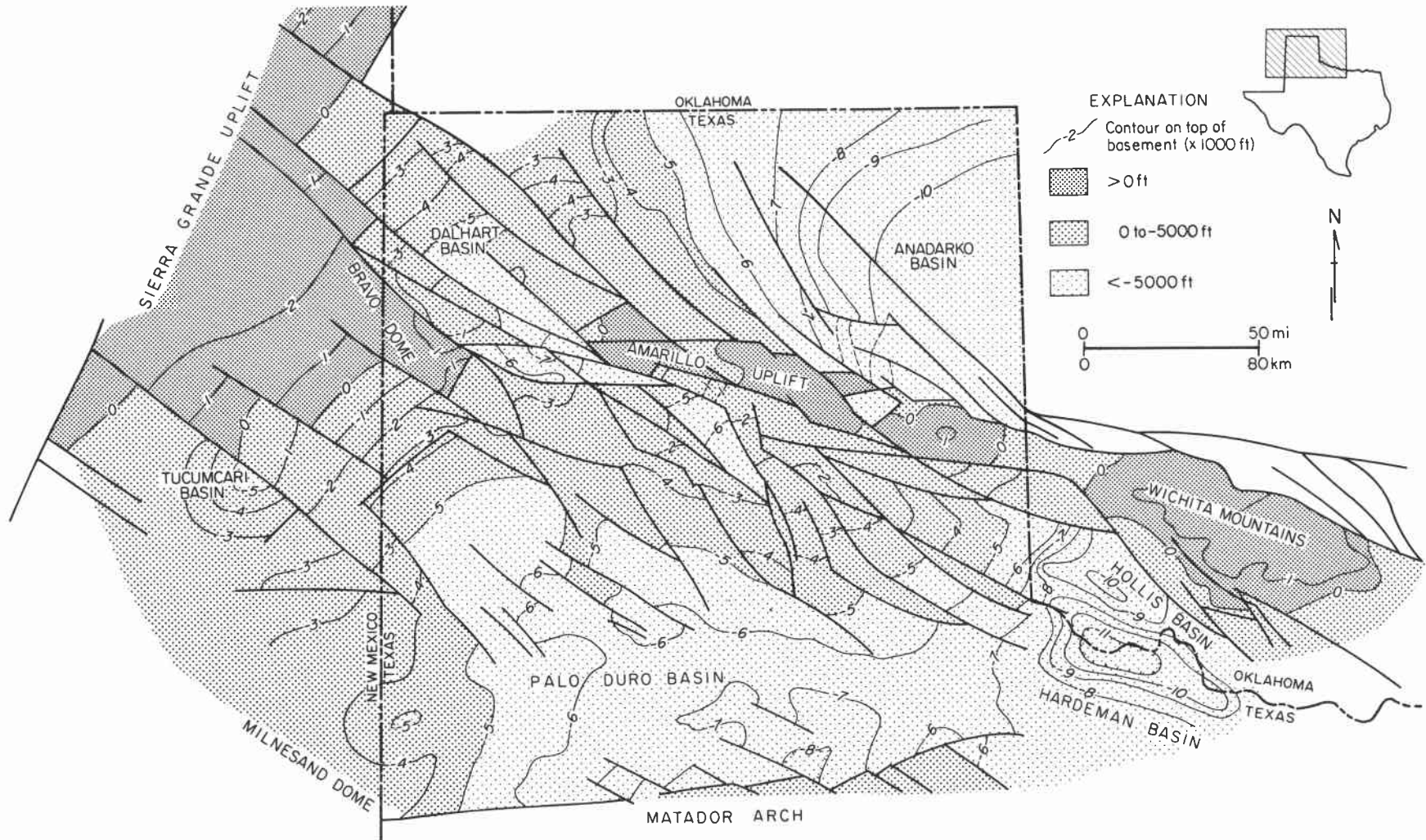


Figure 31. Structure-contour map on the top of Precambrian basement.

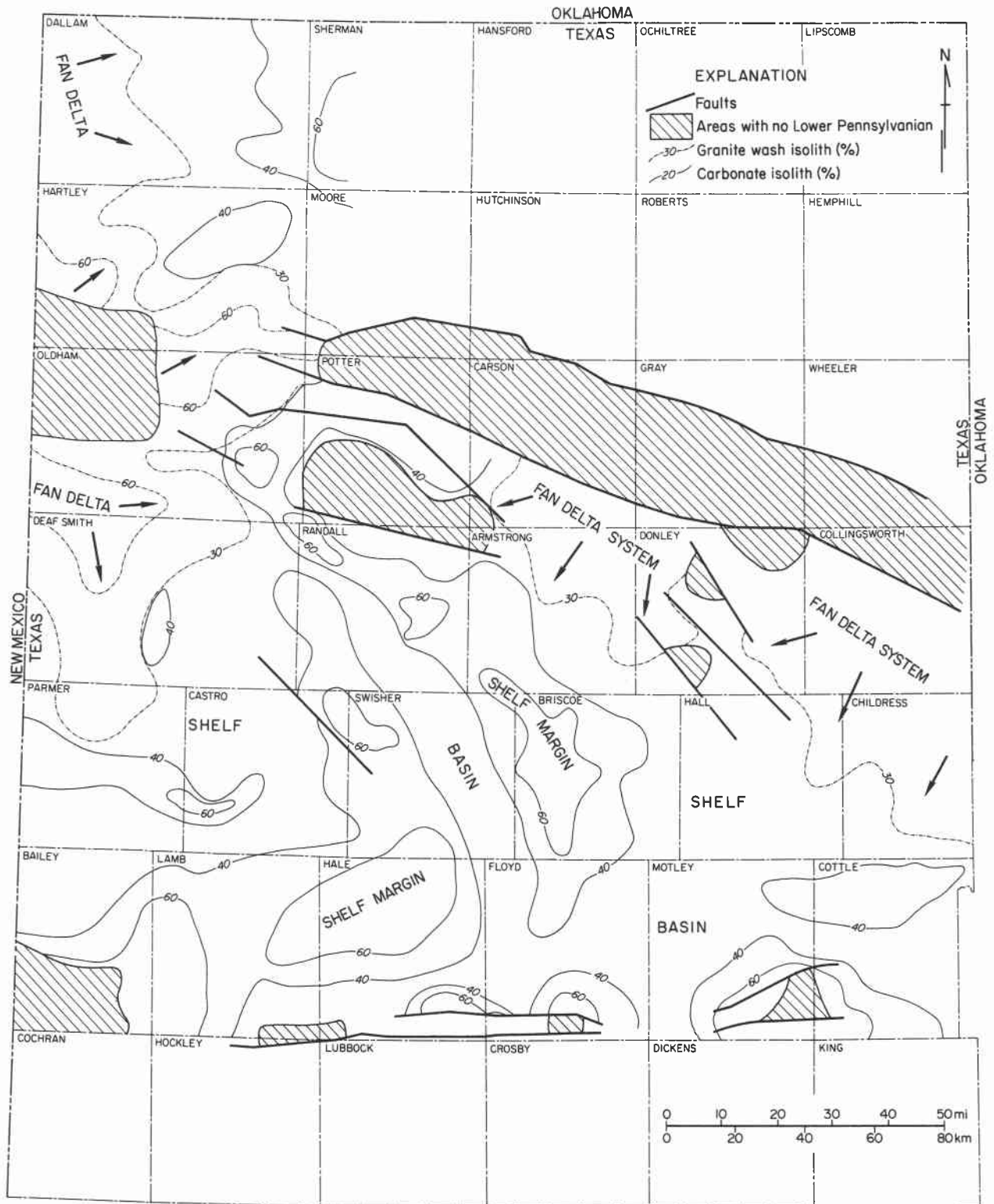


Figure 32. Facies distribution map of Lower Pennsylvanian System. After Dutton (1980 and unpublished data).

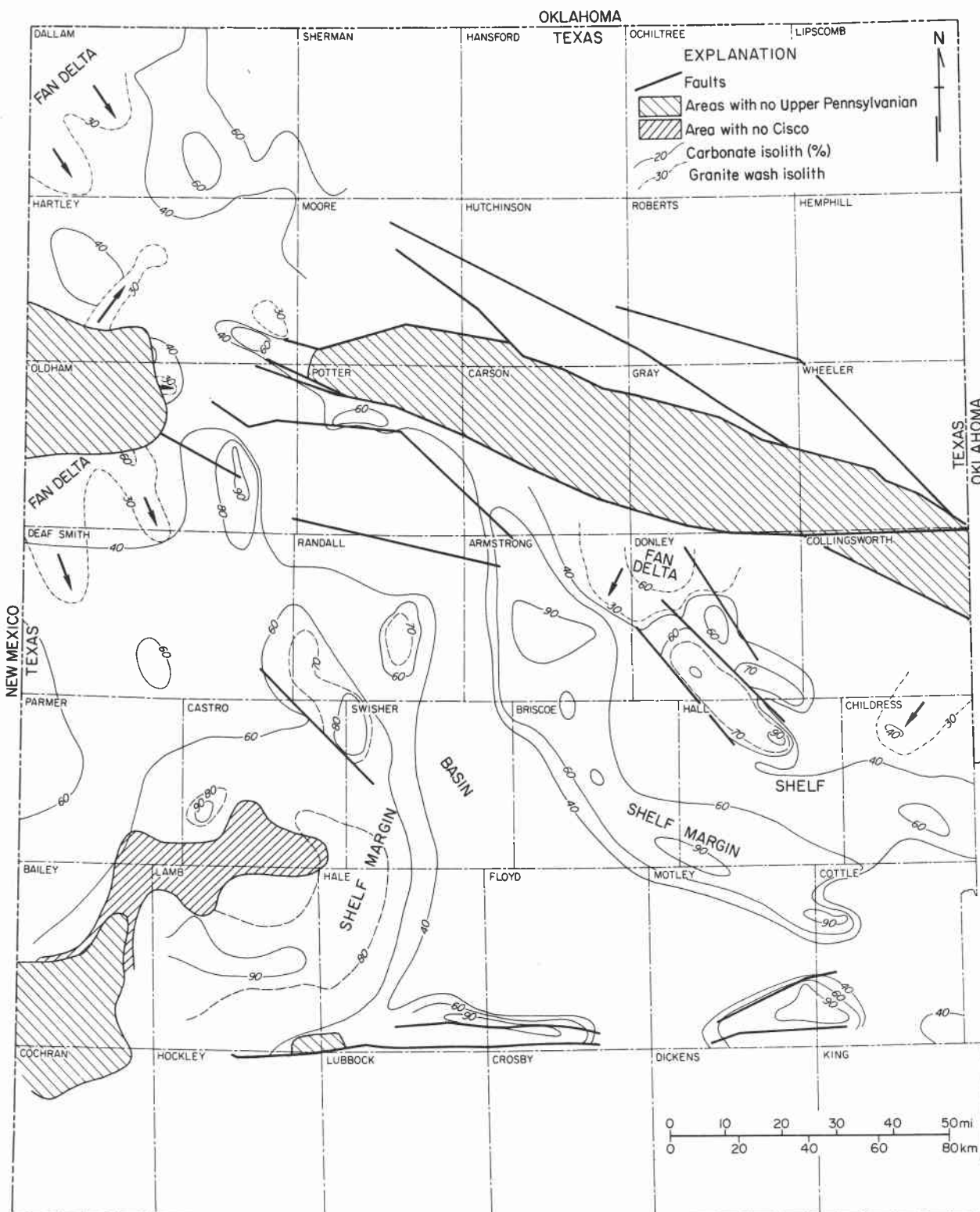
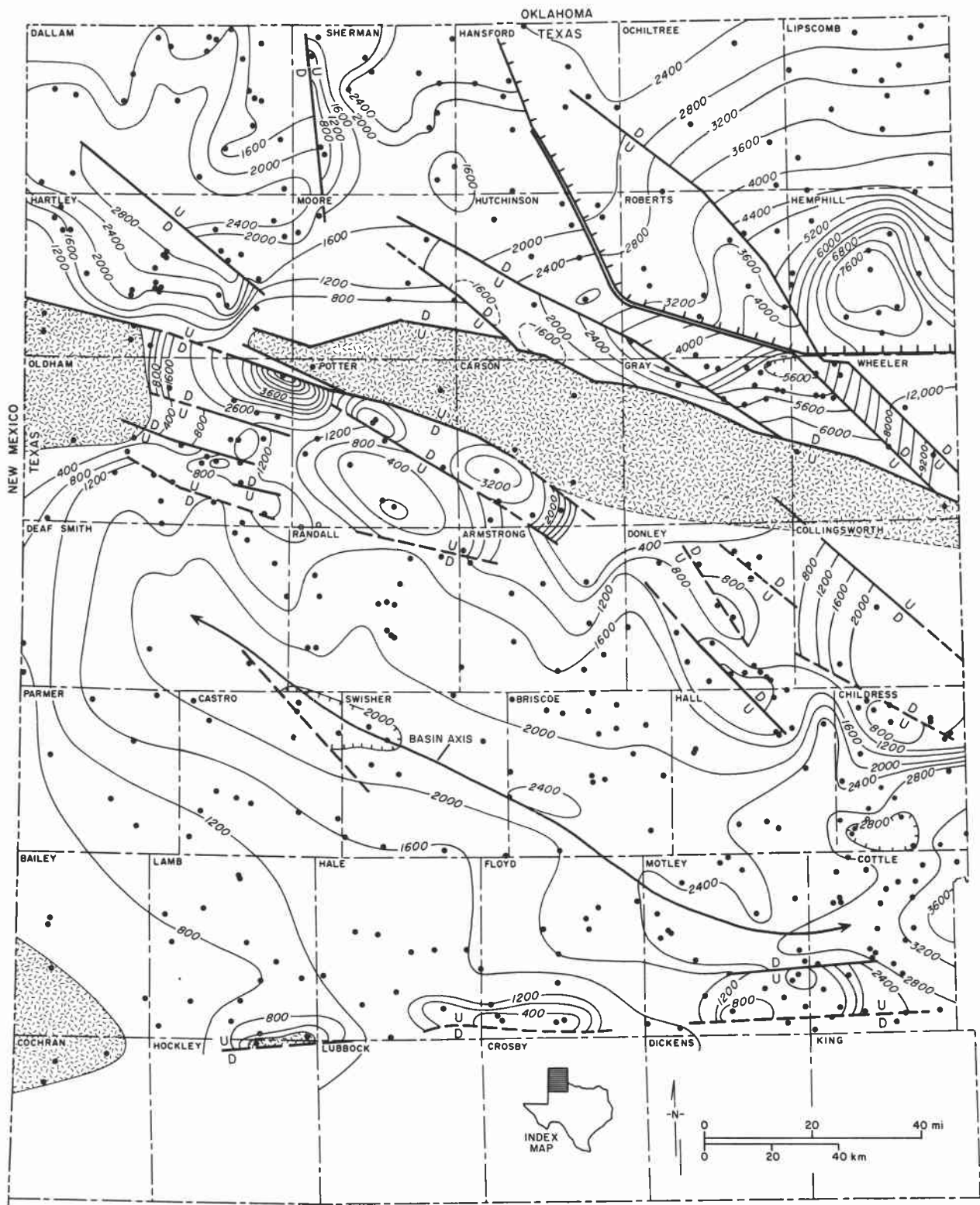


Figure 33. Facies distribution map of Upper Pennsylvanian System. After Dutton (1980).



- EXPLANATION**
- |  |   |  |
|--|---|--|
| <ul style="list-style-type: none"> <li> Precambrian basement exposed throughout Pennsylvanian</li> <li> Faults</li> <li> Well control</li> </ul> | <ul style="list-style-type: none"> <li>Contour interval = 400 ft</li> <li> Axis of basin</li> </ul> | <ul style="list-style-type: none"> <li>Area northeast of hachured line shows thickness from top of Mississippian to top of Missourian Series.</li> </ul> |
|--|---|--|

Figure 34. Isopach map of Pennsylvanian System. After Dutton and others (1982).

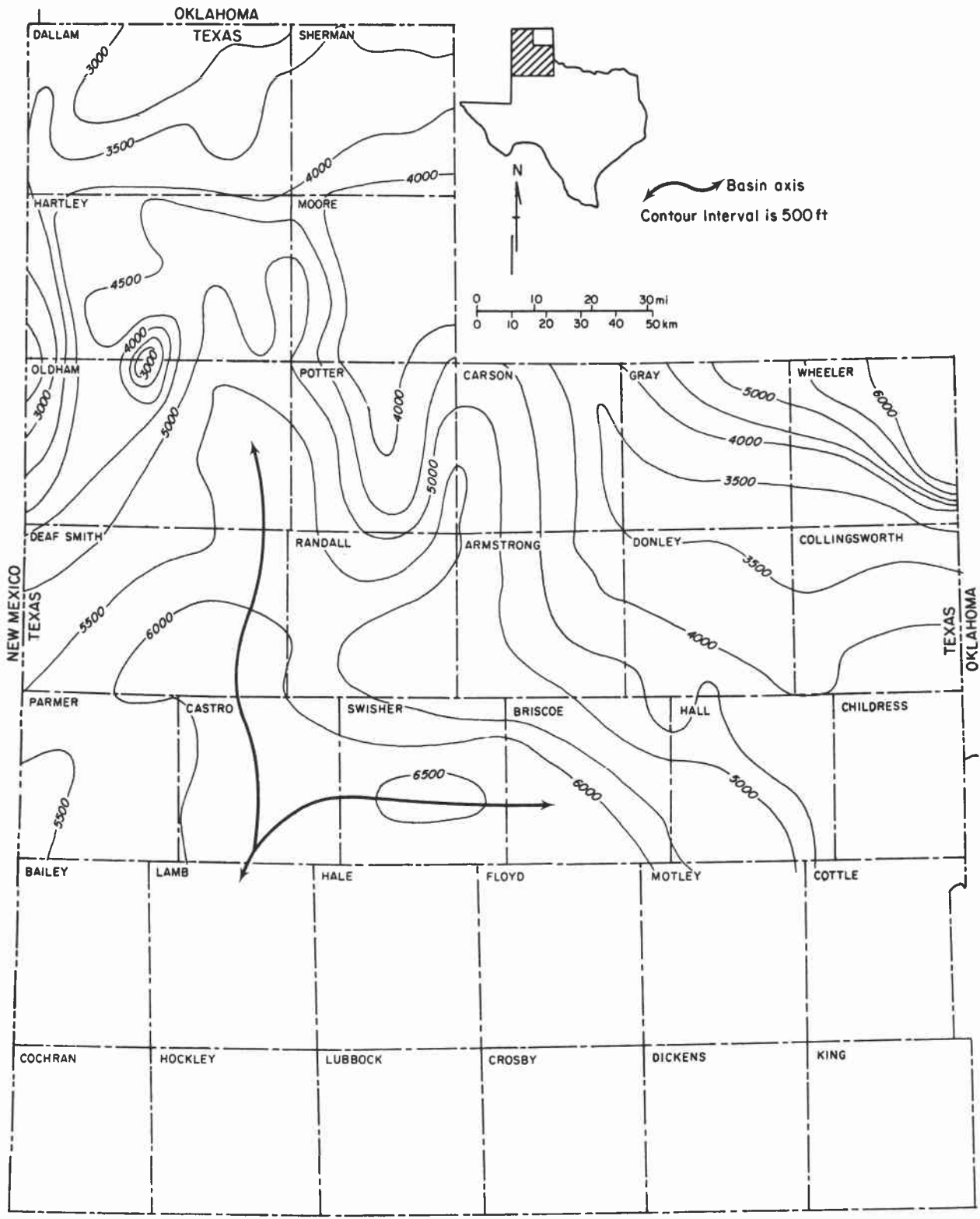


Figure 35. Isopach map of Permian System. From McKee and Oriel (1967).

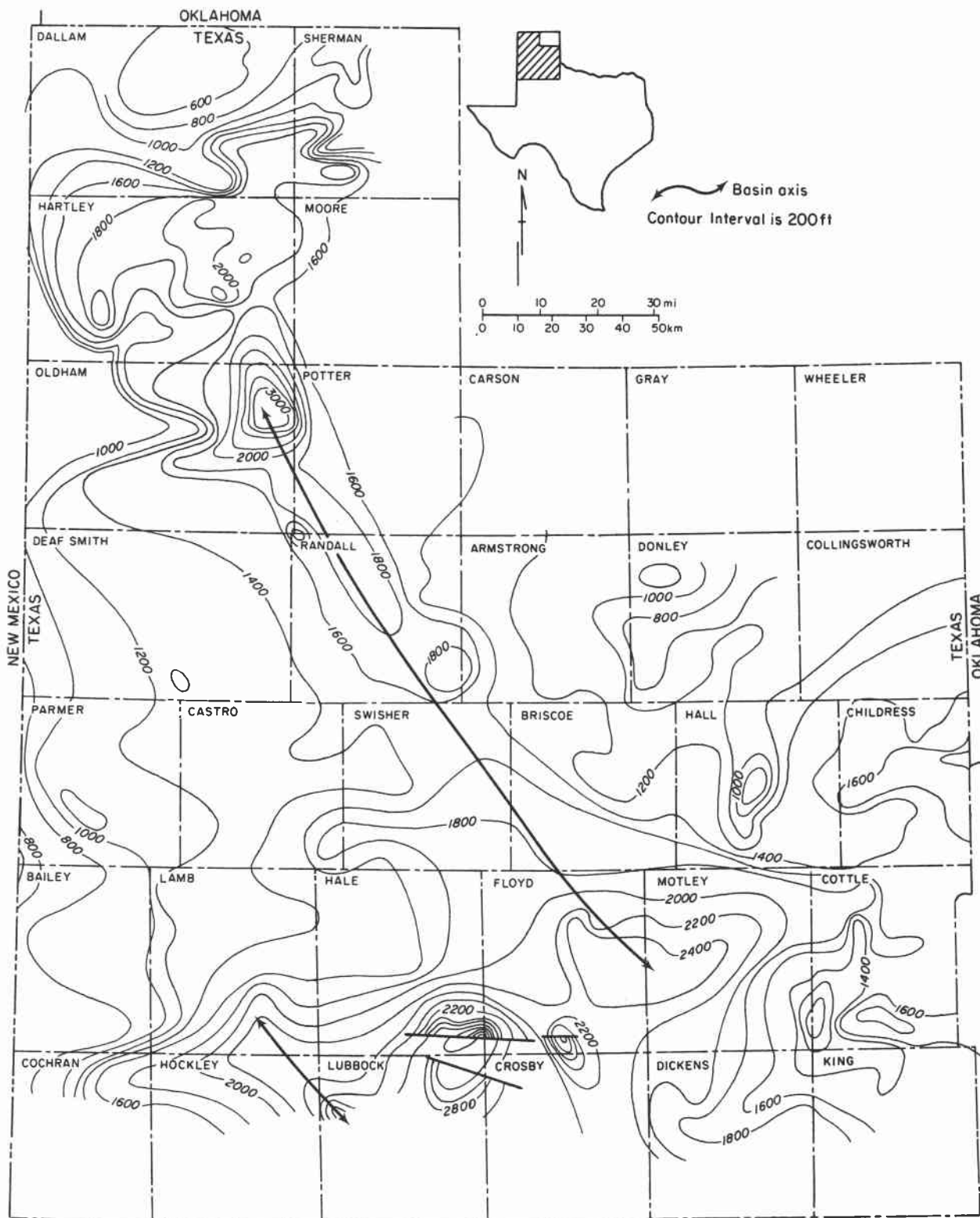


Figure 36. Isopach map of Wolfcamp Series.

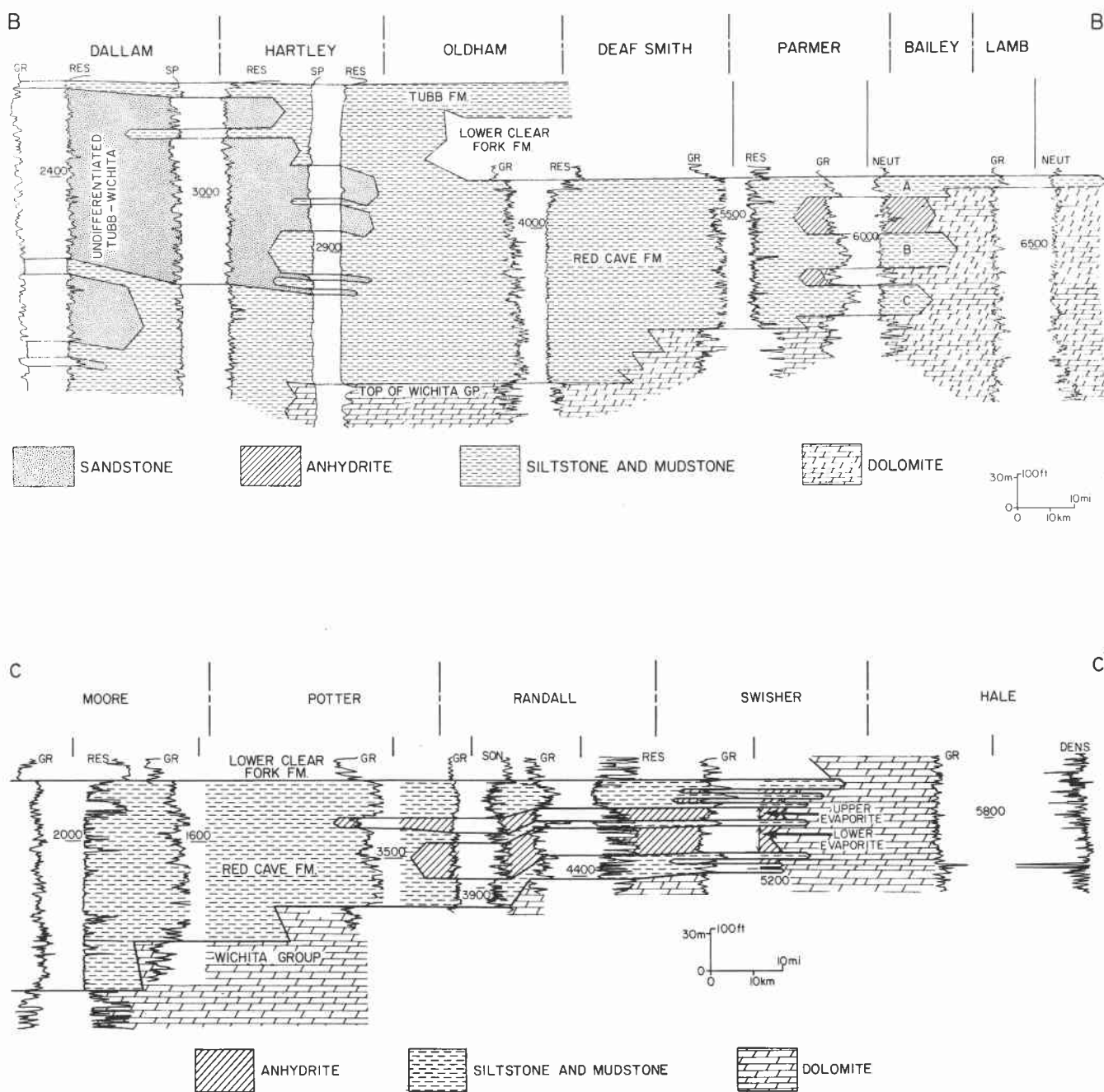


Figure 37. North-south cross sections B-B' and C-C' through the Red Cave Formation. From Handford and Fredericks (1980). See figure 54 for locations.

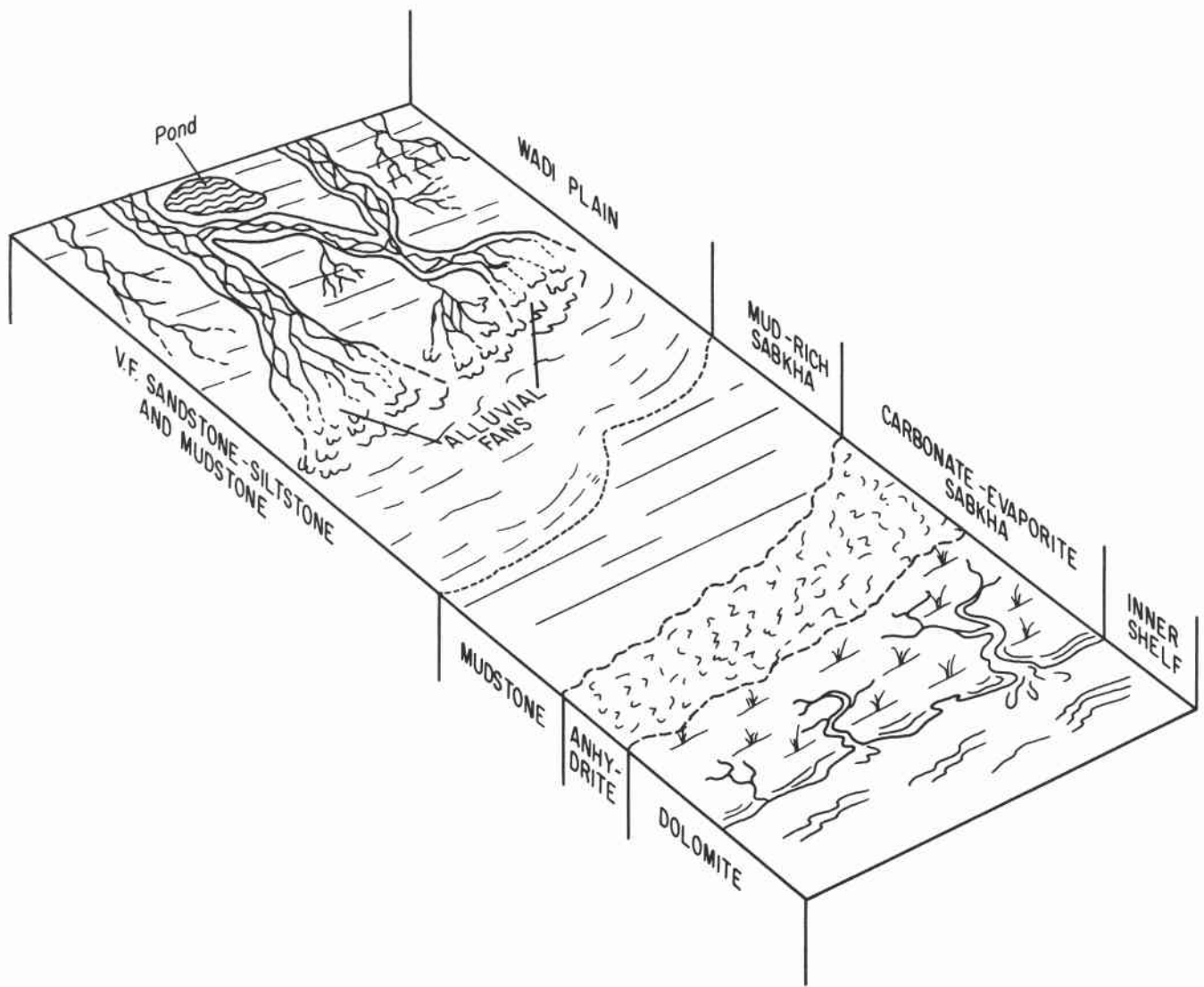


Figure 38. Composite depositional model for Red Cave carbonate, evaporite, and clastic facies (from Handford and Fredericks, 1980).

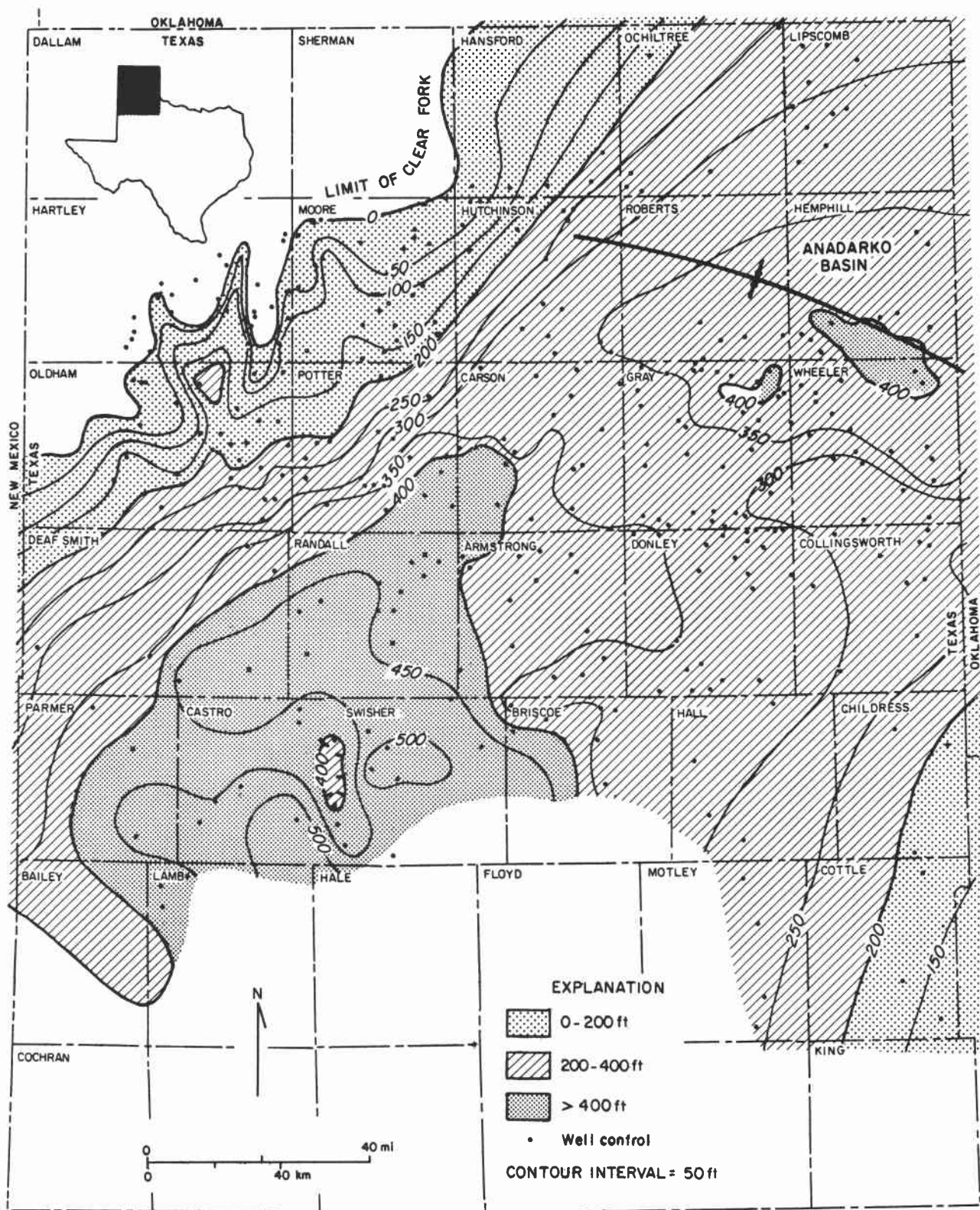


Figure 39. Isopach map, lower Clear Fork Formation, Texas Panhandle.

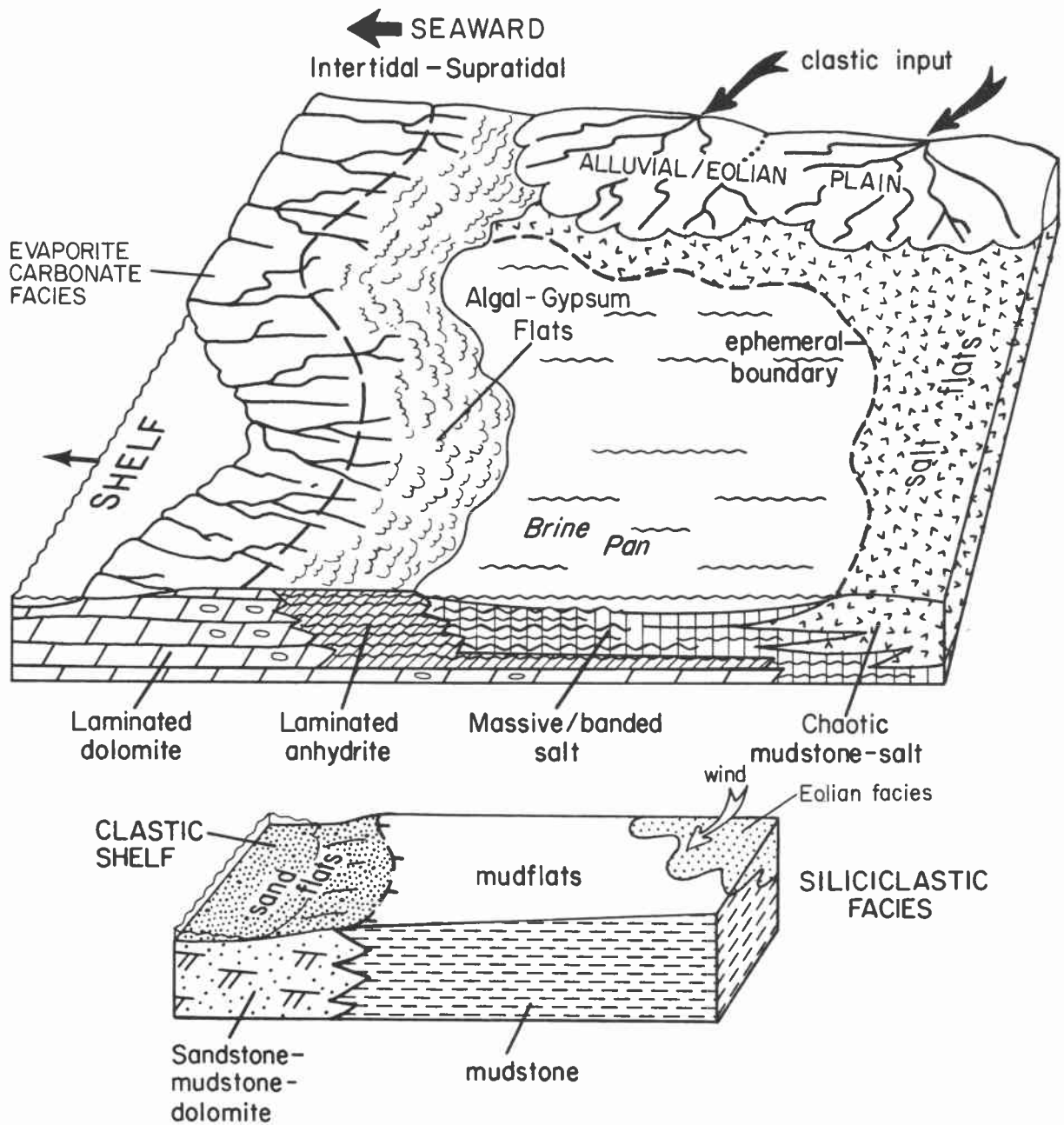


Figure 40. Facies and environments recorded in Tubb strata of the Palo Duro and Dalhart Basins. Evaporite-carbonate facies record a gradual basinward shift in environments. Siliciclastic (red-bed) facies dominate the Tubb sequence, and were deposited in tidal mud flats, which graded basinward into tidal sand flats. From Presley (1980b).

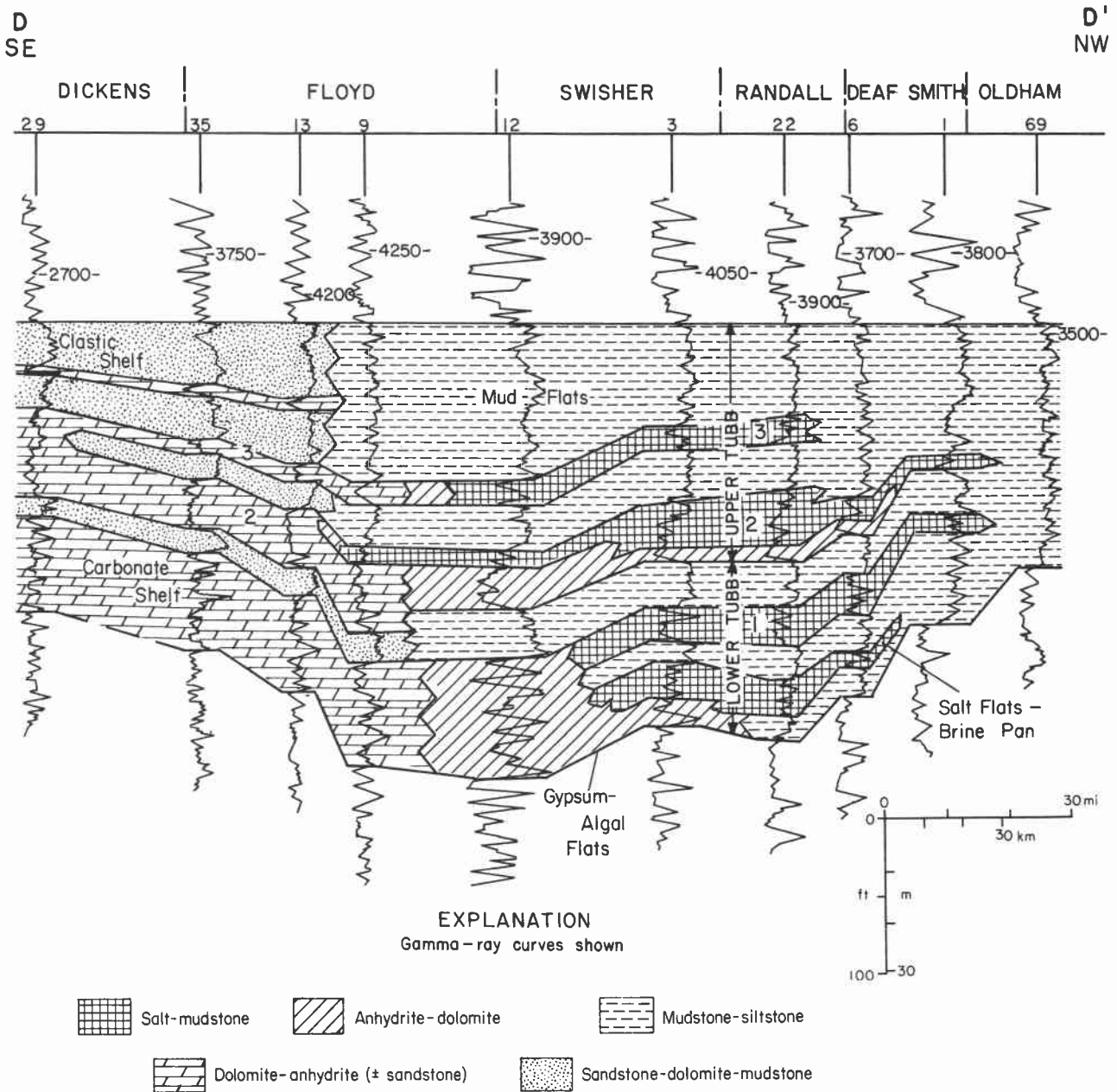


Figure 41. Northwest-southeast cross section, Tubb Formation, Palo Duro Basin. Line of cross section is indicated in figure 87. From Presley (1980b).

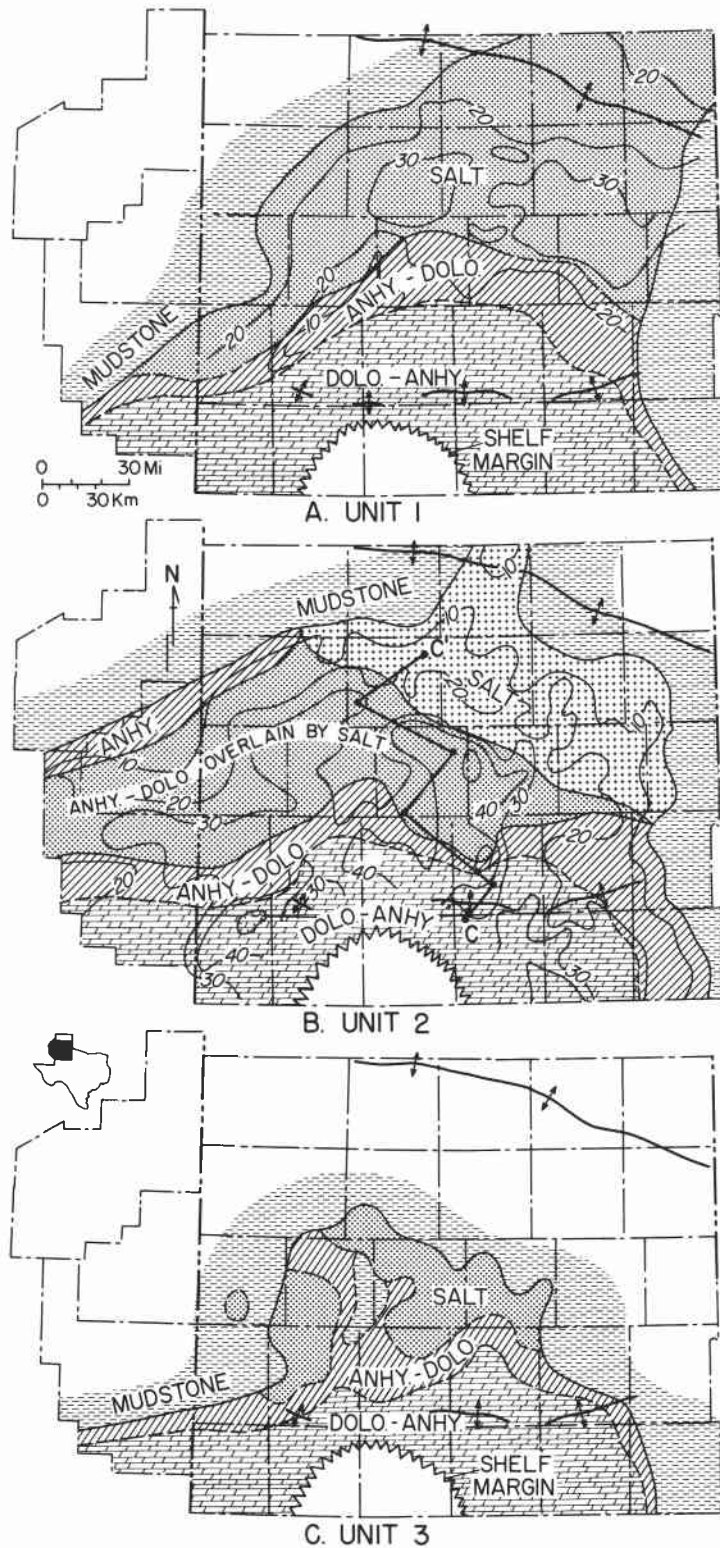


Figure 42. Facies maps of evaporite-carbonate units 1, 2, and 3 (oldest to youngest) of the Tubb Formation. Salt is dominant in updip regions to the north; carbonate is dominant to the south. These units show progressive southerly migration of evaporite-carbonate facies. From Presley (1980b).

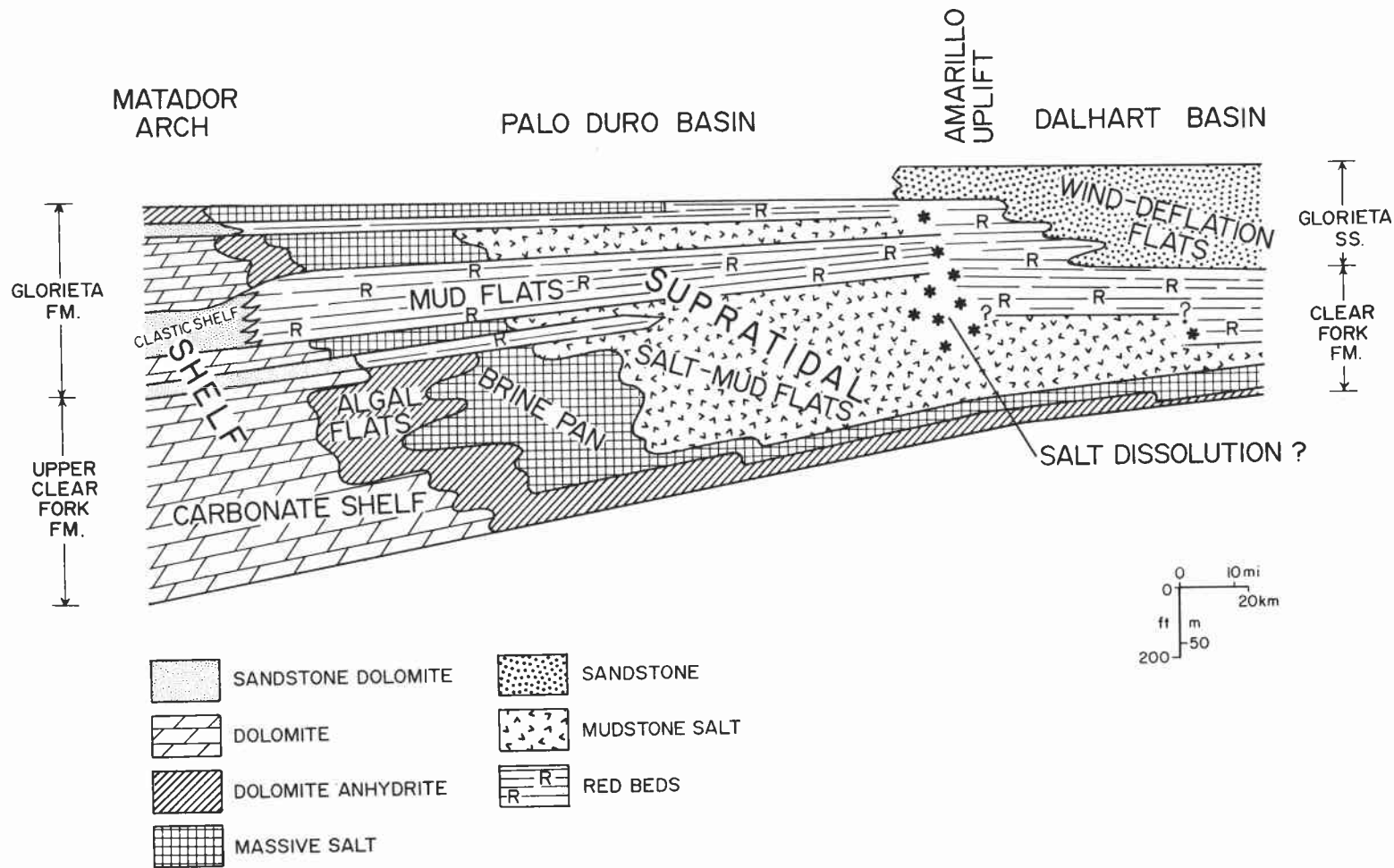


Figure 43. North-south facies cross section through Palo Duro and Dalhart Basins showing relation of environments for the upper Clear Fork and Glorieta Formations. From Presley (unpublished data).

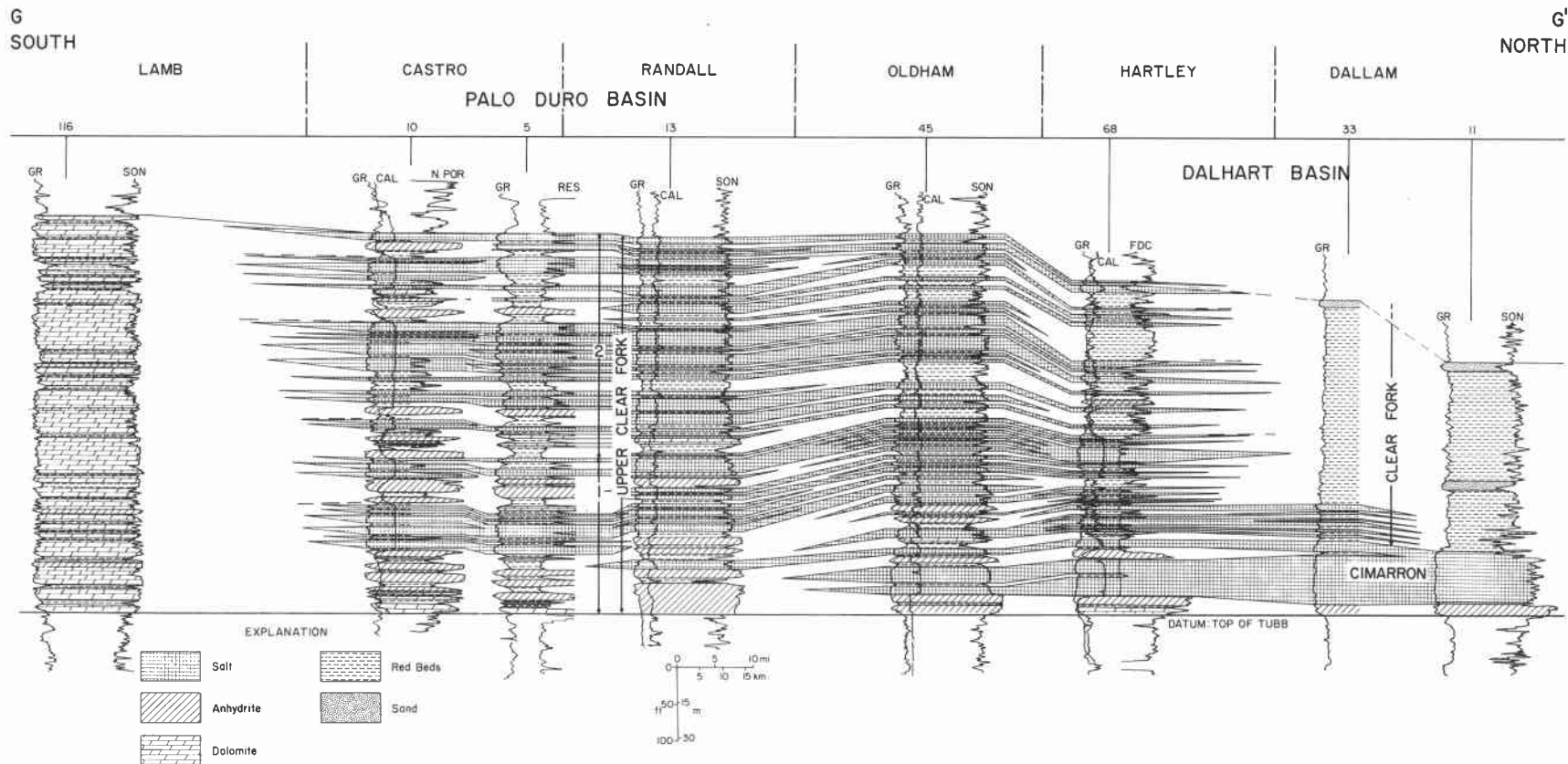


Figure 44. Regional north-south cross section G-G' of upper Clear Fork Formation showing generalized lithologic interpretations. See figure 45 for location. From Presley and McGillis (1981a).

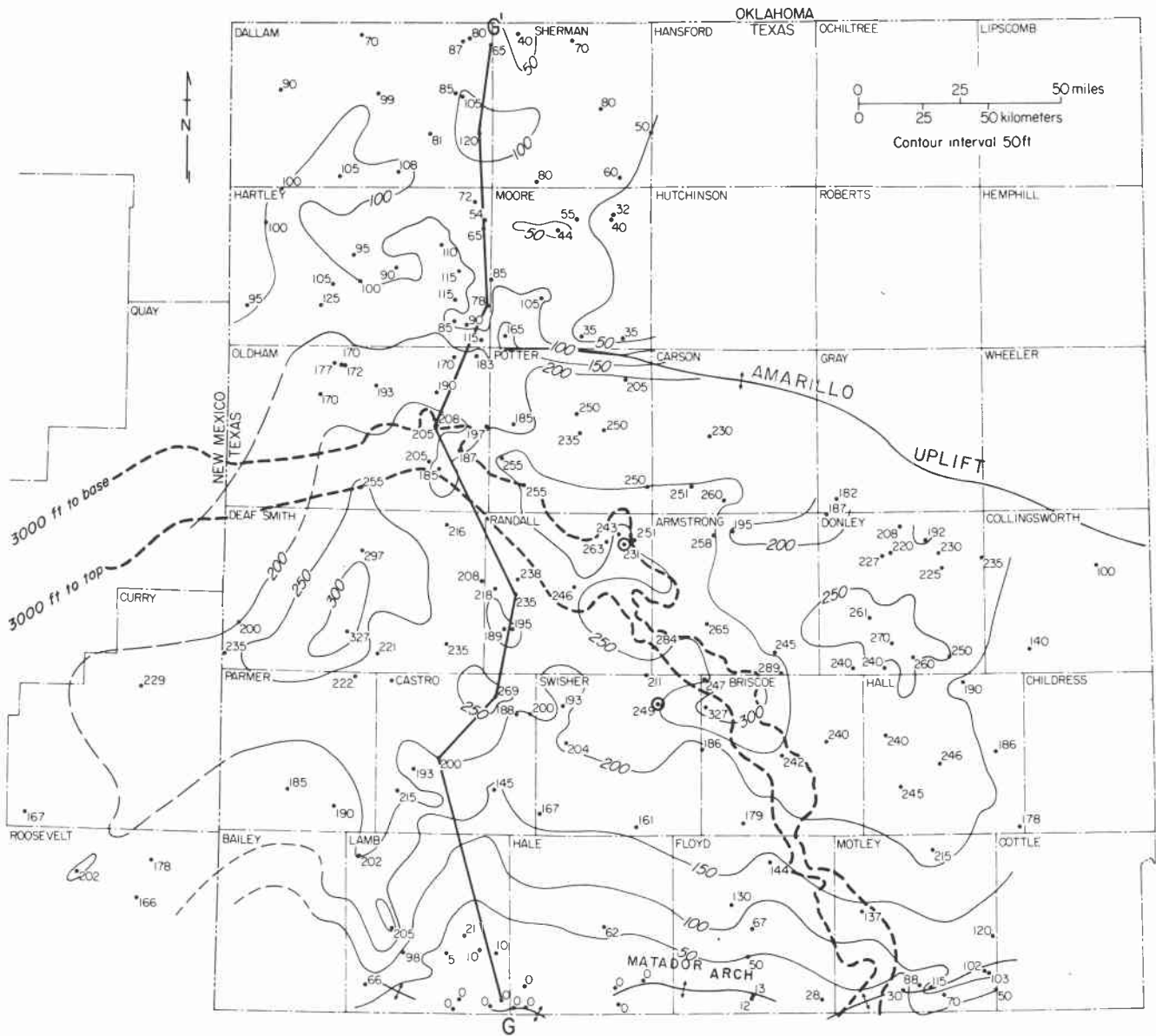


Figure 45. Net-salt map of upper Clear Fork Formation. From Presley and McGillis (1981a).

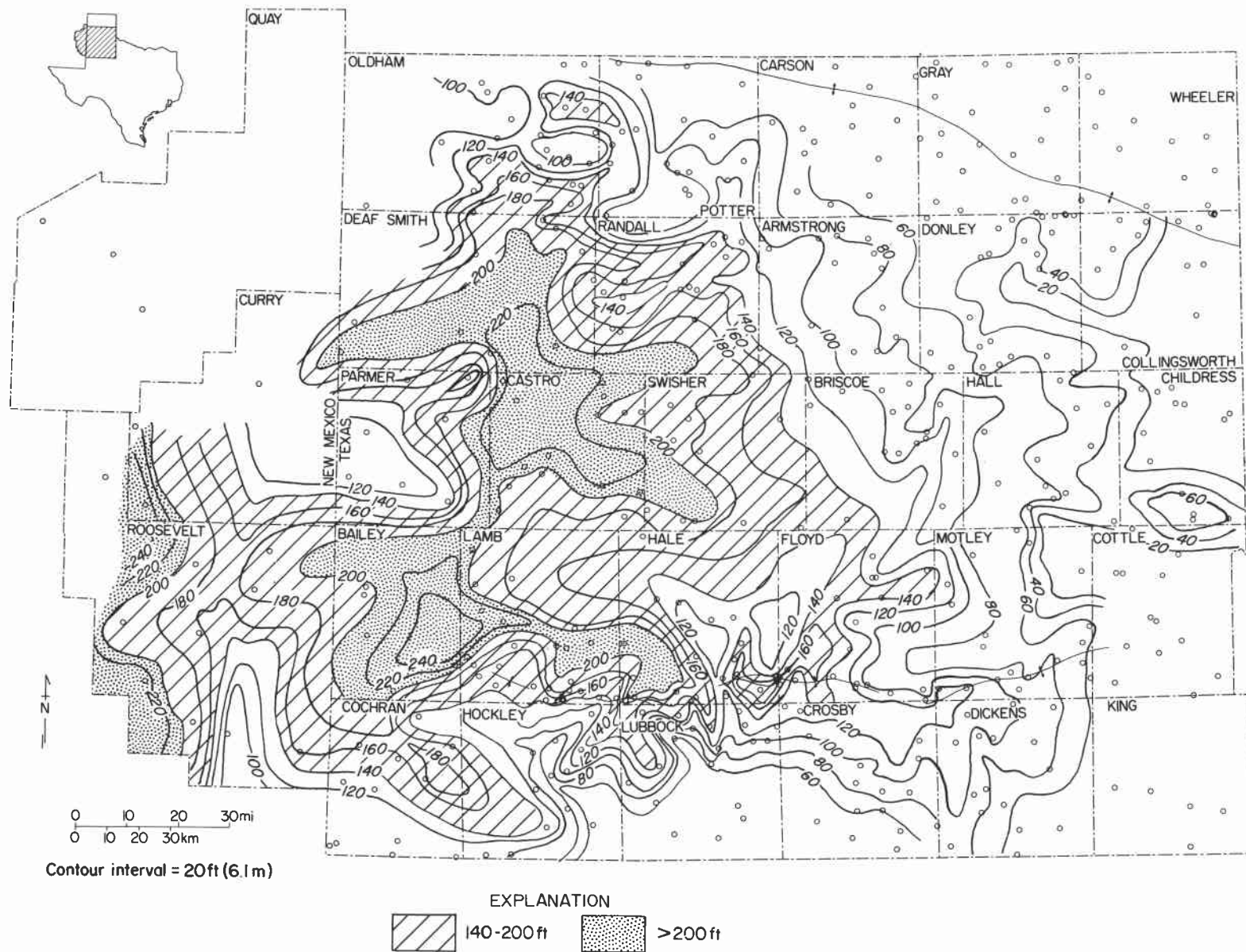


Figure 46. Isopach map of net clastics, Glorieta Formation, Palo Duro Basin and east-central New Mexico (Presley, unpublished data).

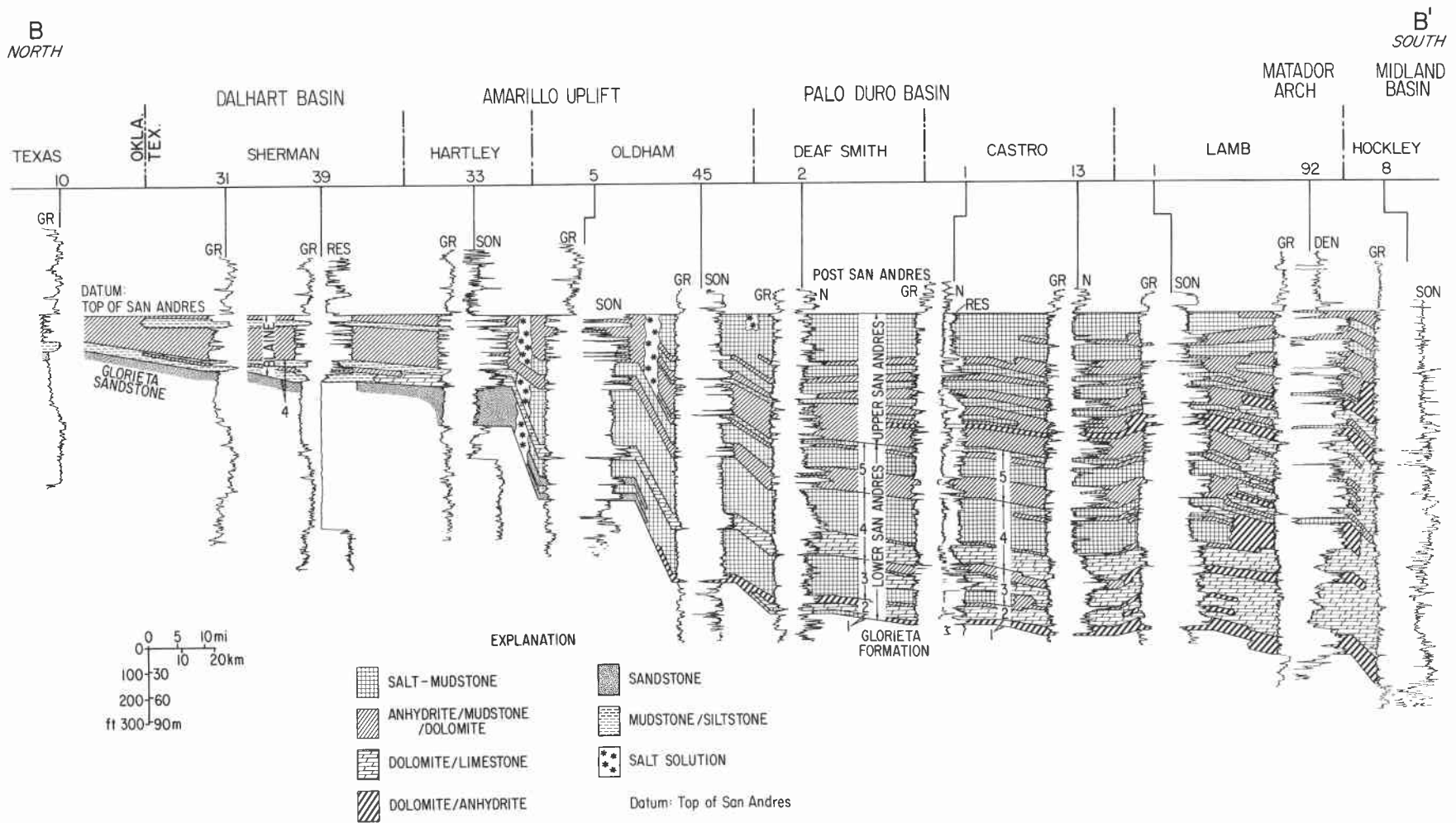


Figure 47. Regional north-south cross section B-B' of the San Andres Formation showing interpretation of lithic composition. Location is shown in figure 48. From Presley (1981c).

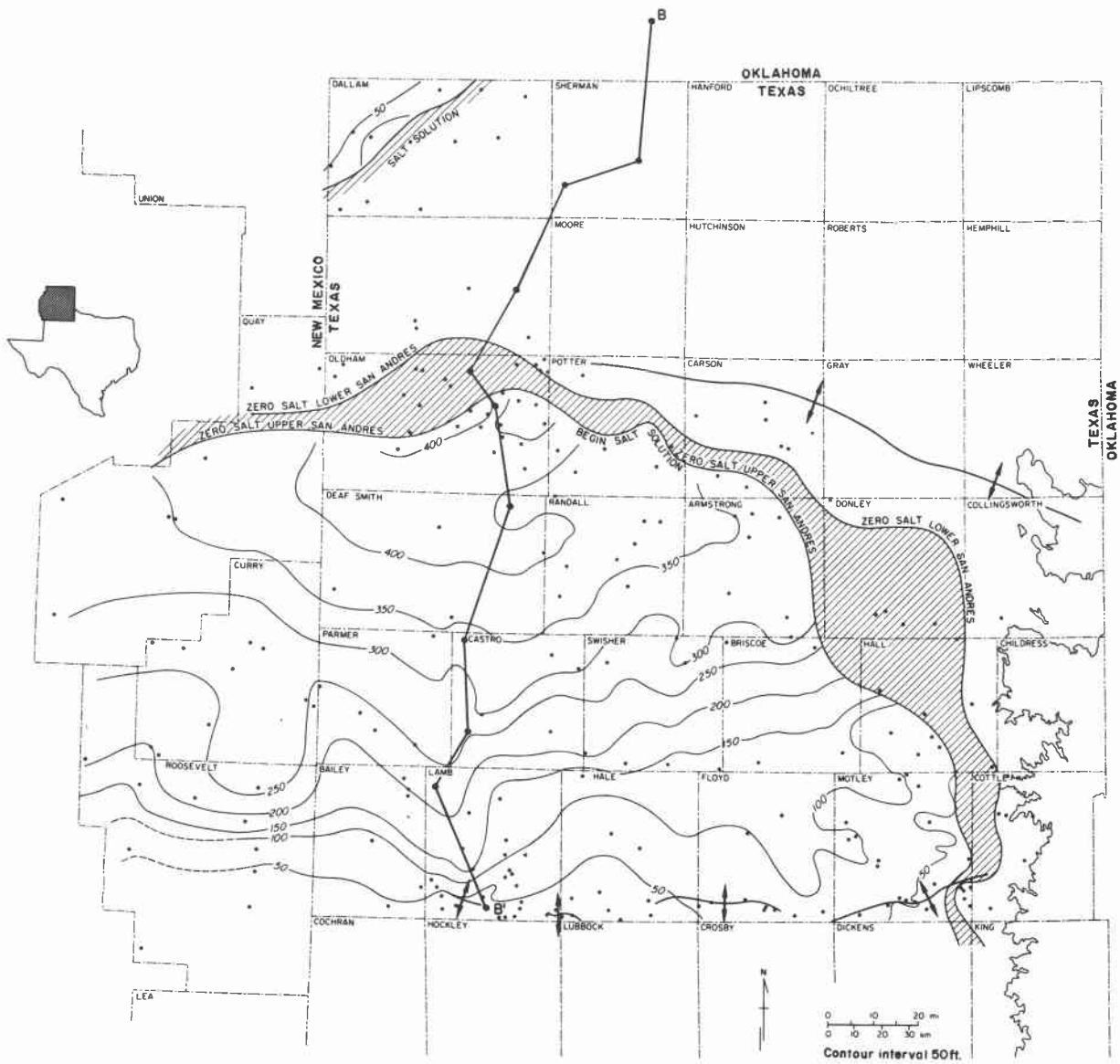


Figure 48. Net-salt map, lower part of the San Andres Formation. Patterned region is the zone of subsurface dissolution of salt by ground-water processes. From Presley (1981c).

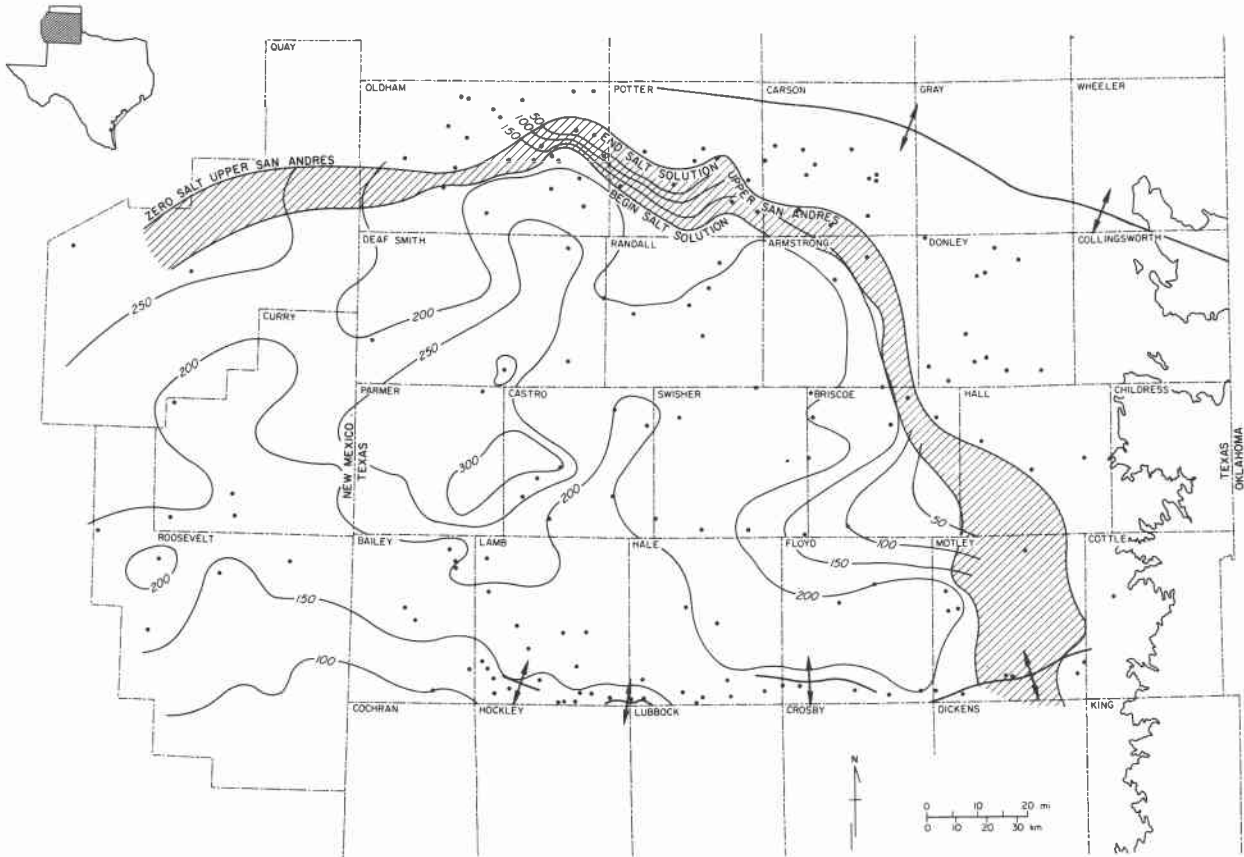


Figure 49. Net-salt map, upper part of the San Andres Formation. Patterned region is the zone of subsurface dissolution of salt by ground-water processes. From Presley (1981c).

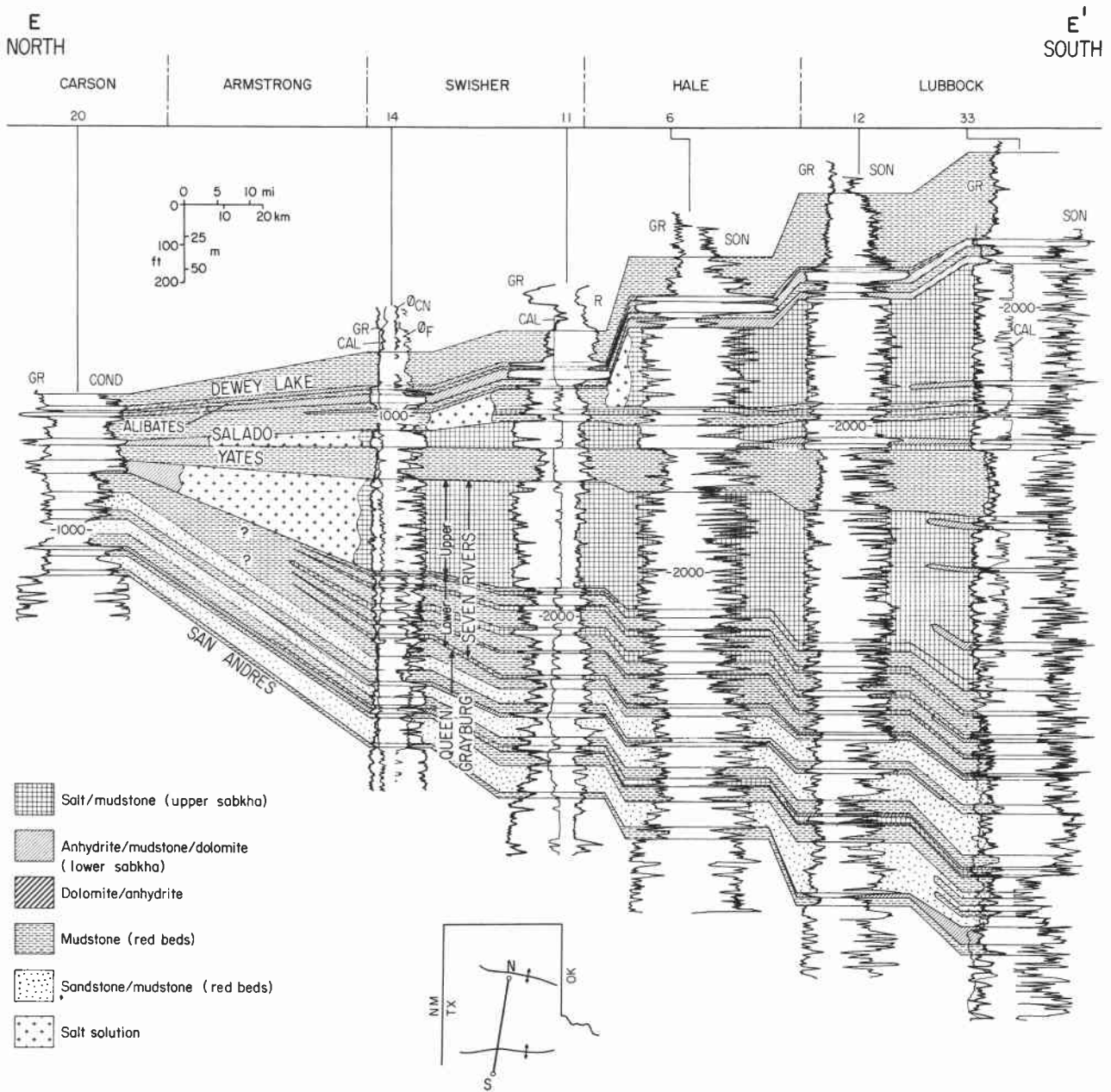


Figure 50. Post-San Andres formations, north-south cross section E-E'. From Presley (1980a).

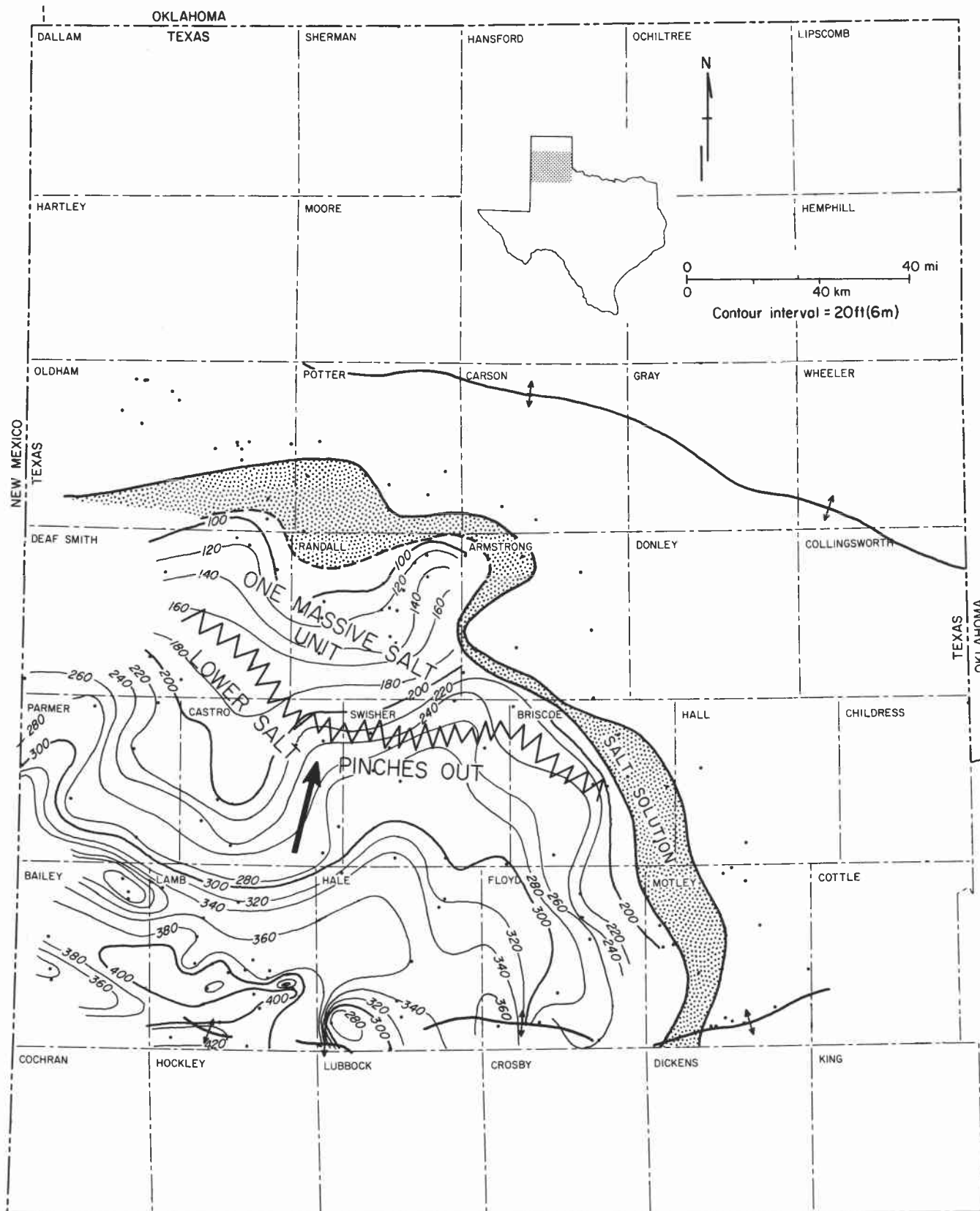


Figure 51. Net salt in Seven Rivers Formation. Lower Seven Rivers salt beds intertongue with red beds to the north. The upper Seven Rivers is a single, relatively massive salt unit. From Presley (1979b).

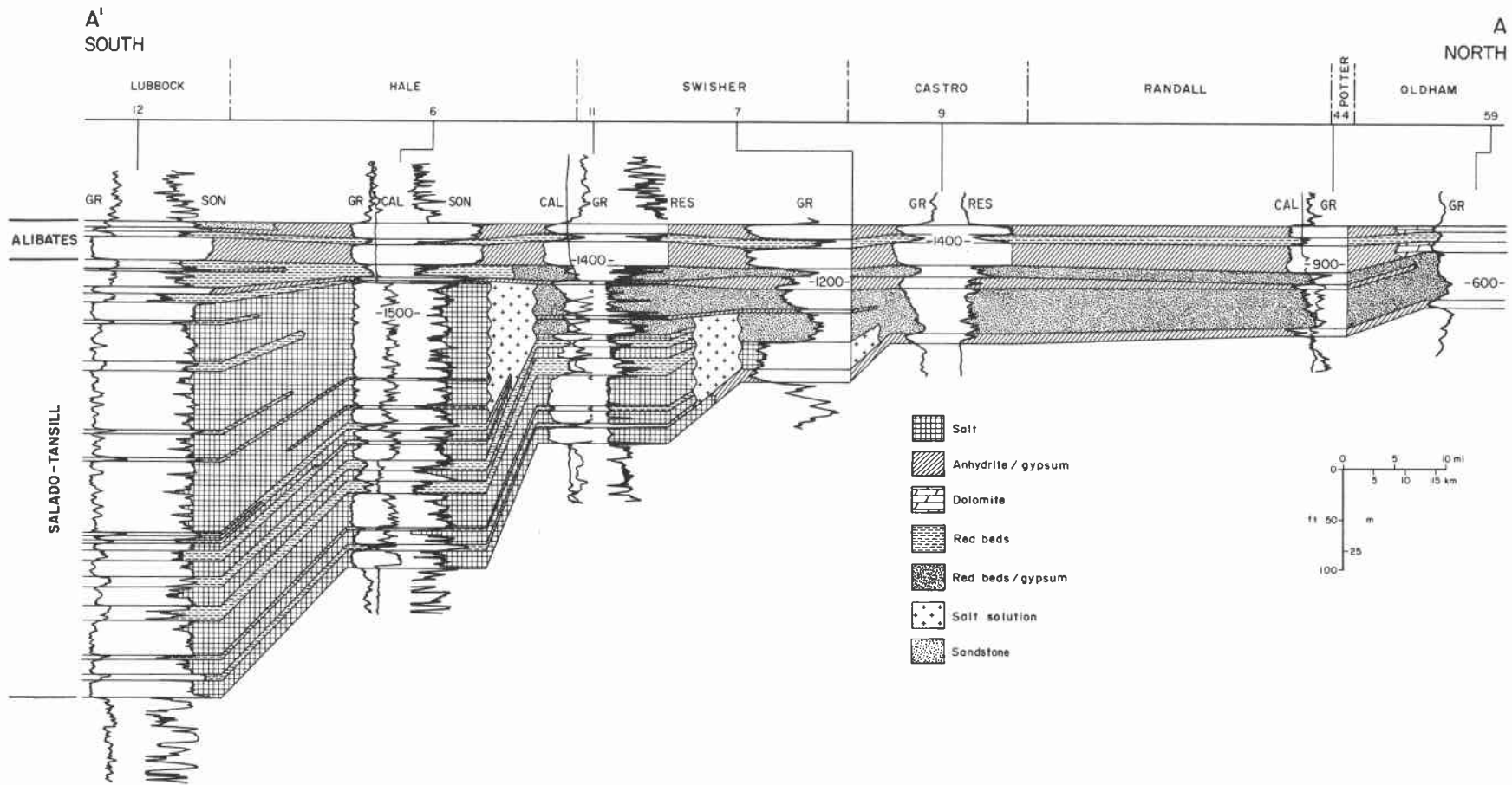


Figure 52. North-south cross section A-A', Salado, Tansill, and Alibates Formations, Palo Duro Basin. For line of section see figure 53. Red beds and gypsum units are composed of collapse breccia caused by salt dissolution. From McGillis and Presley (1981b).

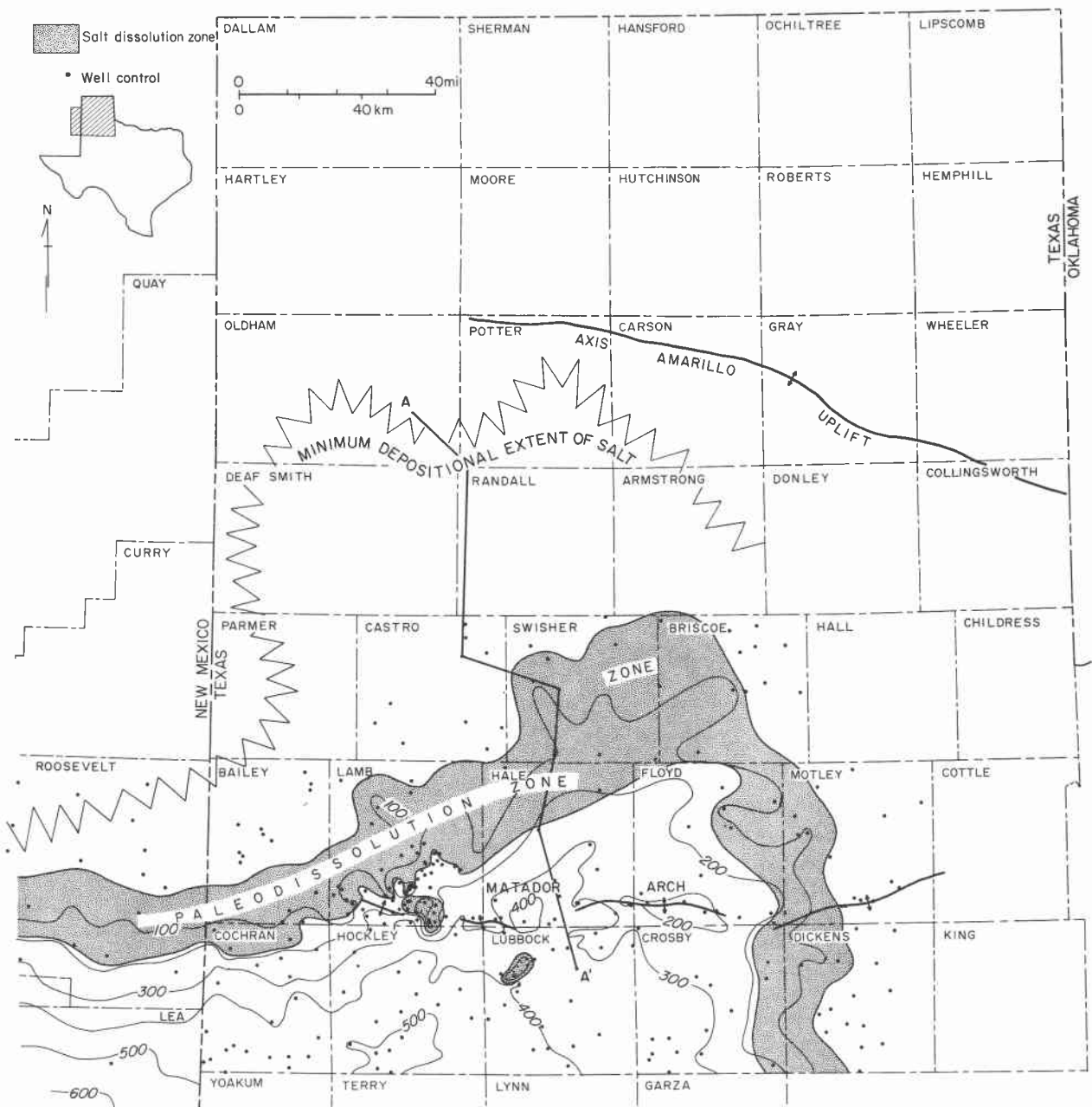


Figure 53. Net salt, Salado-Tansill Formation. Values determined from gamma-ray logs. Salt thickens southward and is bounded on northwest by zone of paleodissolution and on east by zone of modern dissolution. Minimum original extent of salt shown by serrate line; dissolution-collapse breccia occurs south of line. From McGillis and Presley (1981b).

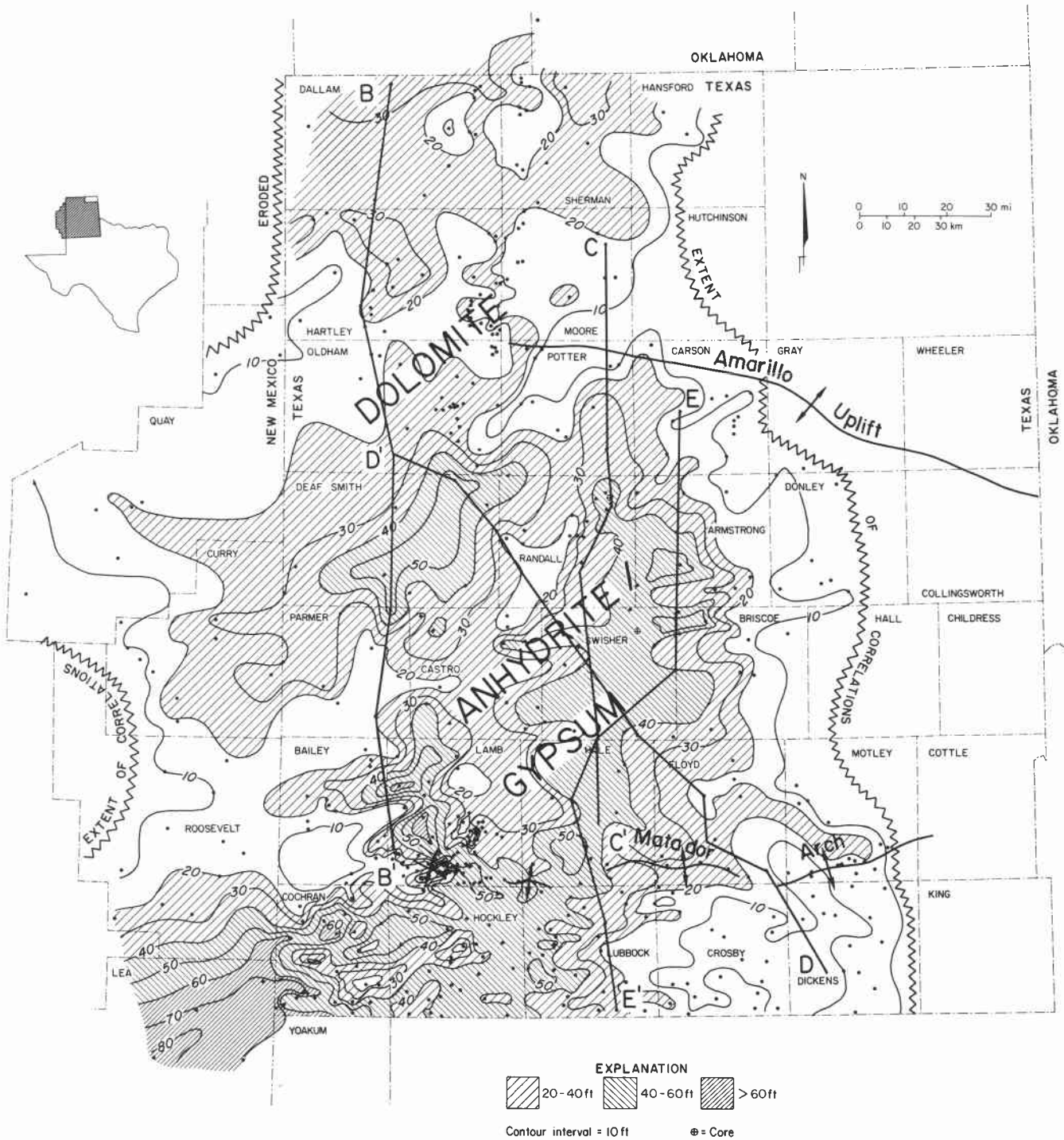


Figure 54. Isopach map, Alibates Formation. Serrate lines mark depositional and erosional boundaries of formation. Dominant lithology of Alibates as recorded on sample logs is noted. From McGillis and Presley (1981b).

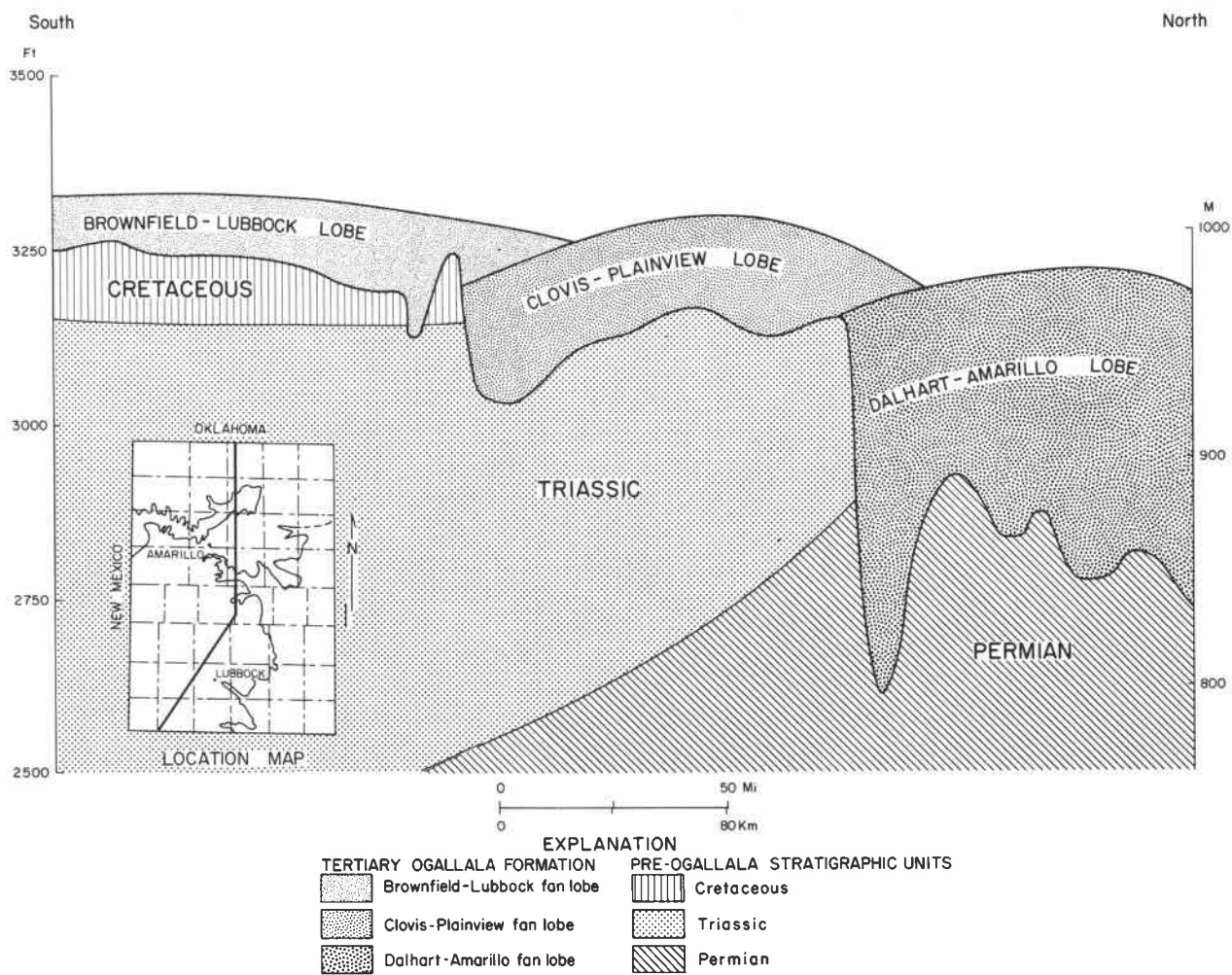


Figure 55. Generalized cross section emphasizing relief of pre-Ogallala surface. Pre-Ogallala surface exhibits three distinct levels that are related to geology of underlying units and their response to salt solution and erosion. Upper surface of Ogallala fans is shown unmodified by postdepositional erosion. From Seni (1980).

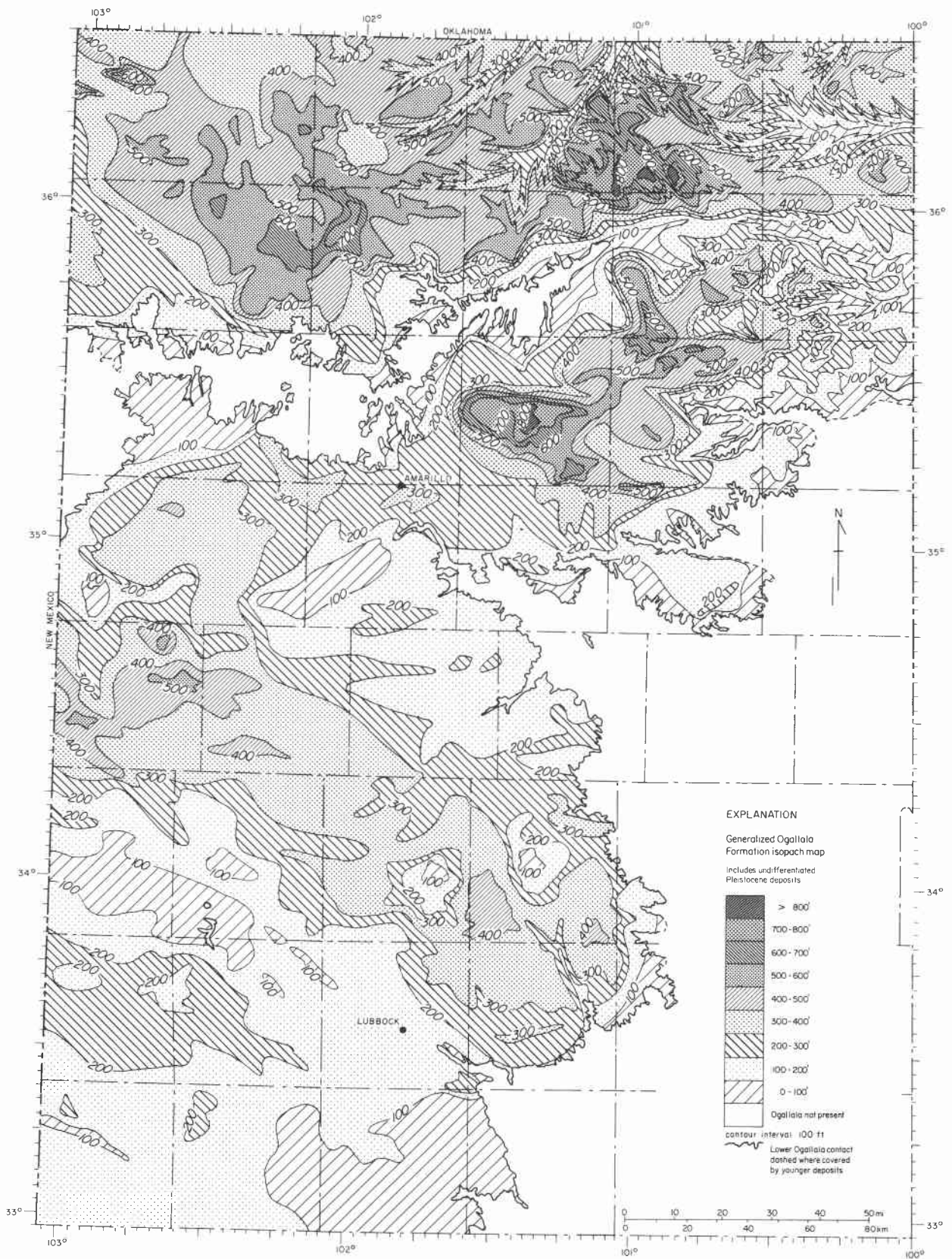


Figure 56. Isopach map, Ogallala Formation. Ogallala thickness is defined as net thickness of all deposits above base of the Ogallala Formation. Undifferentiated Pleistocene deposits (normally less than 7 m [20 ft] thick) may be included in this total. From Seni (1980).

## DEPOSITIONAL HISTORY AND RESERVOIR QUALITY OF GRANITE WASH

Shirley P. Dutton

*Oil and gas fields in granite-wash reservoirs are controlled by both structural and stratigraphic traps. Porosity and permeability within granite wash are related to the amount and kind of authigenic cements present.*

Coarse granite-wash sandstones and conglomerates were deposited adjacent to basement uplifts in the Texas Panhandle during Pennsylvanian and Early Permian time. The regional extent and total thickness of granite wash in the Atoka (Lower Pennsylvanian) through Wolfcamp (Lower Permian) interval are shown by a granite-wash isolith map of the Texas Panhandle (fig. 57). A prism of granite wash more than 5,000 ft (1,500 m) thick accumulated in the Anadarko Basin (figs. 57, 58) north of the bounding Amarillo Uplift fault. Subsidence in the southern Anadarko Basin apparently occurred at a rate comparable to sedimentation, thus allowing accumulations of thick shallow-marine and nonmarine sediment adjacent to the fault. Greater displacement north of the Amarillo Uplift allowed much more sediment to accumulate there than in the Palo Duro Basin (fig. 59). Granite wash south of the uplift is about 20 percent as thick as it is north of the uplift (fig. 57).

Mobeetie Field, which produces oil and gas from granite wash, is located on a northwest-trending basement uplift parallel to the Amarillo Uplift (fig. 58). The principal hydrocarbon-trapping mechanism in Mobeetie Field is structural draping of Pennsylvanian beds over the underlying horst block, forming a doubly-plunging anticline. However, depositional environment and diagenetic history influenced reservoir quality within the area of closure. Porosity in fan-delta sands that were reworked into carbonate environments was occluded by early precipitation of calcite cement. Precipitation of other authigenic cements, including ankerite, Fe-calcite, chlorite, quartz, feldspar, and kaolinite, also reduced porosity. Porosity measured in thin sections varies from 14 percent in uncemented sandstones to zero in highly cemented sandstones. Permeability varies from 1,450 to less than 0.1 md.

Granite wash in the Palo Duro Basin is a potential hydrocarbon reservoir facies. Therefore, the thick granite-wash deposits there are possible targets of oil and gas exploration. Such exploration could threaten the integrity of nuclear waste isolation sites; therefore, knowledge of possible areas of future hydrocarbon exploration is necessary for siting nuclear waste repositories.

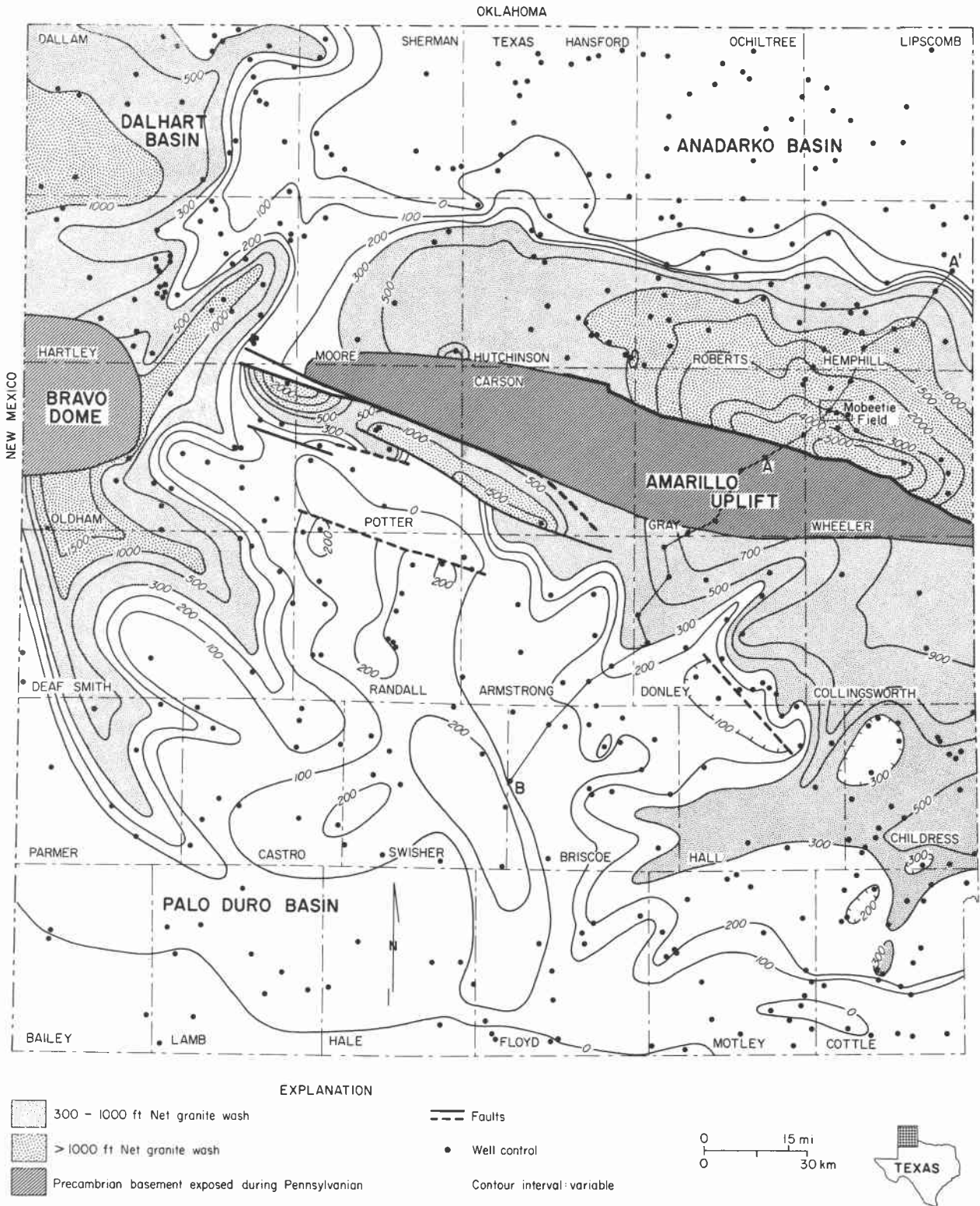


Figure 57. Granite-wash isolith map of Lower Pennsylvanian to Lower Permian strata in the Texas Panhandle. Also shown are lines of cross sections A-A' (fig. 58) and A-B (fig. 59).

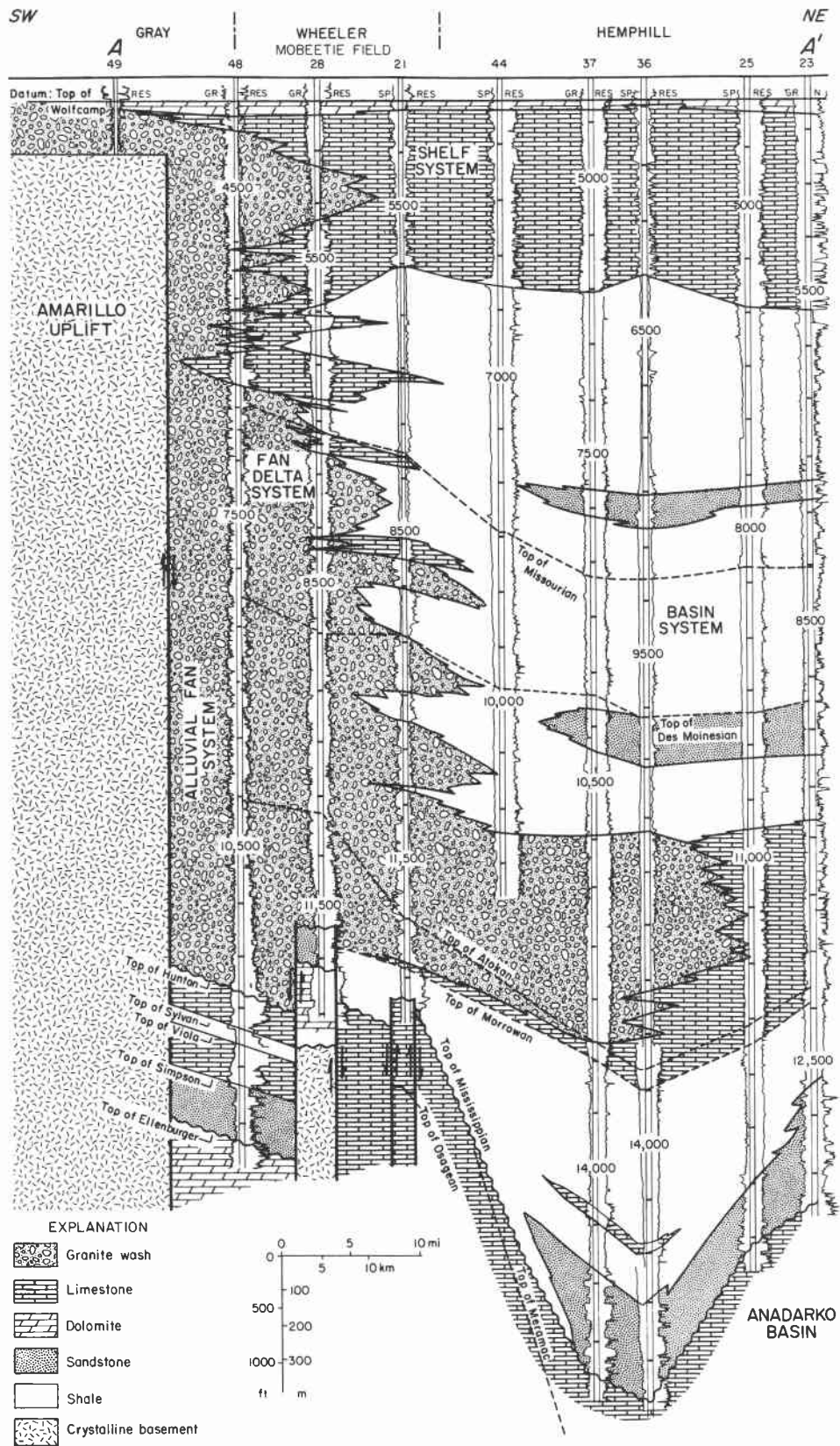


Figure 58. North-south regional cross section A-A' from the Amarillo Uplift into the Anadarko Basin. Line of section shown in figure 57.

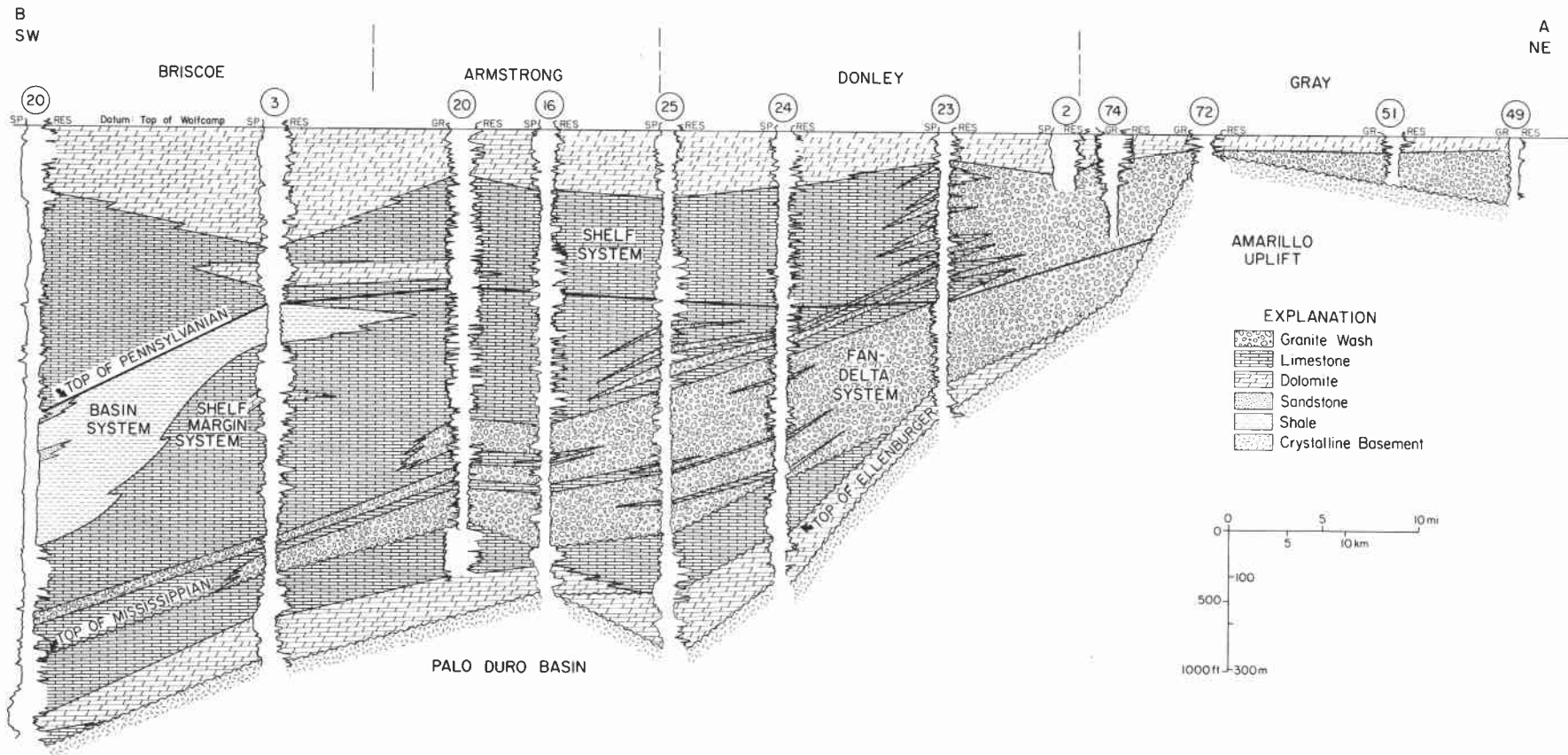


Figure 59. North-south regional cross section A-B from the central Palo Duro Basin to the Amarillo Uplift. Line of section shown in figure 57.

## PETROGRAPHIC SUMMARY OF PERMIAN ROCKS FROM THE DOE/GRUY FEDERAL NO. 1 GRABBE WELL, SWISHER COUNTY

S. D. Hovorka, E. R. Naiman, and J. H. McGowen

*Petrographic analysis of 359 thin sections from the Permian section of the DOE/Gruy Federal No. 1 Grabbe core has provided information about depositional environments. Terrigenous clastics with bimodal grain size reflect eolian transport before deposition in sabkha environments. Dolomites were deposited in more saline water than were partially dolomitized limestones. Halite and anhydrite formed both as primary sediments and as interstitial displacive and replacive deposits.*

The DOE/Gruy Federal No. 1 Grabbe well, in Swisher County, Texas, yielded 3,480 ft (1,478 m) of nearly continuous core of Permian sediments (lower Clear Fork through Dewey Lake Formations). A description of a measured section of this core has been published (McGowen, 1981). Depositional environments of most formations in the core have been described in previous reports (Bein and Land, 1982; Handford and others, in press; Presley and McGillis, 1981, 1982; Ramondetta, 1982). This report presents the results of petrographic analysis of 359 thin sections selected from representative intervals throughout the core. Petrographic features and genetic implications of these features are described for four major lithologies: (1) terrigenous clastics, (2) carbonates, (3) halite rocks, and (4) anhydrite rocks.

### Terrigenous Clastics

Terrigenous clastics include mudstone, siltstone, sandstone and claystone. The siltstones and sandstones are classified (Folk, 1974) as arkose, subarkose, lithic arkose, and arkosic litharenite (fig. 60). The lower part of the Permian section has an average quartz:feldspar:rock-fragment ratio of 76:17:7. The units above the base of the San Andres Formation exhibit an average ratio of 66:20:14. Rock fragments include quartz-mica metamorphic rock fragments, chert, and possible altered volcanic rock fragments. Feldspars include plagioclase, orthoclase, perthite, and microcline; most are fresh, although some are partially sericitized or vacuolized. Sedimentary structures in siltstones and sandstones include small-scale crossbeds, scours, clay drapes, and clay clasts derived from ripped-up drapes (fig. 61). The grain-size distribution is bimodal (figs. 62 and 63). Most sediments contain only angular coarse silt and very fine sand (0.04 to 0.08 mm). Subrounded to very well rounded, fine-, medium-, and coarse-grained sand (0.12 to 0.6 mm) is restricted to a few intervals. This grain-size distribution and the presence of well-rounded bimodal sands may reflect eolian transport of grains before deposition in sabkha environments.

Clay occurs as clay coats on silt grains, as drapes, and as matrix in mudstone. Mudstones contain a mixture of clays and fine, silt-size carbonate, sericite, mica, and anhydrite. The typical sedimentary structure in mudstone is a disrupted intraclastic fabric (fig. 64), which is tentatively attributed to the displacive interstitial growth of halite in laminated mud, subsequent removal of the halite, and collapse of the mud. This relation between mudstone and evaporite minerals is evidence of deposition in a sabkha facies tract.

Diagenesis of terrigenous clastics has been simple. A few feldspar grains have authigenic feldspar overgrowths, especially in the Queen/Grayburg Formation. A minor amount of carbonate cement precipitated, possibly nucleated on detrital carbonate grains. Anhydrite exists as poikilotopic spherulites cementing sand grains and as displacive nodules within mudstone. Halite cement fills all other pore spaces, with the exception of the uncemented near-surface part of the core (above 1,042 ft).

#### Carbonates

Carbonates in the No. 1 Grabbe core can be divided into four categories:

- (1) Mudstones, composed of very finely crystalline to aphanocrystalline, anhedral carbonate mosaic and 2 to 25 percent medium- and coarse-grained, subangular siliciclastic silt. Dolomite mudstones are horizontally laminated or contain very small scale ripples and minute scour surfaces with structures outlined by siliciclastic silt.
- (2) Packstones or wackestones containing a restricted marine fauna and halite-filled moldic porosity. Allochems are difficult to recognize because they have been dissolved, but include small, articulated bivalves, gastropods, and green algae. The matrix is dolomite mudstone.
- (3) Transported grainstones or packstones composed of well-sorted, abraded, skeletal debris, coated grains, oolids, and pellets (figs. 65 and 66). Grainstones are crossbedded and have dolomite or halite cement. In many samples, allochems have been dissolved and molds are filled with halite.
- (4) Extensively burrowed packstones and wackestones with normal faunal diversity, including punctate brachiopods with intact spines, echinoid plates, coral colonies, pelecypods, gastropods, foraminifers, and green algae.

The first three categories of carbonates are 5 to 10 ft thick throughout the Lower Permian Clear Fork and Glorieta Formations. These carbonates have been dolomitized, forming 3 to 10  $\mu$  anhedral and rhombs. Normally diverse fauna of the fourth category

exist only in the 40- and 80-ft-thick cycle 2 and cycle 4 carbonate units of the Upper Permian lower San Andres Formation, which have been only partly dolomitized. The dolomitized carbonates were deposited under conditions of high salinity, as indicated by low faunal diversity, whereas slightly dolomitized limestones were deposited in normal marine waters. The limestone sequences contain anhydrite cement in the upper part and halite cement throughout, indicating subsequent interaction with hypersaline brines.

#### Halite Rocks

Halite and anhydrite were precipitated from hypersaline brine pools or interstitial waters. Halite precipitated from brine pools and deposited at the sediment/water interface can be identified by (1) upward-pointing, chevron-shaped zones of fluid inclusions within salt crystals (fig. 67), an indication of variations in growth rate of crystals on the brine pool floor, and (2) relatively undisturbed horizontal drapes of terrigenous mudstone or anhydrite representing influx of other sediment into the brine pool.

Halite also formed interstitially as displacive cubes, hopper-shaped crystals, and anhedral crystals. Evidences of displacive growth are (1) compression of anhydrite and intraclastic mudstone between halite crystals (fig. 68); (2) large euhedral crystals (fig. 69); and (3) disrupted, intraclastic fabrics in initially well-sorted clastics adjacent to displacive halite.

#### Anhydrite Rocks

Anhydrite, like halite, exists as both a primary precipitate (initially gypsum) at the sediment/water interface, and as a displacive and replacive precipitate within the sediment. Pseudomorphs after blades of gypsum and presence of horizontal dolomite laminae are evidence of formation as primary precipitates. Displacive anhydrite exists as nodules within carbonate or terrigenous mudstone. Isolated, noncompressed nodules (fig. 70) are composed of randomly oriented blades of anhydrite; compressed nodules (fig. 71) are composed of horizontally oriented anhydrite blades.

Diagenesis in evaporites includes (1) conversion of all gypsum to anhydrite, (2) recrystallization and grain enlargement in halite and anhydrite, destroying primary fabrics, (3) replacement of gypsum blades, commonly by halite; (4) minor amounts of halite at grain boundaries replaced by bladed anhydrite and by limpid 0.05 to 0.7  $\mu\text{m}$  dolomite with unusual crystal faces (Naiman and others, in press), and (5) dissolution of halite and hydration of anhydrite to gypsum less than 1,050 ft below surface caused by the effects of low-salinity ground waters in this interval.

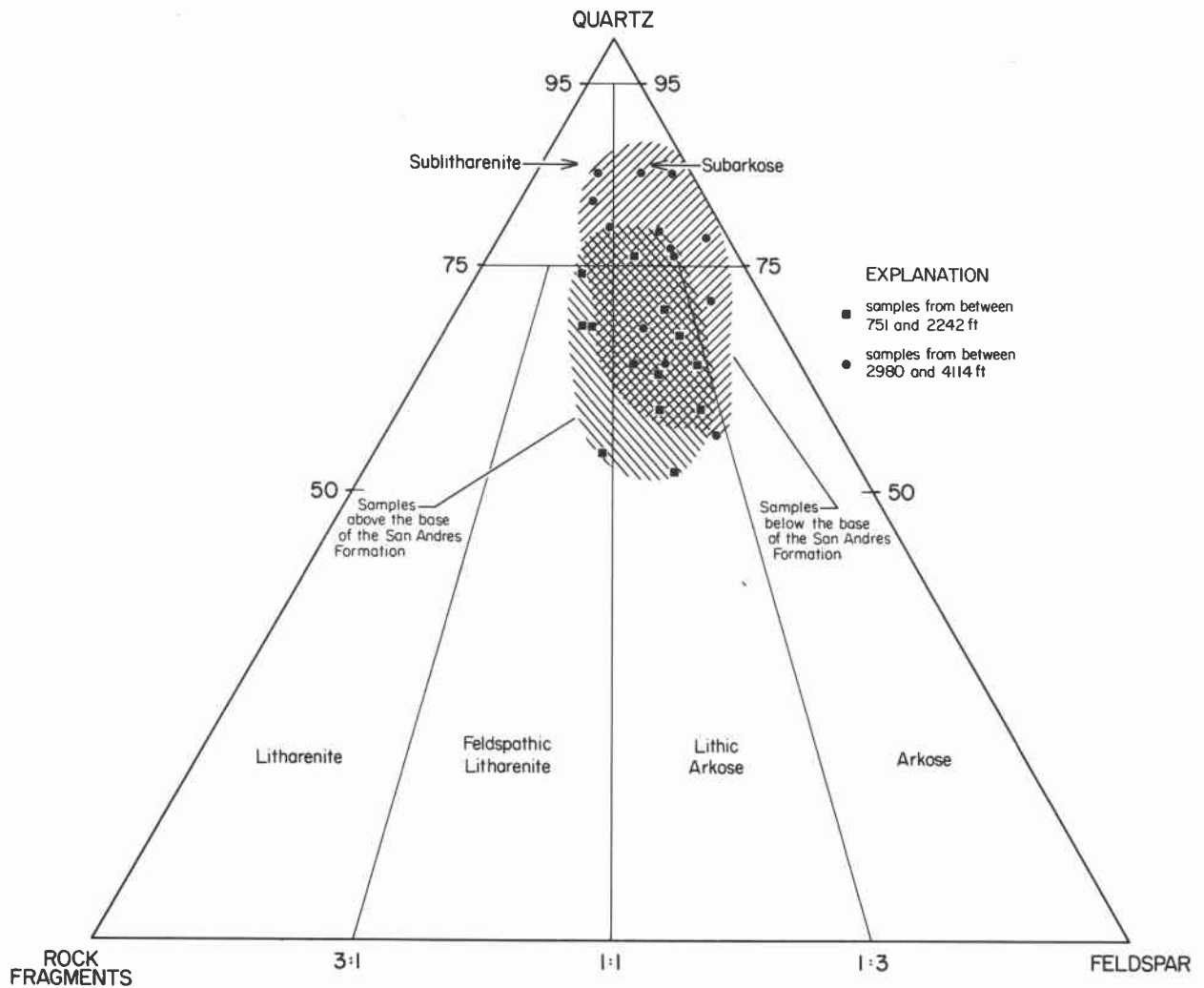


Figure 60. Plot of quartz-feldspar-rock fragment ratios from 28 samples from the No. 1 Grabbe core, based on point counts of 100 to 200 grains. Sandstones and siltstones in the Upper Permian section are richer in rock fragments than the Lower Permian section.

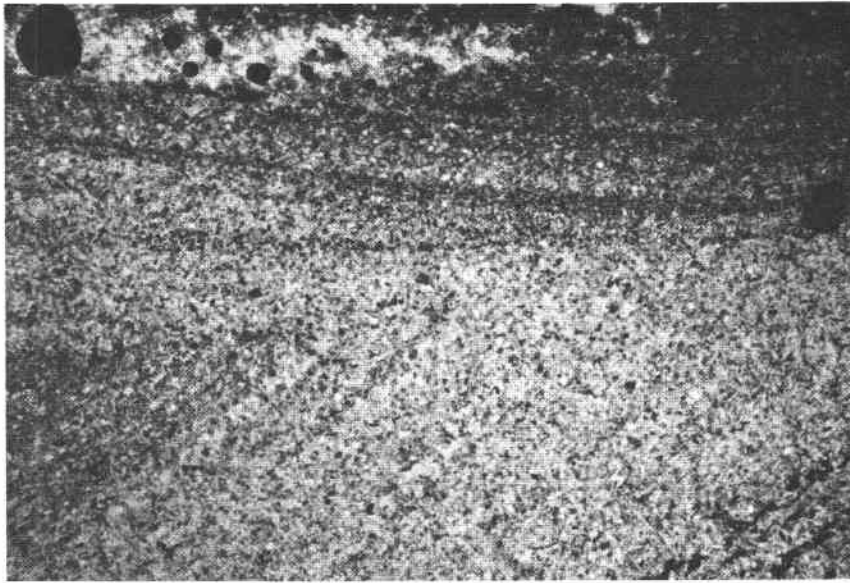


Figure 61. Trough crossbeds visible in very fine, subarkosic sandstone because of placers of opaque minerals and clay intraclasts. Width = 6.15 mm, plane light, depth is 2,976.0; Glorieta Formation.

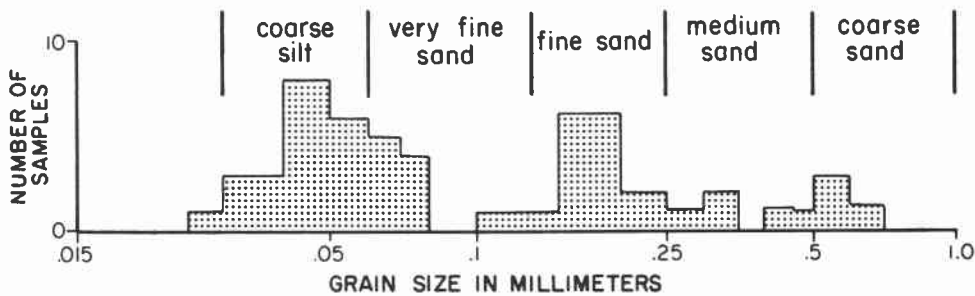


Figure 62. Histogram of grain sizes observed in Permian siliciclastics in the No. 1 Grabbe core. Mean grain sizes for 44 samples were estimated petrographically. In multimodal samples, a mean was estimated for each population. Coarse silt and very fine sand with diameters between 0.03 and 0.08 mm are most common.

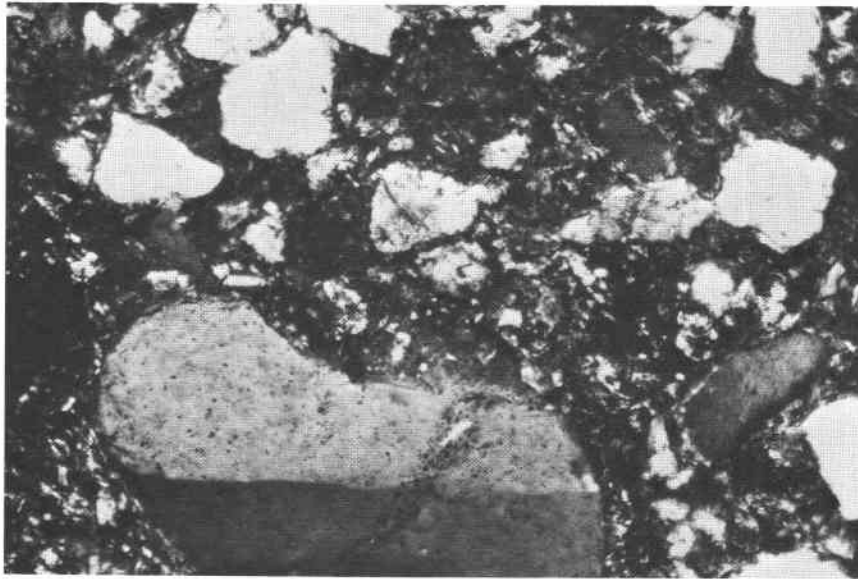


Figure 63. Muddy, very fine sandstone: immature subarkose, showing bimodality. The coarse grains are well rounded, but the finer grains are angular. The matrix is clay. Width = 2.6 mm, crossed nicols, depth is 2,980.6; Glorieta Formation.

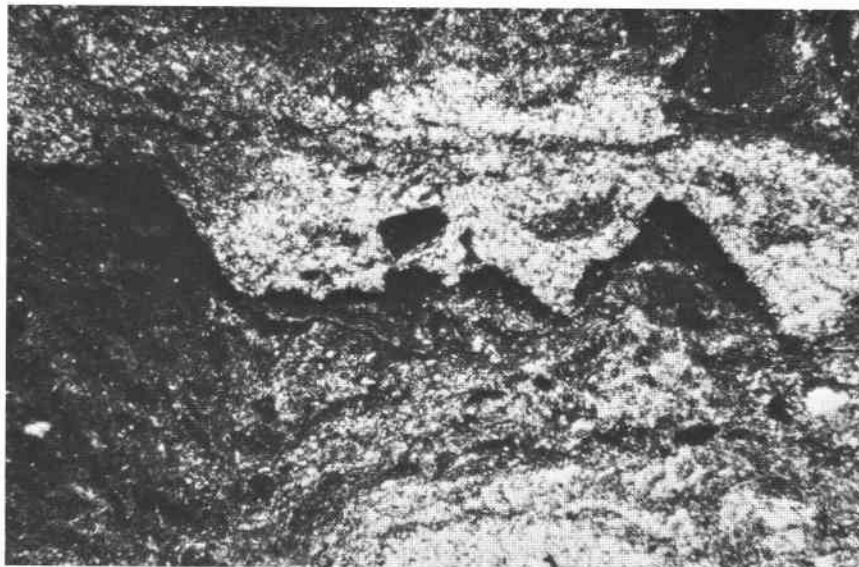


Figure 64. Red clay intraclasts and clay drapes (dark) within coarse, muddy siltstone exhibiting disrupted textures. The straight, sharp contacts of the clay layer with the overlying silt may have been formed by dissolution of halite and deposition of silt in the resulting molds. Width = 6.15 mm, plane light, depth is 3,985.0; Tubb Formation.

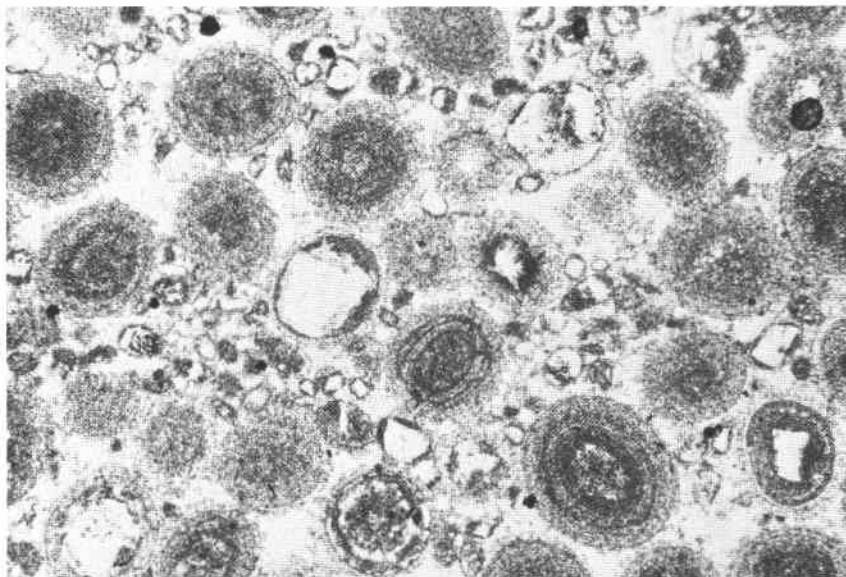


Figure 65. Poikilotopic halite cement filling both intragrain and moldic porosity in silty, dolomitized pellet oosparite. Angular quartz and feldspar grains form nuclei for some ooids and coated grains. Width = 2.6 mm, plane light, depth is 3,582.2; upper Clear Fork Formation.

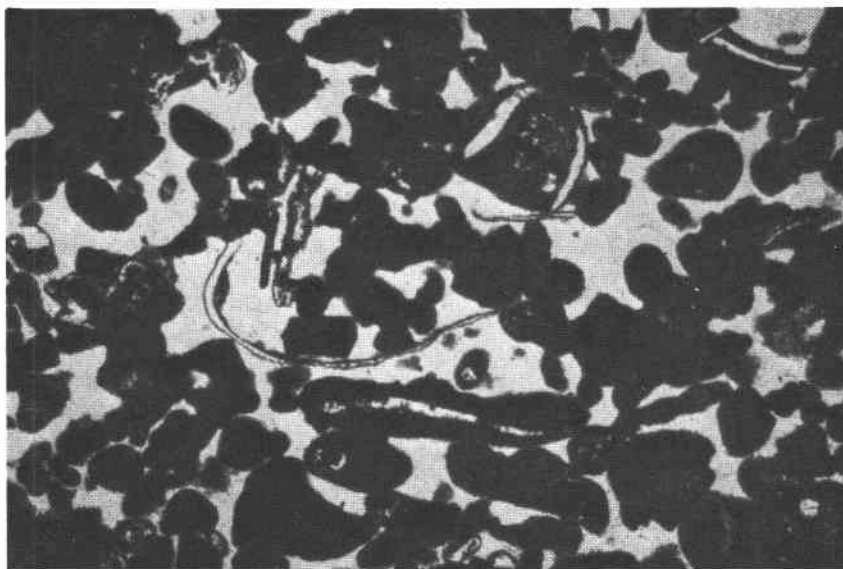


Figure 66. Dolomitized fossiliferous intrasparite containing intraclasts, pellets, and coated skeletal fragments (foraminifer and pelecypod fragments). Halite fills moldic and intragranular porosity. Width = 6.15, plane light, depth is 4,135.0; lower Clear Fork Formation.

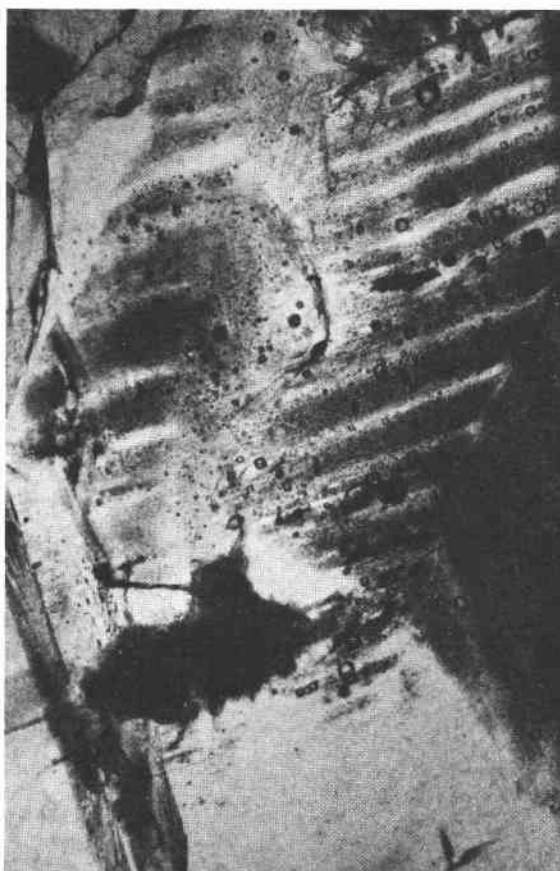


Figure 67. Chevron structure in halite. Concentrations of cubic fluid inclusions alternating with thin bands of clear halite define growth bands. Width = 6.15 mm, plane light, depth is 2,561.9; lower San Andres Formation, cycle 4.

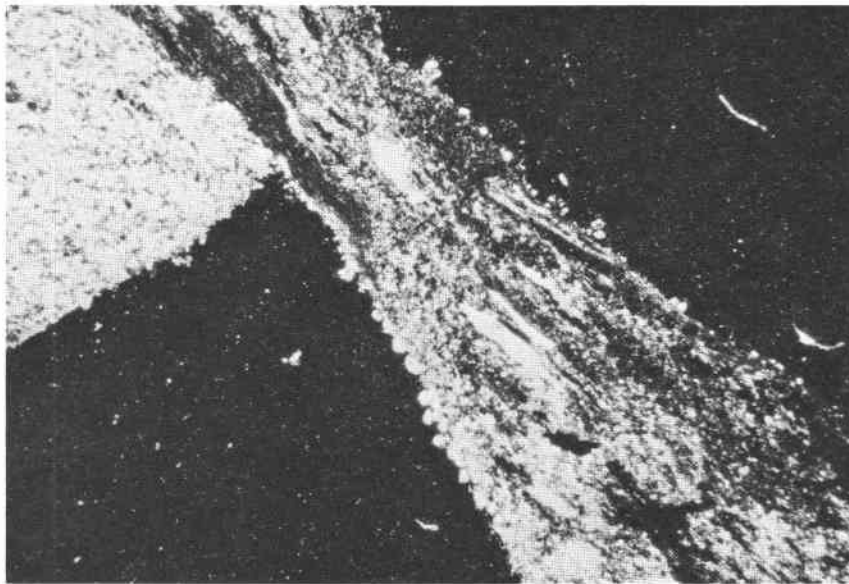


Figure 68. Large cubes of halite (dark areas) that disrupted and compressed originally well-laminated red clay and silt during displacive growth of halite cubes within the sediment. Dolomite crystals nucleated on clay and silt invaded the halite. Width = 6.15 mm, crossed nicols, depth is 3,985.0; Tubb Formation.

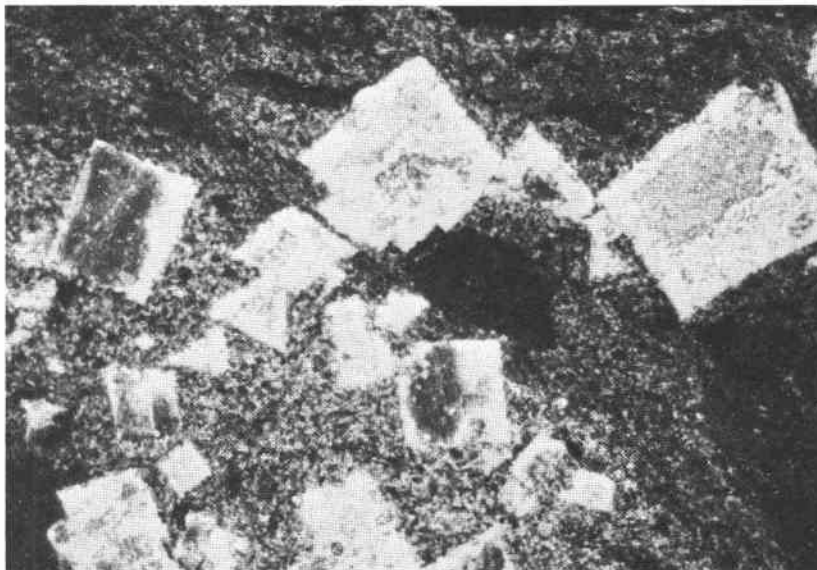


Figure 69. Well-formed cubes of halite that disturbed initially well-laminated, muddy, coarse siltstone, indicating that most halite growth occurred displacively within silt. Dark areas within clear halite cubes are flaws in the thin section. Width = 6.15 mm, plane light, depth is 3,985.0; Tubb Formation.

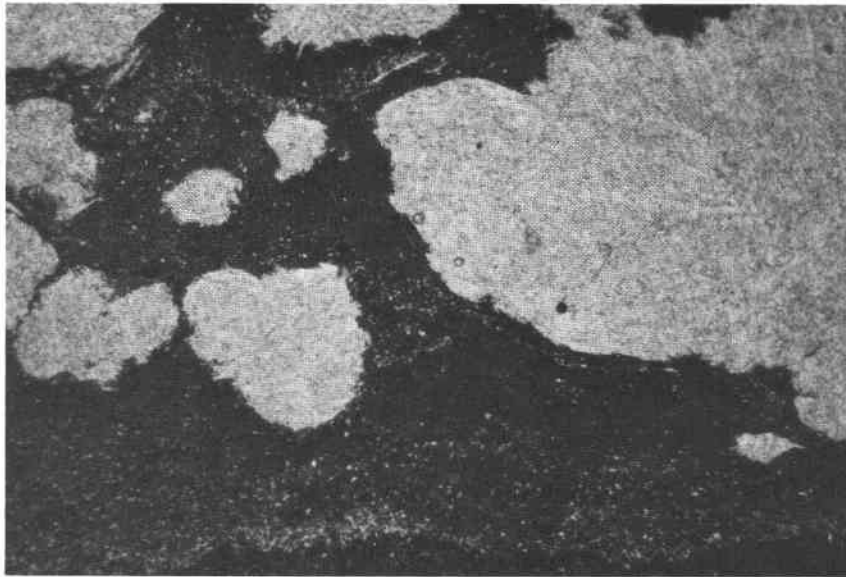


Figure 70. Contact between silty aphanocrystalline dolomite (dark) and displacive anhydrite nodules composed of felted, medium crystalline laths. Width = 6.15 mm, plane light, depth is 4,182.6; lower Clear Fork Formation.

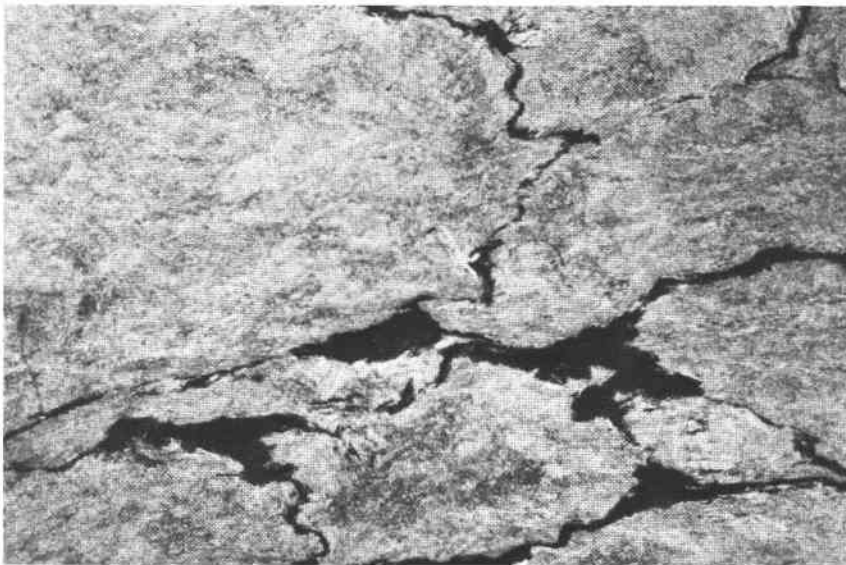


Figure 71. Compressed anhydrite nodules are elongated parallel to bedding and composed of finely crystalline, bladed anhydrite also aligned parallel to bedding. Opaque material between the nodules is very finely crystalline dolomite and hematitic clay. Width = 6.15 mm, crossed nicols, depth is 2,286.7; upper San Andres Formation.

## POSSIBLE PERMIAN DIURNAL PERIODICITY IN NaCl PRECIPITATION, PALO DURO BASIN, TEXAS

Edwin Roedder<sup>1</sup>

*Individual crystals from the Permian salt beds of the Palo Duro Basin show a regular pattern of bands that may reflect diurnally changing conditions during crystallization. The bands (0.40 to 0.85 mm thick) may correspond to complete evaporation of a maximum of 3 to 6 mm of salt-saturated seawater per day. They indicate very shallow water conditions. These bands are much thinner features than, and appear to be quite distinct from, the presumably annual, cyclic bands of different mineralogy found in many saline deposits.*

During an investigation into the nature and amount of water present in salt beds of the Palo Duro Basin in Texas, a series of doubly polished, thick (0.2 to 0.4 inch, 5 to 10 mm) plates was prepared from salt-rich horizons in the Randall County core (DOE-Gruy Federal, Rex White No. 1 well). A regular banding appears within some of the 0.2 to 0.6 inch (0.5 to 1.5 cm) halite crystals in a sample from the lower part of the San Andres Formation at a depth of 1,785.7 ft (figs. 72 through 74). Some similar banding was present in other samples from the core. The banding consists of a regular alternation of clear and dark-gray salt, arranged parallel to the cube face (100). The dark-gray color arises from numerous, minute, slightly rounded, cubic fluid inclusions (fig. 74). Although a few of these inclusions are 30  $\mu\text{m}$  on an edge, or even larger, most are less than a few micrometers, or even less than 1  $\mu\text{m}$ . The gray salt contains as many as  $10^9$  to  $10^{10}$  inclusions per  $\text{cm}^3$ . Because the clear bands are much thinner than the dark-gray bands, in effect they divide an otherwise uniform dark-gray salt into separate compartments and, hence, are here called septa. They are essentially free of inclusions and average about 20  $\mu\text{m}$  wide in most crystals; in a few, they are  $\sim 100$   $\mu\text{m}$  wide. On either side of the clear zone, the density of inclusions increases abruptly. The spacing between septa (perpendicular to the banding) generally is rather uniform within a given crystal but differs from one crystal to another. The average spacings for septa in individual crystals range from 0.40 to 0.85 mm. Some individual crystals show 10 or more bands (fig. 72).

The fluid inclusions between the septa are commonly arranged in parallel bands (fig. 74), and some larger ( $\sim 200$   $\mu\text{m}$ ) cubic inclusions exhibit one very flat cube face directly against the septum. In contrast, the other cube faces, against dark-gray salt, are rounded and only subcubic in outline.

---

<sup>1</sup>959 U.S. Geological Survey, Reston, VA 22092

In some of the banded salt crystals, particularly the elongated ones, two sets of such clear septa join at a sharp  $90^\circ$  angle along what is more or less the center line in the long direction through the crystal. An additional similar clear septum is visible connecting these apices, effectively bisecting the  $90^\circ$  angle (that is, approximately in the plane of the dodecahedron [110]; see arrows in figs. 72 and 73). Both types of clear septa may be invisible unless the sample is tipped for viewing parallel to the clear septa.

A statistical determination of the orientation of the banded crystals with respect to the original bedding would best be made on new plates, cut for that purpose, but the available plates indicate that the elongated banded crystals, and the nested rows of apices, are roughly subparallel and originally pointed more or less vertically in the salt bed. Although much of the salt consists of irregular, completely clear areas, most crystals of halite in these beds have at least some irregular areas of gray, inclusion-rich salt, similar to that between the septa. Because the boundary between the gray areas and these masses of clear salt is a sharp curving surface, even within a single crystal, which cuts across the banding of the gray salt, I believe that the inclusion-rich salt has been dissolved and recrystallized to yield the areas of clear salt. The clear salt contains a few randomly arrayed, large, fluid inclusions.

The distribution of the inclusions in the banded salt crystals indicates that they are almost certainly primary; that is, they must have formed during euhedral growth of the host crystals from a solution. If so, these inclusions presumably contain samples of partly evaporated Permian seawater. The occurrence of a stacked sequence of apices ("chevron" structure) has been described in bedded salt. Salt may crystallize at the air-water interface, yielding small, flat, hollow "hopper" crystals floating on the surface, which subsequently sink. These little crystals contain many planes of tiny fluid inclusions arrayed parallel to the cube face (100). The salt crystals containing the structures described here, however, are obviously too large to have floated; presumably, they grew up from the bottom as a series of subvertical spikes, each a cube corner, as the cube corner (the normal to the octahedron face) is the fastest growing face in salt. This competitive growth procedure has been well documented by Wardlaw and Schwerdtner (1966) for Devonian salt beds in Canada and by Shearman (1970) for Recent salt in Baja California.

The depth at which such chevron growth may have occurred has been a subject of much discussion (Dellwig, 1955; Wardlaw and Schwerdtner, 1966; Arthurton, 1973; Friedman, 1978), and the banding described here bears on that discussion. Evaporation at the surface will yield a dense, supersaturated solution, which is gravitationally unstable

and will sink in a pattern of convection cells, or "stream tubes" (Bradley, 1965). On contact with the halite crystals at the bottom, the excess salt in solution will crystallize. In nearly all crystal-growth studies, a high degree of supersaturation results in fast growth and imperfect crystals containing many inclusions, and slow growth yields more nearly perfect crystal growth.

Alternation of inclusion-rich and inclusion-poor zones forms the chevron texture in the many salt deposits where it has been described, but this alternation is generally shown to be highly irregular, both in spacing of the bands and in the density of inclusions in each band. The highly regular alternation of inclusion-rich and inclusion-free salt within the Palo Duro crystals suggests a regular alternation of the degree of supersaturation of the liquid, as might be expected to occur diurnally; the inclusion-rich salt probably crystallized during the day, and the clear septa at night, as proposed by Holser (1979). A crude upper bound can be placed on the amount of evaporation this crystallization might have entailed. The sea bottom might have had relatively few such crystals protruding into the liquid, or a complete carpet of them. If a carpet of crystals existed, the maximum amount of precipitation of salt during a given 24-hour cycle would be a layer ~0.85 mm thick over the entire bottom. This would correspond to the total evaporation of water from about 3 to 6 mm of salt-saturated seawater in that 24 hours. The actual amount of evaporation could be considerably less than this if the precipitation was not over the entire bottom. Similar evaporation rates have been recorded before, although they were based on measurements of presumed annual cycles (Dellwig, 1955; Wardlaw and Schwerdtner, 1966).

If the previously described mechanism is correct, it also places some constraints on the depth of the water under which this salt crystallized. The deeper the water, the more mixing will occur as the currents of dense, supersaturated fluid flow downward, and the less sharp will be the changes in conditions at the bottom throughout a given cycle. Bradley (1965) has shown experimentally that vertical density currents ("stream tubes") tend to break up in a few centimeters of movement. If we assume that these bands were deposited during a 24-hour cycle, we eventually should be able to place some limits on the water depth, using estimates of the density contrasts and temperature gradients, expected turbulence and diffusion rates, and the thickness of the individual bands. At present, it appears highly unlikely that periodic density currents from a few millimeters of denser surface water could travel down vertically more than a few feet without mixing (Bradley, 1965), thus losing periodicity in the precipitated salt.

Many bedded halite deposits show a regular banding or lamination parallel to the bedding (Dellwig, 1955; Wardlaw and Schwerdtner, 1966; Arthurton, 1973; Nurmi and Friedman, 1977). These laminae, which have sometimes been assumed to reflect annual variations in the conditions of deposition, are defined by differences in NaCl color or grain size and particularly by a band of calcite or anhydrite (or gypsum) grains for each cycle. For example, in the Michigan Basin, the calcite-anhydrite layers are 2.5 to 30 cm thick, and the intervening salt layers are 2.5 to 150 cm thick, yielding 5 to 180 cm of bed per cycle (Nurmi and Friedman, 1977). This sequence of change in composition of the material being precipitated agrees with the sequence of phases, if not with the quantities, that would be expected during the evaporation of a given unit of seawater (see Dean, 1978; Friedman, 1978). The periodicity of the salt crystals described in this paper, however, occurred while a single phase (NaCl) was being precipitated, and each cycle represents the deposition of two to three orders of magnitude less material.

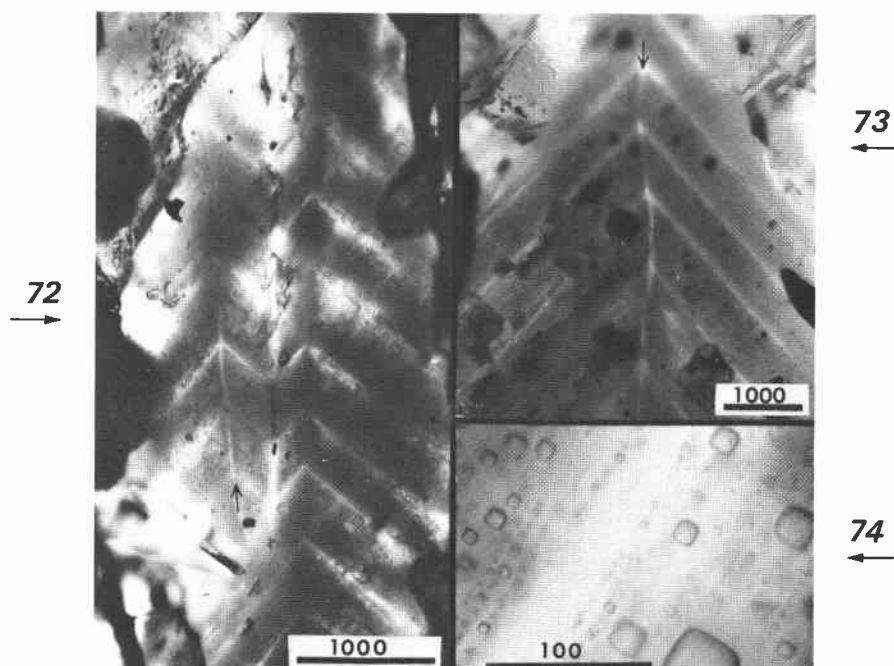


Figure 72. Part of two elongated single crystals (~2x8 mm) showing 12 bands, averaging 0.39 mm/band (clear septum to clear septum, perpendicular to the bands). Note that the separate crystal on the left has an additional clear septum along its center line (arrow).

Figure 73. Part of an elongated single crystal (~5x12 mm) showing 14 bands, averaging 0.54 mm/band. Note additional clear septum along center line (arrow).

Figure 74. Detail of salt across one clear septum shown in figure 73, in same orientation.

## USE OF GEOPHYSICAL WELL LOGS FOR THE DETERMINATION OF MUD AND ANHYDRITE CONTENT IN BEDDED SALT

Paul J. Ramondetta and Robert M. Merritt

*The mud and/or anhydrite content of bedded salt of the San Andres Formation, Palo Duro Basin, Texas, correlates with gamma-ray intensity, neutron porosity, bulk density, and interval transit time (sonic).*

Middle and Upper Permian salt deposits of the Palo Duro Basin are being evaluated as a possible nuclear waste isolation repository. One of the factors affecting the feasibility of waste isolation is the relative purity of the salt host rock. Impurities include mud, anhydrite, and fluid inclusions. Results of studies of fluid inclusions are reported elsewhere (Roedder, this report; Bassett and Roedder, 1981).

The salt-bearing interval had been cored at two locations in the basin by September 1980. Mud and/or anhydrite content was determined from point counts on the slabbed core. However, two control points are insufficient to characterize the entire basin; no other salt cores existed at the time that this report was written. Several hundred exploratory holes, however, have been drilled throughout the basin, and many of these wells have been logged by various geophysical devices. A full suite of geophysical logs was run on the two test wells. If a relationship can be established between the various impurities within the cored salt and the geophysical log response, then salt purity can be assessed throughout the basin. Presley (1981) showed that geophysical log response is related to facies in the Palo Duro Basin. Presley (in preparation) also has used these relations to construct several facies cross sections through the basin. This approach is critical for choosing an appropriate salt bed and an area upon which to concentrate the search for a repository site. This technique also may be helpful in evaluating bedded salt in other basins.

The San Andres Formation contains the greatest part of massive salt deposits, and of these, the cycle 4 salt is the thickest and most widespread. For these reasons the cycle 4 salt was used for the calibration study.

Coarsely crystalline massive salt is by far the most abundant component of the cycle 4 salt (approximately 90 percent of the interval); finely crystalline salt is rare. The most common form of mud is red mud. In general, mud may occur as discrete seams (up to 3 inches thick) or as chaotic mud-salt. Chaotic texture is very common in other salt units of the Permian section but is relatively unusual in the cycle 4 salt. The chaotic mud-salt may represent a shallowing of the brine pan, whereas the discrete mud seams

may represent a sudden influx of terrigenous sediment during storms. Relative concentrations of the various impurities are shown in figure 75.

Massive salt may be transparent, dark, reddish, pinkish, or milky. It is commonly banded; bands are dark and consist of finely disseminated clay and/or organic material (Handford and others, in preparation). Dark salt commonly is nearly opaque, making point counts difficult.

Figures 76 through 78 illustrate some of the relationships between geophysical logs and various impurities. Compensated neutron porosity (excluding sidewall neutron porosity) offers the best log correlation with mud content (fig. 76). Correlation with gamma-ray intensity (fig. 77) is not quite as good but overall is more useful due to the abundance of gamma-ray intensity logs relative to compensated neutron logs in the Palo Duro Basin. Sonic logs provide poor correlation with mud content.

Bulk density correlates well with percent anhydrite (fig. 78); the relationship is linear. A somewhat poorer correlation exists between anhydrite and sonic logs. Impurities, either mud and/or anhydrite, tend to increase the density of the rock beyond the density of pure halite. Therefore, the bulk density log can be used to estimate total impurities.

This technique has, in fact, been used to map percent mud (in salt) throughout the study area. The percent mud increases in the landward direction (where red beds dominate) as one would expect, which further justifies using this technique.

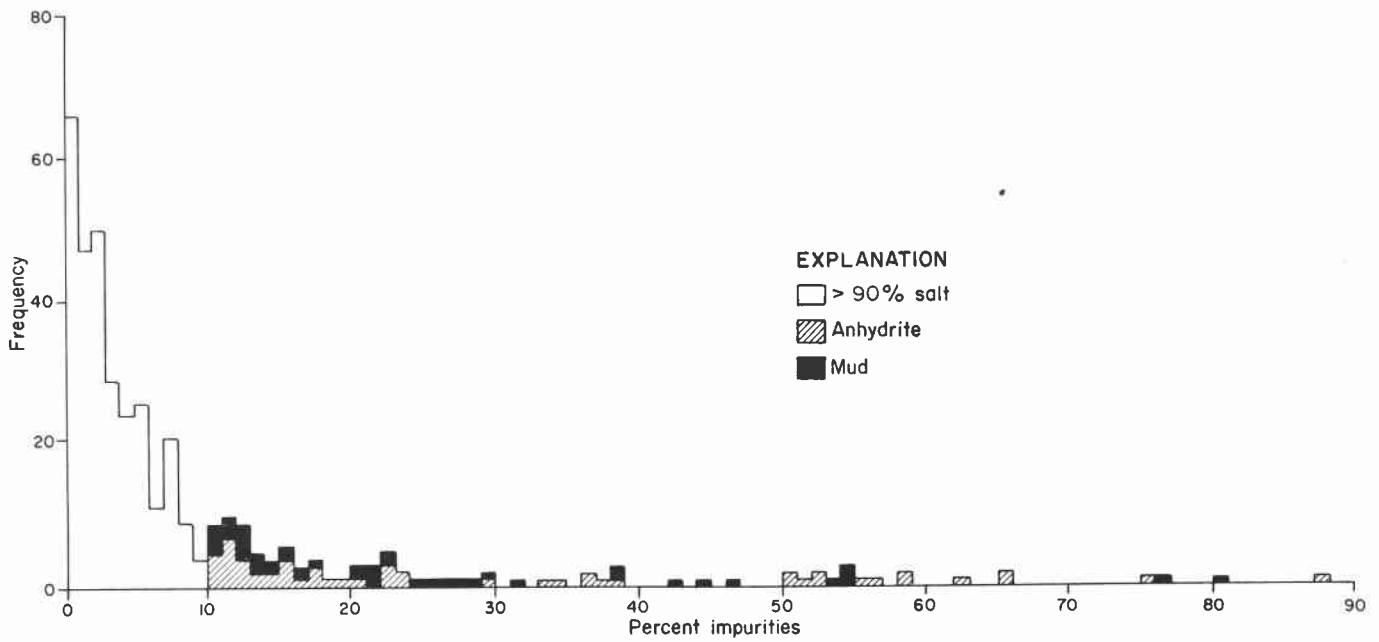


Figure 75. Histogram of impurities in 1-foot samples from the San Andres cycle 4 salt, DOE-Gruy Grabbe No. 1 and DOE-Gruy White No. 1, Randall and Swisher Counties, Texas.

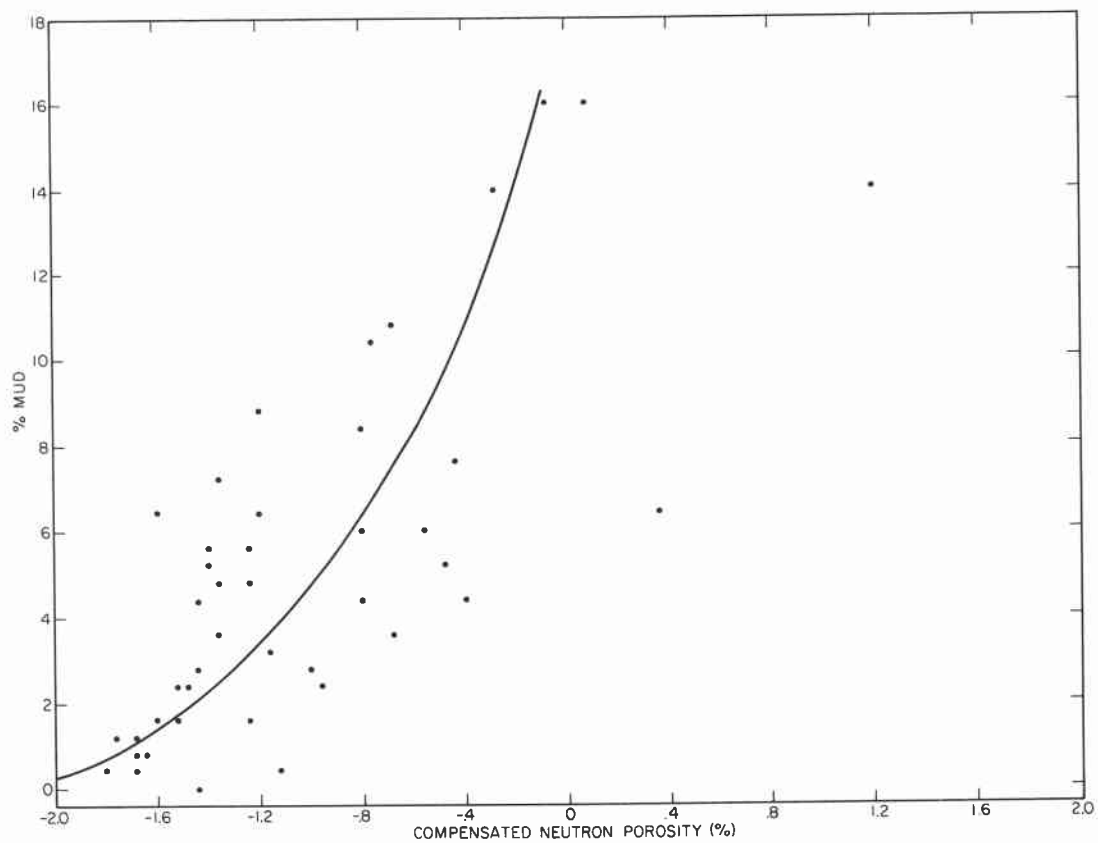


Figure 76. Compensated neutron porosity correlated with mud content.

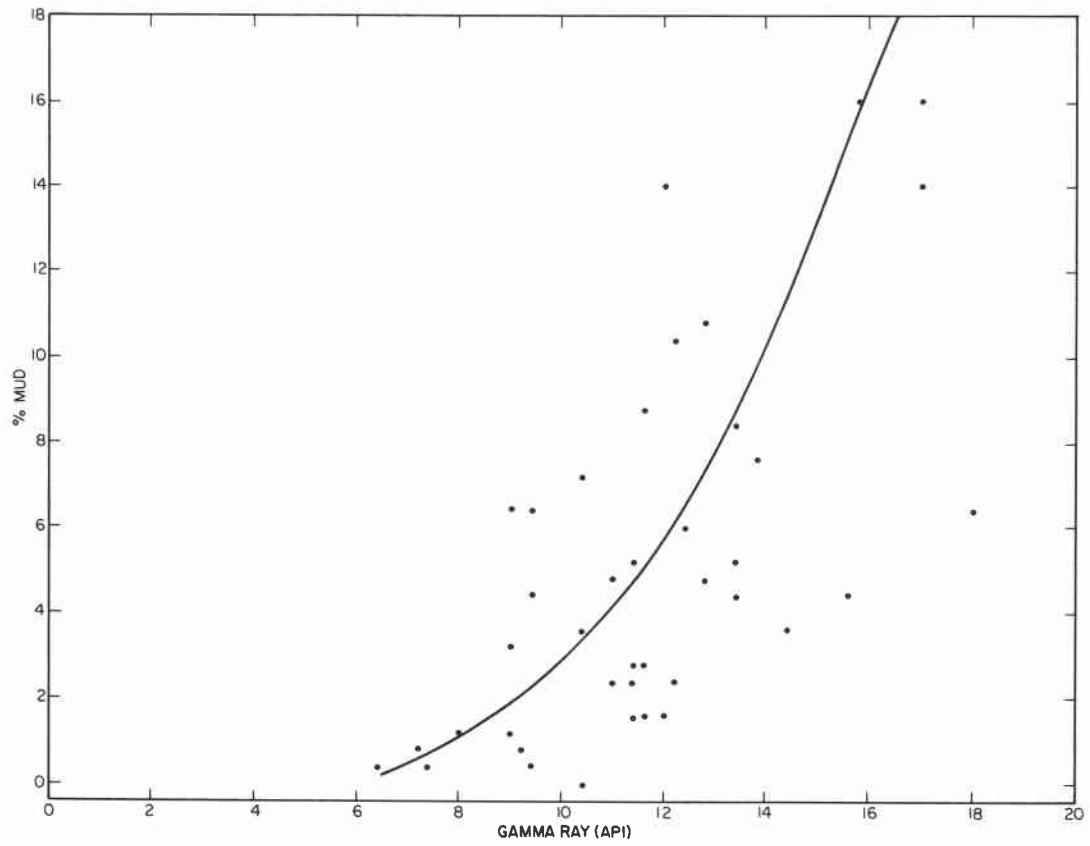


Figure 77. Gamma-ray intensity (API) correlated with mud content.

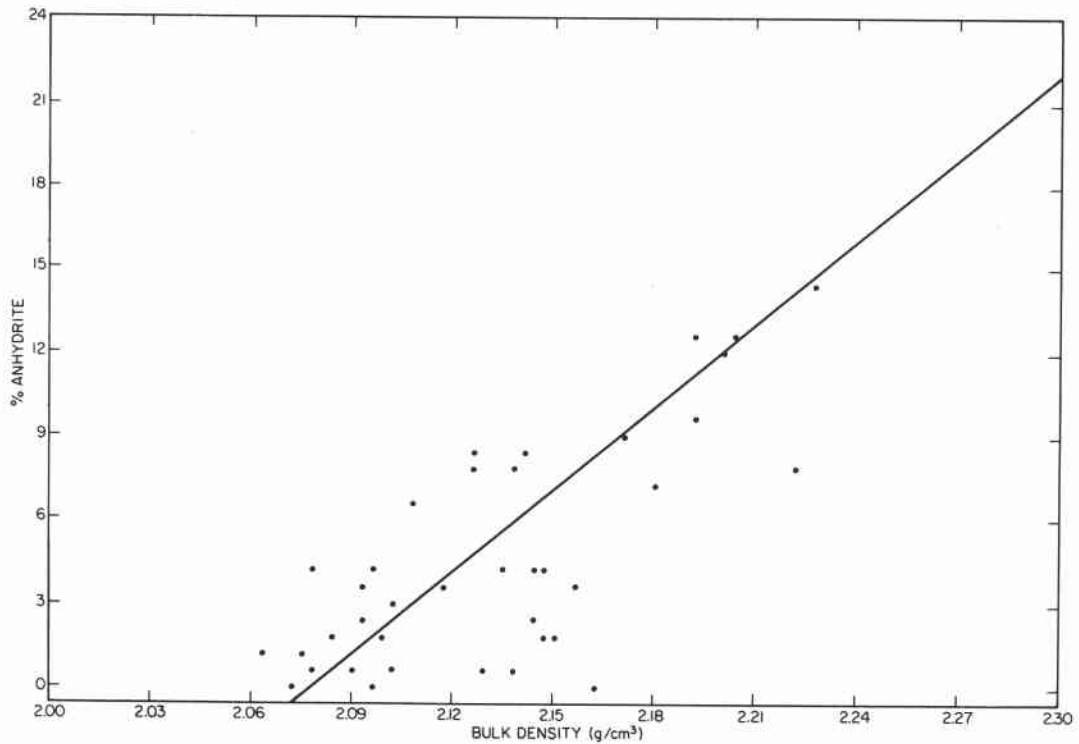


Figure 78. Bulk density correlated with anhydrite content.

## TRAPPING MECHANISMS OF OIL IN THE SAN ANDRES FORMATION, NORTHERN SHELF OF THE MIDLAND BASIN

Paul J. Ramondetta

*Large amounts of oil are trapped in a discontinuous, structurally high and stratigraphically thin belt that rims the deep Midland Basin and overlies older shelf margins. Additional oil is trapped in a series of steplike updip porosity pinch-outs having little or no structural control.*

Nearly 13 percent of Texas oil production is from lower San Andres reservoirs on the Northern Shelf of the Midland Basin (figs. 79 and 80) (Railroad Commission of Texas, 1981). Oil that is produced from San Andres dolomites is not indigenous to the San Andres but has migrated onto the Northern Shelf from deep Wolfcampian basinal shales. This migration occurred mostly through vertical fractures along the Abo Reef trend (Ramondetta, in press). It is important to assess San Andres oil and gas potential in the Palo Duro Basin, where San Andres salt deposits are being evaluated as a possible nuclear waste isolation repository.

The San Andres Formation over the Northern and Northwestern Shelves of the Midland Basin is a progradational unit consisting predominantly of carbonate facies. Lithofacies include dolomite, laminated anhydrite/dolomite, massive bedded anhydrite, limestone, salt, and red beds. These lithofacies represent depositional environments that include deep-water outer shelf, shallow-water inner shelf, shallow-water to emergent shoals, and a sabkha complex including intertidal to supratidal algal mud flats, hypersaline lagoons or brine pans, and terrigenously derived mud flats (fig. 81).

Deposition was cyclic; a cycle began with transgression, followed by a gradual shoaling-upward sequence. These cycles commonly ended with subaerial exposure before renewed transgression initiated a new cycle. Dolomitization and porosity development probably occurred during periods of subaerial exposure as a result of schizohaline environments (Folk and Land, 1975). Surface topography probably exerted considerable control on these processes. Additional diagenetic alteration of carbonates may have occurred as a result of an influx of hypersaline brine (Bein and Land, 1982).

Higher order cycles are also present within inner shelf dolomite units, as exhibited by rapid vertical fluctuations of porosity and permeability (fig. 82); this provides updip porosity pinch-out traps. The dolomites thicken to the south and coalesce south of the Matador Arch to form one thick, porous section (the major porosity zone, >300 ft) in the lower San Andres (fig. 83).

South and east of the Northern Shelf (inner shelf) was a discontinuous belt of shoals. Stratigraphic thinning along this structurally high belt (fig. 84) verifies that this belt was a topographic high. These shoals coincide with the location of the older (Strawn to Clear Fork) shelf margin positions (fig. 80). Differential compaction of shelf margin carbonates relative to basinal shales (source rocks) and landward sediments produced a hingeline and was probably responsible for the irregular depositional topography during San Andres time. This highly productive belt rims the outer shelf and was a depositional high, and hence, subject to longer periods of subaerial exposure. Such conditions could lead to a thicker porous zone along the shoals because of increased leaching of unstable carbonates (Todd, 1976; Hills, 1972) and dolomitization. In contrast, the deeper part of the shelf to the east was probably never exposed and consists mainly of relatively nonporous limestone (fig. 83). In general, structurally high areas tend to have thicker porosity zones.

Updip (west) of the shoal area, the San Andres evaporitic shelf was exposed less frequently than the shoals and thus has a thinner porous zone (underlain by nonporous limestone) and thicker sections of siliciclastics and anhydrite (Schneider, 1943; Chuber and Pusey, 1967). Deposition of nonporous anhydrite/dolomite and salt in southward-prograding sabkhas eventually capped the major porosity zone (fig. 83). Evaporitic minerals plugged porosity in the San Andres of the Palo Duro Basin (Handford and others, in press; Dunlap, 1967). For this reason, little or no San Andres oil production is anticipated north of the present limit of oil production. Attempts to extend the Yellowhouse-Littlefield trend farther north have been unsuccessful (fig. 85).

The nature of structural control ranges from subtle to very obvious (Ramondetta, in press b). Prolific San Andres and Clear Fork oil production exists in the large Wasson and Anton Irish structures (fig. 86); both of these domal structures exhibit closure greater than 100 ft (30.5 m). In contrast, a subtle, south-plunging anticline (striking NE.-SW.) controls production along the eastern margin of Slaughter and Levelland Fields; no San Andres production occurs east (basinward) of the anticline (fig. 86). This productive trend (which coincides with the position of the older Wolfcampian shelf margin [fig. 80]) continues northeast through Yellowhouse, Littlefield, and Illusion Lake Fields (figs. 85 and 86). Note the steeper basinward (southeastern) flank of this anticline, and note also the mild structural closure along the crest where entrapment occurs (fig. 85). Similar structural relations exist throughout the Northern and Northwestern Shelves, thus controlling some San Andres production (fig. 86). These structural trends are often associated with fractures, enhancing the reservoir potential. In other fields, such as Cato or the central and western parts of Levelland-Slaughter, only a slight nosing or regional dip alone is present (fig. 86).

Structural closure alone is insufficient to account for the thick oil columns observed in the Northern Shelf, as in Wasson and Reeves Fields (Chuber and Pusey, 1967). The presence of porosity pinch-outs updip from productive structures accounts for a large proportion of the trapped oil, especially in fields where no structures exist. The Levelland-Slaughter trend is caused by a steplike updip porosity pinch-out (fig. 87).

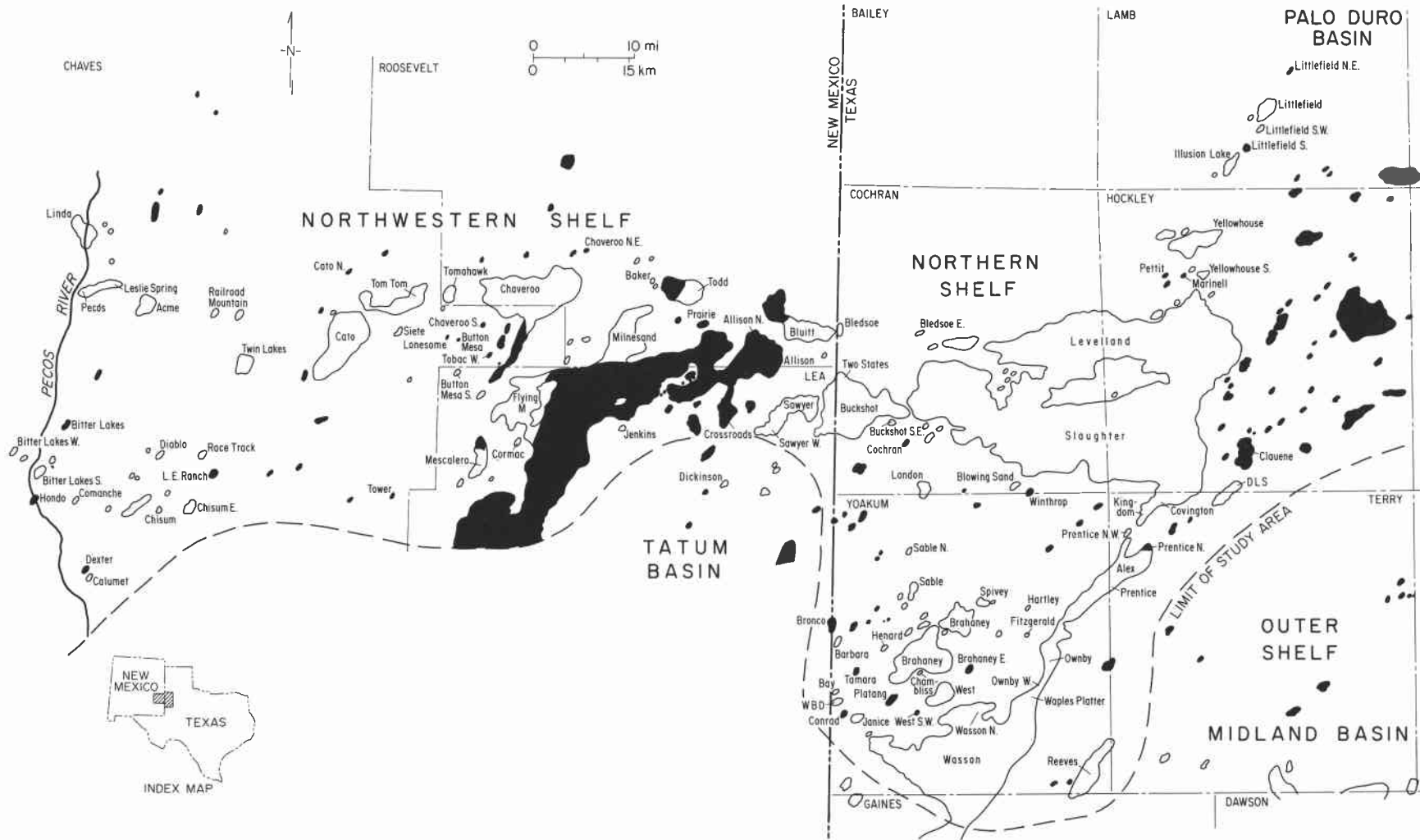


Figure 79. Map of the Northern and Northwestern Shelves showing oil fields and percent total cumulative oil production within each region.

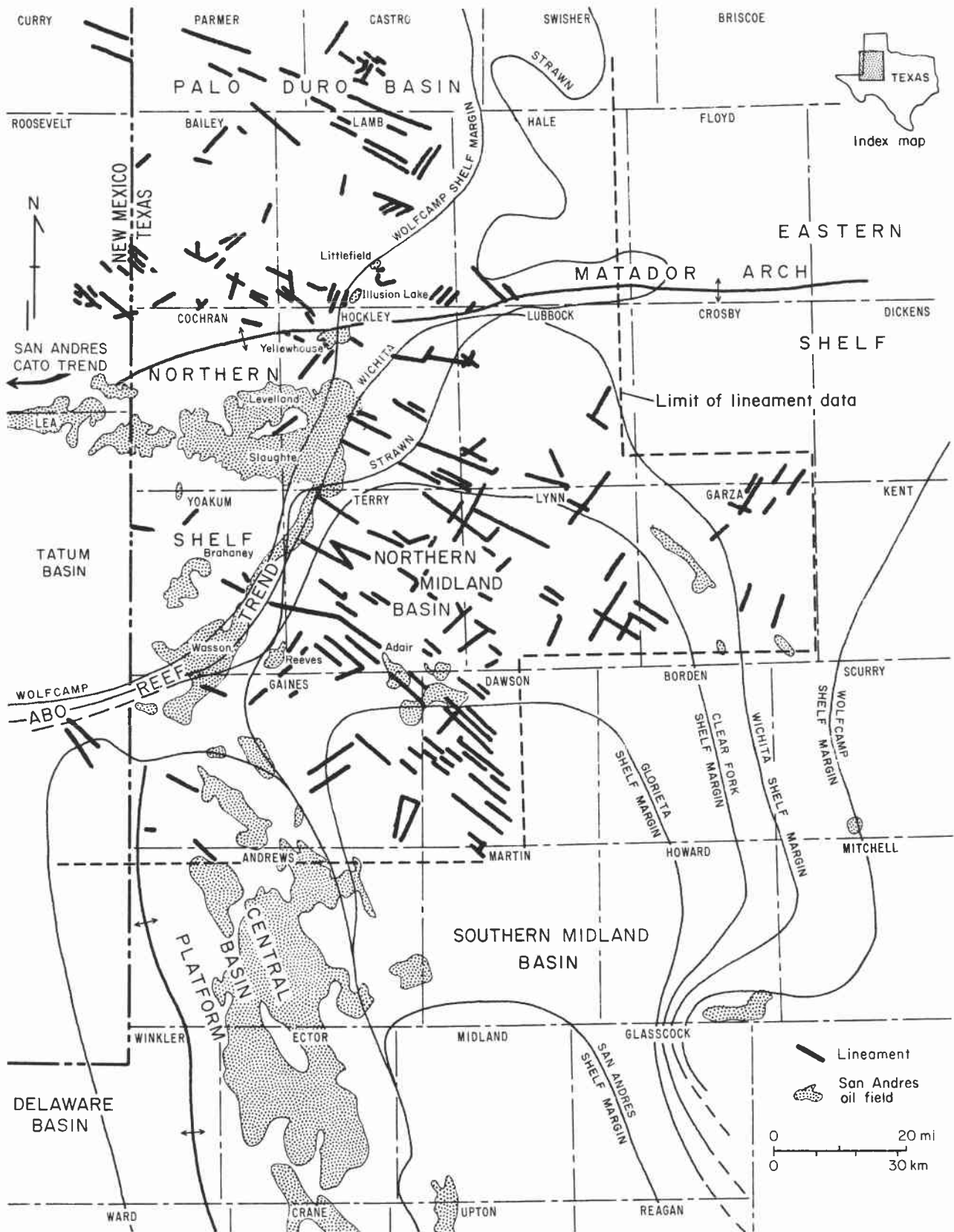


Figure 80. Map of study area in Texas showing San Andres oil production, shelf margins, and surface lineaments (from Finley and Gustavson, 1981).

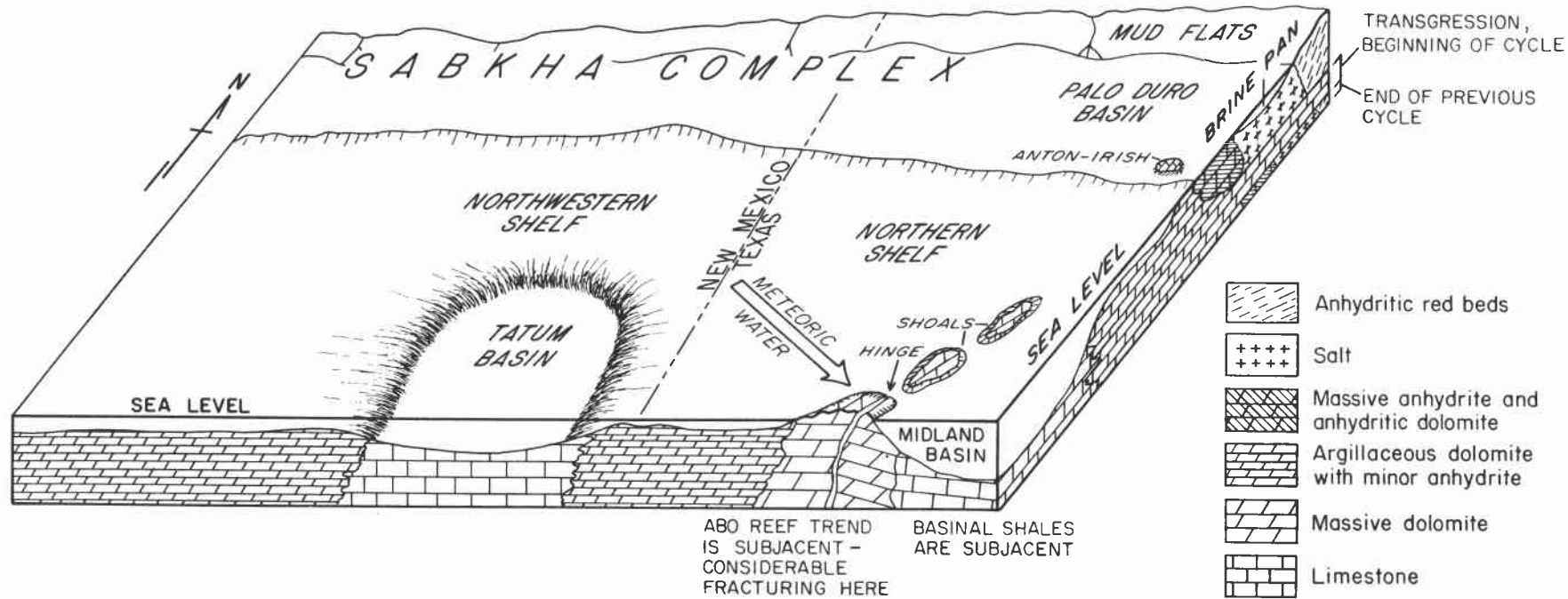


Figure 81. Schematic block diagram of depositional environments during a regressive depositional phase in early San Andres time.

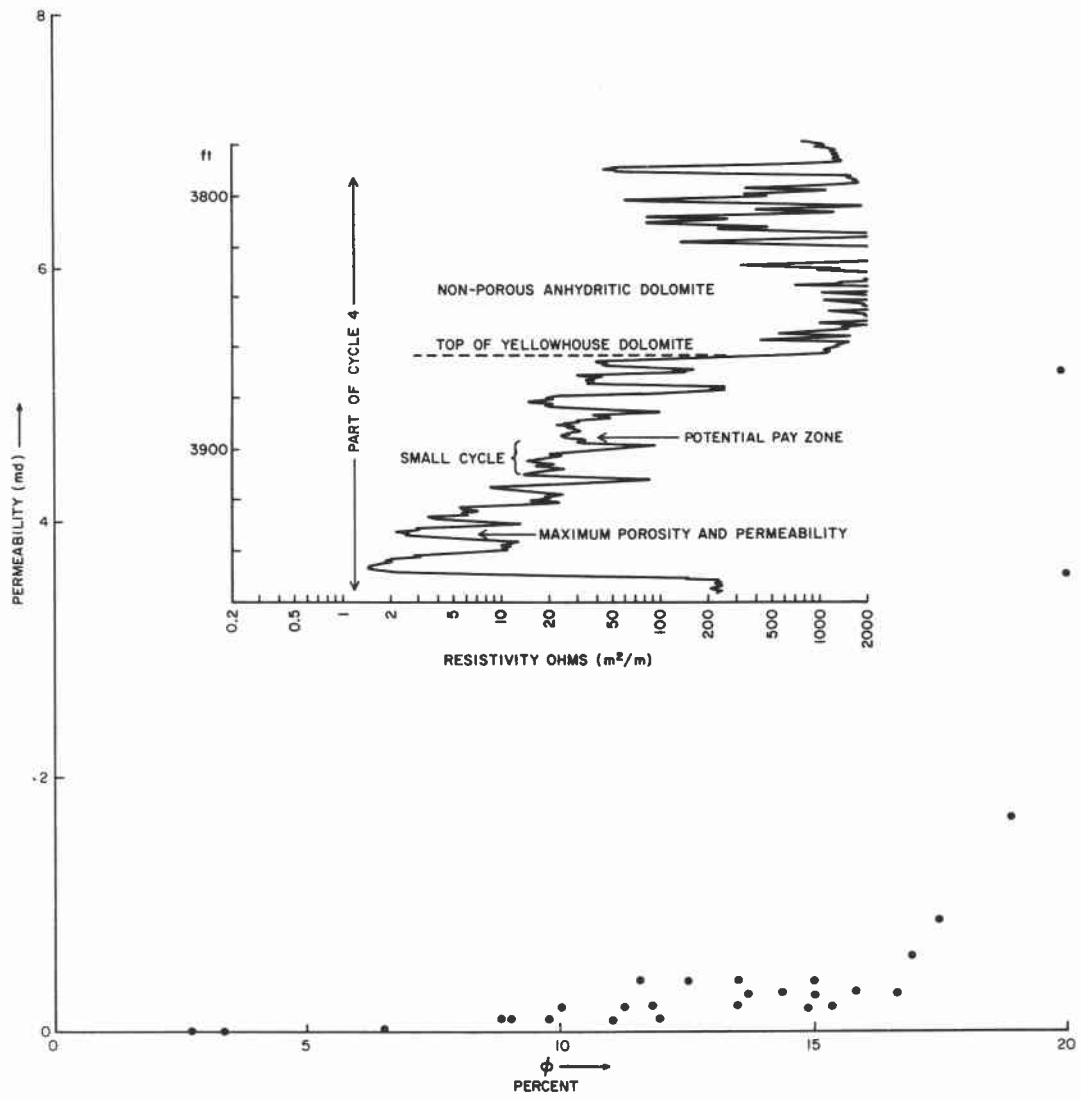
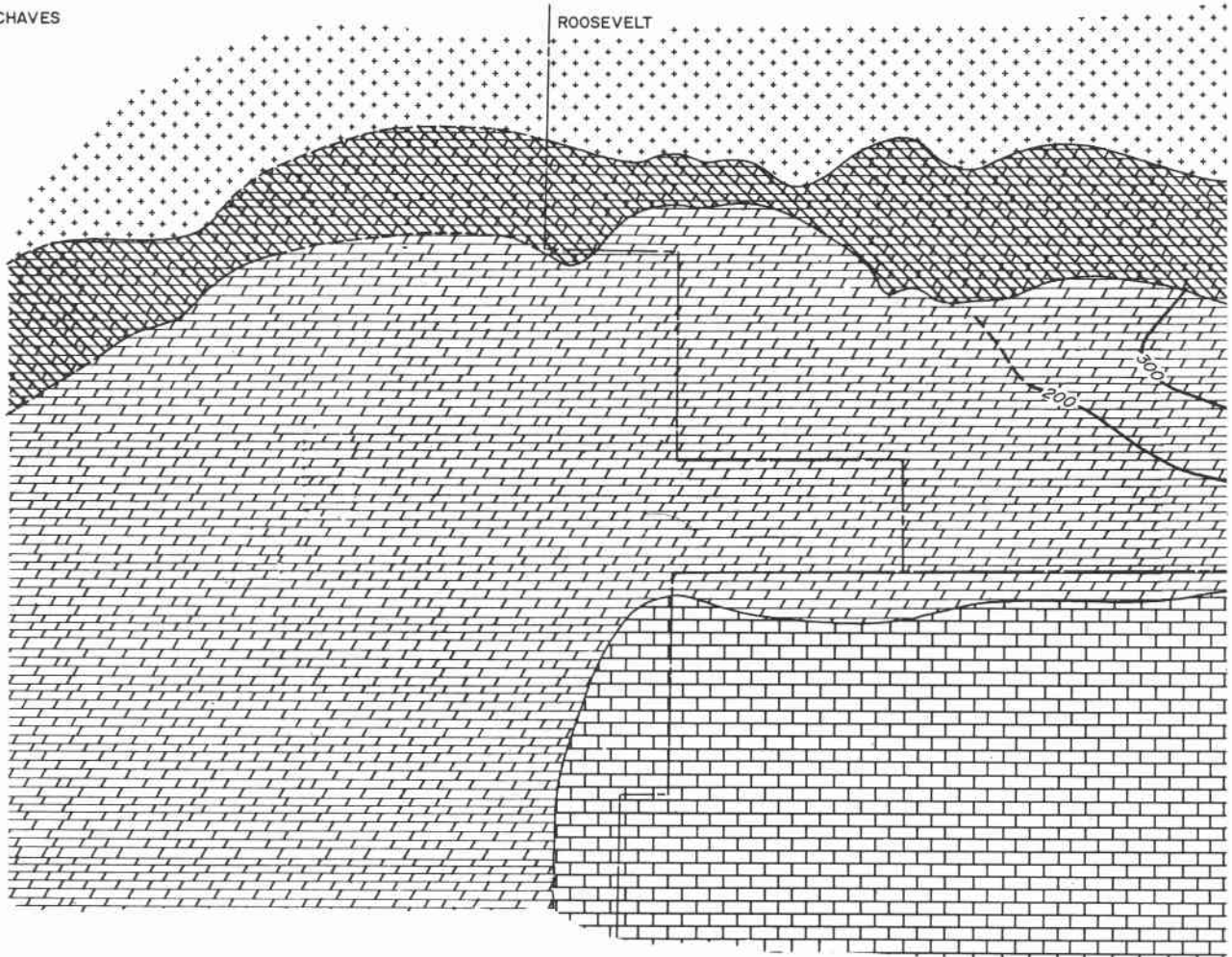


Figure 82. Plot of porosity versus permeability in the Yellowhouse dolomite; resistivity log of same interval is included, Littlefield Northeast field, Lamb County, Texas.

CHAVES

ROOSEVELT



EXPLANATION

-  Continuous thickness of major porosity zone
-  Cycle 4 salt is present
-  Major porosity zone is interbedded with cyclic nonporous anhydrite/dolomite strata
-  Porous argillaceous dolomite and minor anhydrite constitutes major porosity zone
-  Porous massive dolomite constitutes major porosity zone
-  Nonporous limestone is dominant lithology in the lower San Andres

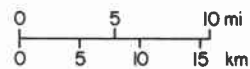


Figure 83. Distribution of lithofacies during much of early San Andres time. The thickness of the major porosity zone is also shown.

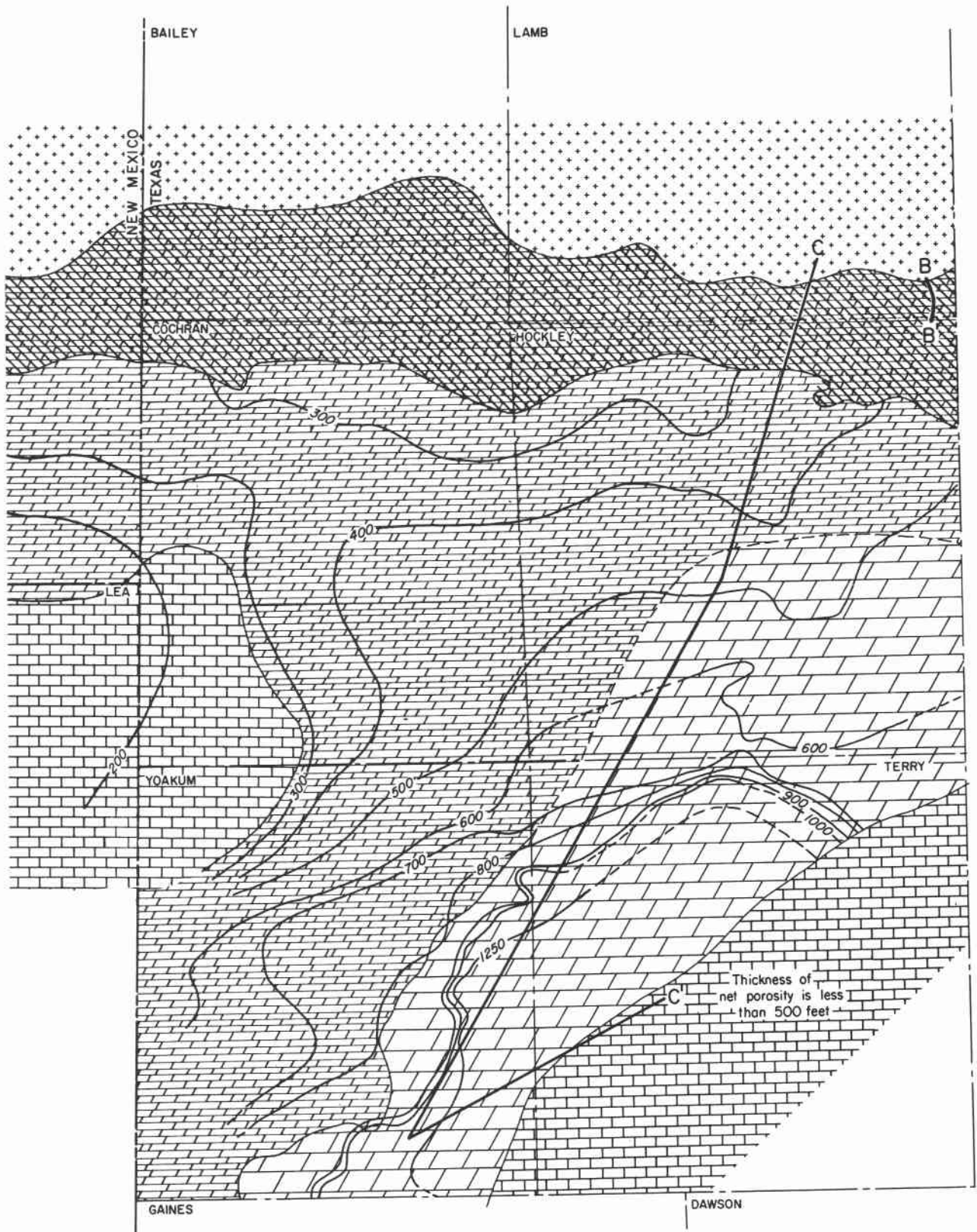
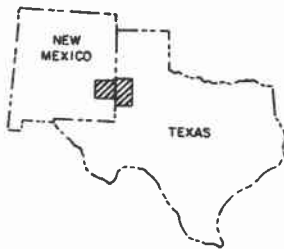
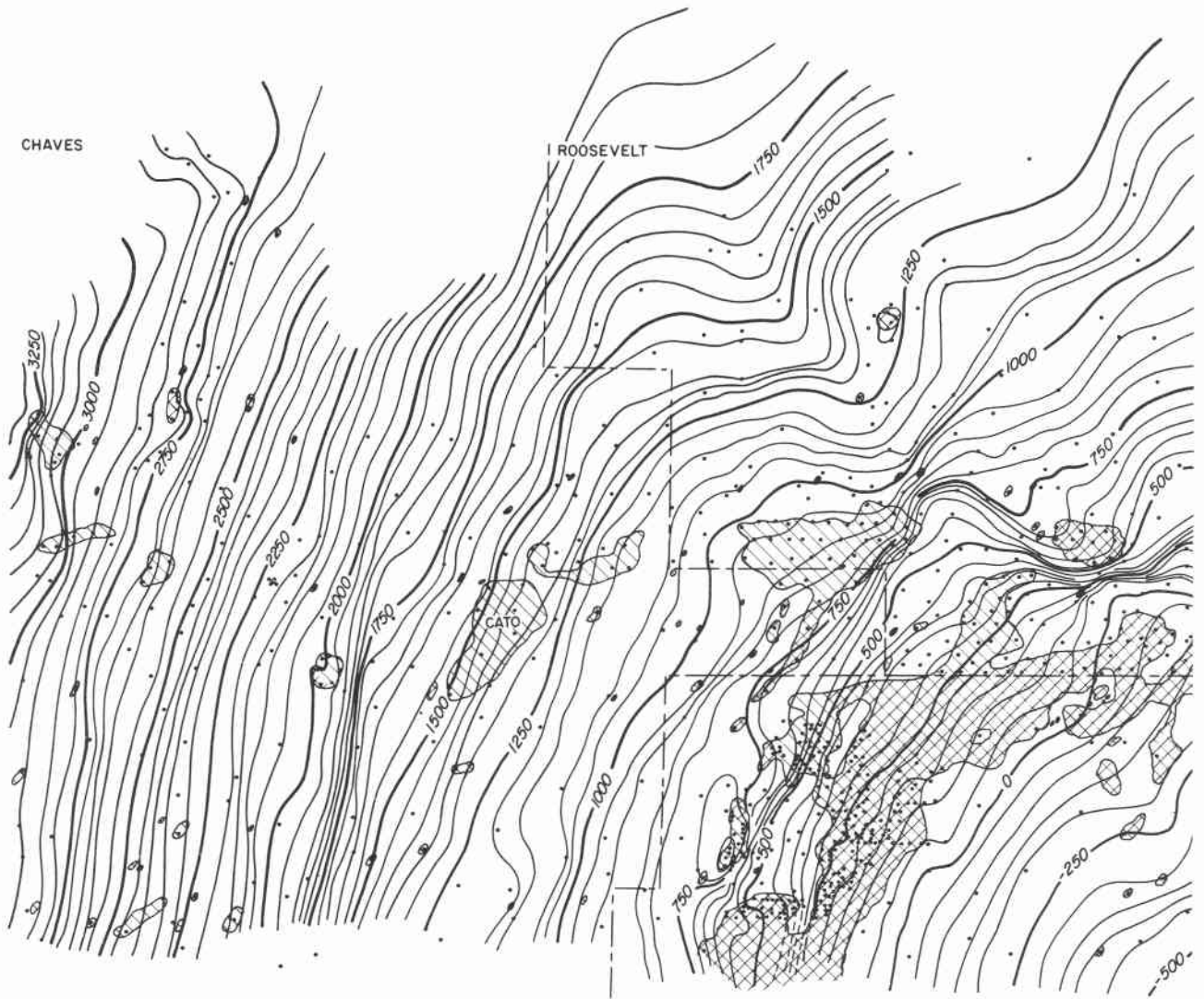


Figure 83 (continued)



INDEX MAP

- EXPLANATION**
- Control well
  - San Andres oil production
  - Pre-San Andres oil production
- Contour interval = 50 ft

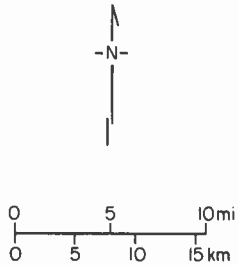
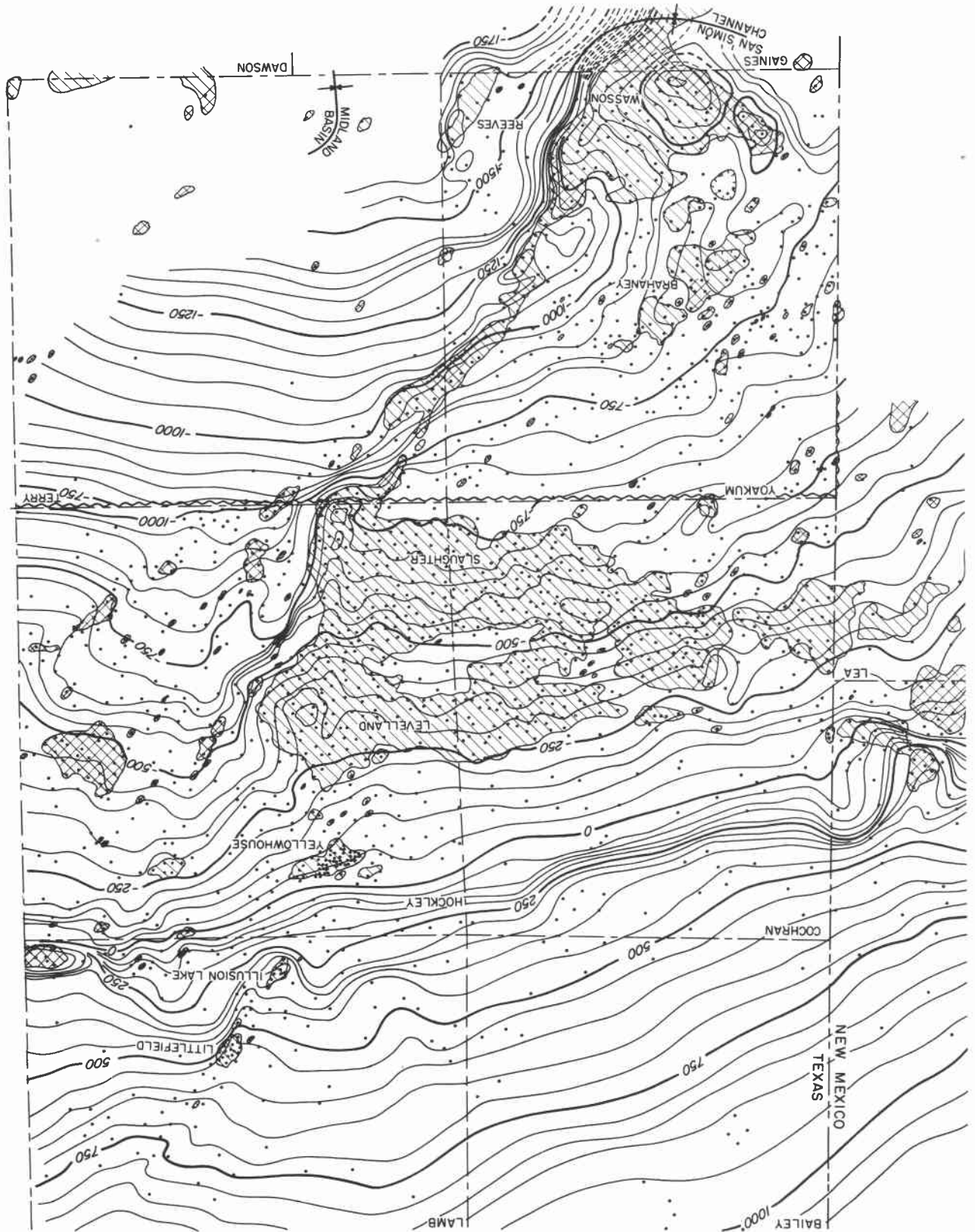


Figure 84. Structure map, top of San Andres Formation.

Figure 84 (continued)



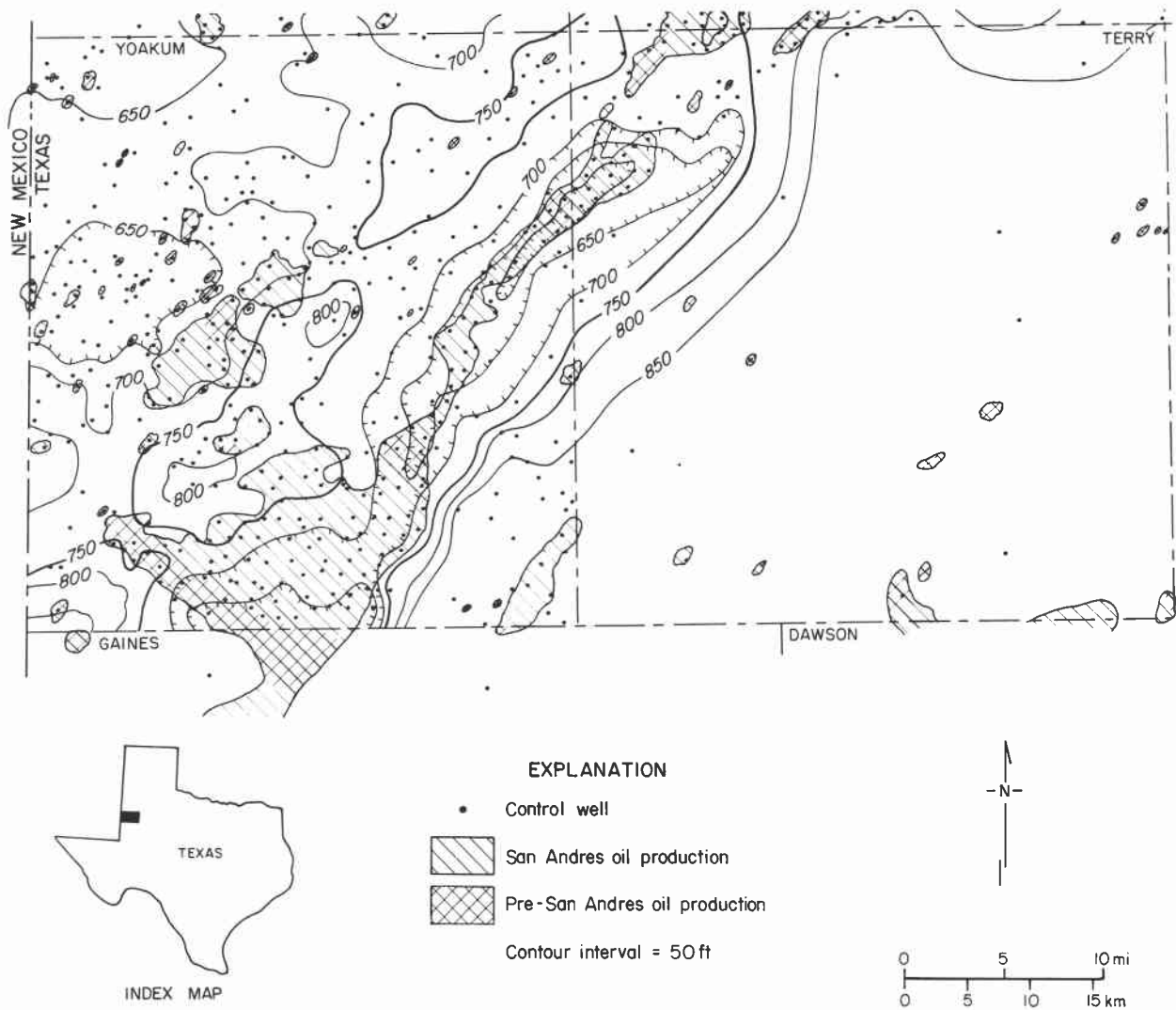


Figure 85. Isopach map, upper San Andres Formation, Yoakum and Terry Counties, Texas.

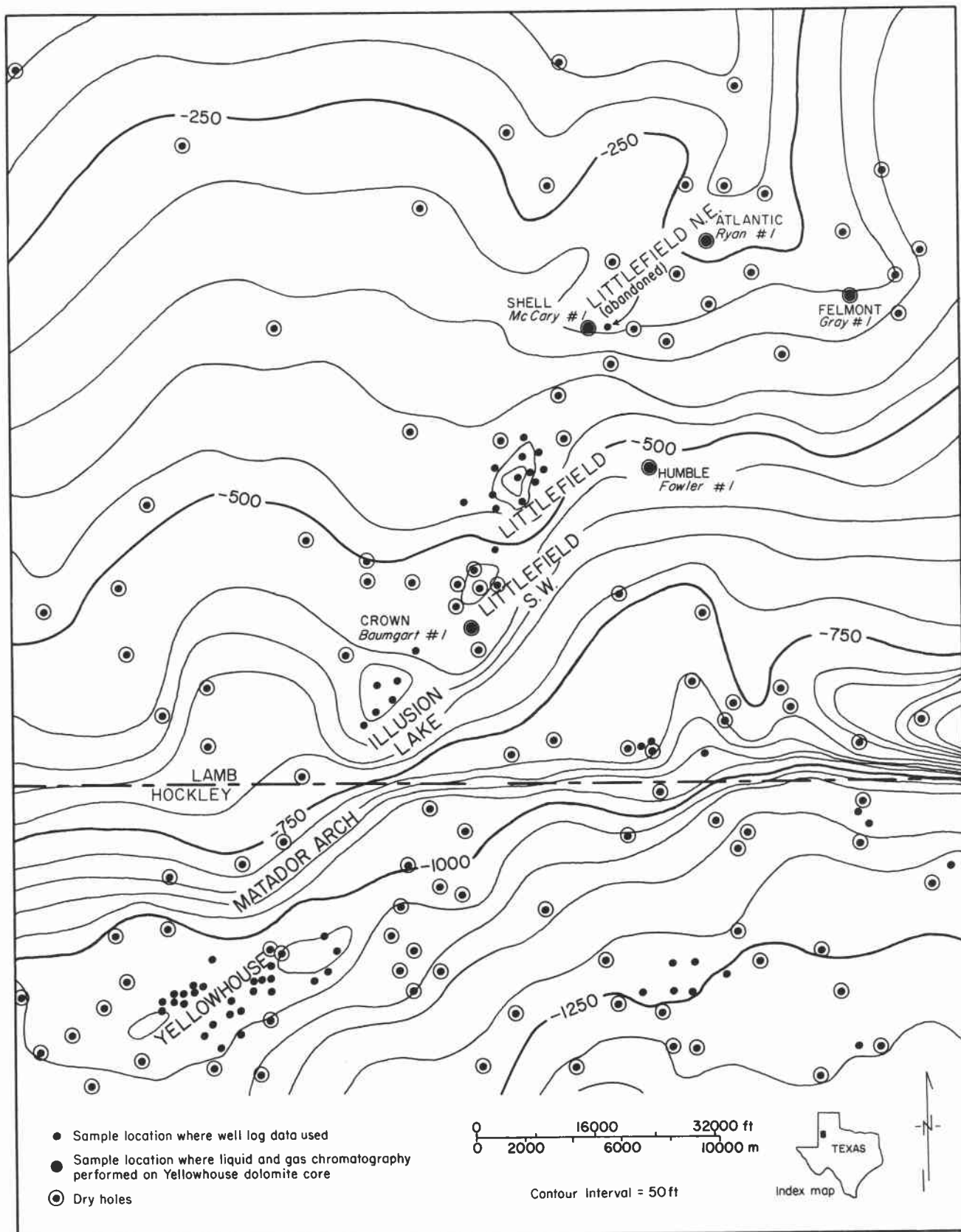


Figure 86. Structure map, top of Yellowhouse dolomite, San Andres Formation, northern Hockley and southern Lamb Counties, Texas.

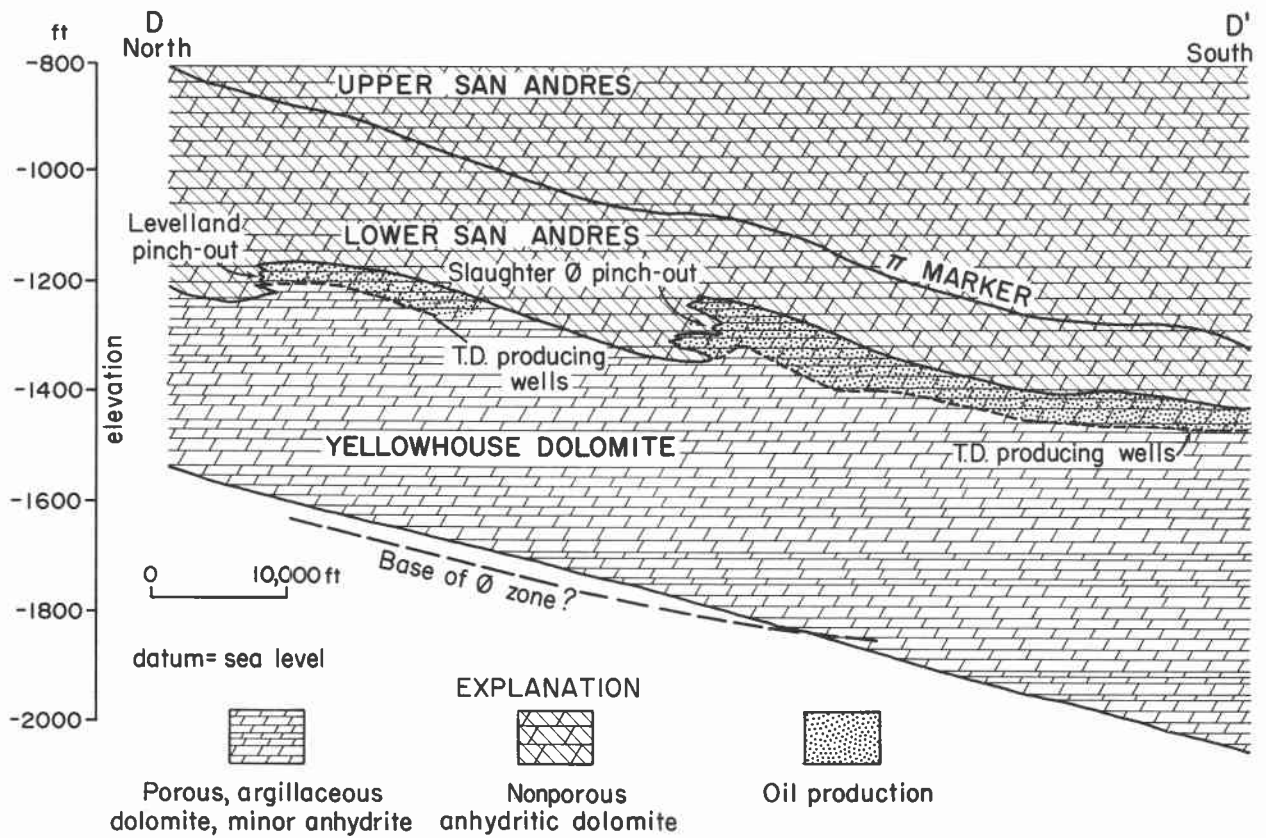


Figure 87. North-south cross section of San Andres Formation across Levelland and Slaughter fields, Texas.

## PERMEABILITY OF WOLFCAMP CARBONATES

R. L. Bassett, D. A. Smith, and M. E. Bentley

*Permeability estimated from analysis of drill-stem-test charts ranges from 0.03 to 44.0 md in the Wolfcamp carbonates. The range of 1 to 10 md probably is representative of average permeability of carbonates in the region except for zones along the dolomitized shelf edge, where porosity is extremely high and permeabilities may consistently average greater than 100 md.*

Hydraulic head data for deep aquifers in the Palo Duro Basin are available almost exclusively from in situ testing of formation pressure during petroleum exploration activities. A regional head map was constructed for the Wolfcamp aquifer by analyzing shut-in pressure data from drill-stem-tests (DST's) conducted during the previous few decades (Bassett and Bentley, in press). Abbreviated DST reports are tabulated for large regions of the nation and are available from commercial data bases.

Hydraulic parameters such as permeability or transmissivity are not included in commercial data compilations; however, they can be approximated from a detailed analysis of the DST chart or measured directly on core material. The DST charts for wells of interest were requested from operators who had worked in the Palo Duro Basin. Unfortunately, most of the tests were conducted years ago, and the records were not always transferred as leases and companies changed ownership. Of the scores of charts received, only 19 tests (table 3) for the Wolfcamp carbonates were adequate for a pressure buildup analysis using the Horner method. Certainly these few values (fig. 88) are insufficient for an accurate description of permeability distribution in the basin; however, they probably represent a reasonable sampling, on the high side, of the permeability one could expect from the Wolfcamp carbonates. The wells were drilled for exploration; consequently, the horizons tested generally will be the more permeable targets suspected of containing hydrocarbons. The majority of the DST charts are for pre-Wolfcamp formations, and they will be analyzed in the near future for a more complete understanding of flow through the basin. Results presented here are for only the Wolfcamp carbonates.

An alternate source of permeability data is direct analysis of cores in the laboratory. Results of laboratory analysis of core from three wells, two in Hartley County and one in Carson County, are given in table 4. Permeability values obtained in this fashion are strongly constrained by sample size, method of handling, and analytical procedure; other workers should be consulted concerning the applicability of such data to field conditions (Johnson and Beeson, 1944; Reeve, 1953; McNeal and Coleman, 1966).

One serious source of error is the preselection against fractures that may actually provide substantial permeability. Cores are usually selected because they are consolidated and maintain integrity; consequently, broken and fractured core is not tested. The laboratory values are for zones with intercrystalline and vuggy porosity. There is no information to determine if this kind of void space exerts a more significant influence on permeability than do fractures in the intervals tested.

#### Analysis of Error

A DST is a transient pressure test; consequently, accurate information is required on the change in pressure with time, the quantity of fluid produced, the interval tested, and the location of gages. The test usually includes a brief production period, a short shut-in period allowing the formation pressures to begin recovering, and longer production and shut-in periods to complete the test. Mechanical problems, such as poor seating of packers, plugging of perforations in the tool; drill-pipe leakage, sticking valves, and malfunctioning clocks and pressure gages, can all cause a test failure or contribute to error in the results. The pressure-time data are analyzed with a semi-log plot (Horner, 1951), and the straight line section of the plot corresponds to predicted theoretical behavior. The slope ( $m$ ) of the linear part of the plot is frequently determined by only a few points and, therefore, may not be well constrained. Ambiguity such as this may also contribute to error in the computation of permeability (fig. 89). The ISIP or FSIP subscript denotes whether the analysis was done on the initial or the final shut-in pressure data.

$$k = \frac{(162.6)(Q)(\mu)}{(m)(h)}$$

- $k$  = average permeability (md)
- $Q$  = flow rate (bbl/day)
- $\mu$  = viscosity (cp)
- $m$  = slope of the Horner Plot (psi)
- $h$  = interval thickness (ft)

A second serious error may occur in computing  $Q$ , which depends on the quantity of fluid produced during the flowing period of the test. Fluid recovery is estimated from the first observance of fluid as the drill string is broken down, thereby introducing the uncertainty of the quantity of fluid that drains onto the derrick floor from above the joint. An alternative scheme is to compute recovery from the hydrostatic pressure within the pipe; however, fluid height (and consequently volume) will depend on density, which varies with mud, hydrocarbon, and brine content.

Although there are several sources of error in the estimation of permeability, the propagated error for one test is smaller than the range of permeabilities computed for the Wolfcamp strata. These estimates are probably representative of the average permeability for the intervals tested and are accurate to an order of magnitude. A histogram of the permeability variation in the Wolfcampian carbonates is shown in figure 90.

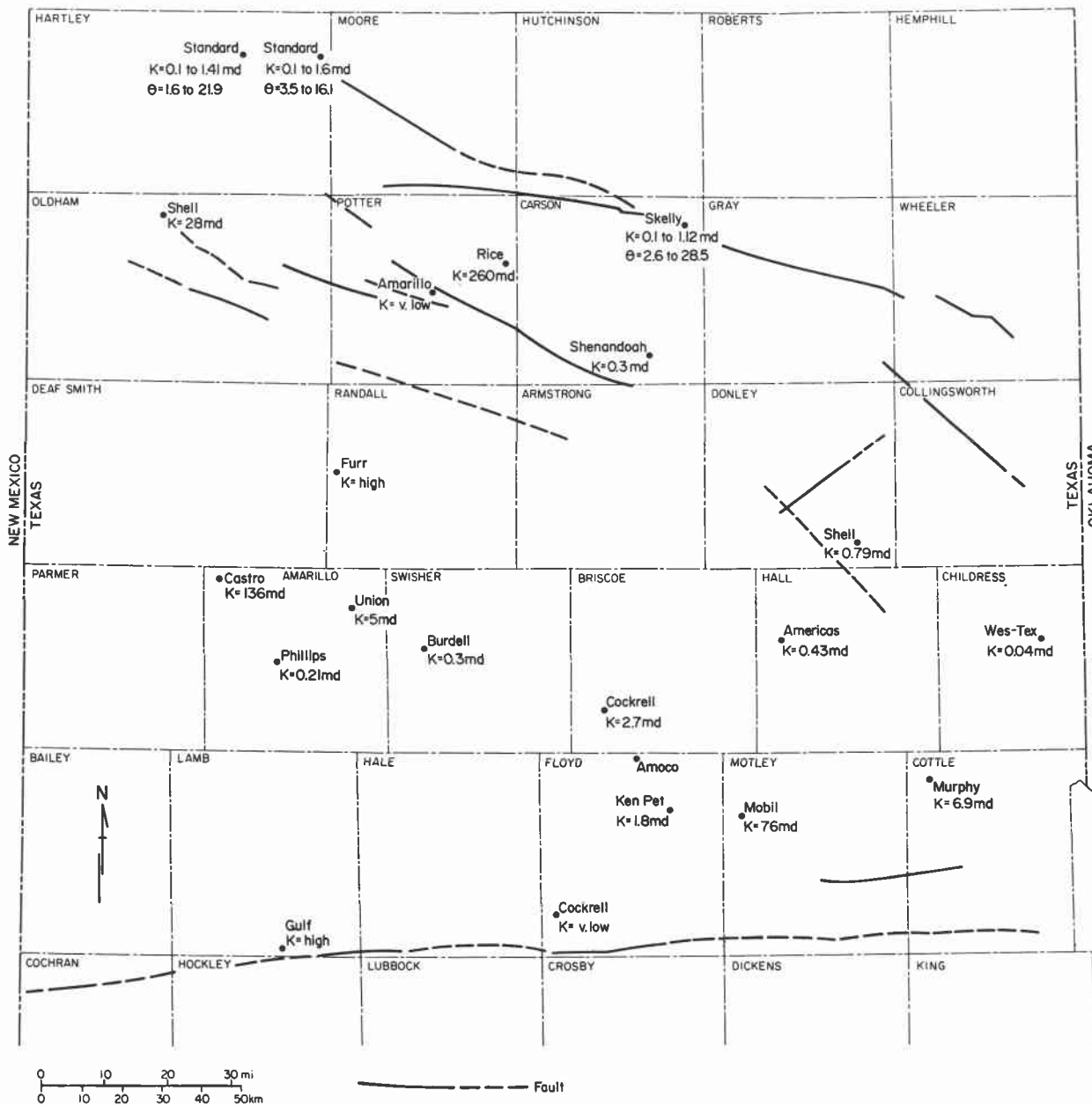


Figure 88. Permeability of carbonate rocks in the Permian Wolfcamp Series. Structure data from Goldstein (this report). Permeability data are tabulated in tables 3 and 4.

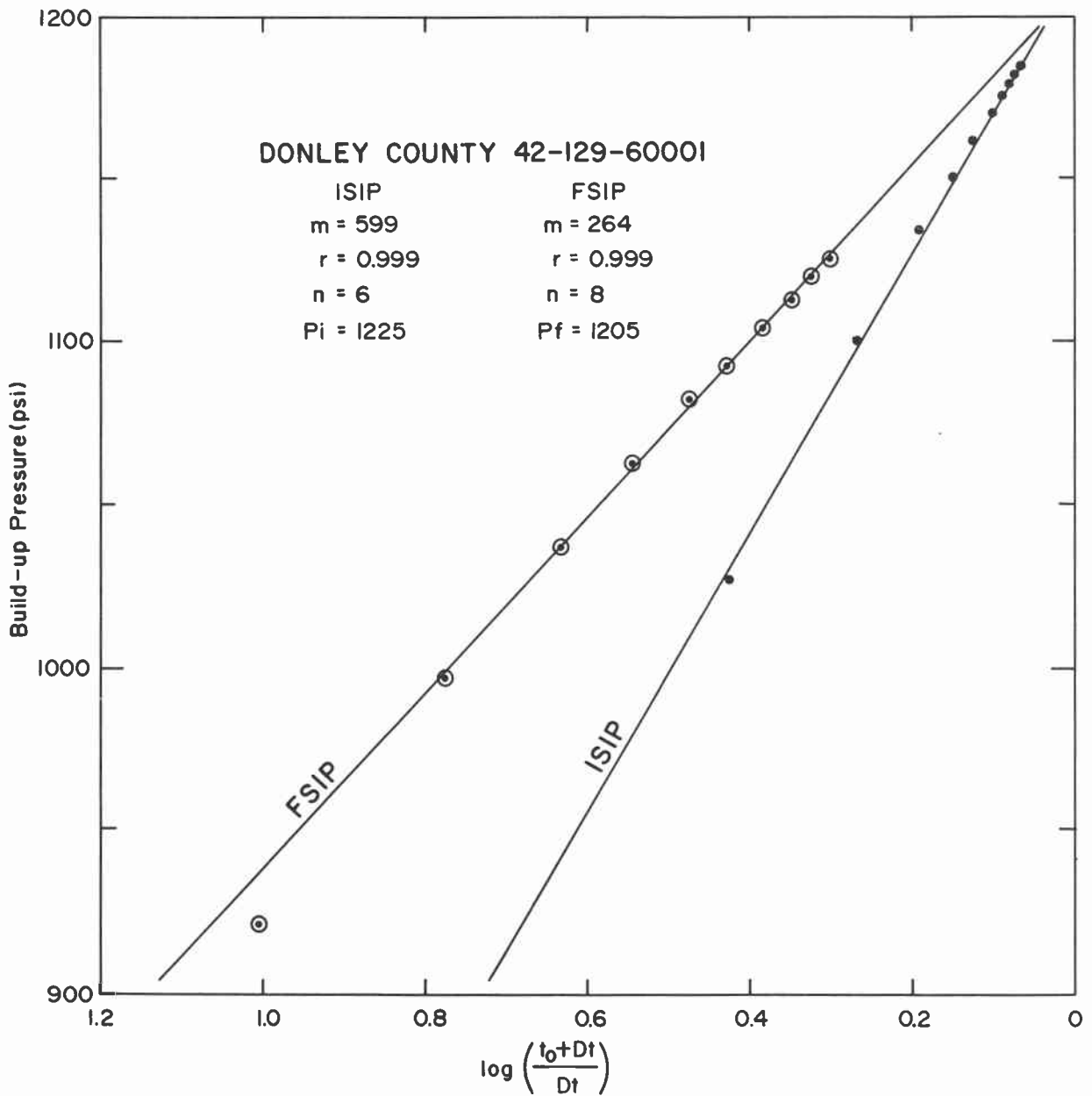


Figure 89. Pressure buildup analysis using the Horner (1951) method. Data for this example are from a DST on a well in Donley County. The buildup pressure is plotted against the logarithm of time elapsed ( $t_0$  = length of time for previous flowing period,  $Dt$  = elapsed time in the buildup test). Additional information on the well and the computed permeabilities are given in table 3.

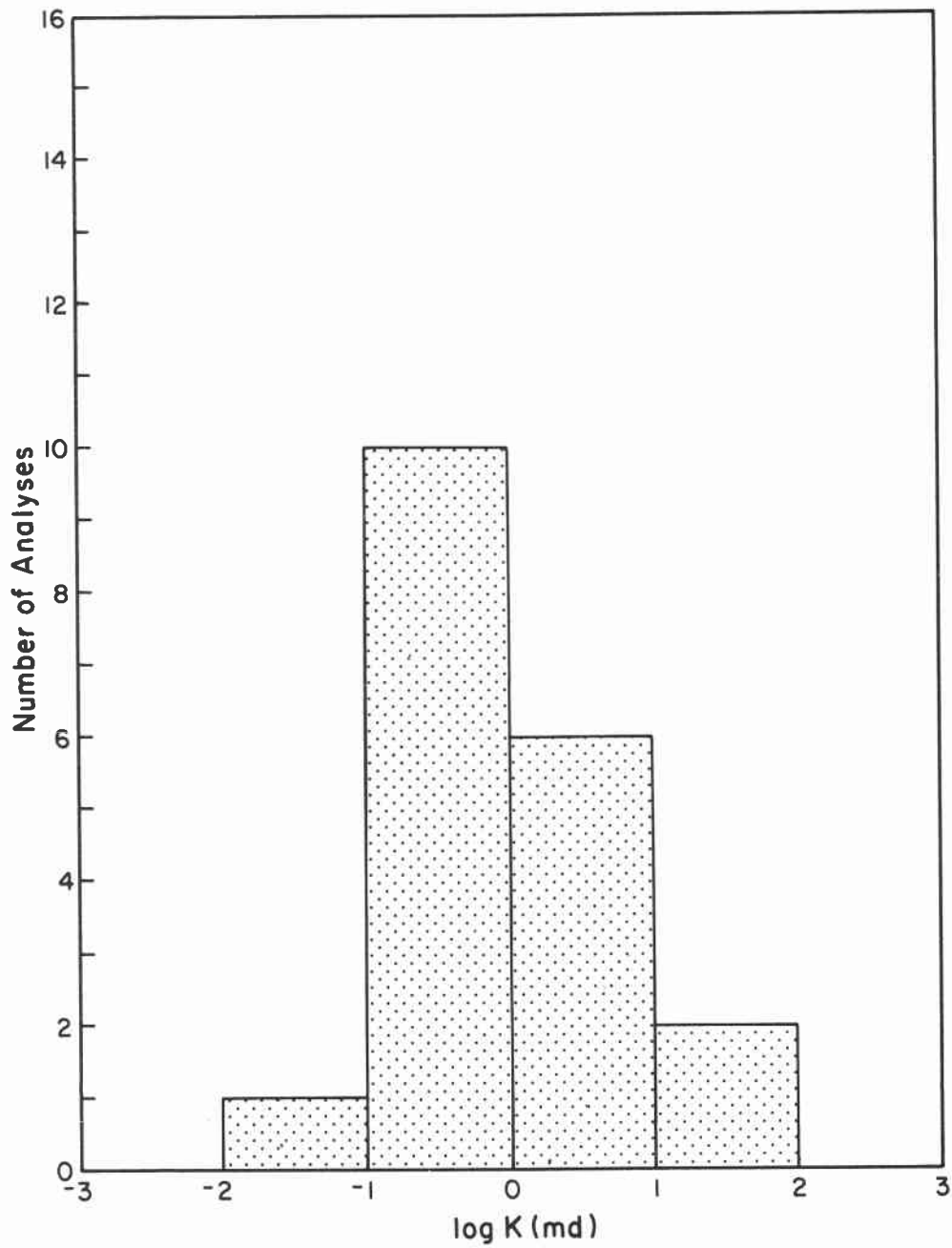


Figure 90. Frequency distribution of the effective permeability in Wolfcamp carbonates determined by analysis of 19 drill-stem-test charts. Data range from 0.03 to 44 md, with a mean of 5.3 md and a median of 0.77 md (table 3).

Table 3. Hydraulic parameters derived from an analysis of drill-stem-tests charts using the Horner method (1951). The selected permeability and hydraulic values are underscored in the table. From Bassett and Bentley (in press).

| County name | BEG well no. | Company    | API no.      | Depth tested (ft) | Thickness (ft) | K <sub>ISIP</sub> (md) | K <sub>FSIP</sub> (md) | H <sub>ISIP</sub> (ft) | H <sub>FSIP</sub> (ft) | Comments†††                              |
|-------------|--------------|------------|--------------|-------------------|----------------|------------------------|------------------------|------------------------|------------------------|--|
| Briscoe     | 21           | Cockrell   | 42-045-30001 | 6,344-6,411       | 67             | 8.5                    | <u>1.31</u>            | <u>3,105</u> †         | 2,964†                 | L. Wfc. shelf**                          |
| Carson      | 38           | Shenandoah | 42-065-30182 | 3,601-3,615       | 14             | 1.1                    | <u>0.24</u>            | <u>1,551</u>           | 1,551                  | M. Wfc. back shelf**                     |
| Castro      | 1            | Amarillo   | 42-069-60003 | 6,909-7,059       | 150            | <u>64.0</u>            | <u>26.0</u>            | 2,500                  | 2,505                  | M. Wfc. por. dol.                        |
| Castro      | 7            | Union      | 42-069-60014 | 5,183-5,228       | 45             | <u>6.0</u>             | —                      | <u>2,750</u>           | —                      | T. Wfc. sl. por. (sabk.)                 |
| Castro      | 7            | Union      | 42-069-60014 | 5,838-5,932       | 94             | ***                    | ***                    | 2,206                  | 2,206                  | M. Wfc. chalky ls.                       |
| Castro      | 10           | Phillips   | 42-069-30002 | 6,762-6,782       | 20             | 0.36                   | <u>0.27</u>            | <u>2,560</u>           | 2,483                  | U. Wfc. sl. por. dol. ls. (sabk.)        |
| Childress   | 76           | Westex     | 42-075-60068 | 2,633-2,663       | 30             | 0.95                   | <u>0.03</u>            | <u>1,818</u>           | 1,781                  | U. Wfc. dol. and ls.**                   |
| Cottle      | 10           | Murphy     | 42-101-10217 | 3,169-3,178       | 9              | 15.5                   | <u>8.8</u>             | 1,867                  | 1,897                  | U. Wfc. sl. calc. dol. (sabk.)           |
| Donley      | 31           | Shell      | 42-129-60001 | 3,350-3,399       | 49             | 0.51                   | <u>0.79</u>            | 1,797                  | 1,754                  | U. Wfc. por. ls. (sabk.)                 |
| Floyd       | *            | Amoco      | 42-153-30194 | 5,500-5,581       | 81             | 8.9                    | <u>8.3</u>             | <u>2,081</u>           | 2,081                  | *  |
| Floyd       | *            | Ken Pet.   | 42-153-30008 | 4,660-4,750       | 90             | 0.68                   | <u>0.59</u>            | <u>3,597</u> ††        | <u>2,392</u> ††        | *  |
| Hale        | 6            | Mobil      | 42-189-10202 | 7,864-8,036       | 172            | 1.04                   | <u>0.1</u>             | 2,583                  | 2,461                  | L. Wfc. sl. por. ls. (?) may be U. Penn. |
| Hall        | *            | Americas   | 42-191-30001 | 3,365-3,390       | 25             | 0.62                   | <u>0.44</u>            | 1,890                  | 1,830                  | *  |
| Hartley     | 13           | Standard   | 42-205-35008 | 3,520-3,623       | 66             | <u>0.77</u>            | —                      | 1,381                  | —                      | T. Wfc. an. dol. (sabk.)                 |
| Hartley     | 13           | Standard   | 42-205-35008 | 3,824-3,890       | 66             | <u>1.0</u>             | —                      | 1,796                  | —                      | U. Wfc. dol. ls. (sabk.)                 |
| Hartley     | 13           | Standard   | 42-205-35008 | 4,896-4,940       | 44             | <u>0.24</u>            | —                      | 1,574                  | —                      | L. Wfc. calc. ss.                        |
| Hartley     | 16           | Standard   | 42-205-00023 | 3,916-3,957       | 41             | <u>1.75</u>            | —                      | 3,007                  | —                      | U. Wfc. dol. ls. (sabk.)                 |
| ***Lamb     | *            | Gulf       | 42-279-30045 | 7,352-7,404       | 52             |                        | ***                    | 2,522                  | 2,510                  | *  |
| ***Motley   | 13           | Mobil      | 42-345-00015 | 4,674-4,715       | 41             |                        | ***                    | 1,950                  | 1,947                  | U. Wfc. dol. (sabk.)                     |
| Oldham      | 4            | Shell      | 42-359-00026 | 3,446-3,471       | 25             | 27.0                   | <u>44.0</u>            | 1,945                  | 1,908                  | U. Wfc. **                               |
| Oldham      | 48           | Shell      | 42-359-30001 | 5,340-5,367       | 27             | 1.0                    | <u>0.6</u>             | 1,824                  | 1,741                  | M. Wfc. ls.                              |
| ***Potter   | 26           | Rice       | 42-375-35013 | 3,907-4,050       | 143            |                        | ***                    | 1,486                  | —                      | T. Wfc. por. dol.                        |
| Swisher     | 8            | Burdell    | 42-437-60012 | 5,765-5,796       | 31             | <u>0.1</u>             | —                      | 2,360                  | —                      | U. Wfc. por. ls.                         |

† The head values appear to be anomalously high compared with surrounding values; however, the test appears acceptable mechanically.

†† A 1,000-psi difference between ISIP and FSIP is not explainable at this time; the higher value is selected.

††† L. = lower, M. = mid, U. = upper, ls. = limestone, dol. = dolomite, por. = porous, sl. = slightly, T. = top, Wfc. = Wolfcamp, calc. = calcareous, sabk. = sabkha may have influenced dolomitization, Penn. = Pennsylvanian, an. = anhydritic.

\* no log information \*\*no sample log \*\*\*build-up test reached formation pressure; permeability cannot be computed.

— only one shut-in period.

Table 4. Permeability of core samples from the Wolfcamp Series.  
 (Data provided from Standard Oil and Skelly Oil Companies.)

| Location (Operator)     | Interval<br>(ft) | Number<br>of samples | Mean<br>k<br>(md) | St.<br>dev. | Variance | Min.<br>k<br>(md) | Max.<br>k<br>(md) |
|-------------------------|------------------|----------------------|-------------------|-------------|----------|-------------------|-------------------|
| <u>Hartley County</u>   |                  |                      |                   |             |          |                   |                   |
| Standard Oil (Johnston) | 3,556-3,623      | 38                   | 0.19              | 0.29        | 0.08     | <0.1              | 1.6               |
| Standard Oil (Lantham)  | 4,604-4,614      | 7                    | 15.8              | 38.0        | 1,245.0  | <0.1              | 102.0             |
| <u>Carson County</u>    |                  |                      |                   |             |          |                   |                   |
| Skelly (Shaffer Ranch)  | 2,709-3,049      | 243                  | 8.5               | 31.5        | 988.0    | <0.1              | 335.0             |

## PRELIMINARY MODELING OF GROUND-WATER FLOW NEAR SALT DISSOLUTION ZONES, TEXAS PANHANDLE

William W. Simpkins and Graham E. Fogg

*A two-dimensional finite-element ground-water model was constructed in the vertical plane along a stratigraphic cross section of Tertiary Ogallala Formation, Triassic Dockum Group, and Permian sediments in Swisher, Briscoe, Hall, and Childress Counties. Preliminary runs of the model suggest that the salt dissolution process is sustained by (1) downward flow of fresh ground water from the Ogallala aquifer into the salt dissolution zone, (2) eastward movement of resultant brine waters through transmissive dolomite/anhydrite beds of the Blaine Formation, and (3) discharge of the brine water to saline springs in topographically low areas. Discharge of brine waters from the model area via lateral subsurface flow is negligible compared with the magnitude of spring discharge.*

The rate and magnitude of subsurface salt dissolution in the Texas Panhandle are tied to the ground-water flow system, particularly at the margins of the Caprock Escarpment (fig. 91). A digital computer model was constructed to demonstrate the ground-water flow in the salt dissolution zone and to identify the most important hydrodynamic components of the salt dissolution process.

### Ground-Water Model

The ground-water model simulates two-dimensional ground-water flow in the vertical plane and is based on the stratigraphic cross section from Gustavson and others (1980) shown in figure 92. The model is oriented in the vertical plane to take advantage of the detailed stratigraphic framework provided by the cross section and to examine vertical components of ground-water flow. Vertical flow is particularly important because it is the mechanism by which the brines from salt dissolution are discharged to the surface at previously identified saline springs in the Rolling Plains region (U. S. Army Corps of Engineers, 1976).

The ground-water model used the computer program FLUMP, which employs a finite element, mixed explicit-implicit numerical scheme for solving linear and nonlinear subsurface water flow problems. The theory behind FLUMP was developed by Neuman and Narasimhan (1977) and applied to ground-water problems by Narasimhan and others (1977), Neuman and others (1977), Narasimhan and Witherspoon (1977), and Fogg and others (1979).

The finite-element mesh (fig. 93) was designed to accommodate reasonably the heterogeneities of the local stratigraphic system and to provide greatest accuracy near the Caprock Escarpment, where hydraulic gradients are steepest. Hydraulic

conductivities (K) of the various units were compiled from various sources (table 5). Most values were estimates of a range of K data from pumping tests. Where data were not available, K was estimated either by extrapolation from other data for units of similar lithology or by selection of a "typical value" from the literature (such as in Freeze and Cherry, 1979). Vertical K values (Kv) of the Upper Permian "mudstones" are not from field or lab tests but are based primarily on the fact that these units are horizontally stratified mudstones containing small amounts of sand. In this type of lithology, Kh/Kv should be large if fracture permeability is absent. The potential for fracture permeability in units east of the escarpment was probed by a stratigraphic test well that was drilled in Donley County. Early simulations with the model in which Kv = Kh in the mudstones yielded results that were unrealistic in that they indicated much more ground-water flow through the systems than would be possible given the rainfall amounts in the region. The K data cause more uncertainty in regard to the model than any other factor.

The upper boundary of the model is the water table based on water-level measurements in the region. Prescribed hydraulic head boundary conditions are imposed on the upper, left, and right boundaries. The lower boundary is a no-flow boundary, and thus we are assuming that any upward leakage out of the deeper units occurs at a negligible rate compared with the rate of flow that occurs in the model area. This appears to be a reasonable assumption.

## Results

Several preliminary simulations were made with the model to determine the sensitivity of the model to K variations. Hydraulic heads and recharge/discharge rates computed by the model using the values of K listed in table 5 are shown in figure 94. Unfortunately, ground-water flowlines cannot be drawn perpendicular to the hydraulic head contours in figure 94 because of anisotropic K values and the extreme vertical exaggerations. Effect of vertical exaggeration is greatest at the escarpment, where the vertical (downward) ground-water flow component in the model is substantial but the head contours seem to indicate only horizontal flow. Much of our preliminary interpretation of the results is therefore based on node-to-node fluxes printed in the model output listing.

The model suggests that the salt dissolution process is sustained by (1) downward flow of fresh ground water from the Ogallala aquifer into the salt dissolution zone, (2) eastward movement of resultant brine through transmissive dolomite/anhydrite beds of the Blaine Formation, and (3) discharge of the brine to saline springs in topographically low areas. This circulation pattern is, of course, based on several assumptions and may be

incorrect owing to errors in K values or to prescribed hydraulic head boundary conditions. However, not all the uncertainties are equally important to the results. Key uncertainties that may be of pivotal importance in determining the results of the model are (1) K<sub>v</sub> values in the vicinity of the Caprock Escarpment, (2) K<sub>v</sub> and K<sub>h</sub> values for the dolomite/anhydrite units, and (3) K<sub>v</sub> values of other units east of the Caprock Escarpment. The K<sub>v</sub> values from near the Caprock Escarpment are an important control on the rate and amount of fresh ground water introduced to Permian salt beds in the subsurface. The K<sub>h</sub> and K<sub>v</sub> values of the dolomite/anhydrite units east of the Caprock Escarpment govern how the brine waters from salt dissolution exit the ground-water flow system and how topography affects the ground-water flow system. Early simulations of the model in which K<sub>v</sub> values of the Permian mudstone units were unrealistically high depicted only local ground-water circulation cells on the Rolling Plains, wherein water was both locally derived and locally discharged. This was a result of the maximum effect of topography on the system. The saline springs discharge a mixture of both locally derived and deeper ground waters, as evidenced by geochemical and isotopic data (R. Bassett, personal communication, 1981).

In relation to calculations of salt dissolution rates by Gustavson and others (1980), the model indicates that nearly all ground-water discharge from the system can be accounted for by vertical discharge to saline springs, and that horizontal flow of brines out of the region is small. These conclusions support work by Gustavson and others (1980), who calculated salt dissolution rates partly on the basis of the assumption that most of the brine discharge from the system occurs through springs east of the Caprock Escarpment.

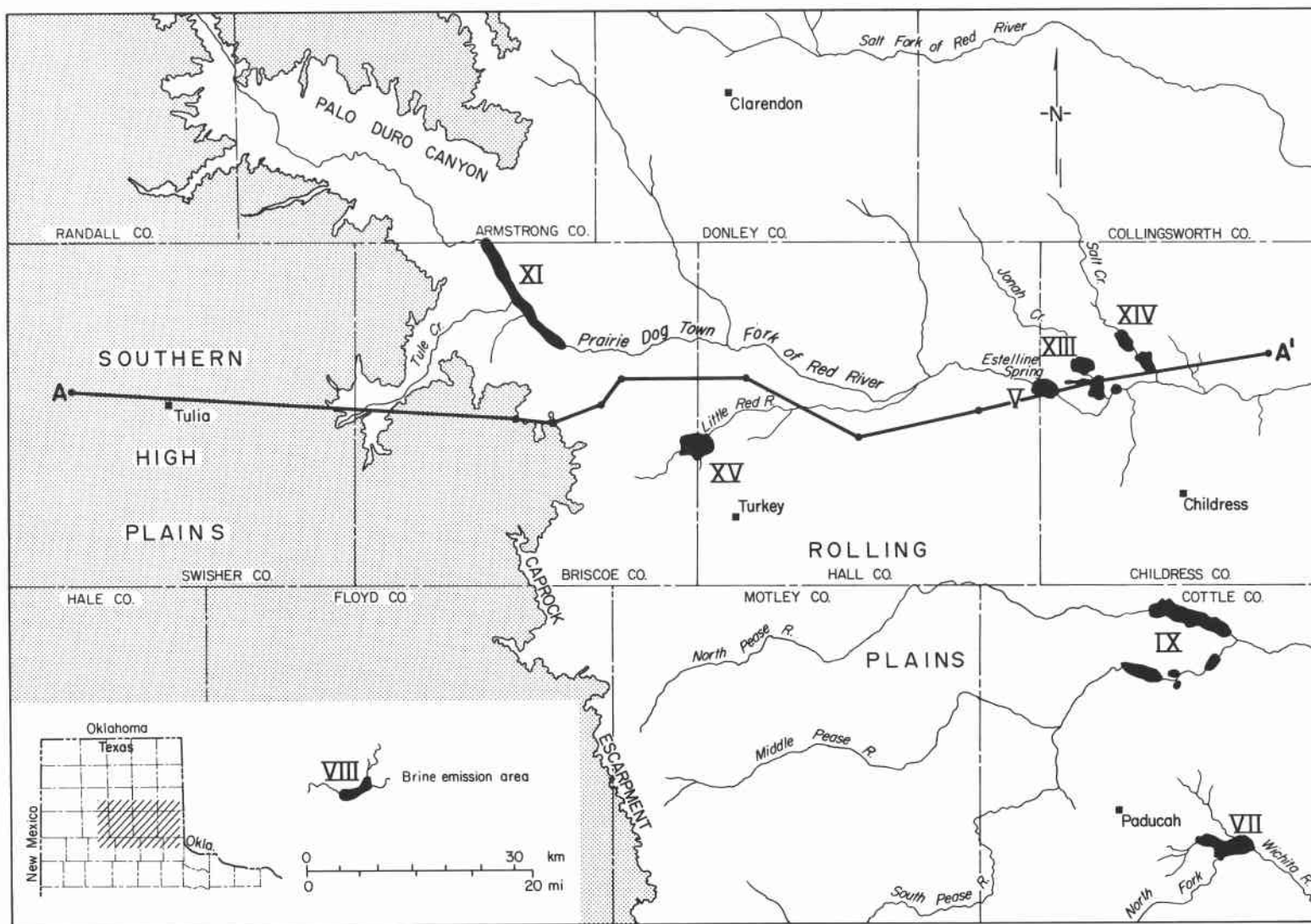


Figure 91. Map of physiographic units and major streams in the study area, Texas Panhandle. Line of section A-A' corresponds to the stratigraphic cross section in figure 93. Brine emission areas identified by the U.S. Army Corps of Engineers (1976) are designated by Roman numerals.

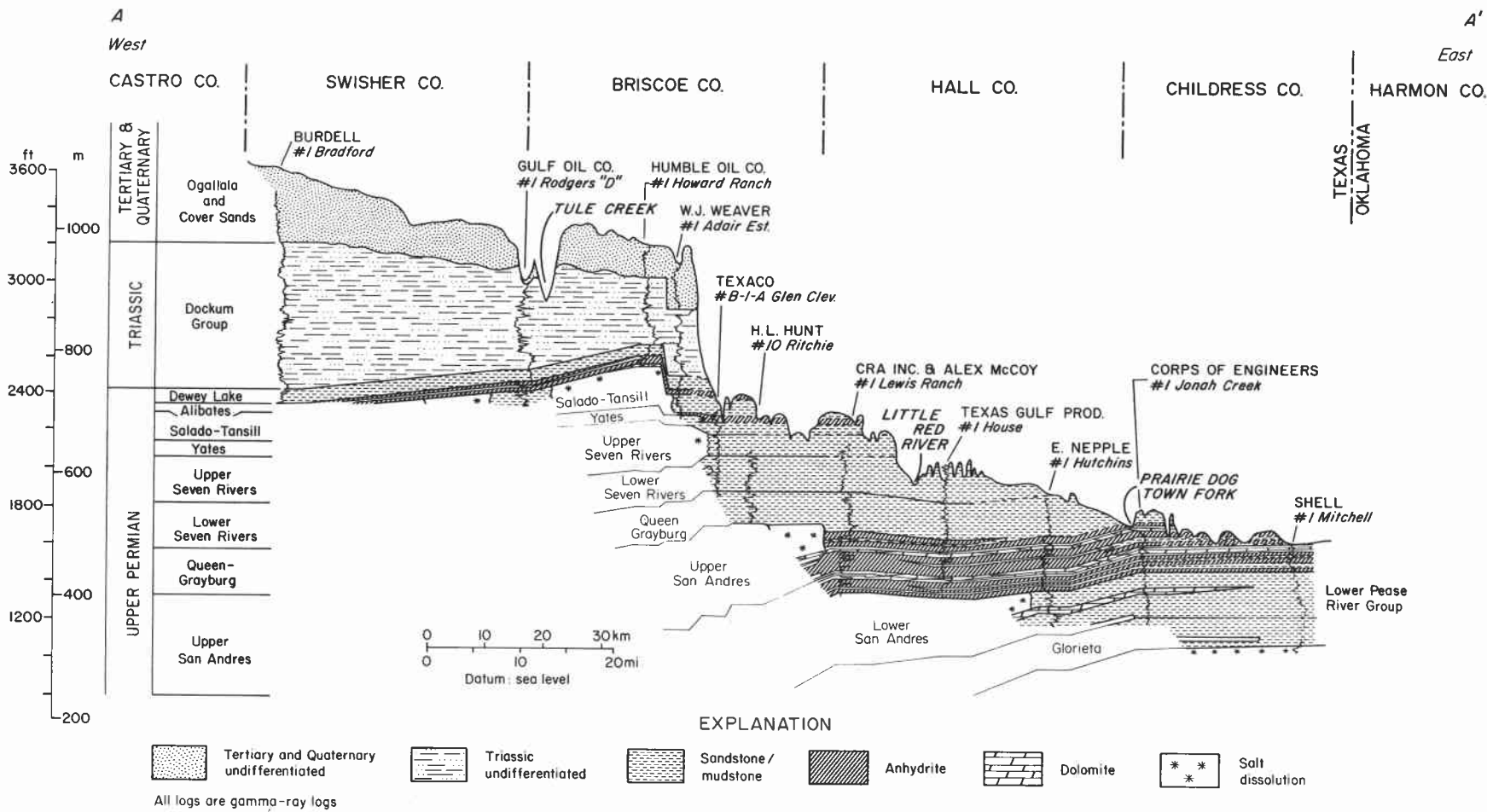


Figure 92. Stratigraphic cross section used for ground-water model. It extends from Briscoe County, Texas, eastward across the Rolling Plains Physiographic Province to the Oklahoma border (modified after Gustavson and others, 1980). Zones of salt dissolution form the lower boundary because units below dissolution are considered to be relatively impermeable. Cross section is located in figure 91.

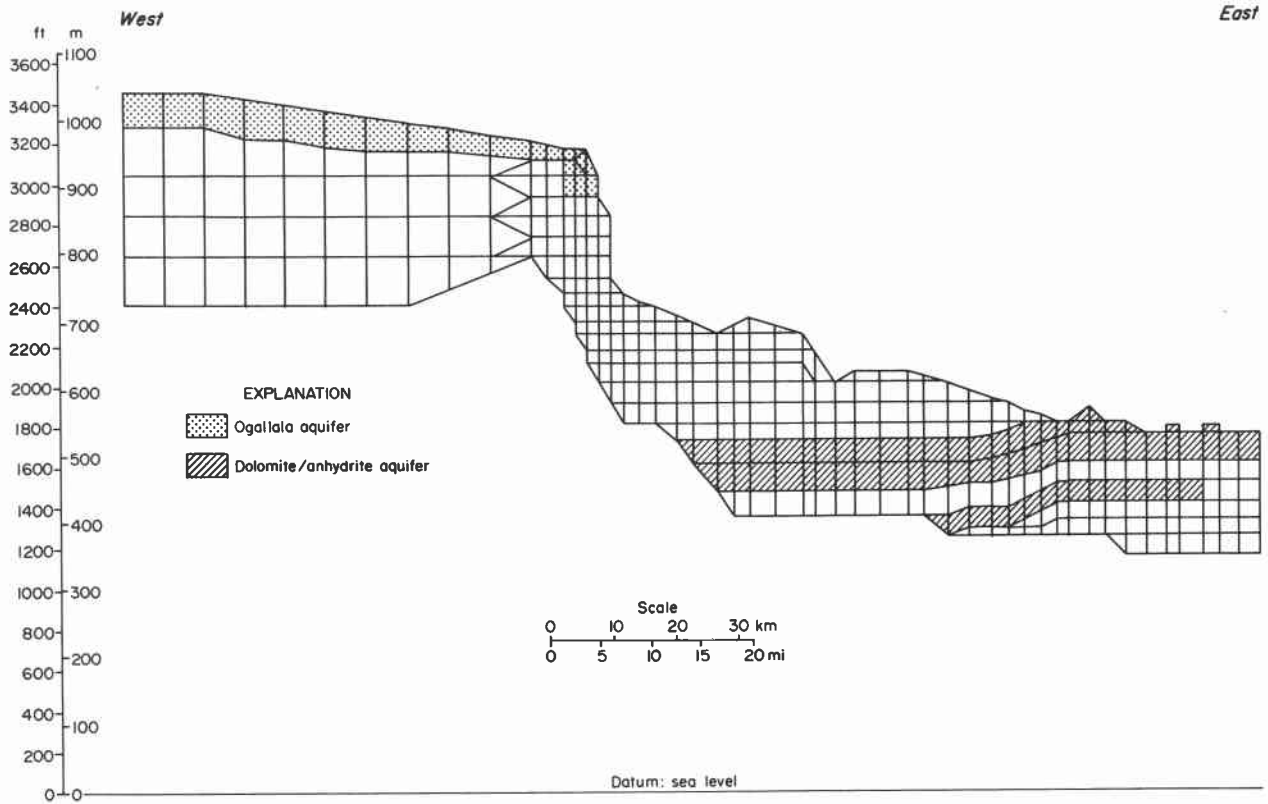


Figure 93. Finite-element mesh designed from the cross section shown in figure 92. The important Ogallala and dolomite/anhydrite aquifers are highlighted. Upper surface is the water table. Lower surface is drawn at zones of salt dissolution.

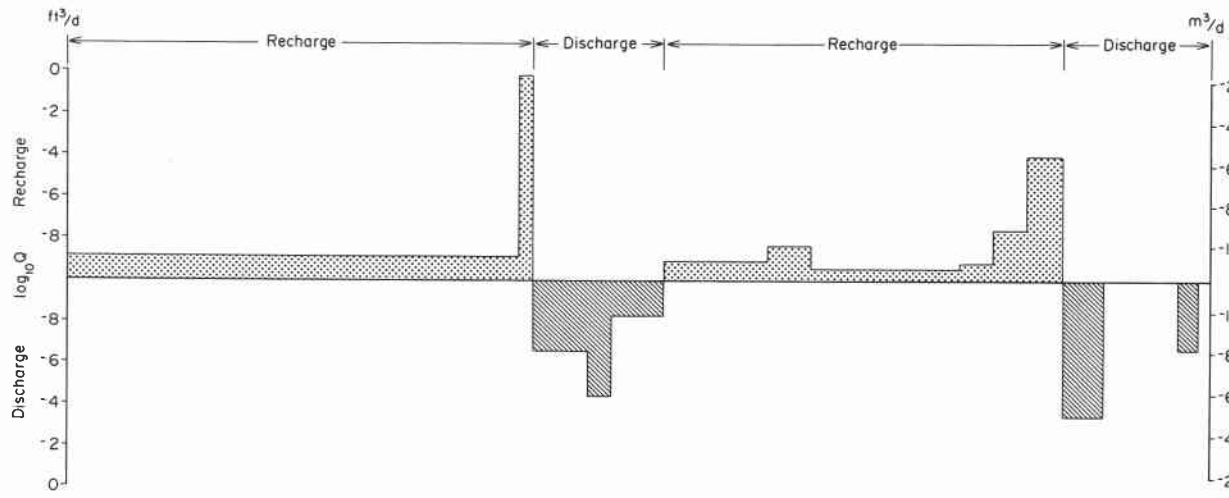
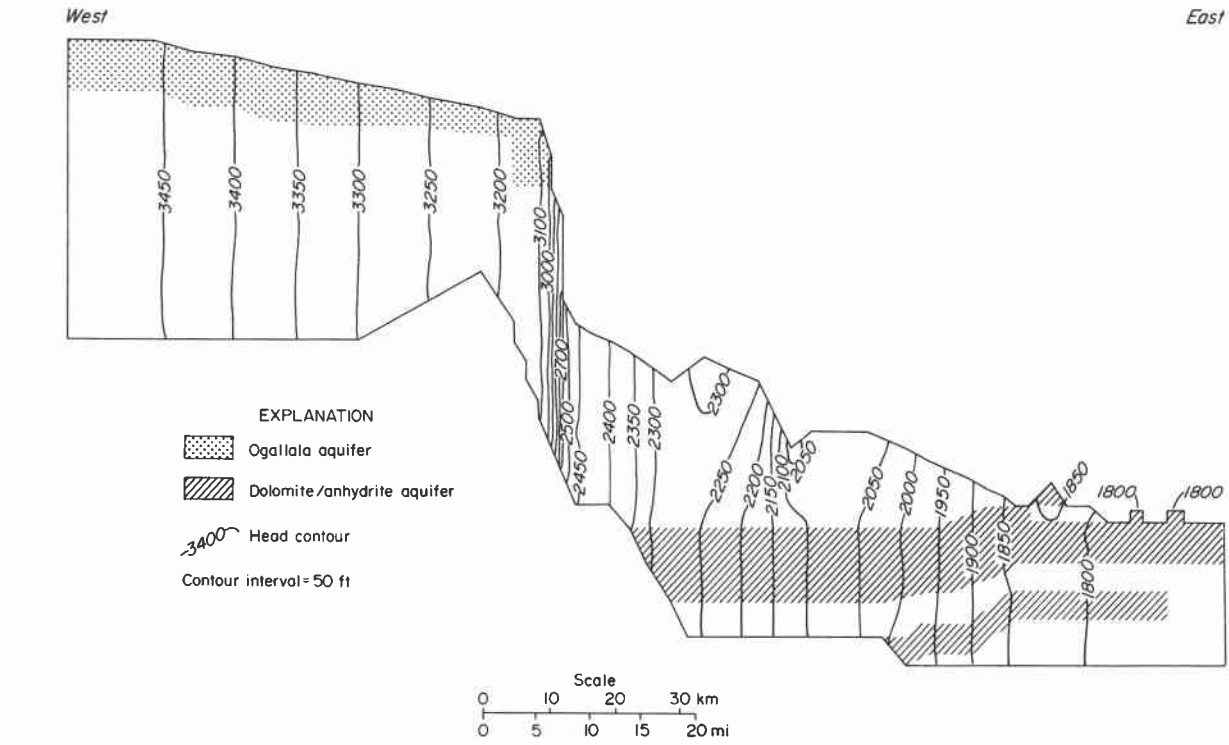


Figure 94. Steady-state hydraulic heads and recharge/discharge rates computed by the model. Flow lines cannot be assumed to be orthogonal to the head contours because of anisotropic K values and because the vertical scale exaggeration is approximately 104 to 1. Contour interval is 50 feet. Ogallala and dolomite/anhydrite units are highlighted. The recharge/discharge rates shown are regional averages of rates computed at groups of nodes and thus reflect only the major recharge and discharge areas. Flow rates through the sides of the model are on the order of  $10^{-9}$  ft<sup>3</sup>/d ( $10^{-11}$  m<sup>3</sup>/d), which is minute compared with the rates shown above.

Table 5. Hydrostratigraphic units and hydraulic conductivities utilized in the ground-water model. Values marked with an asterisk (\*) were estimated not from field or lab tests, but are based on the fact that these units are horizontally stratified mudstones containing small amounts of sand (and thus Kh/Kv should be large).

| <u>Hydrostratigraphic Unit</u>   | <u>Kh(ft/day)</u> | <u>Kv(ft/day)</u> | <u>Source</u>   |
|--|-------------------|-------------------|---|
| Ogallala (sand and gravel)   | 26.7              | 26.7              | (Myers, 1969)   |
| Dockum (sand, silt, clay)  | 2.7               | 2.7               | (Myers, 1969)   |
| Quartermaster/Cloud Chief<br>(mudstone)                                      | 0.27              | 0.00027           | Kh=(Stevens, written<br>communication, 1980)Kv=*                    |
| Whitehorse (sandstone)   | 3.0               | 3.0               | (Freeze and Cherry, 1979)   |
| Blaine and San Andres<br>cycle 4 in shallow subcrops<br>(dolomite/anhydrite) | 10.0              | 10.0              | (U.S. Army Corps of<br>Engineers, written communi-<br>cation, 1980) |
| Flowerpot (mudstone)   | 0.27              | 0.00027           | Kh=(Stevens, written<br>communication, 1980)Kv=*                    |

## REGIONAL SALINITY AND CHEMICAL COMPOSITION OF WATERS IN DEEP AQUIFERS IN THE PALO DURO BASIN

R. L. Bassett and E. A. Duncan

*Brines in the deep aquifers of the Palo Duro Basin derive their salinity primarily from dissolution of halite in the overlying evaporite section or from evaporites encountered early in the flow path. Brines appear to be near saturation with respect to anhydrite except in regions of active sulfate reduction and generation of H<sub>2</sub>S.*

The brines produced from Upper Pennsylvanian and Lower Permian formations in the Palo Duro Basin appear to be part of a continuous system, moving eastward under a gradient of less than 2 m/km (Bassett and Bentley, in press). Lithostratigraphy below the evaporites in this basin is dominated by carbonates (limestone, micritic limestone, dolomite) with substantial intertonguing of arkosic clastic facies (fig. 95). Because of the regional nature of brine migration, the lateral continuity of carbonate facies, and the long residence and reaction times, it should be expected that the brine composition would reflect the composition of the host rock. Dissolved solids values from chemical analyses and geophysical data show this spatial similarity; however, regional variations of individual brine concentrations are less well known.

Electric logs are particularly useful for lithologic correlation, and the spontaneous potential (SP) log may be used as an additional indicator of fluid resistivity (Keys and MacCary, 1971; Schlumberger, 1972). The resistivity of the formation water is measured relative to the resistivity of the borehole fluid, then converted to an equivalent resistivity (or salinity) of a sodium chloride solution. According to Keys and MacCary (1971), at least three assumptions must hold: (1) Both fluids must be dominantly sodium chloride; (2) shales are treated as ideal membranes and sands are not; and (3) formation fluid and matrix have a lower resistivity than borehole fluid. If these constraints are satisfied, then the following relation may be used:

$$SP = - K \log R_m/R_w$$

SP = deflection in SP log (millivolts)

K = 60 + 0.133 T

T = temperature at the formation depth (°F)

R<sub>m</sub> = resistivity of the borehole fluid (ohm-meters)

R<sub>w</sub> = resistivity of the formation water (ohm-meters)

Brines from the Palo Duro Basin appear to meet these criteria. Information about drilling fluids is given in the header of the log chart. SP logs that satisfied the

prerequisites of the method were selected from the Wolfcamp (Lower Permian) carbonates and granite-wash facies. Resistivities (or salinities) have been computed and the values converted to total dissolved solids as sodium chloride (g/L), then plotted on both Wolfcamp and granite-wash isopach maps (figs. 96 and 97). For comparison, the dissolved solids values from actual chemical analyses are also included on the map. Reasonable similarity is apparent. The maps indicate that there is little need to correct the fresh-water head maps for salinity difference owing to the rather uniform salinity across the Palo Duro Basin. North of the Amarillo Uplift in the Anadarko Basin, higher salinities exist; this anomaly may be explained by the relative hydraulic isolation and long residence times. Hydraulic isolation is evidenced by overpressure in the deep Anadarko Basin east of the mapped area.

As is common in sedimentary basins, the brine composition is dominated by sodium and chloride, and salinity is several times that of seawater. A number of mechanisms have been proposed to explain the evolution of brines, including membrane filtration, dissolution of evaporites, or mixing with metamorphic or magmatic waters.

Development of salinity in this basin is almost certainly related to the presence of evaporites. Of incidental note is the absence of post-Paleozoic magmatic activity within the basin; membrane effects are not evidenced through any detected chemical or head gradients. Mudstones and shales required for membrane filtration are volumetrically insignificant in this basin, which is dominated by evaporites, coarse-grained siliciclastics, and carbonates.

Carpenter (1978) suggested that brine compositions greater than 100,000 mg/L TDS in sedimentary basins are influenced by evaporite dissolution. The deep formations in the Palo Duro and Dalhart Basins have been overlain by evaporites since the Late Permian. Now, head declines with depth through the evaporite section below the elevated Southern High Plains area, and any fluid migrating through this section would be saturated with sodium chloride. Upon discharge from the evaporites, those brines would mix with brines in the Wolfcamp carbonates (fig. 95). Permeability of evaporites is extremely low (Geotechnical Engineers, 1978); consequently, flux through this section must be low. Although some mixing with waters leaking downward from evaporite strata has surely occurred, a more reasonable origin of the salinity is dissolution earlier in the flow history and relatively near the recharge areas in New Mexico.

Ancient salt dissolution zones (originating as early as the Triassic) have been identified near the margins of the basin (Gustavson and others, 1980). Regional hydraulic gradients during the Triassic are uncertain; however, the Panhandle area was still a

topographic low, as evidenced by inward movement of sediments from fluvial to lacustrine environments (McGowen and others, 1980).

During the Late Cretaceous, the Panhandle area was still at or below sea level, and broad carbonate platforms covered the Triassic basin fill. Marine regression accompanied by Laramide tectonism (Late Cretaceous to Paleocene) in New Mexico most likely initiated the ambient regional eastward topographic and hydraulic gradients. Fluids migrating through the deep basin may have entered the system primarily in New Mexico. Owing to the extreme anisotropy between vertical permeability in the evaporites and horizontal permeability in the carbonates (a ratio of  $1:10^6$ ), most recharge may come from areas where outcropping aquifers are juxtaposed with updip limits of evaporite beds undergoing dissolution. If hydraulic gradients have remained unchanged since the Late Cretaceous and permeability and porosity of 2.0 md and 0.5 percent can be considered average for the carbonates (Bassett and Bentley, in press), the fluid from western recharge areas could replace the basinal brines approximately every one million years. During the time since the Laramide orogeny, the entire mass of fluid in strata of Wolfcamp age from outcrop to the basin center may have been displaced more than 60 times. Any residual brine from the sabkha deposits would have been displaced early in the development of the regional flow regime. The brines present today in the carbonate rocks and sandstones cannot be connate water. Original fluids have been driven out by the regional flow. Brine composition is dominated by dissolution of evaporites early in the flow path and by subsequent modification in transit.

Calcium, magnesium, and sodium compositions from analyses of both Wolfcamp and granite-wash brines have been plotted on trilinear diagrams (fig. 98a, b), a prominent feature of which is the dominance of sodium chloride. Of the 121 values plotted for analyzed Wolfcamp samples, most are aligned along a ray emerging from the sodium apex, which indicates a common magnesium to calcium ratio.

It should be noted that the slope of the salinity ray of fluids in carbonates (fig. 98a) corresponds to a higher magnesium to calcium ratio than that of fluids in clastic rocks (fig. 98b), a suggestion that brines in the granite-wash facies are depleted in magnesium or that the calcium content has been elevated.

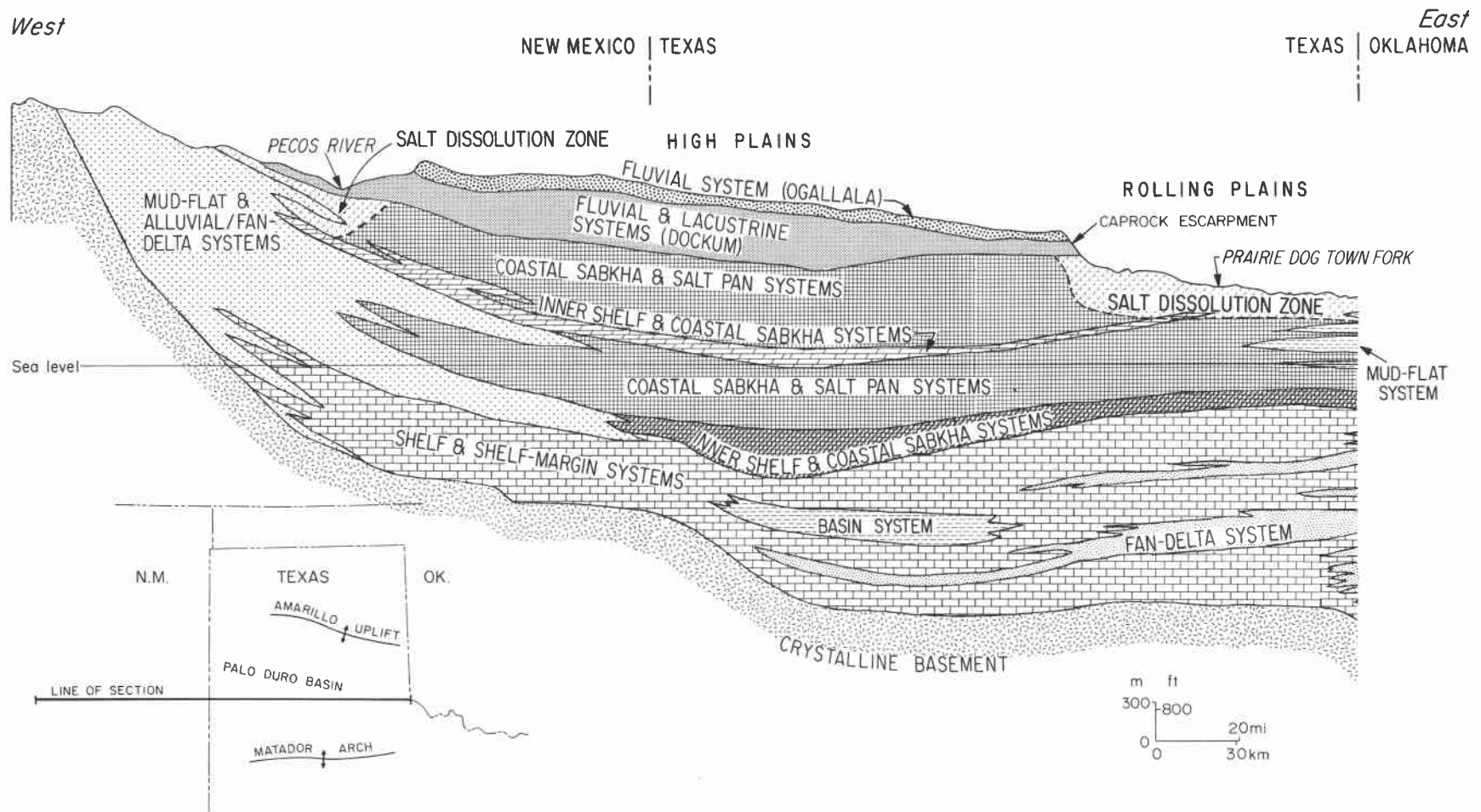


Figure 95. Regional east-west cross section illustrating spatial relations among the major depositional systems in the Palo Duro Basin.

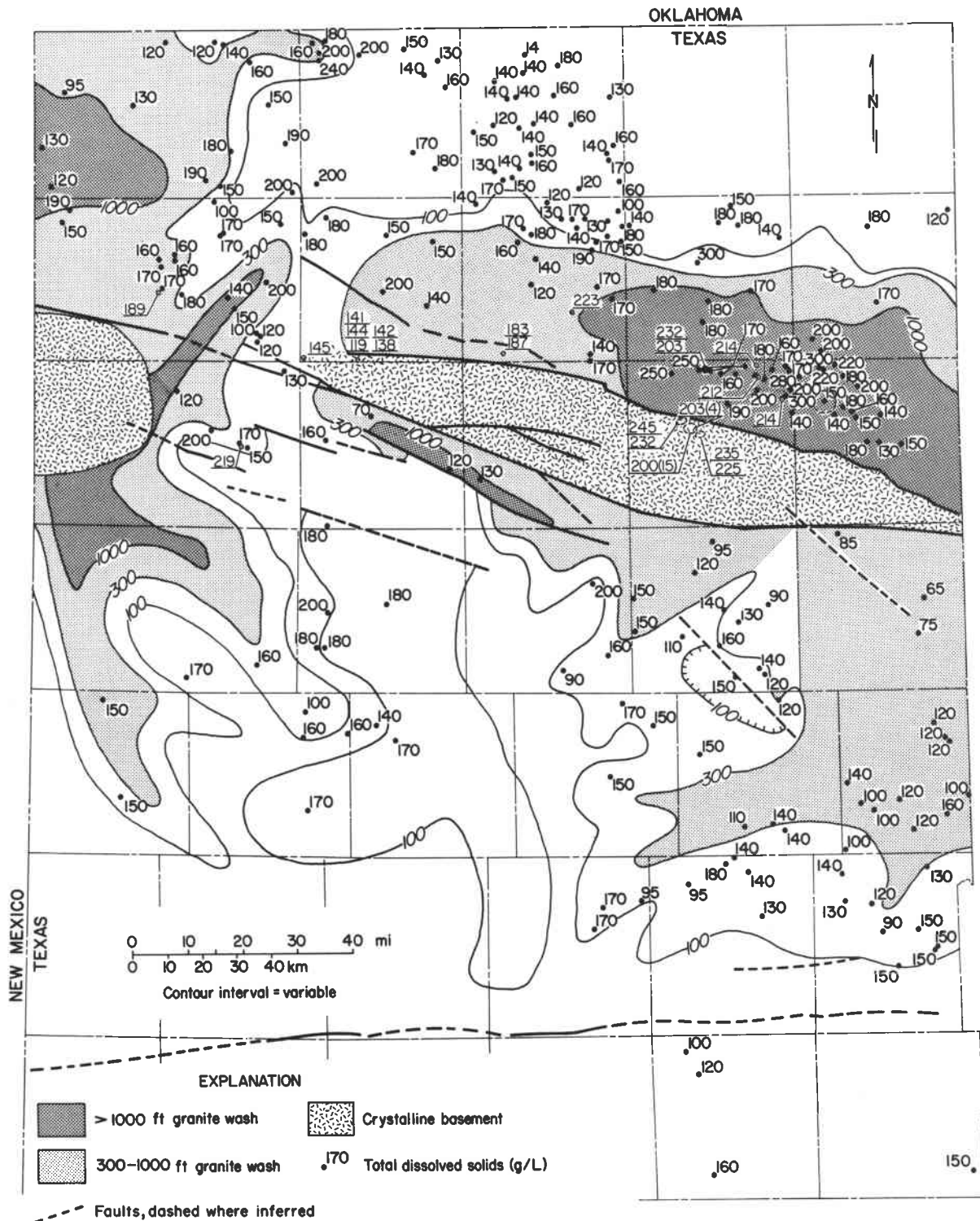


Figure 96. Isopach map of granite wash in the deep-basin brine aquifer (Dutton, in preparation). Data points indicate total dissolved solids (g/L) from chemical analyses of the brines (underscored) or computed from spontaneous potential log. Structure data are from Goldstein (personal communication, 1981).

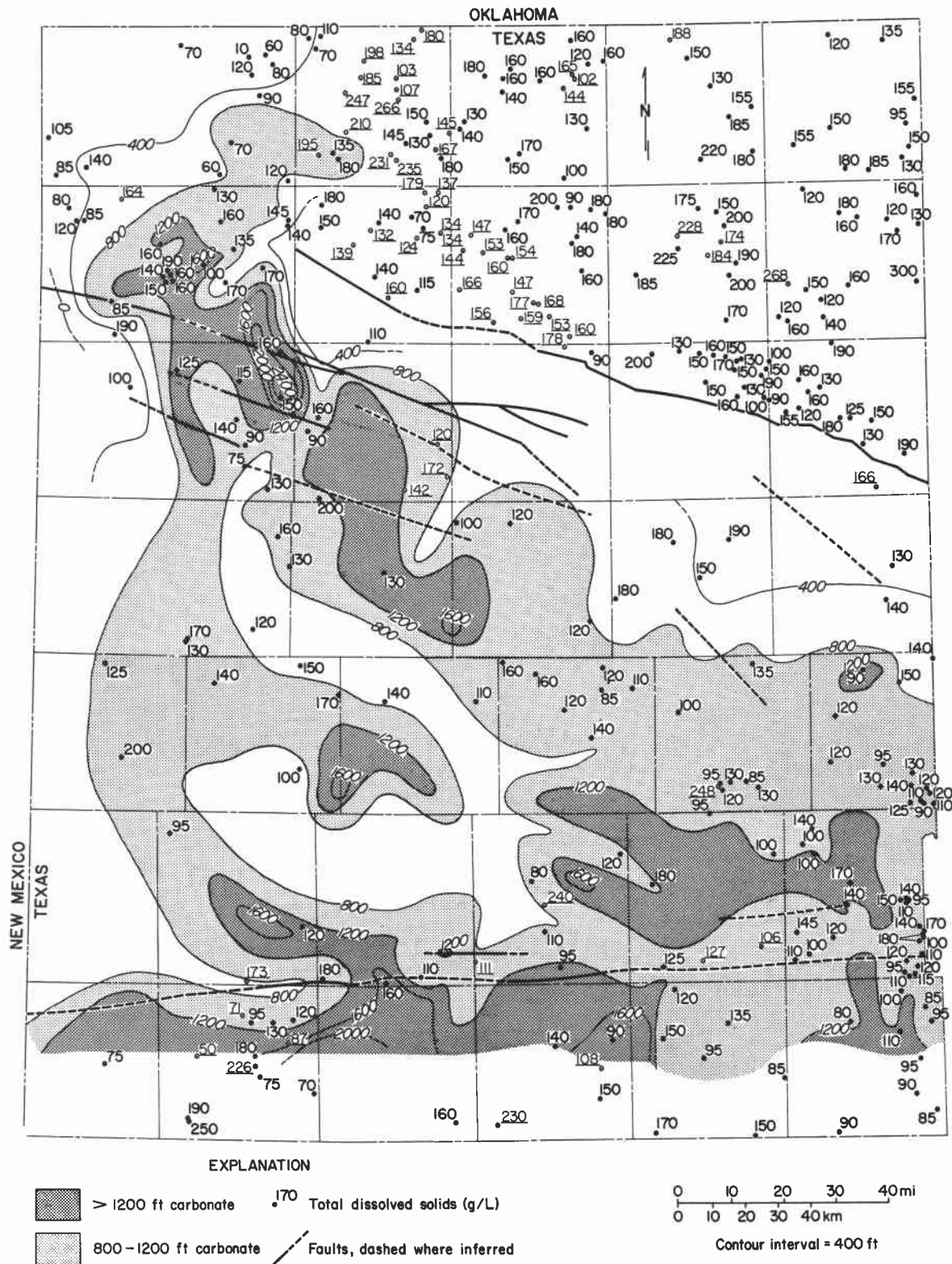


Figure 97. Carbonate isoliths for the Wolfcampian-age section of the deep-basin brine aquifer (C. R. Handford, written communication, 1981). Data points indicate total dissolved solids (g/L) from chemical analyses of the brines or computed from spontaneous potential logs. Structure data are from Goldstein (1981, written communication).

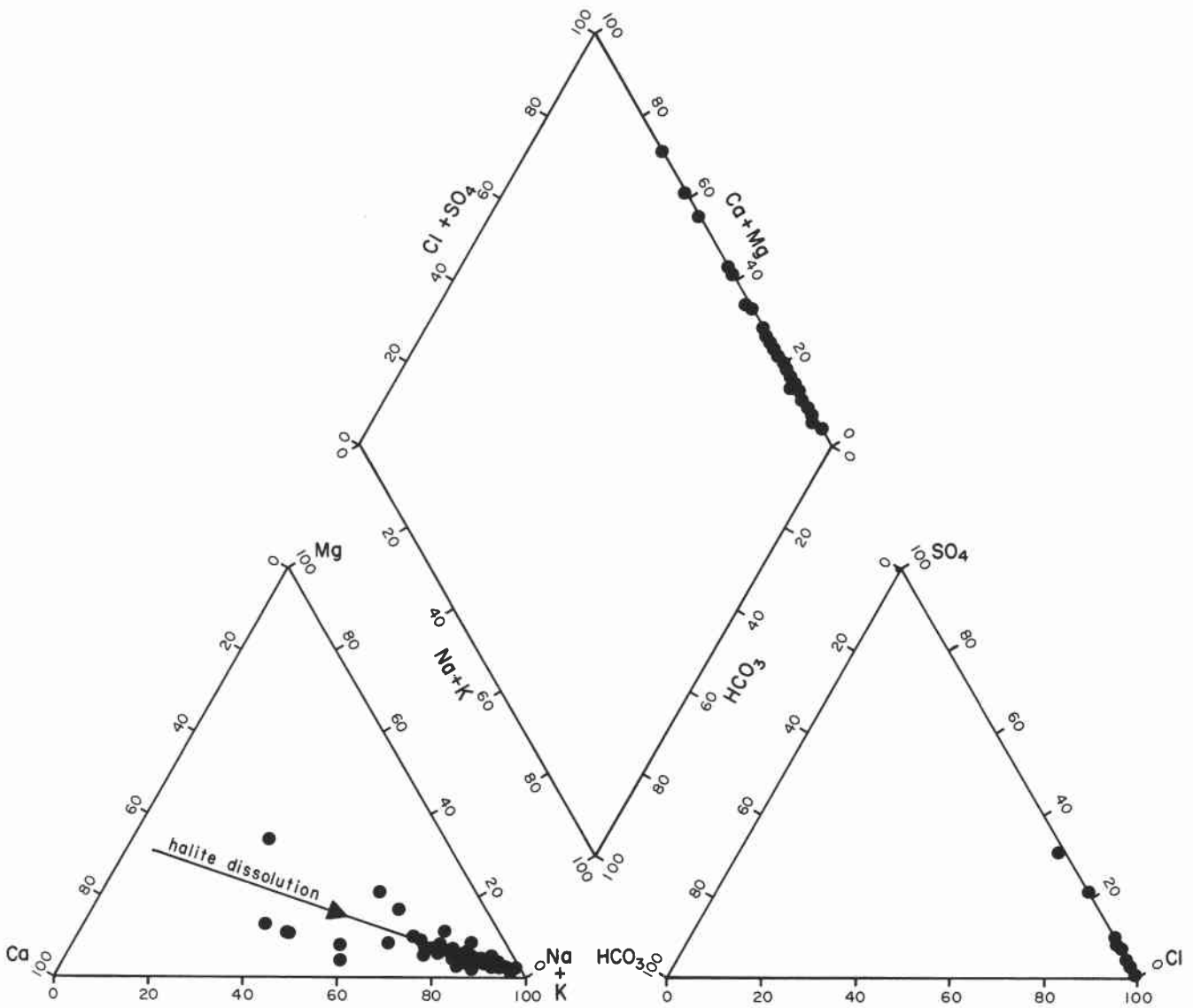


Figure 98a. Trilinear diagram illustrating the compositional variation of brine samples from the Permian Wolfcamp carbonate aquifer.

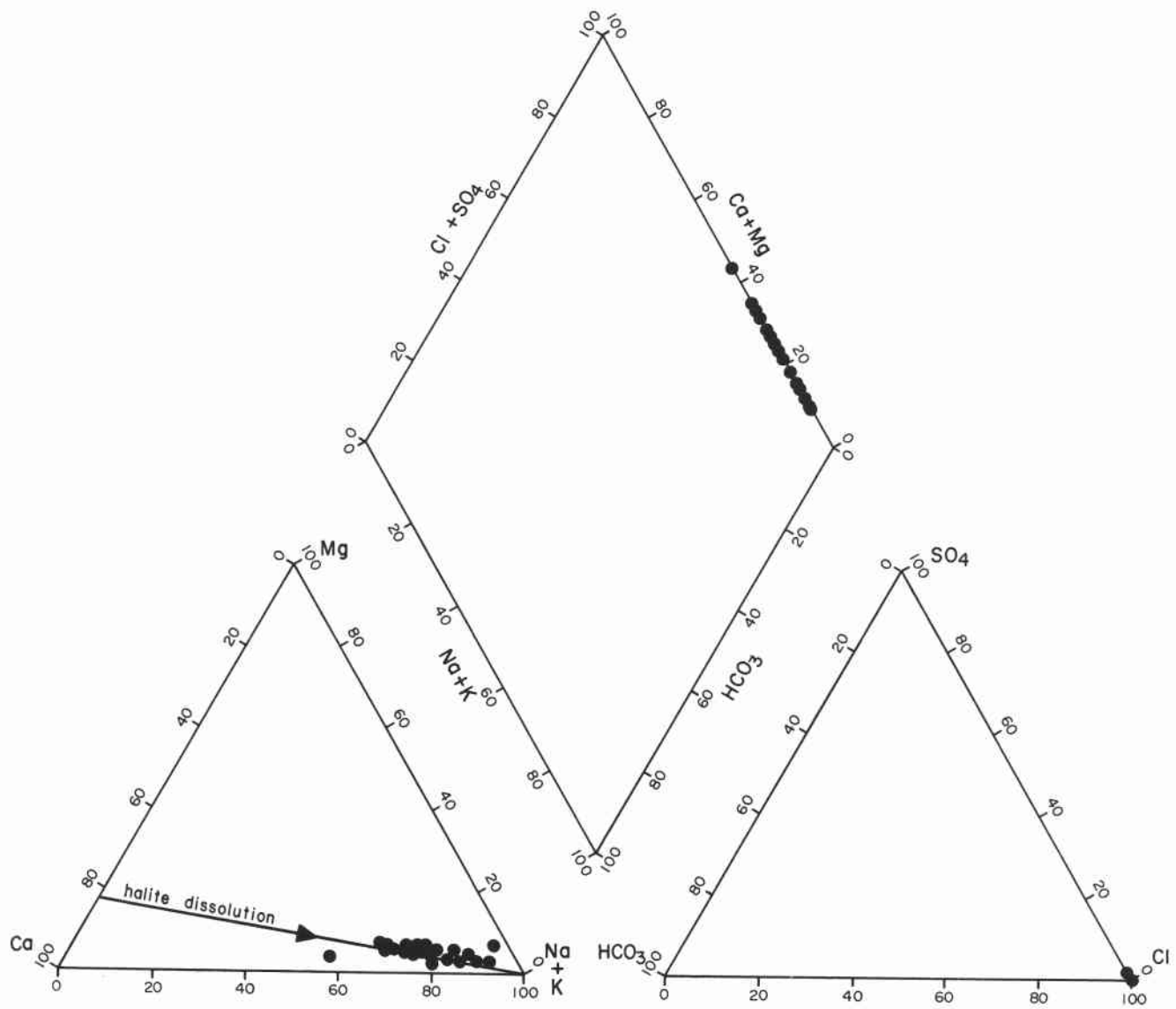


Figure 98b. Trilinear diagram illustrating the compositional variation of brine samples from the Pennsylvanian-Permian granite-wash facies.

## AQ/SALT: CALIBRATION OF A BRINE MODEL

R. L. Bassett and J. A. Griffin

*The AQ/SALT model is a reliable tool for evaluating the reaction state between brines and host rock owing to the ability to predict the potential for reaction or the likelihood of equilibrium. Calibration with well-controlled experimental data verifies the algorithms employed.*

Compositions of deep saline formation brines have been determined from analysis of fluids collected during drill-stem tests or from producing oil and gas wells. Fluid compositions and the attendant geochemical interpretations provide information concerning flow path, fluid origin, and diagenesis, and are also important in predicting the safety of long-term storage of radioactive waste. Brines may be agents for corrosion of containers, dissolution of host rock, expansion of engineered barriers, and transport of contaminants; consequently, an effective method for evaluating their reactivity and determining the dominant reactions controlling composition is essential in predicting long-term stability. Only recently have mathematical algorithms been developed that allow a rigorous chemical description of the brine. A computer program (AQ/SALT) has been developed to assist in the interpretation of mass transfer in formations containing brines.

AQ/SALT is written as a general code that can easily accept newly acquired experimental data. The model computes the activity coefficients of the free ions (Bassett and Griffin, 1981); consequently, the difficulties encountered with the ion-pairing models, namely the ill-defined character of weak ion associations, and the poor fit to measured values given by the Debye-Hückel equation, is circumvented. The utility of the model to deep-basin chemistry is discussed elsewhere in this report; this section will describe a calibration technique using published solubility data.

For the minerals that have stoichiometries that raise the activities to higher powers, such as bischofite ( $\text{MgCl}_2 \cdot 6\text{H}_2\text{O}$ ):

$$I_{\text{ap}} = a_{\text{Mg}^{++}} \cdot a_{\text{Cl}^-}^2 \cdot a_{\text{H}_2\text{O}}^6$$

Small errors in computation of ionic activity are magnified owing to exponentiation. In general, the model illustrates an excellent agreement between experimentally determined equilibrium conditions and predictions of equilibrium based on chemical analysis. The consistently low reaction state for bischofite may indicate that the equilibrium constant currently accepted is erroneous. This possibility is now being investigated.

Ionic strength and activity of water are also given in table 6. The Pitzer approach provides remarkably accurate computations for the activity of water on the basis of

calibration with published data for varying electrolyte compositions (Robinson and Stokes, 1965). Comparisons between computed and experimental values are also shown in figure 99.

The petroleum industry has made available chemical analyses of brines from numerous drill-stem tests in the Texas Panhandle. The saturation values of brines from the Wolfcampian-age carbonates as computed by AQ/SALT are shown in figure 100. It appears that brines in this system are essentially at equilibrium with respect to anhydrite and significantly undersaturated with halite. Anhydrite dissolution is most likely initiated early in the regional flow system, and some shielding from halite in the overlying evaporite system by the anhydritic dolomites of the Lower Permian may occur. Substantial potential for dissolution of halite does exist, however, in brines in the Wolfcamp aquifer.

Although previously investigated Palo Duro Basin brines (Bassett and others, 1981) are not as concentrated as solutions used in these calibration studies, the composition can be related to evaporite minerals with confidence where applicable data are available.

A computer-plotted phase diagram for the Na-K-Mg-Cl-SO<sub>4</sub>-H<sub>2</sub>O system at 25°C is given in figure 99 (P. Uerpmann, written communication, 1981) constructed from solubility data in D'Ans (1933). Each corner on this three-dimensional polyhedron represents a point at which equilibrium has been reached between the solution and the minerals itemized in table 6. For this system, halite and H<sub>2</sub>O are always present and the three axes represent K, Mg, and SO<sub>4</sub> compositions. The minerals known to form in this system, and their German names, are given in table 7. Using the chemical analyses of the equilibrium solutions at the corner points, AQ/SALT then predicted the minerals that should be in equilibrium with the given solution. The data are reported in terms of a saturation index (SI), as shown in table 6. The SI is the logarithm of the ratio of a computed activity product for a given mineral (I<sub>ap</sub>) with respect to the thermodynamic equilibrium constant (K<sub>eq</sub>):

$$SI = \log (I_{ap}/K_{eq})$$

At equilibrium the ratio will be 1.0 and the SI is 0. In almost every instance, the model predicts the correct suite of minerals; however, in four cases the mineral sylvite is predicted as more stable than other potassium phases. It is difficult to establish criteria for deciding whether the solution is at equilibrium (SI  $\cong$  0), slightly supersaturated (SI > 0), or slightly undersaturated (SI < 0). Halite, for example, reaches equilibrium quickly. Although the chloride concentration varies from 37.4 to 105.5 mol/(1,000 mol H<sub>2</sub>O), the model consistently computes that the solution is in equilibrium with an SI range at  $\pm$  0.20.

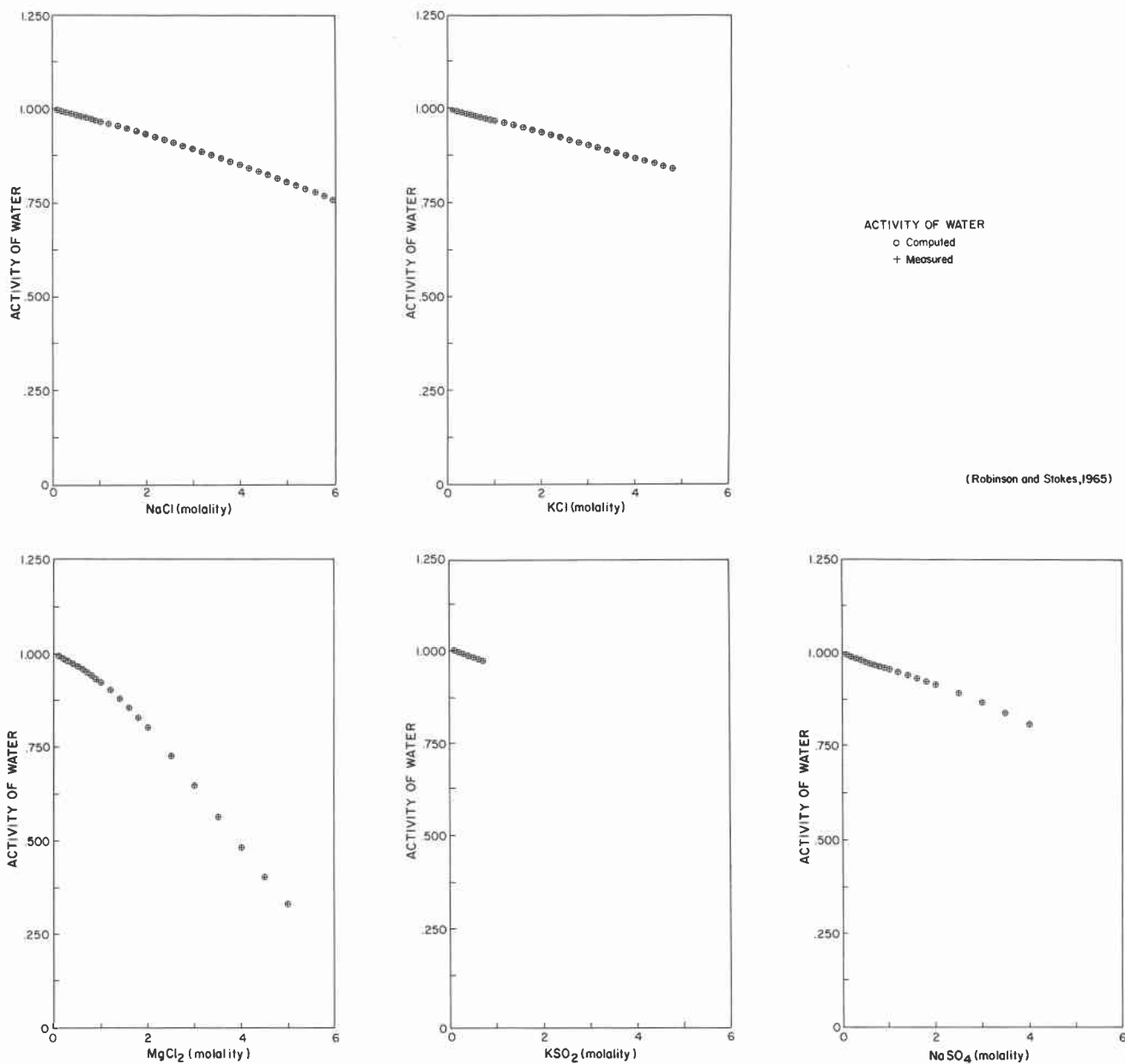


Figure 99. Measured values for the activity of water in solutions with varying electrolyte compositions (Robinson and Stokes, 1965) compared with the computed value for activity of water using AQ/SALT. Solutions examined are (a) NaCl, (b) KCl, (c) MgCl<sub>2</sub>, (d) KSO<sub>4</sub>, and (e) NaSO<sub>4</sub>.

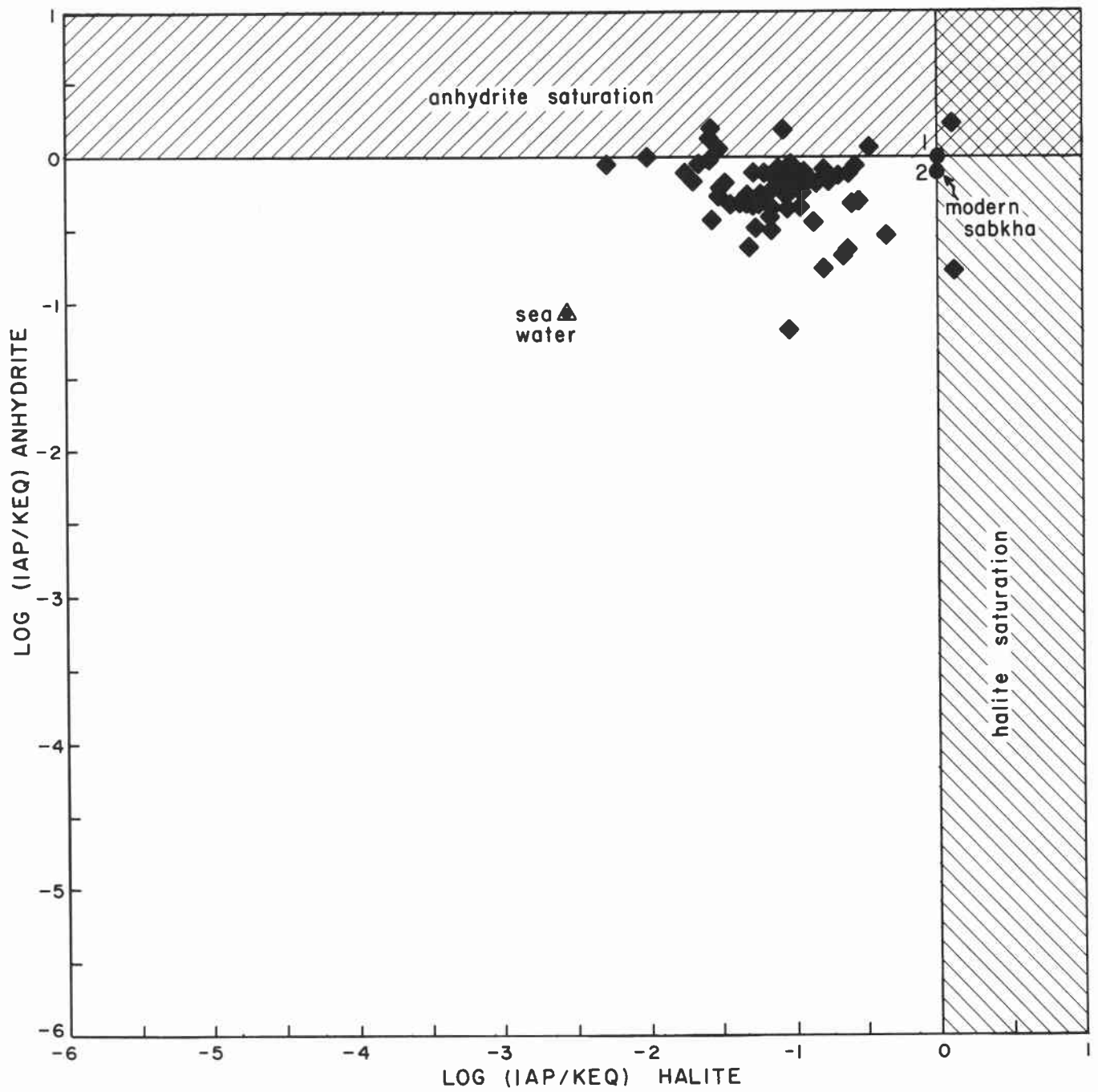


Figure 100. Saturation state of brine samples from Wolfcamp carbonate facies as computed with AQ/SALT.

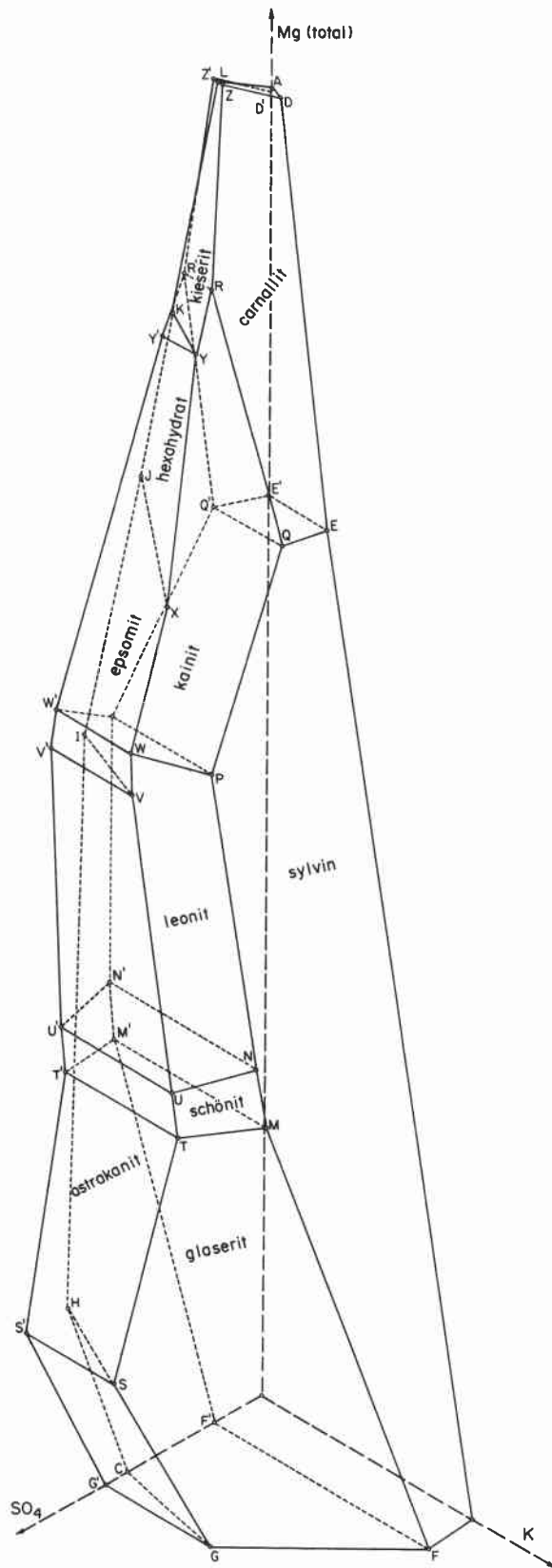


Figure 101. Phase diagram for the Na-K-Mg-Cl-SO<sub>4</sub>-H<sub>2</sub>O system at 25°C (after D'Ans, 1933). Halite is in equilibrium with the brine at all points. Brine compositions and equilibrium phase assemblages present at the corner points are identified in tables 5 and 6.

Table 6. Chemical compositions of solutions in equilibrium with phases in the Na-K-Mg-Cl-SO<sub>4</sub>-H<sub>2</sub>O system.

| Corner Points | Solution Composition |                |                 |                 |       | Minerals Present At<br>The Corner Points | Activity<br>H <sub>2</sub> O | Ionic<br>Strength | Saturation Indices |      |      |      |      |      |      |     |      |      |      |      |
|---------------|----------------------|----------------|-----------------|-----------------|-------|--|------------------------------|-------------------|--------------------|------|------|------|------|------|------|-----|------|------|------|------|
|               | Mg                   | K <sub>2</sub> | Na <sub>2</sub> | SO <sub>4</sub> | Cl    |  |                              |                   | Hal                | Bis  | Syl  | Then | Carn | Glas | Bloe | Ep  | Kie  | Sch  | Leo  | Kai  |
| A             | 103.8                | -              | 1.0             | -               | 104.8 | Hal, Bis                                 | 0.23                         | 17.41             | .10                | -.89 | -    | -    | -    | -    | -    | -   | -    | -    | -    | -    |
| B             | -                    | 19.2           | 41.0            | -               | 60.2  | Hal, Syl                                 | 0.74                         | 6.69              | -.14               | -    | -.07 | -    | -    | -    | -    | -   | -    | -    | -    | -    |
| C             | -                    | -              | 49.8            | 12.4            | 37.4  | Hal, Then                                | 0.79                         | 6.22              | -.37               | -    | -    | -.30 | -    | -    | -    | -   | -    | -    | -    | -    |
| D             | 103.6                | 0.9            | 1.0             | -               | 105.5 | Hal, Bis, Carn                           | 0.23                         | 17.47             | .10                | -.88 | -    | -    | -.19 | -    | -    | -   | -    | -    | -    | -    |
| E             | 71.7                 | 5.5            | 3.8             | -               | 81.0  | Hal, Carn, Syl                           | 0.44                         | 12.98             | -.10               | -    | -.01 | -    | -.47 | -    | -    | -   | -    | -    | -    | -    |
| F             | -                    | 20.0           | 48.6            | 4.4             | 64.2  | Hal, Syl, Glas                           | 0.70                         | 7.86              | .30                | -    | .01  | -    | -    | -.19 | -    | -   | -    | -    | -    | -    |
| G             | -                    | 9.8            | 58.5            | 14.4            | 53.9  | Hal, Glas, Then                          | 0.71                         | 8.36              | .02                | -    | -    | .00  | -    | .02  | -    | -   | -    | -    | -    | -    |
| H             | 16.0                 | -              | 46.9            | 18.1            | 44.8  | Hal, Then, Bloe                          | 0.70                         | 8.88              | -.06               | -    | -    | -.02 | -    | -    | -.07 | -   | -    | -    | -    | -    |
| I             | 61.1                 | -              | 12.5            | 16.9            | 56.7  | Hal, Bloe, Ep                            | 0.53                         | 12.51             | .00                | -    | -    | -    | -    | -.21 | -.24 | -   | -    | -    | -    | -    |
| J             | 79.2                 | -              | 4.2             | 11.8            | 71.6  | Hal, Ep                                  | 0.41                         | 14.32             | -.03               | -    | -    | -    | -    | -    | -.50 | -   | -    | -    | -    | -    |
| K             | 90.7                 | -              | 1.7             | 9.0             | 83.4  | Hal, Kie                                 | 0.32                         | 15.80             | -.10               | -    | -    | -    | -    | -    | -    | .15 | -    | -    | -    | -    |
| L             | 106.8                | -              | 1.0             | 4.9             | 102.9 | Hal, Kie, Bis                            | 0.21                         | 18.18             | .14                | -.95 | -    | -    | -    | -    | -    | .59 | -    | -    | -    | -    |
| M             | 35.4                 | 14.2           | 23.0            | 13.9            | 58.6  | Hal, Syl, Glas, Sch                      | 0.62                         | 10.80             | -.04               | -    | -.02 | -    | -    | .14  | -    | -   | -.13 | -    | -    | -    |
| N             | 40.0                 | 13.8           | 19.3            | 14.4            | 58.7  | Hal, Syl, Sch, Leo                       | 0.61                         | 11.14             | -.08               | -    | -.01 | -    | -    | -    | -    | -   | -.10 | -.03 | -    | -    |
| O             | -                    | -              | 55.5            | -               | 55.5  | Hal                                      | 0.75                         | 6.17              | .01                | -    | -    | -    | -    | -    | -    | -   | -    | -    | -    | -    |
| P             | 61.2                 | 9.3            | 9.7             | 14.3            | 65.9  | Hal, Syl, Leo, Kai                       | 0.51                         | 13.10             | -.001              | -    | .02  | -    | -    | -    | -    | -   | -    | -    | -.16 | -.12 |
| Q             | 73.2                 | 6.4            | 3.5             | 5.1             | 78.0  | Hal, Syl, Kai, Carn                      | 0.43                         | 13.58             | -.15               | -    | .06  | -    | -.50 | -    | -    | -   | -    | -    | -    | -.25 |
| R             | 93.3                 | 2.5            | 1.7             | 7.9             | 89.6  | Hal, Carn, Kai, Kie                      | 0.30                         | 16.45             | .00                | -    | -    | -    | -.27 | -    | -    | .25 | -    | -    | -    | .09  |
| S             | 15.7                 | 8.2            | 48.0            | 21.8            | 50.1  | Hal, Then, Glas, Bloe                    | 0.67                         | 10.07             | .02                | -    | -    | .07  | -    | -.02 | .05  | -   | -    | -    | -    | .09  |
| T             | 34.9                 | 10.5           | 27.5            | 18.4            | 54.5  | Hal, Glas, Bloe, Sch                     | 0.62                         | 11.06             | .00                | -    | -    | -    | -    | -.05 | -.05 | -   | -    | -.20 | -    | -    |
| U             | 38.7                 | 10.4           | 22.5            | 18.9            | 52.1  | Hal, Bloe, Sch, Leo                      | 0.63                         | 11.12             | -.10               | -    | -    | -    | -    | -.21 | -    | -   | -.17 | -.12 | -    | -    |
| V             | 61.3                 | 7.5            | 10.3            | 19.9            | 59.2  | Hal, Leo, Bloe, Kie                      | 0.52                         | 13.30             | -.07               | -    | *    | -    | -    | -    | -.32 | -   | -.50 | -    | -.14 | -    |
| W             | 64.2                 | 6.9            | 8.9             | 19.5            | 60.5  | Hal, Leo, Kai, Kie                       | 0.50                         | 13.54             | -.07               | -    | *    | -    | -    | -    | -    | -   | -.44 | -    | -.20 | -.18 |
| X             | 73.9                 | 6.6            | 5.3             | 15.9            | 69.9  | Hal, Kai, Kie                            | 0.44                         | 14.52             | -.04               | -    | *    | -    | -    | -    | -    | -   | -.19 | -    | -    | .07  |
| Y             | 89.3                 | 3.2            | 2.5             | 10.0            | 85.0  | Hal, Kai, Kie                            | 0.33                         | 16.07             | .05                | -    | *    | -    | -    | -    | -    | -   | .19  | -    | -    | .15  |
| Z             | 107.3                | 0.9            | 0.7             | 5.4             | 103.5 | Hal, Carn, Kie, Bis                      | 0.21                         | 18.36             | .00                | -.95 | -    | -    | -.25 | -    | -    | -   | .64  | -    | -    | -    |

Table 7. Mineral names and chemical formulas.

| <u>Symbol</u> | <u>Mineral Name</u> |              | <u>Formula</u>   |
|---------------|---------------------|--------------|--|
| H             | Halite              | (Halit)      | NaCl   |
| B             | Bischofite          | (Bischofit)  | MgCl <sub>2</sub> -6H <sub>2</sub> O                                 |
| S             | Sylvite             | (Sylvin)     | KCl  |
| T             | Thenardite          | (Thenardit)  | Na <sub>2</sub> SO <sub>4</sub>                                      |
| C             | Carnallite          | (Carnallit)  | KMgCl <sub>3</sub> -6H <sub>2</sub> O                                |
| G             | Glaserite           | (Glaserit)   | Na <sub>2</sub> K <sub>6</sub> (SO <sub>4</sub> ) <sub>4</sub>       |
| Bl            | Bloedite            | (Astrakanit) | Na <sub>2</sub> Mg(SO <sub>4</sub> ) <sub>2</sub> -4H <sub>2</sub> O |
| E             | Epsomite            | (Epsomit)    | MgSO <sub>4</sub> -7H <sub>2</sub> O                                 |
| Ki            | Kieserite           | (Kieserit)   | MgSO <sub>4</sub> -H <sub>2</sub> O                                  |
| Sch           | Schoenite           | (Schönit)    | K <sub>2</sub> Mg(SO <sub>4</sub> ) <sub>2</sub> -6H <sub>2</sub> O  |
| L             | Leonite             | (Leonit)     | K <sub>2</sub> Mg(SO <sub>4</sub> ) <sub>2</sub> -4H <sub>2</sub> O  |
| Ka            | Kainite             | (Kainit)     | KMgCl SO <sub>4</sub> -3H <sub>2</sub> O                             |

## GEOCHEMISTRY AND MASS TRANSFER IN BRINES FROM PERMIAN WOLFCAMP CARBONATES IN THE PALO DURO, DALHART, AND ANADARKO BASINS

R. L. Bassett

*Brines in Wolfcamp carbonates are probably in equilibrium with calcite, as determined by chemical analyses of samples collected during wildcat drilling. Mass transfer computations corrected for CO<sub>2</sub> outgassing indicate that the P<sub>CO<sub>2</sub></sub> of Palo Duro, Dalhart, and Anadarko brines is remarkably similar to the P<sub>CO<sub>2</sub></sub> observed in producing gas fields in the basin.*

Of the several thousand chemical analyses of brines originally located for the Palo Duro, Dalhart, and Anadarko Basins, we have eliminated from consideration those for which (1) dilution with drilling fluid is suspected, (2) the brine originated from a production or injection well in an enhanced recovery process, (3) either depth or location data are unavailable, or (4) the host formation is unrelated to this study. The remaining data are subject to error of three types: (1) collection procedure, (2) sample preservation, and (3) analytical procedure. Chemical compositions of fluids used in this investigation were determined by petroleum companies and are predominantly from analyses of samples collected during wildcat drilling programs. The Bureau of Economic Geology obtained these chemical data from both the petroleum industry directly and from commercial petroleum information service companies.

The reaction state of Wolfcamp brines was computed with SOLMNEQ and AQ/SALT using 121 analyses. The models indicate that almost all Wolfcamp brines are supersaturated with respect to calcite (fig. 102) and dolomite (fig. 103). Outgassing of carbon dioxide at the surface during sample collection is undoubtedly the cause of the apparent over-saturation with respect to carbonate minerals. In an attempt to estimate the in situ partial pressure of carbon dioxide (P<sub>CO<sub>2</sub></sub>) and determine if calcite was in equilibrium with the brine, two approaches were taken. The first approach was to seek an analogy between in situ brine P<sub>CO<sub>2</sub></sub> and the P<sub>CO<sub>2</sub></sub> in natural gas from nearby producing fields. Second, a mass transfer approach using a computer equilibrium model was used to simulate the stepwise addition of CO<sub>2</sub> back into the sample. The variation in speciation was monitored along the reaction path, and a new "in situ" pH and P<sub>CO<sub>2</sub></sub> were computed at the calcite phase boundary.

During the period from 1917 to 1974, the Bureau of Mines (U.S. Department of Interior) surveyed the worldwide helium potential by analyzing natural gas samples from 37 states and 23 foreign countries. Numerous oil and gas fields from the Texas Panhandle were included in this study (Moore, 1976). Data on wellhead pressures, depth, and mole

percent CO<sub>2</sub> were used to compute a field P<sub>CO<sub>2</sub></sub> (atm). Although substantial variation in wellhead pressures exists among the producing fields, the P<sub>CO<sub>2</sub></sub> across the region is defined within a relatively narrow range (fig. 104a, b). Without stable isotopic data, one can only assume that the CO<sub>2</sub> was derived from within the basin during hydrocarbon maturation. The fields are too deep to be associated with biogenic methane (Hunt, 1979), and there is certainly no evidence of carbonate decomposition attending volcanic intrusion. It seems doubtful that CO<sub>2</sub> pressures would be so uniform across the basin (fig. 105) were there not some buffering mechanism. I suggest that the brines and the carbonate host rocks are in equilibrium, and the P<sub>CO<sub>2</sub></sub> is constrained to follow the calcite phase boundary.

It is significant that a plot of calcite saturation index against pH indicates a strong correlation toward a slope of unity for the Wolfcamp samples (figs. 103 and 104). The stepwise addition of CO<sub>2</sub> to the solution with recalculation of pH, speciation, and saturation state moves the computed saturation toward the calcite phase boundary, always following this slope of one.

The change in the saturation state with pH is simply the derivative of the activity product (I<sub>ap</sub>) minus the equilibrium constant with pH:

$$\left( \frac{\partial (\log I_{ap} - \log K_{eq})}{\partial \text{pH}} \right)_{T,P} = \left( \frac{\partial \log I_{ap}}{\partial \text{pH}} \right)_{T,P}$$

Inserting the activity product for calcite:

$$\left( \frac{\partial \log I_{ap}}{\partial \text{pH}} \right)_{T,P} = \left( \frac{\partial \log (a_{\text{Ca}^{++}} \cdot a_{\text{CO}_3^{=}})}{\partial \text{pH}} \right)_{T,P} = \left( \frac{\partial \log (\gamma_{\text{Ca}^{++}} \cdot m_{\text{Ca}^{++}} \cdot \gamma_{\text{CO}_3^{=}} \cdot m_{\text{CO}_3^{=}})}{\partial \text{pH}} \right)_{T,P}$$

Ionic strength changes are negligible, temperature and solution composition remain constant, and the change in ion pairing with pH over the range of interest does not alter significantly the concentration of free calcium; consequently,

$$\left( \frac{\partial \log I_{ap}}{\partial \text{pH}} \right)_{T,P} = \left( \frac{\partial \log m_{\text{CO}_3^{=}}}{\partial \text{pH}} \right)_{T,P}$$

$$\left( \frac{\partial \log I_{ap}}{\partial \text{pH}} \right)_{T,P} \approx 1.0$$

All Wolfcamp brine analyses from samples in the Panhandle were translated to the calcite phase boundary by CO<sub>2</sub> addition. The equilibrium P<sub>CO<sub>2</sub></sub> over these solutions was compared with that of natural gas reservoirs (fig. 105), and the data are shown as histograms (fig. 104a, b). The computed P<sub>CO<sub>2</sub></sub> for brines compares remarkably well with waters in the reservoirs, and the values from within the basin show no significant variation in P<sub>CO<sub>2</sub></sub> distribution. This suggests that CO<sub>2</sub> is buffered by the carbonate host rock and that the brines are in equilibrium with calcite. The linear distribution of computed saturation states when plotted with pH also indicates that the brines were in equilibrium, but CO<sub>2</sub> loss has occurred during sampling.

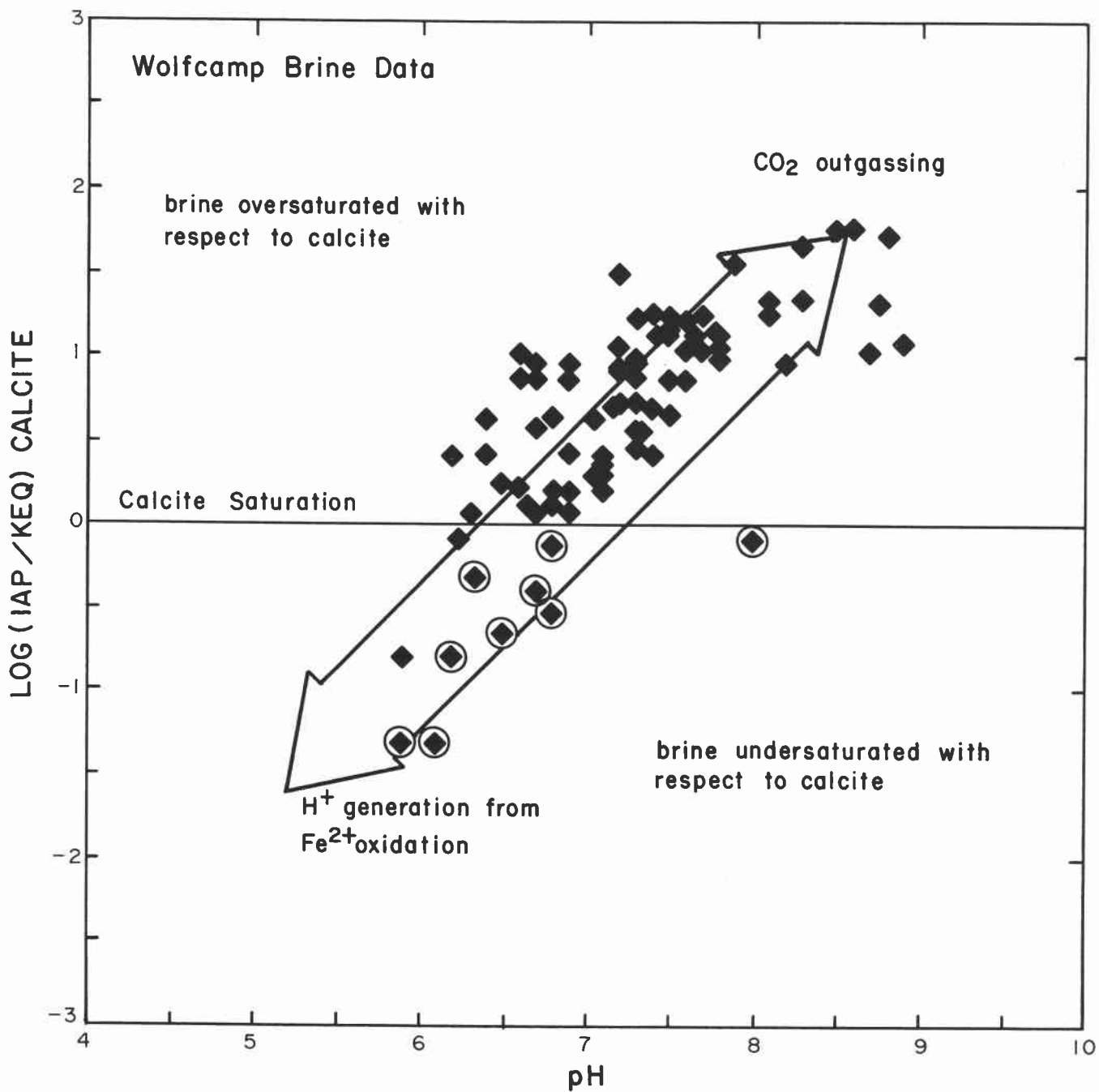


Figure 102. Saturation states computed with AQ/SALT and SOLMNEQ for Lower Permian Wolfcamp brines illustrate the effect of outgassing of CO<sub>2</sub> and iron oxidation. Circled data points represent compositions of fluid from Sherman County.

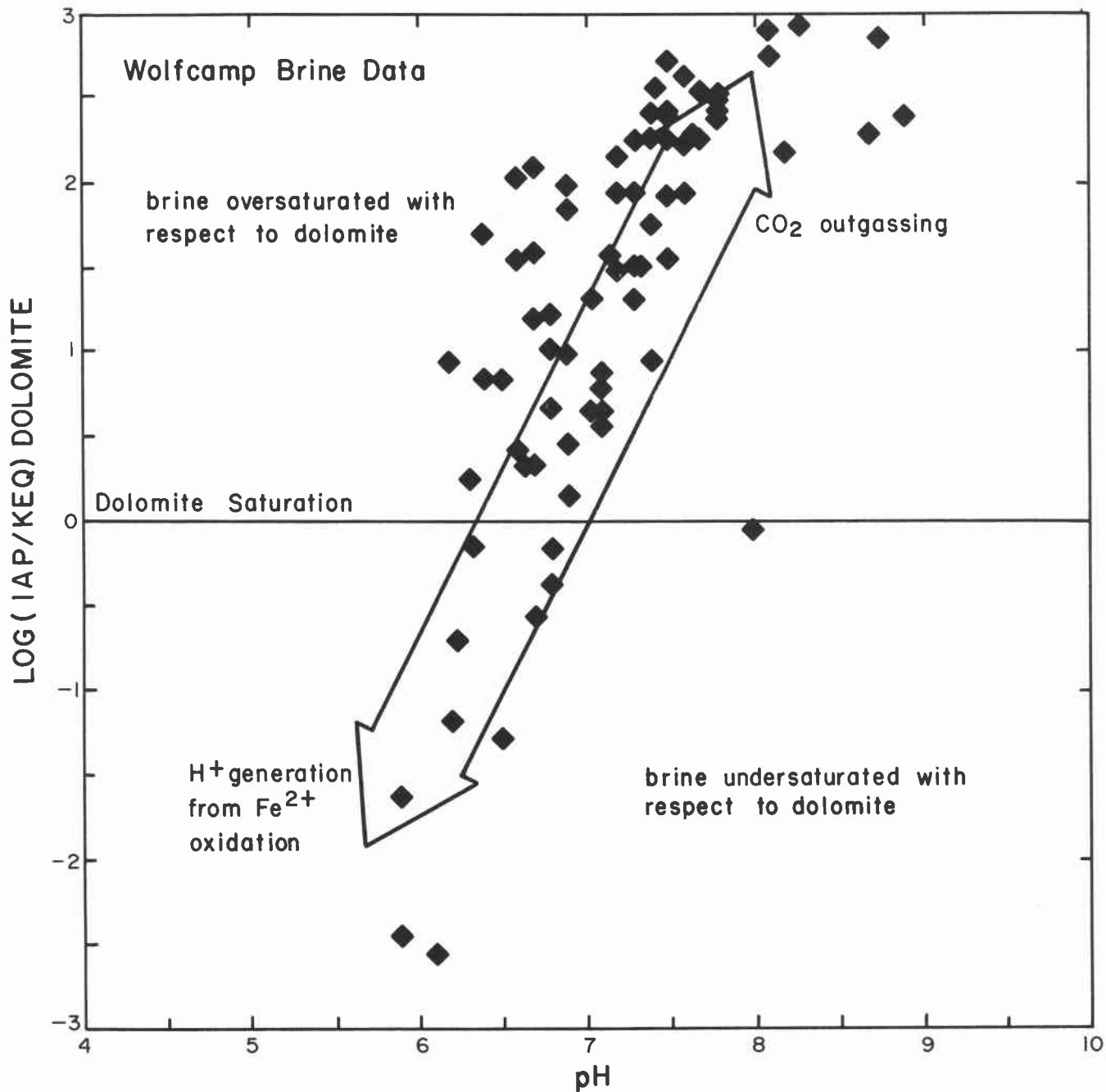


Figure 103. Saturation state of Lower Permian Wolfcamp brine with respect to dolomite as computed with AQ/SALT and SOLMNEQ.

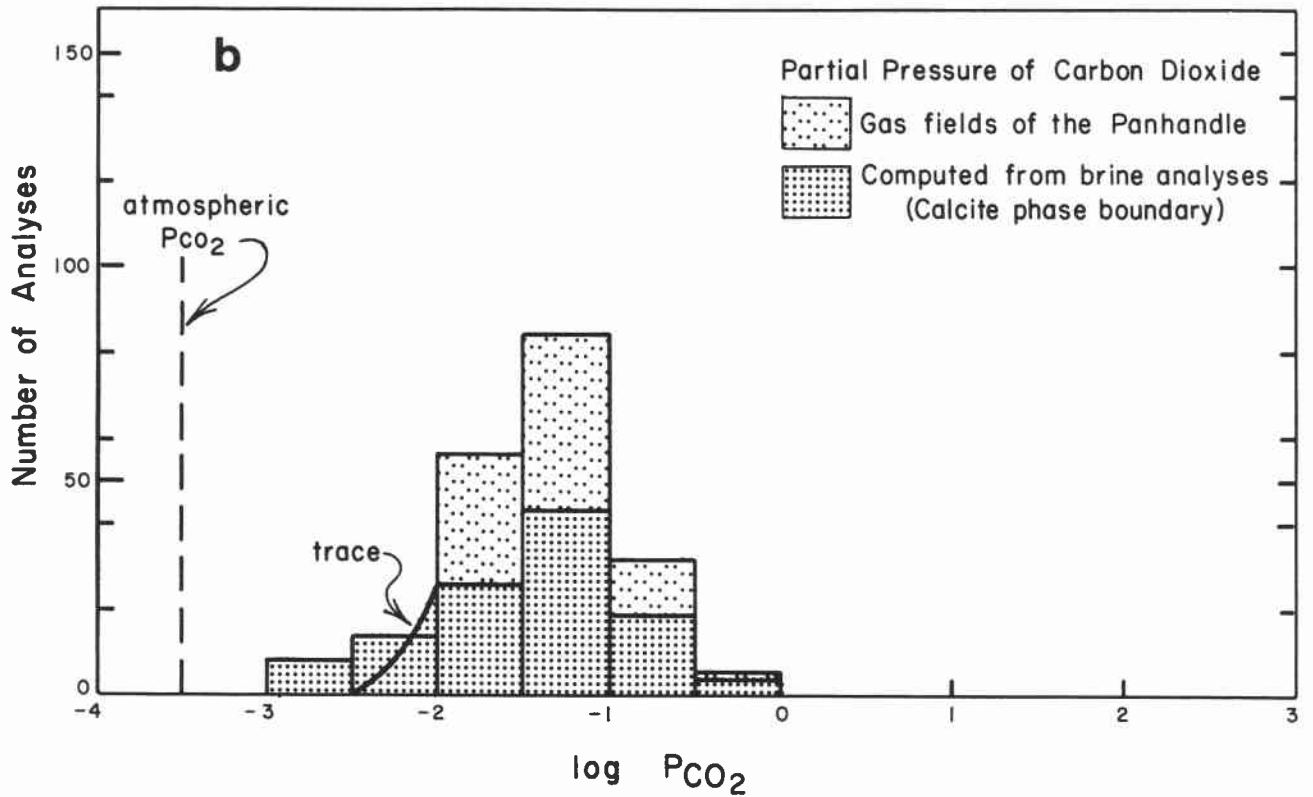
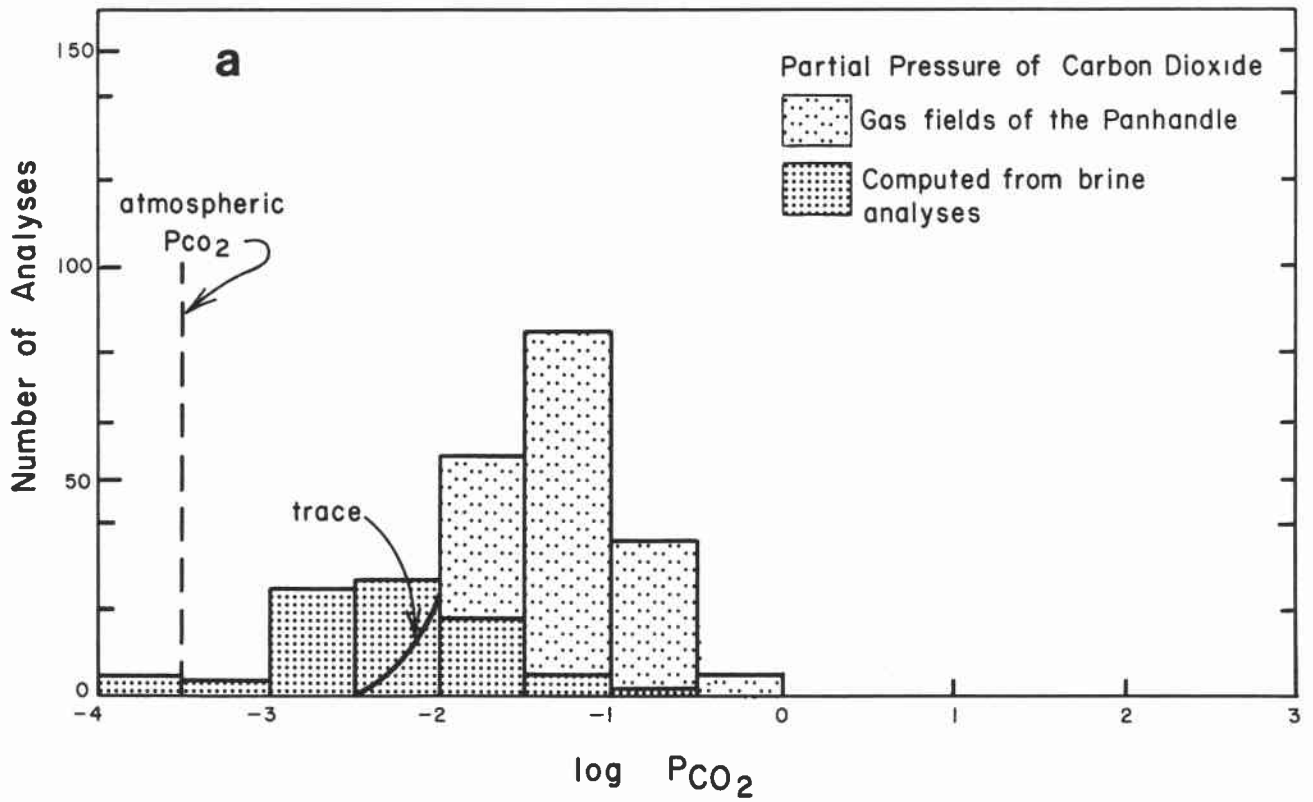


Figure 104. Distribution of  $CO_2$  partial pressure in oil and gas fields in the Palo Duro and Dalhart Basins. Also shown is the distribution of computed  $\log P_{CO_2}$  with (a) reported pH and with (b) the computed pH at the calcite phase boundary.

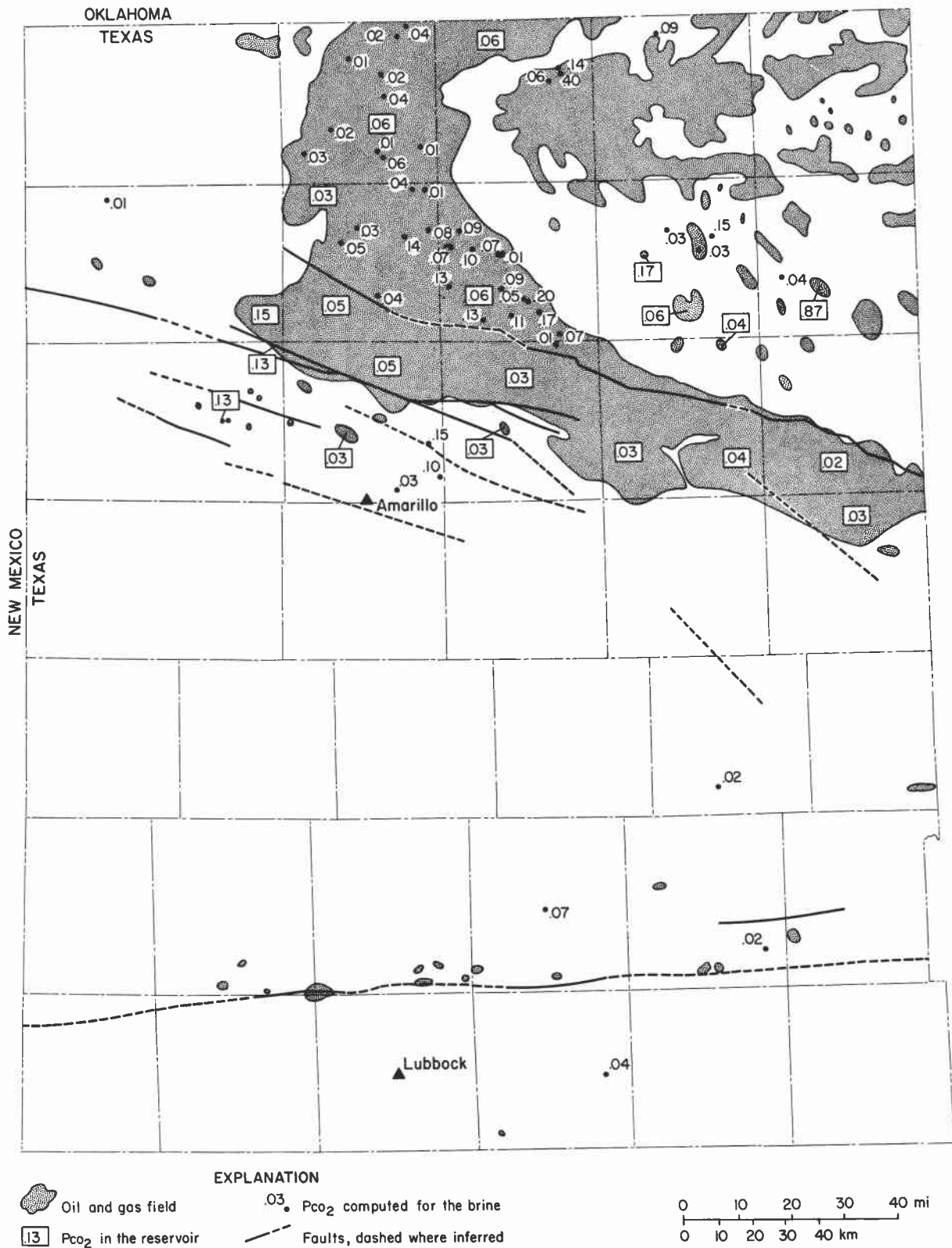


Figure 105. Location map showing (1) the  $PCO_2$  of oil and gas fields in the Palo Duro, Dalhart, and Anadarko Basins, based on the results of analyses of gas samples (Moore, 1976), and (2)  $PCO_2$  computed from analytical results obtained from brine in wildcat and production wells.

## STREAM INCISION AND SCARP RETREAT RATES BASED ON VOLCANIC ASH DATE FROM THE SEYMOUR FORMATION

William W. Simpkins and Robert W. Baumgardner, Jr.

*The Seymour Formation contains alluvial sediment eroded from the Ogallala Formation, and deposited east of the westward-retreating Caprock Escarpment. Volcanic ash deposits within the Seymour in North-Central Texas yield a minimum age for the Seymour deposits, and from this age, maximum rates of stream incision and escarpment retreat can be calculated.*

Pleistocene sands and gravels of the Seymour Formation (Hibbard and Dalquest, 1966) are recognized throughout North-Central Texas. These fluvial deposits were probably derived from the Ogallala Formation (Menzer and Slaughter, 1971). A bed of volcanic ash 1.6 to 6.6 ft (0.5 to 2.0 m) thick occurs at the type section of the Seymour Formation (figs. 106 and 107), overlying both fluvial and lacustrine deposits within the Seymour. Small-scale current ripples with wavelengths of 0.8 to 1.6 inches (2 to 4 cm) occur within the ash deposit in conformable beds 4 inches (10 cm) thick. Locally, the upper part of the ash deposit contains nodules of calcium carbonate (caliche). The primary sedimentary structures in the ash suggest that it was deposited in a fluvial or lacustrine environment.

Samples of volcanic ash from the formation near Seymour were age-dated by the U.S. Geological Survey. Chemical analyses and comparison to previous fission-track-dated volcanic ashes in the Great Plains indicate that the Seymour ash is Pearlette "Type O" ash (G. Izett, personal communication, 1981) as distinguished from other volcanic ashes described by Naeser and others (1971). Accordingly, the ash is 600,000 years old (Kansan in age). This age is substantiated by the similar age of the Pleistocene Cudahy fauna in Meade County, Kansas, which underlies a volcanic ash deposit, and the Vera Faunule in the lacustrine beds, which underlie the ash at the Seymour type section (Hibbard and Dalquest, 1973).

Assuming that the volcanic ash was deposited contemporaneously with the Seymour deposits, then rates of stream incision and escarpment retreat can be calculated. The volcanic ash date yields a minimum age for the Seymour and hence a maximum rate of incision and escarpment retreat.

Average incision rates were calculated by assuming that the ash was originally deposited at about the elevation of the proto-South Wichita and Brazos Rivers, and dividing the present-day difference in elevation between outcrops of the ash and those rivers by the age of the ash (600,000 ybp). The Seymour type locality is 180 ft (55 m)

above and 1.6 mi (2.6 km) south of the South Wichita River (fig. 106), and another distinctive ash outcrop 1 mi (1.6 km) south of the type locality is 140 ft (42.7 m) above and 2.6 mi (4.1 km) north of the Brazos River. Both outcrops are of the so-called Seymour terrace (Pleistocene). Incision rates derived from these sites are 0.0036 inch/yr (0.091 mm/yr) and 0.0028 inch/yr (0.071 mm/yr), respectively. Such rates are average rates for a 600,000-year period, because there were undoubtedly periods of deposition or no net change that alternated with periods of erosion. Instantaneous incision rates would be greater than the average rates calculated from this analysis.

A rate of westward retreat for the Caprock Escarpment was estimated by measuring the distance from the present position of the Caprock Escarpment to the Seymour Formation type locality and then dividing the result by the age of the volcanic ash deposit. Using a linear distance of 71 mi (114 km) (fig. 106), the average retreat rate over the last 600,000 years has been 7.5 inches/yr (19 cm/yr). This is a maximum retreat rate, based on the assumption that the Caprock Escarpment was immediately west of the Seymour type section when ash was deposited.

Calculation of retreat and incision rates is necessary to determine if a repository might be breached by erosional processes. These rates compare closely with those rates derived from different data for the same area (Gustavson and others, 1980, 1981).

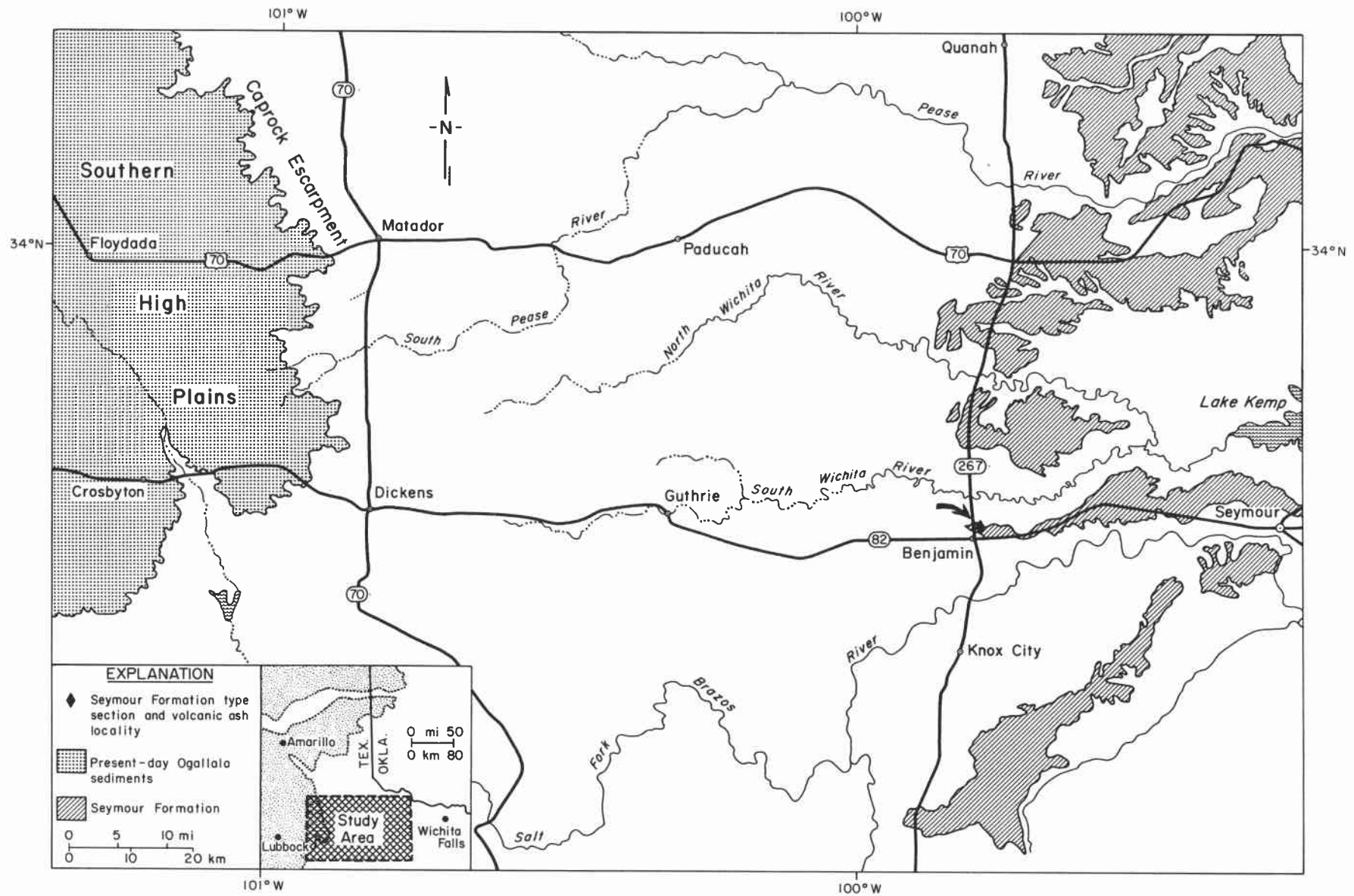


Figure 106. Location of type section, Seymour Formation. Straight-line distance to the Caprock Escarpment is 114 km (71 mi).

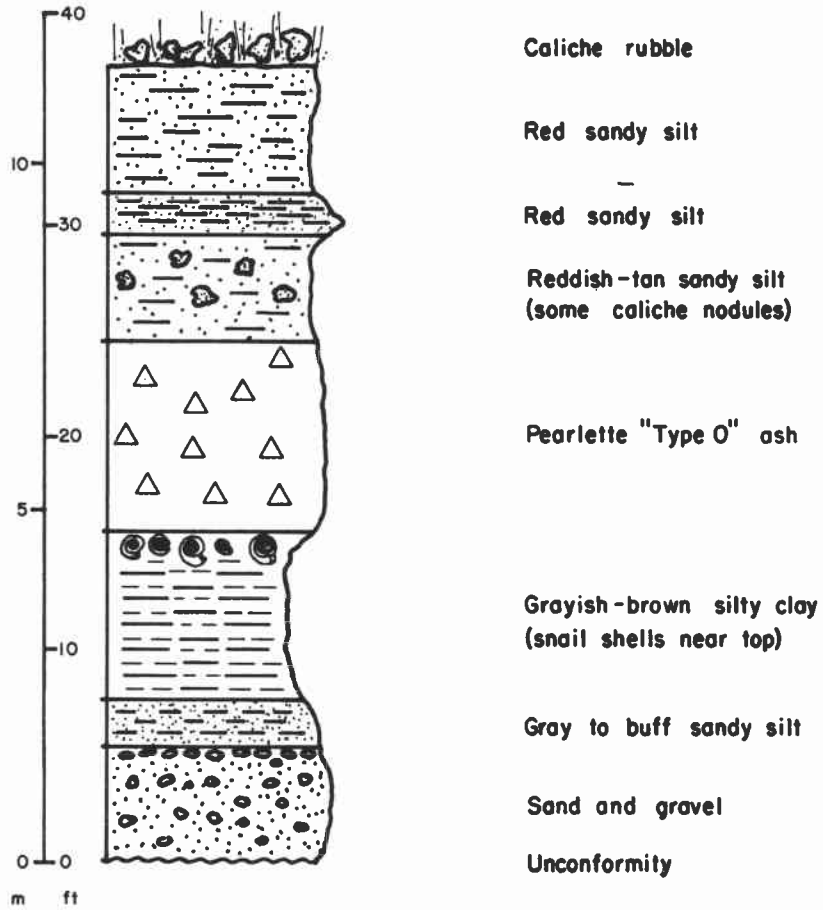


Figure 107. Stratigraphic column, type section, Seymour Formation. A deposit of Pearlette "Type O" volcanic ash crops out near the middle of the type section, forming a resistant cliff. Vertebrate fauna beneath the ash have been correlated with the Pleistocene Cudahy fauna in Kansas (Hibbard and Dalquest, 1973). Adapted from Hibbard and Dalquest, 1966.

## GEOMORPHIC STUDIES OF REPRESENTATIVE DRAINAGE BASINS

Robert W. Baumgardner, Jr.

*Morphometric studies of drainage basins along the Caprock Escarpment are used to describe regional geomorphic characteristics. Results of localized erosion monitoring are thereby placed in a regional perspective.*

Five drainage basins are being studied to characterize the geomorphology of the area surrounding the retreating edge of the Caprock Escarpment. Four basins were chosen to complement detailed field studies completed in the Little Red River Basin within Caprock Canyons State Park (fig. 108). Because of limited ground access none of the other basins can be examined in as much detail as the Little Red River. These basins were chosen on the basis of four criteria. Each basin has (1) stream-gaging records, (2) headwaters along the Caprock Escarpment, (3) surface geology different from that of the Little Red River Basin, and (4) an areal extent approximately the same as that of the Little Red River Basin. Morphometric studies are used to compare the basins in terms of their capacity for transporting sediment and runoff.

Drainage density is defined as the length of streams per unit area. It is a useful measure of drainage basin dynamics because it is influenced by several different factors, including permeability and erodibility of the ground surface, vegetation cover, local relief, and type of precipitation. In the representative basins, values of drainage density normally are higher near the headwaters along the Caprock Escarpment and lower near the mouth of the basin (fig. 109). The same is true of local relief values (fig. 109). High-relief areas enhance the development of drainage pathways that eventually may be incorporated into the stream network. Because drainage density is a measure of the efficiency of the basin in conveying sediment and runoff, areas with high values of drainage density are likely to be sites of elevated erosion rates. Low values of drainage density in Duck Creek Basin (table 8) correspond to low-relief areas, where most natural drainage pathways have been obliterated by terracing and plowing.

Values of the hypsometric integral for each basin can be used to estimate long-term denudation rates in the basin (Finley and Baumgardner, 1981). Values also indicate how much the basin has developed from an original subhorizontal surface. Lower values indicate a higher degree of development and may indicate greater age.

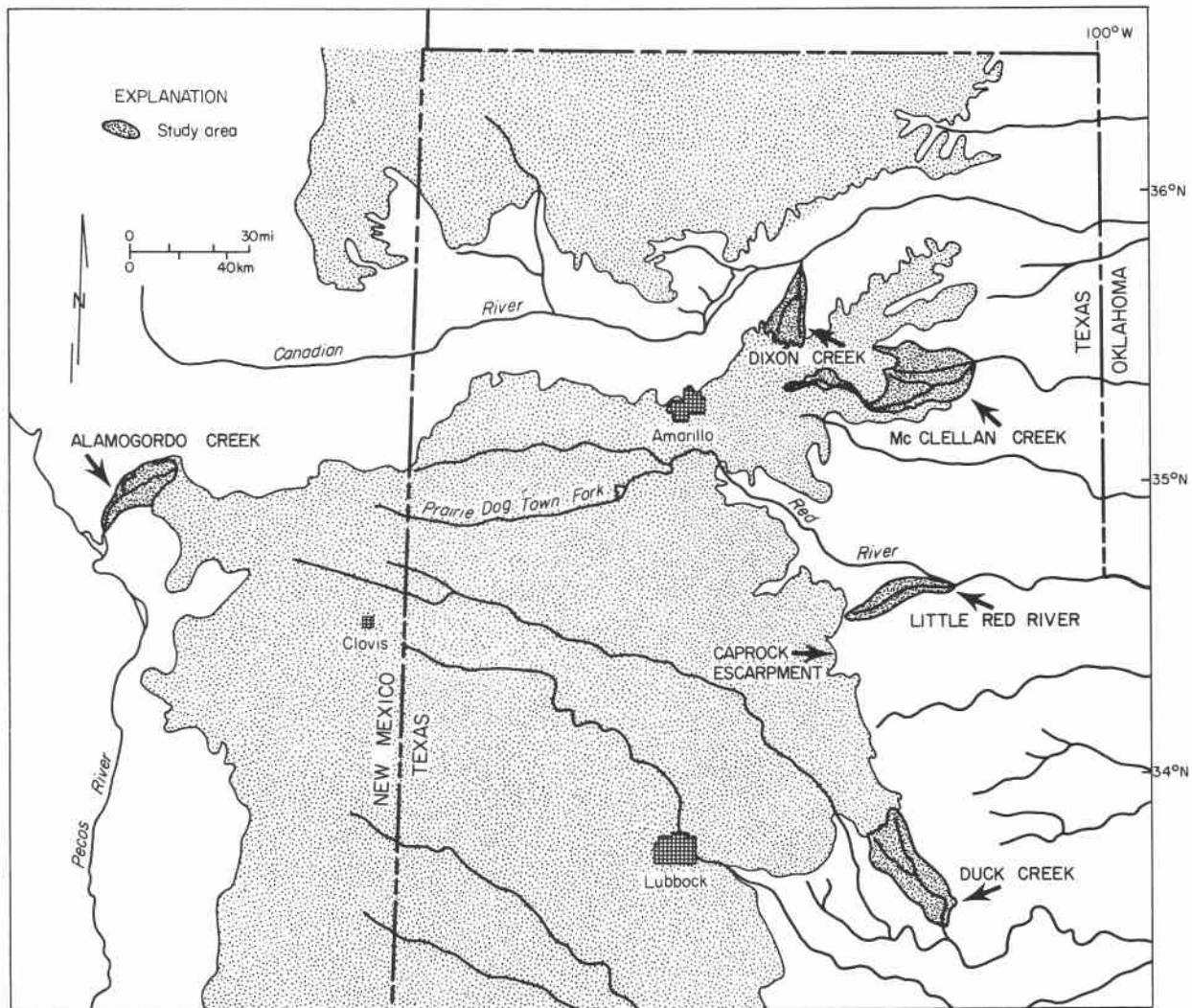


Figure 108. Location of representative drainage basins selected for morphometric study.

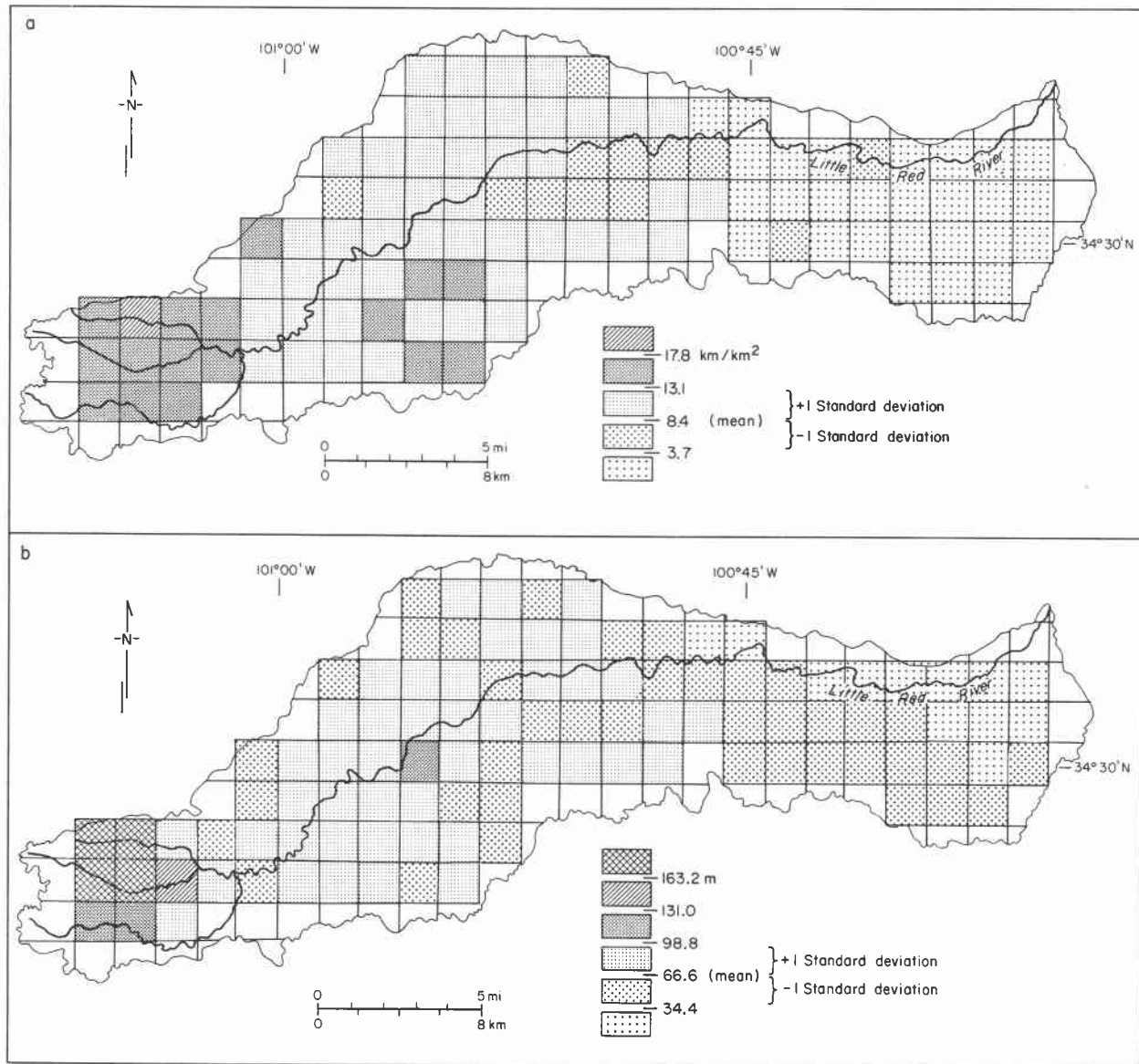


Figure 109. Morphometric data from the Little Red River Basin. (a) Drainage density ( $\text{km}/\text{km}^2$ ) values for  $2.56 \text{ km}^2$  ( $1 \text{ mi}^2$ ) areas. (b) Local relief (m) values. Note close correspondence between high values and low values for both parameters.

Table 8. Selected morphometric parameters for representative drainage basins. Drainage density and local relief are measured on 2.56-km<sup>2</sup> (1-mi<sup>2</sup>) squares.

| Basin      | Area (km <sup>2</sup> ) | Drainage density (km <sup>-1</sup> ) |      |      | Basin Relief (m) | Mean Local relief (m) | Hypsometric integral |
|------------|-------------------------|--------------------------------------|------|------|------------------|-----------------------|----------------------|
|            |                         | Mean                                 | Max. | Min. |                  |                       |                      |
| Alamogordo | 466                     | 5.7                                  | 11.5 | 1.4  | 390              | 61                    | .41                  |
| Dixon      | 340                     | 5.8                                  | 12.1 | 1.1  | 247              | 43                    | .59                  |
| Duck       | 768                     | 3.6                                  | 13.1 | 0.0  | 335              | 28                    | .45                  |
| Little Red | 474                     | 8.4                                  | 19.1 | 0.0  | 415              | 67                    | .27                  |
| McClellan  | 640                     | 7.3                                  | 14.5 | 0.0  | 305              | 40                    | .55                  |

## EROSION PROCESS STUDIES IN THE TEXAS PANHANDLE--ANALYSIS OF A TWO-YEAR DATA RECORD

William W. Simpkins, Thomas C. Gustavson, and Robert J. Finley

*Data have been collected over a 2-year period at six erosion- and climate-monitoring stations in the Texas Panhandle. Net erosion predominates at four stations; mean annual net erosion rates range from 0.11 inch/yr (0.27 cm/yr) to 0.31 inch/yr (0.79 cm/yr). Mean annual net retreat rates taken from rebar measurements range from 1.1 inches/yr (2.9 cm/yr) to 3.4 inches/yr (8.7 cm/yr). Previously published correlations of erosion with slope angle and vegetative cover are most clearly indicated at the Muleshoe station. Linear regression analysis indicates some correlation of increased erosion rates with increasing cumulative rainfall over all stations.*

Erosion process monitoring continues at six stations in the Texas Panhandle. These stations consist of continuously recording temperature and rainfall gages, in addition to 526 erosion pins deployed across a variety of soil types, slopes, and vegetative cover densities. Twenty-seven rebars are emplaced in near-vertical gully walls to record headcut retreat. Data have been accumulated for approximately 2 years at six stations, encompassing 310 erosion pins and 23 rebars. Calculated net erosion rates for erosion pins at these stations appear in tables 9 and 10. Since measurement periods and times of pin emplacement were slightly different at each station, erosion data were converted to annual rates and thus normalized to the same time period. Mean annual net erosion rates range from 0.11 inch/yr (0.27 cm/yr) at the Quitaque station in Caprock Canyons State Park to 0.31 inch/yr (0.79 cm/yr) at the Palo Duro Canyon State Park station. A maximum net erosion rate of 2.09 inches/yr (5.30 cm/yr) is shown for the Caprock Canyons station. According to an analysis of variance test (F-test), the differences in mean annual net erosion rates can be shown to be insignificant at the  $\alpha=0.05$  significance level. Thus, the apparent differences in mean values could be due entirely to measurement variation. It is significant to note, however, that 70 percent of the total number of pins show net erosion during the period of record. Erosion pins also display nearly equal mean annual net erosion rates for different slope classes (table 10), and these rates can be shown by an F-test to not differ statistically at the  $\alpha=0.05$  level of significance. A maximum net erosion rate of 1.46 inches/yr (3.70 cm/yr) occurs in the  $10^{\circ}$  to  $19^{\circ}$  slope class. Rates shown for the higher slope classes may be misleading because in many cases pins are driven into the bedrock that holds up some of the steeper slopes in the area.

Erosion pins favoring net deposition amount to only 30 percent of the total pins measured. Mean annual net deposition rates range from 0.08 inch/yr (0.20 cm/yr) at the

Muleshoe station to 0.22 inch/yr (0.57 cm/yr) at the Buffalo Lake station. The Quitaque station at Caprock Canyons State Park contains the highest percentage (73 percent) of erosion pins showing net deposition for a single station over the 2-year period. The 0° to 9° slope class recorded the highest mean annual net deposition rate of 0.22 inch/yr (0.56 cm/yr) and the maximum rate of 0.75 inch/yr (1.90 cm/yr). A tendency toward more erosion pins showing net deposition on lower-angle slopes is also evident (table 10).

Mass movement processes such as rock fall, debris slides, and avalanches are more important processes on vertical slopes; hence a different measurement technique is utilized than for the rainsplash, sheetwash, and rillwash process that primarily affect erosion pins. Twenty-seven iron-reinforcing rods, or "rebars," have been emplaced in nearly vertical headcuts at the Lake Meredith, Caprock Canyons, and Buffalo Lake sites in an effort to measure these rates of retreat. Highest mean annual net retreat rates of 3.5 inches/yr (8.7 cm/yr) occur at the Buffalo Lake station; the maximum rate of 7.2 inches/yr (18.2 cm/yr) was also recorded there (table 11). An F-test indicated that the mean annual net retreat rates differ statistically at the  $\alpha=0.05$  significance level.

These rates can be compared to other published erosion rates in the region. Bath (1980) reported an erosion rate over a 1-year period of 0.03 inch/yr (0.76 mm/yr) at erosion pins in Palo Duro Canyon State Park. Denudation rates (which include rates of weathering, mass-wasting, and transportation of materials, as well as erosion) given in Gustavson and others (1981) range from 0.02 inch/yr (0.47 mm/yr) on the basis of the geomorphic history of the Little Red River Basin, to 0.17 inch/yr (2.97 mm/yr) according to reservoir sedimentation rates for man-made lakes in the Rolling Plains region. The measured erosion rates for the 2-year analysis compare favorably with these cited denudation rates. Mean headcut retreat rates of 2.0 inches (5.1 cm) were recorded as a result of one 10-year recurrence interval storm at the Buffalo Lake station in 1978 (Finley and Gustavson, in press).

### Factors Affecting Erosion

Factors that may influence erosion rates at each site include slope length and slope angle (Wischmeier and Smith, 1965; Bryan, 1979), vegetation cover (Ellison, 1948; Schumm, 1965), substrate type (Emmett, 1970; Quansah, 1981), rainfall amount and intensity (Wischmeier and Smith, 1965), antecedent moisture conditions (Bryan, 1979) and slope aspect (Melton, 1960). Currently, sufficient data are available only for preliminary evaluation of the influence of vegetation cover, slope angle, and cumulative rainfall.

Scattergrams with least-squares regression lines for slope angle and vegetative cover plotted against net erosion rate are shown for the Muleshoe station (figs. 110 and

111), which displays the best correlation coefficients for slope angle ( $R^2 = .29$ ) and vegetative cover ( $R^2 = .36$ ) with net erosion rate--both significant at the  $\alpha=0.01$  significance level. Other stations in the present study display much lower  $R^2$  values and were not significant at  $\alpha=0.05$  significance level. In Palo Duro Canyon, Bath (1980) obtained values of  $R^2 = 0.0002$  and  $R^2 = 0.0200$  for correlations of erosion with slope angle and vegetation, respectively. Bryan (1979) noted a mean  $R^2$  value of 0.60 for total soil loss (splash and sheetwash) caused by the effect of slope angle alone on various soil types in the northern U.S. and Canada. Leopold and others (1966) and Bryan (1979) noted difficulties in obtaining a significant correlation of slope and vegetation with erosion, indicating that much of the variance in erosion rates was as yet unexplained. Bryan (1979) suggested that the variability is due to microscale variations in soil surface characteristics, thickness of surface-water layers, and raindrop size and point of impact.

Cumulative rainfall over the measurement period apparently has some relation to the rate of erosion at a particular site (fig. 112). Presumably, periods of long, low-intensity rainfall serve to encourage vegetative growth, which would tend to slow erosion rates. However, it is apparent from figure 112 that rainfall creates more erosion than vegetative growth; Wischmeier and Smith (1965) also suggested that rainfall intensity was a more important contributor to soil erosion. Studies of the region by Bath (1980) and Finley and Gustavson (1980) indicated that intense rainfall occurs frequently and causes most of the soil erosion, depending on factors at the particular site. Other studies include calculations of values of kinetic energy expended on the soil from rainfall (Wischmeier and Smith, 1958).

In summary, it appears that the erosion rates calculated from a 2-year data record are valid under current climatic conditions, mostly because of their similarity to other long-term denudation and scarp retreat rates (Gustavson and others, 1981). Certain statistical relations between erosion factors are shown more clearly at some sites than at others, which may indicate that a single factor (such as slope angle or vegetative cover) will not fully explain the variability in the erosion rates at all six stations. Yet, all the stations show mean annual net erosion rates not statistically different from each other, perhaps indicating some uniformity of process. Clearly, additional factors (such as slope aspect, soil type, and antecedent moisture) must be evaluated to add statistical validity to statements regarding the controls on erosion in the Texas Panhandle.

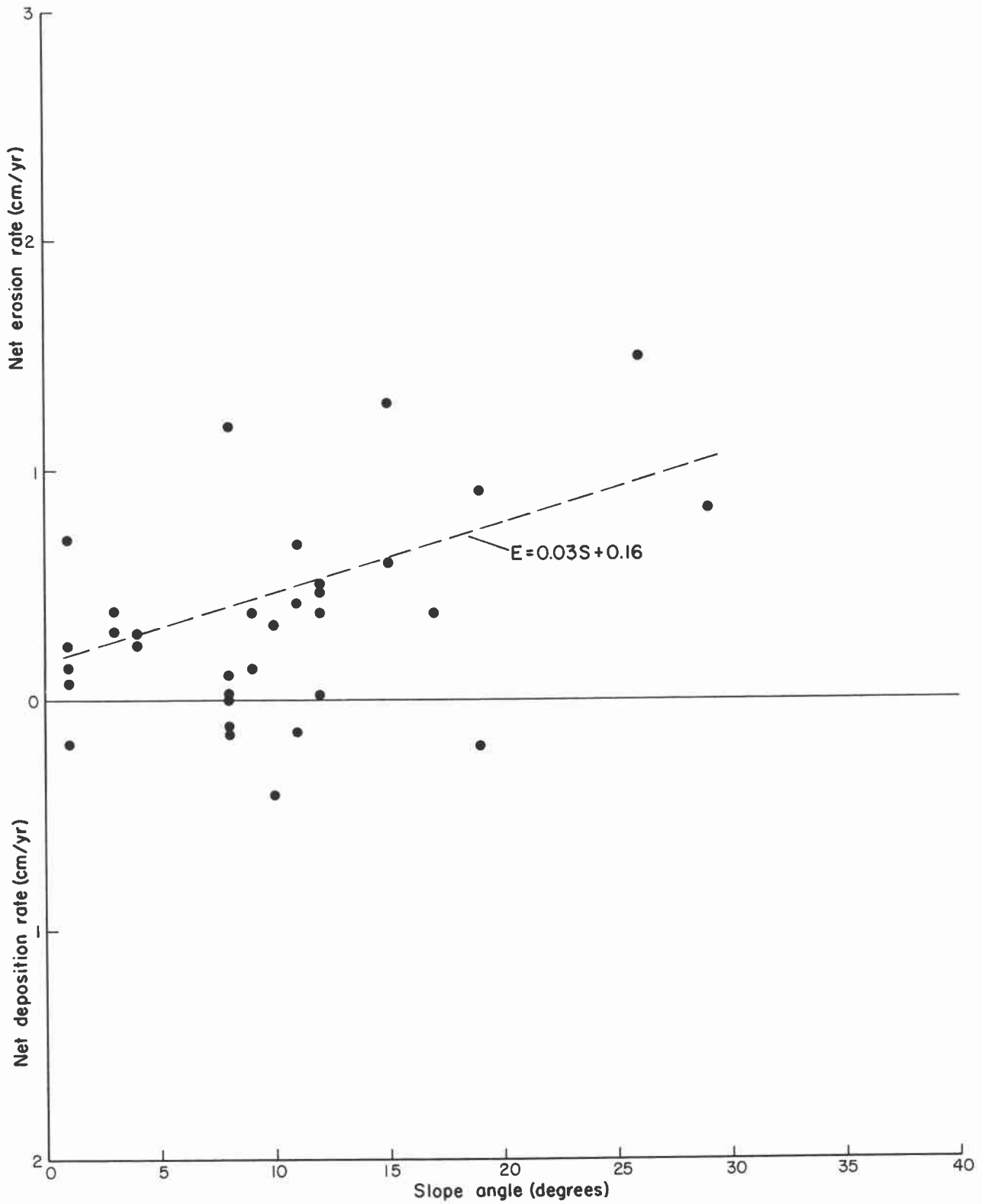


Figure 110. Scattergram showing relation between slope angle and net erosion/deposition rate for the Muleshoe station. Linear least-squares regression line for slope angle versus erosion is shown (dashed), plus the equation for that line.

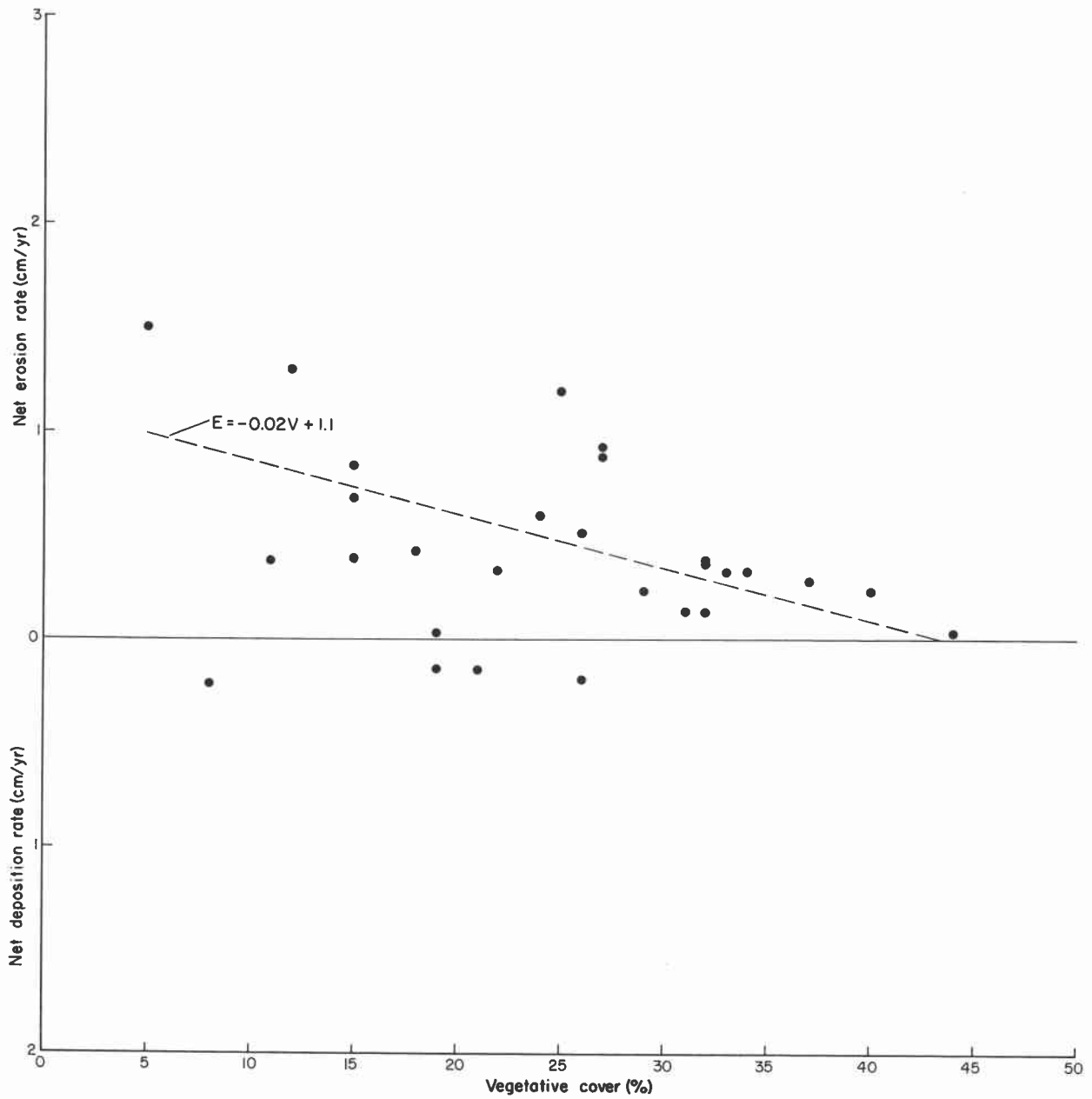


Figure 111. Scattergram showing relation between percent vegetative cover and net erosion/deposition rate for the Muleshoe station. Linear least-squares regression line for vegetative versus erosion is shown (dashed), plus the equation for that line.

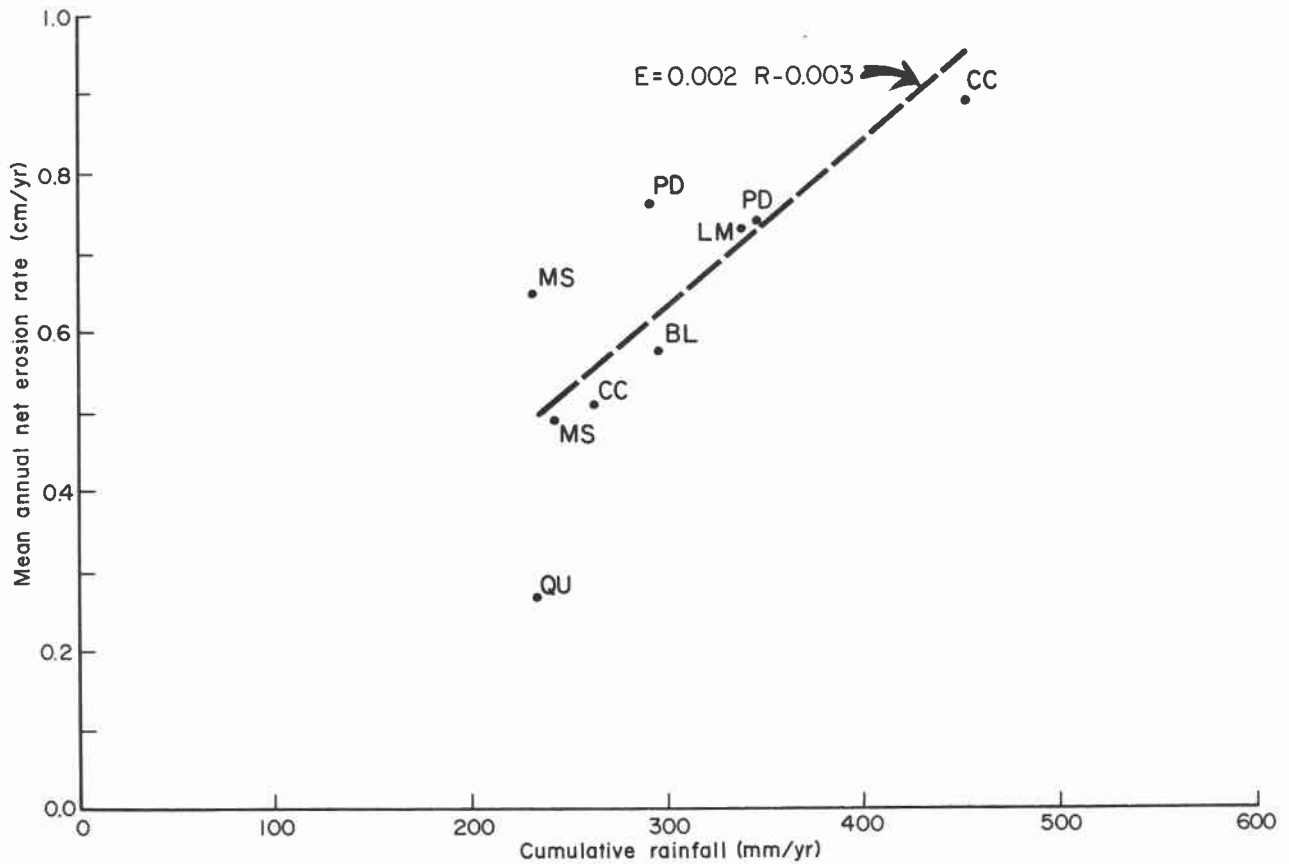


Figure 112. Scattergram showing the relation between cumulative rainfall (per year) and mean erosion rates (per year) for stations in the Texas Panhandle. Stations are shown more than once where lengths of pin emplacement differed within a station. Linear least-squares regression line is shown (dashed), plus the equation for that line.

Table 9. Mean, maximum, and minimum annual net erosion rates for erosion-monitoring stations in the Texas Panhandle. Differences in mean rates are not statistically significant at the  $\alpha=0.05$  level of significance.

| Station          | Pins Eroding | Pins Dep. | No Change | Mean | Annual Erosion Rate (cm/yr) |      |
|------------------|--------------|-----------|-----------|------|-----------------------------|------|
|                  |              |           |           |      | Min.                        | Max. |
| Buffalo Lake     | 19           | 30        | 3         | 0.58 | 0                           | 0.73 |
| Caprock Canyons  | 78           | 16        | 2         | 0.68 | 0                           | 5.3  |
| Lake Meredith    | 38           | 13        | 0         | 0.73 | 0.04                        | 3.7  |
| Muleshoe NWR     | 27           | 5         | 1         | 0.45 | 0                           | 1.5  |
| Palo Duro Canyon | 42           | 13        | 1         | 0.79 | 0                           | 3.0  |
| Quitaque         | 4            | 16        | 2         | 0.27 | 0                           | 0.59 |

Table 10. Mean, maximum, and minimum annual net erosion rates for assigned slope classes at erosion-monitoring stations in the Texas Panhandle. Differences in mean rates are not statistically significant at the  $\alpha=0.05$  level of significance.

| Slope Class | Pins Eroding | Pins Dep. | No Change | Mean | Annual Erosion Rate (cm/yr) |      |
|-------------|--------------|-----------|-----------|------|-----------------------------|------|
|             |              |           |           |      | Min.                        | Max. |
| 0-9°        | 59           | 39        | 3         | 0.49 | 0                           | 2.2  |
| 10-19°      | 56           | 27        | 2         | 0.68 | 0                           | 3.7  |
| 20-29°      | 50           | 18        | 3         | 0.63 | 0                           | 2.6  |
| 30-39°      | 36           | 4         | 2         | 0.65 | 0                           | 2.0  |
| 40-49°      | 6            | 1         | 0         | 0.64 | 0.06                        | 1.2  |
| 50-59°      | 2            | 0         | 0         | 1.08 | 0.76                        | 1.4  |
| 60-69°      | 0            | 1         | 0         | N/A  | N/A                         | N/A  |

Table 11. Mean, maximum, and minimum annual net retreat rates for rebars at three erosion-monitoring stations in the Texas Panhandle. Differences in mean rates are statistically significant at the  $\alpha=0.05$  level of significance.

| Station         | Number of Rebars | Annual Retreat Rate (cm/yr) |         |         |
|-----------------|------------------|-----------------------------|---------|---------|
|                 |                  | Mean                        | Minimum | Maximum |
| Buffalo Lake    | 7                | 8.7                         | 4.5     | 18.2    |
| Caprock Canyons | 6                | 2.9                         | 0.1     | 6.2     |
| Lake Meredith   | 10               | 5.3                         | 0.4     | 10.8    |

## STRUCTURAL CONTROL OF MAJOR DRAINAGE ELEMENTS SURROUNDING THE SOUTHERN HIGH PLAINS

Thomas C. Gustavson

*The Pecos Valley on the western margin, the Canadian River Valley on the northern margin, and the Palo Duro Canyon on the northeastern margin of the High Plains all originated as subsidence troughs caused by dissolution of Permian bedded salts.*

Many geologists have recognized that the Pecos Valley is at least in part the result of subsidence over zones of dissolution of Permian bedded salts. At the end of deposition of the Ogallala Formation, a nearly continuous, eastward-sloping, alluvial surface existed across eastern New Mexico and the Texas Panhandle. In the shallow subsurface, Permian bedded salts occurred around the margins of the Palo Duro Basin beneath Permian, Triassic, and Cretaceous sediments and across the Dalhart and Anadarko Basins where the Dockum Group (Triassic) and younger sediments had been removed before Ogallala sedimentation. Salt dissolution and collapse was active in these shallow areas before (Schultz, 1977) and during (Gustavson and others, 1980) Ogallala sedimentation. As long as Ogallala sedimentation was active, deposition apparently kept up with subsidence, for there is no reason to expect that dissolution stopped during Ogallala time. At the end of Ogallala deposition, subsurface dissolution continued, and collapse was translated to surface subsidence along the zones of active dissolution (figs. 113 through 117).

The regional slope of the Ogallala varied from eastward in the northern Texas Panhandle to southeastward in the Southern High Plains (fig. 118a). Subsidence troughs developed along the dissolution zones and diverted streams that flowed along the regional slope of the Ogallala surface (fig. 118b). As these troughs formed, sediments accumulated in them, but eventually the subsidence troughs coalesced along the dissolution zone and allowed stream waters to be diverted by overtopping divides between adjacent basins (fig. 115). When this began near the present Canadian River, southeasterly flowing streams were diverted by the subsidence basins, but the streams still were influenced by regional slope; consequently they flowed along a line of subsidence basins to the east and northeast, eventually evolving into the Canadian River. Near the present Pecos River Valley, southeasterly flowing streams that were diverted by subsidence basins began to flow along a line of basins that extended to the south to form the Pecos River. Streams probably were not diverted into the valley of the Prairie Dog Town Fork near the present Palo Duro Canyon, but the process of subsidence concentrated the processes of erosion, leading to the development of the Palo Duro Canyon (fig. 118b).

Remnants of these subsidence basins that formed at the end of Ogallala sedimentation may be represented by Blancan-age lacustrine sediments preserved as the Rita Blanca

Beds on the north flank of the Canadian River Valley near Channing, Texas, and at North Cita Canyon, a tributary of the Palo Duro Canyon (fig. 118b). These beds contain late Pliocene to early Quaternary fossils and thus date the time of basin formation. They therefore provide a minimum date for the onset of the process of dissolution subsidence and stream diversion (fig. 118a through d).

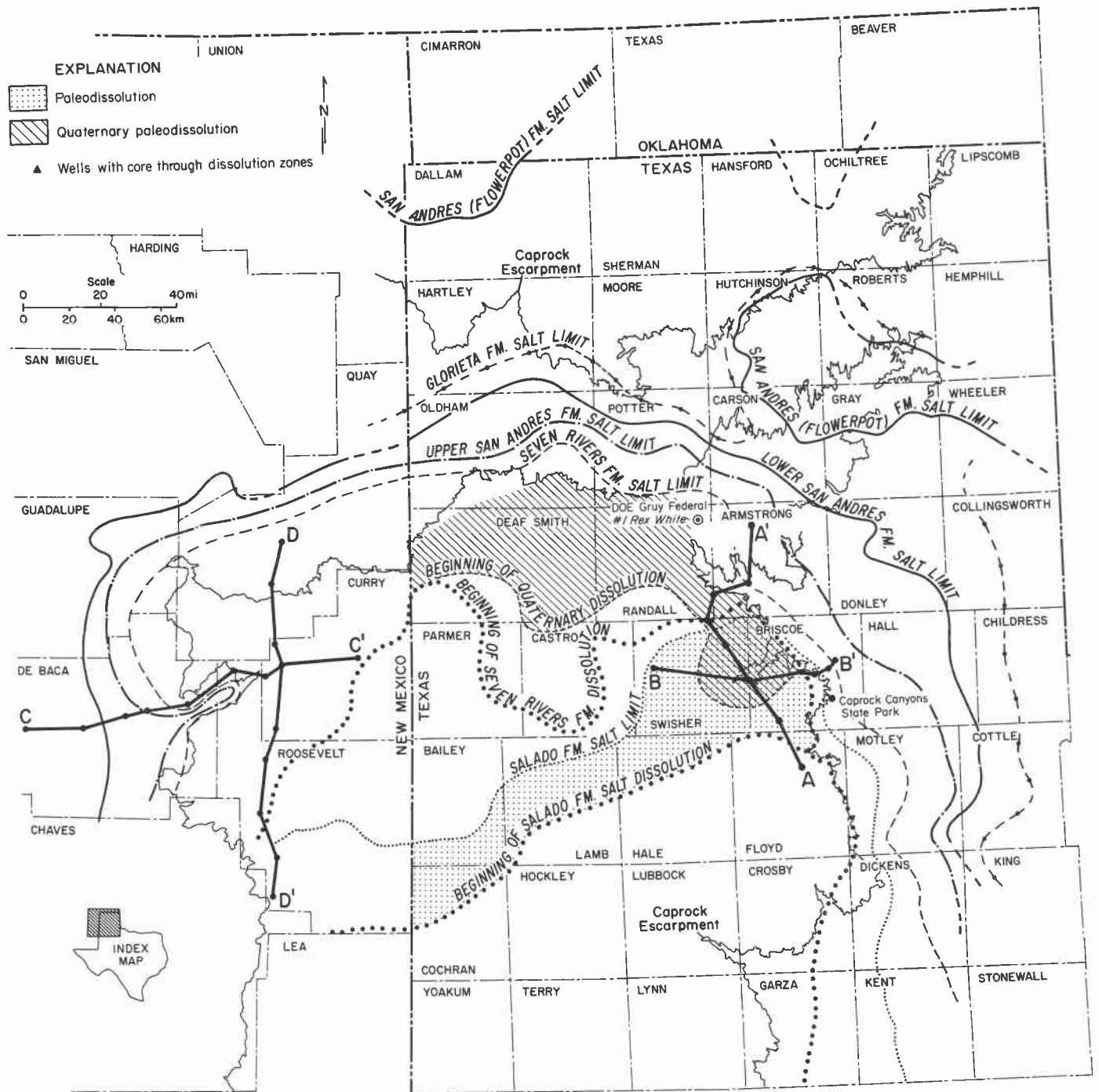


Figure 113. Zones of salt dissolution in eastern New Mexico and in Texas and Oklahoma Panhandles (after Gustavson and others, 1980a). A-A' is figure 116, B-B' is figure 117, C-C' is figure 114, and D-D' is figure 115.

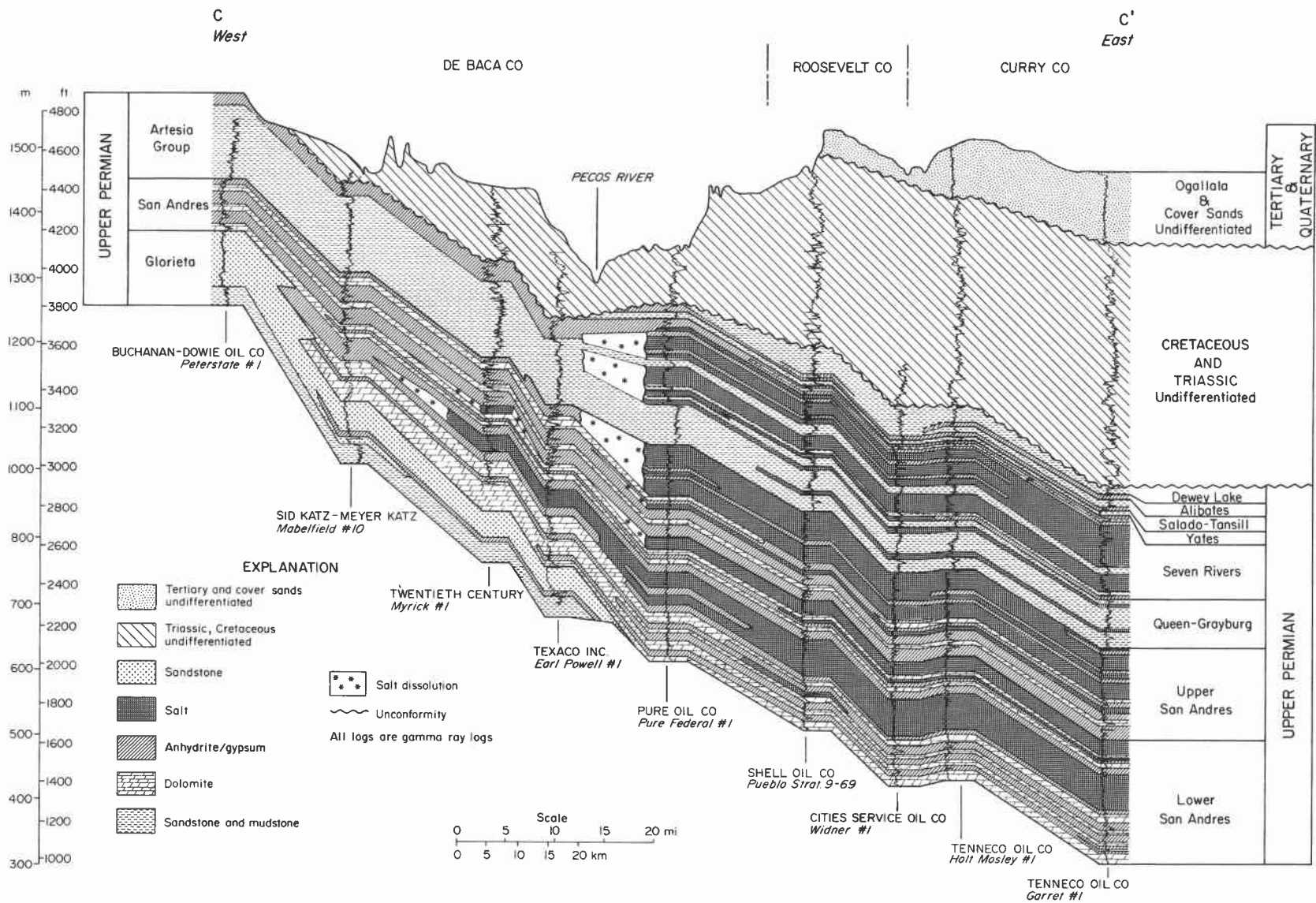


Figure 114. Stratigraphic section illustrating salt dissolution and collapse of strata beneath the Pecos River. See figure 113 for the location of cross section C-C'.

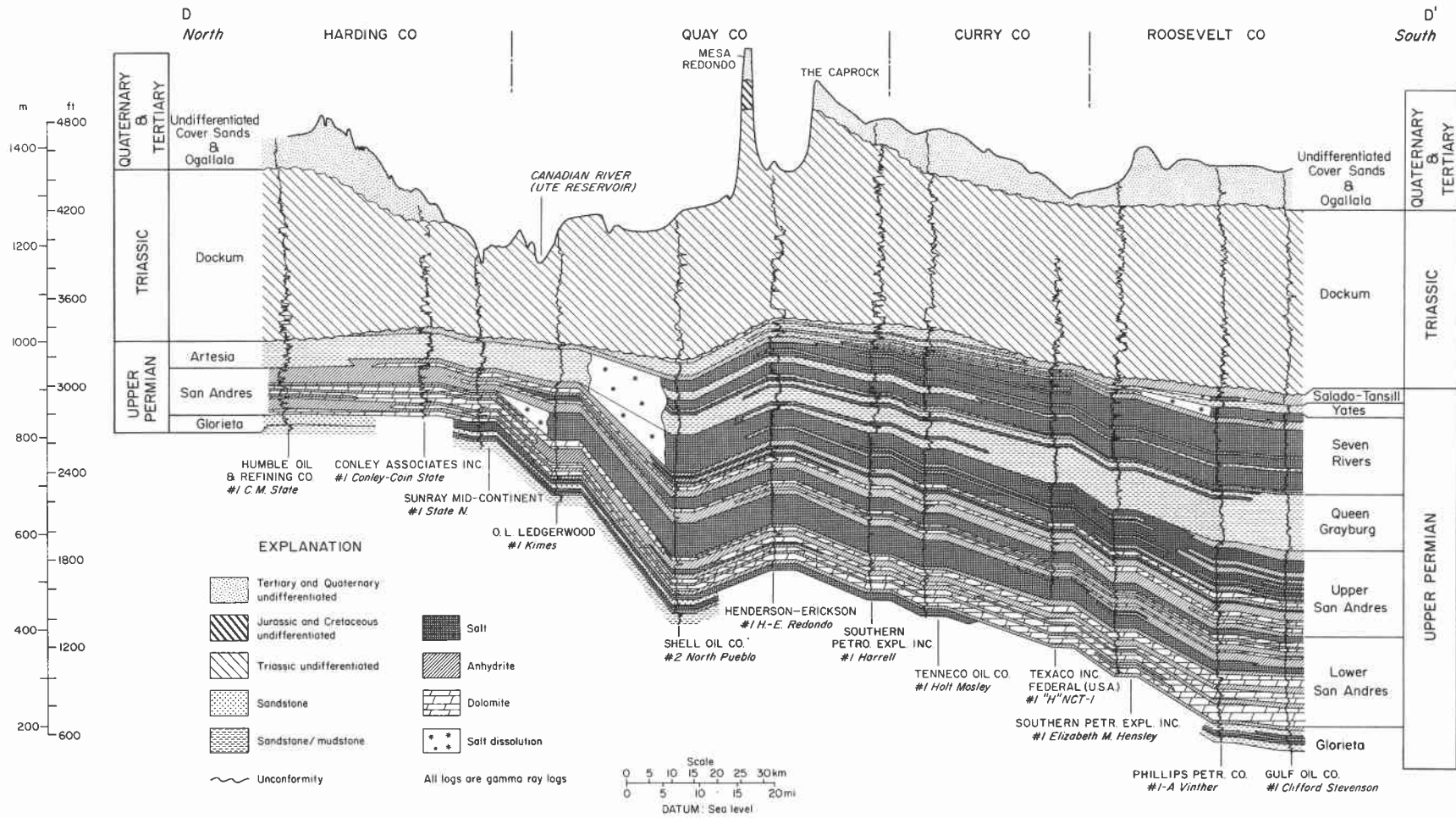


Figure 115. Stratigraphic section illustrating salt dissolution and collapse of strata beneath the Canadian River. See figure 113 for the location of cross section D-D'.

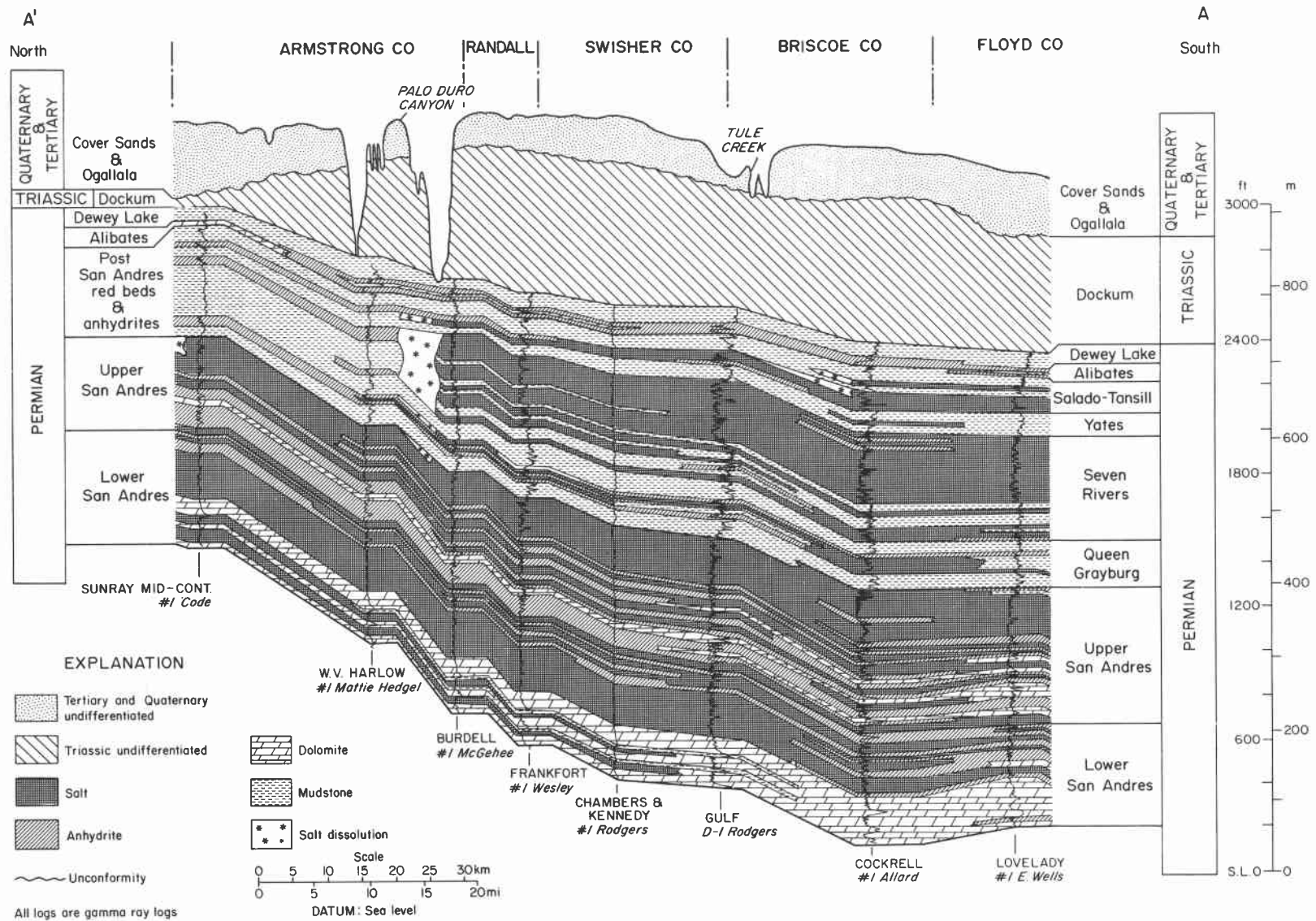


Figure 116. Stratigraphic section illustrating dissolution of Seven Rivers and Salado salts and collapse of overlying strata. See figure 113 for location of section A-A'.

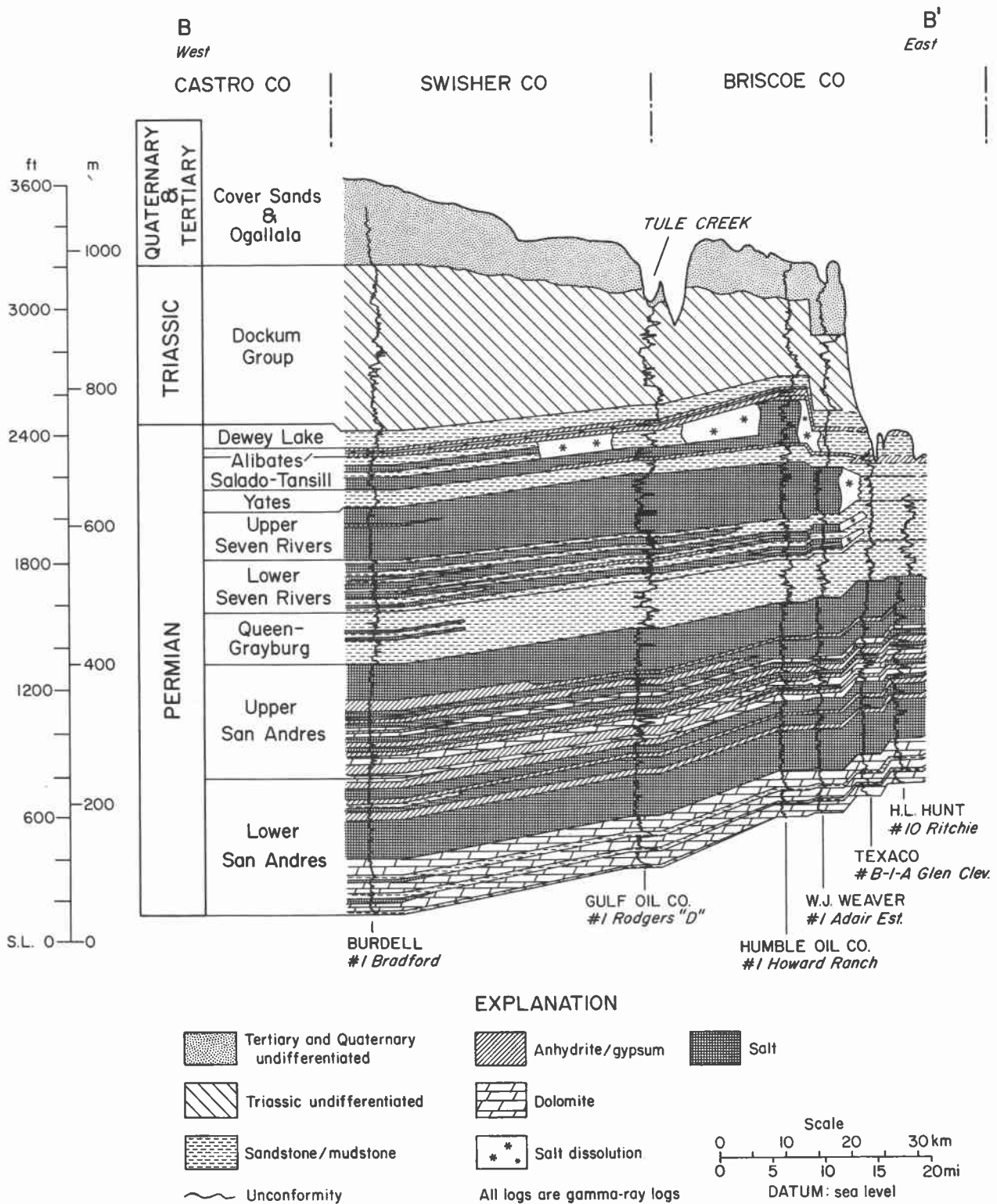


Figure 117. Stratigraphic section illustrating dissolution of Salado Formation salts and collapse of overlying strata. See figure 113 for location of section B-B'.

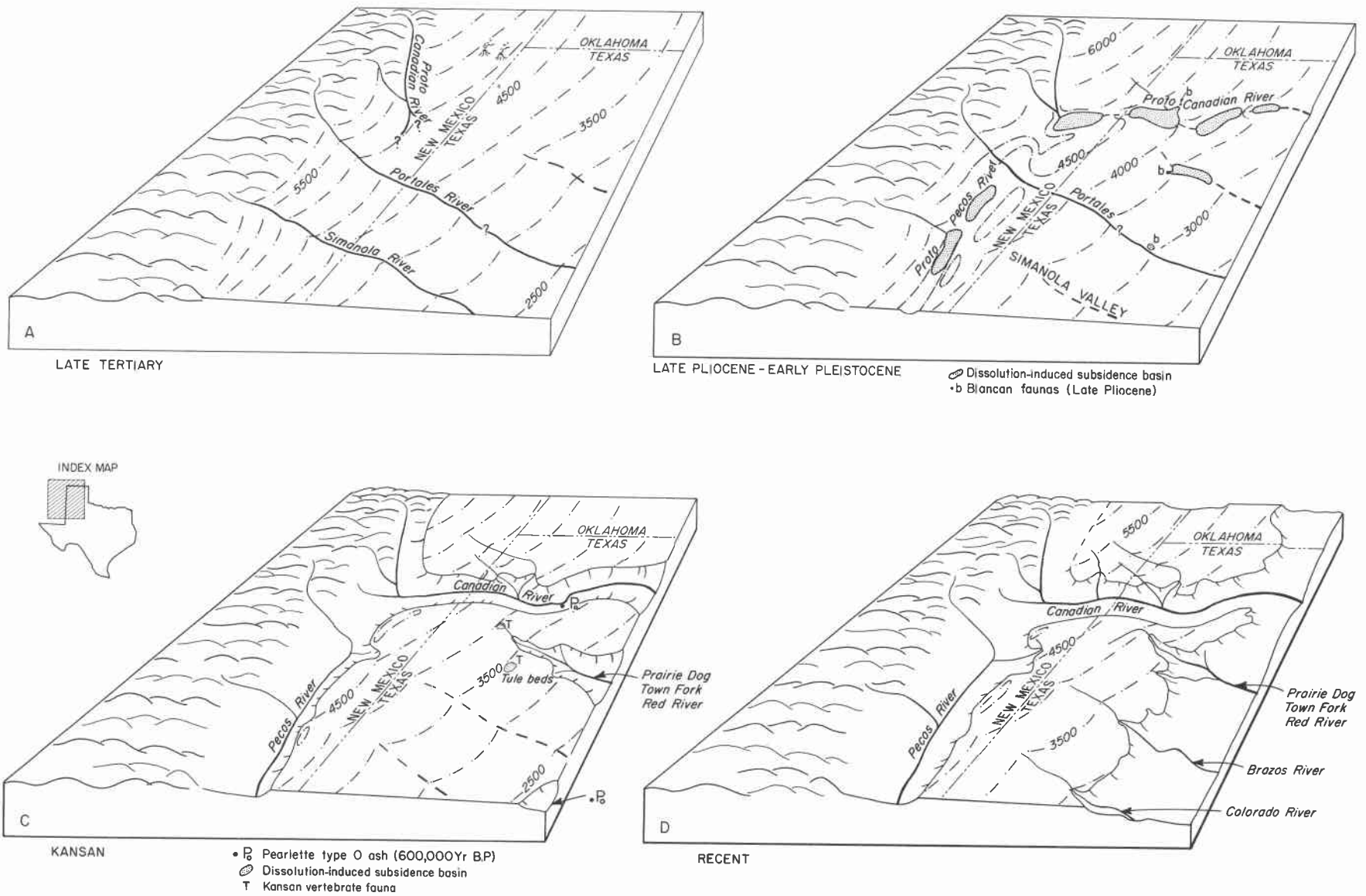


Figure 118. Evolution of drainage in eastern New Mexico and the Texas Panhandle.

## DETERMINATION OF SALT PURITY USING GAMMA-RAY LOGS: SAN ANDRES FORMATION, PALO DURO BASIN

Stephen C. Ruppel and Paul J. Ramondetta

*The mud content of salt deposits in the Palo Duro Basin can be estimated on the basis of gamma-ray logs. Maps have been prepared showing salt purity trends for three San Andres salt intervals: (1) upper San Andres, (2) lower San Andres cycle 5, and (3) lower San Andres cycle 4.*

Previous studies of San Andres bedded salts have illustrated that these deposits are not homogeneous but rather contain varying admixtures of several lithologies including anhydrite and mud (terrigenous clay) as well as halite. Determination of the amounts of impurities (nonhalite proportions) present in these salt beds may be important in locating the best deposits for possible nuclear waste isolation.

Ramondetta and Merritt (this volume) have previously demonstrated the use of geophysical borehole logs in determining mud and anhydrite content in the San Andres cycle 4 salt unit. As they pointed out, both neutron and gamma-ray logs are useful indicators of mud content; density logs give good estimates of the anhydrite fraction. Although porosity logs (neutron and density) are relatively rare in the Palo Duro Basin, gamma-ray logs are common. The approximate mud content of bedded salts across the Palo Duro Basin can thus be determined using available gamma-ray logs.

Gamma-ray values were "calibrated" by comparing them to mud contents determined by point counting the cycle 4 salt in core from two test wells (DOE-Gruy Federal--Rex White No. 1 in Randall County and DOE-Gruy Federal--Grabbe No. 1 in Swisher County; tables 12 and 13) (figs. 119 and 120). Typical variables in borehole conditions that may affect gamma-ray readings (such as mud weight and hole size) were closely controlled and monitored in these wells; gamma-ray calibration is thus based on these known variables. In other wells, gamma-ray logs were recorded under typical wildcat drilling conditions that were different from those in these test wells; the hole size in oil field wells is usually much higher, generally beyond the reach of caliper measurement, owing to the use of fresh-water drilling fluid. To compensate for differing conditions in the DOE test wells that were used for calibration and other wells in the basin, a correction was applied. This was empirically determined by comparing the gamma-ray log from the DOE-Gruy Federal No. 1 Rex White test well in Randall County with gamma-ray logs from six immediately adjacent (less than 4 mi away) wildcat wells. By assuming uniform salt purity in this small area, a correction factor of 1.5X was determined. This was subsequently applied to all gamma-ray values taken from wildcat wells throughout the basin.

Specific procedures were as follows:

- (1) Average gamma-ray values (measured directly in API units or calculated by multiplying Mg/eq ton units by 11.7) were estimated for 10-ft intervals in each salt unit on 1"-100' logs (sonic, density, or neutron).
- (2) API values were corrected for borehole effects by multiplying by 1.5.
- (3) Shale breaks less than or equal to 30 ft within salt units were averaged in with the salt (in practice, breaks greater than 10 ft occurred only in the upper San Andres).
- (4) Shale breaks greater than 30 ft were used to separate salt beds into more than one unit (this also occurred only in the upper San Andres).
- (5) An average value was calculated for each salt unit in each well by averaging corrected values.

Salt purity maps were prepared for salt intervals in the upper San Andres (fig. 121), the lower San Andres cycle 5 (fig. 122), and the lower San Andres cycle 4 (fig. 123). These maps define areas of more pure (lower API values) and muddier (higher API values) salt beds. Comparison of gamma values with core in DOE test wells (figs. 119 and 120) indicates the following correlation between API values and percent mud:

12-15 API  $\approx$  6-12% mud

15-20 API  $\approx$  12-30% mud

>20 API  $\approx$  >30% mud

Although these values are relatively consistent, some variability can be observed (figs. 119 and 120). Probably the major cause of this is variation in the radioactivity of the clays. Unrecognized anhydrite mixed in with clays could also account for some discrepancy between gamma-ray values and point count data.

It should be emphasized that no attempt has been made to separate anhydrite from halite. There are two reasons for this. First, no evidence has yet been presented to indicate that anhydrite is any less suitable than halite as a waste repository host rock. Second, gamma-ray logs, which are far more numerous than other types of logs in the basin, cannot differentiate anhydrite from halite.

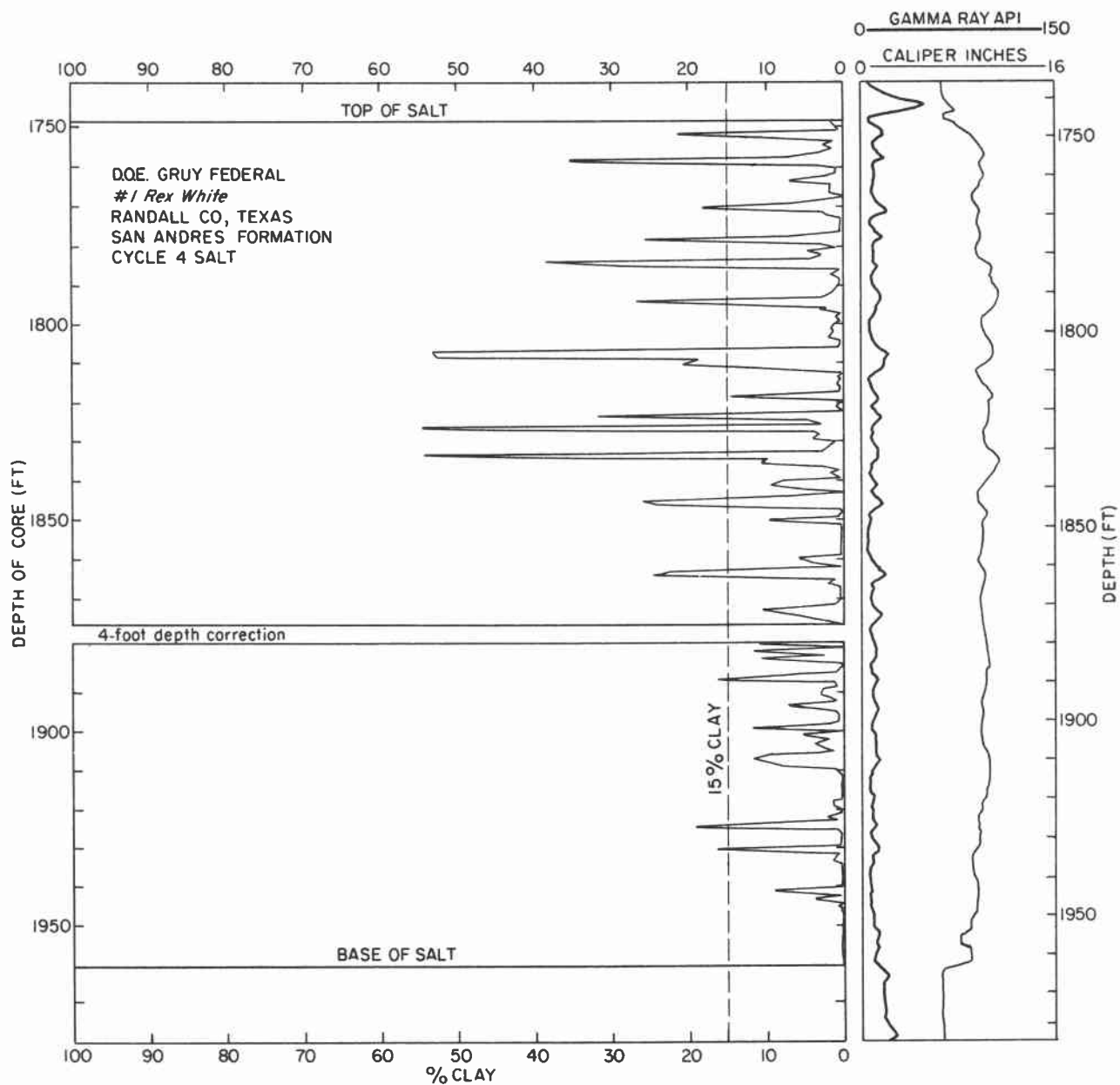


Figure 119. Correlation between gamma-ray log response and mud content in San Andres Formation cycle 4 salt interval, DOE-Gruy Federal Rex White No. 1, Randall County. See explanation for figure 123. Note: Point count plot is 2 ft deeper than gamma-ray log above 1,877 ft and 2 ft shallower below 1,877 ft.

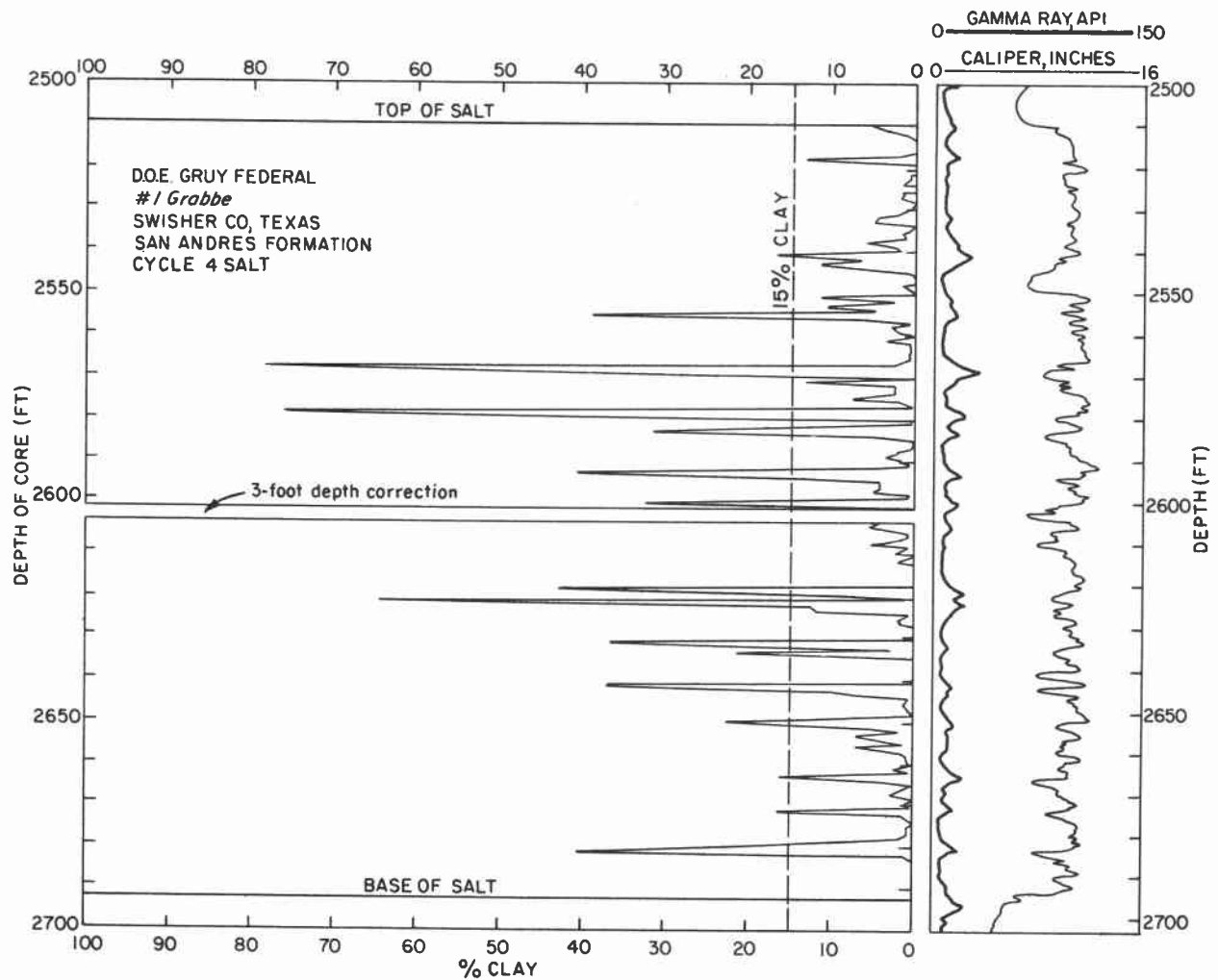


Figure 120. Correlation between gamma-ray log response and mud content in San Andres Formation cycle 4 salt interval, DOE-Gruy Federal Grabbe No. 1, Swisher County. Mud content includes (1) gray, green, and black clay, (2) red clay, (3) anhydritic (?) mud. Anhydrite is not separated from halite in this plot since such a distinction cannot be made by the gamma-ray log. Note: Point count plot is shifted down 3 ft at 2,602 ft to align with gamma-ray log.

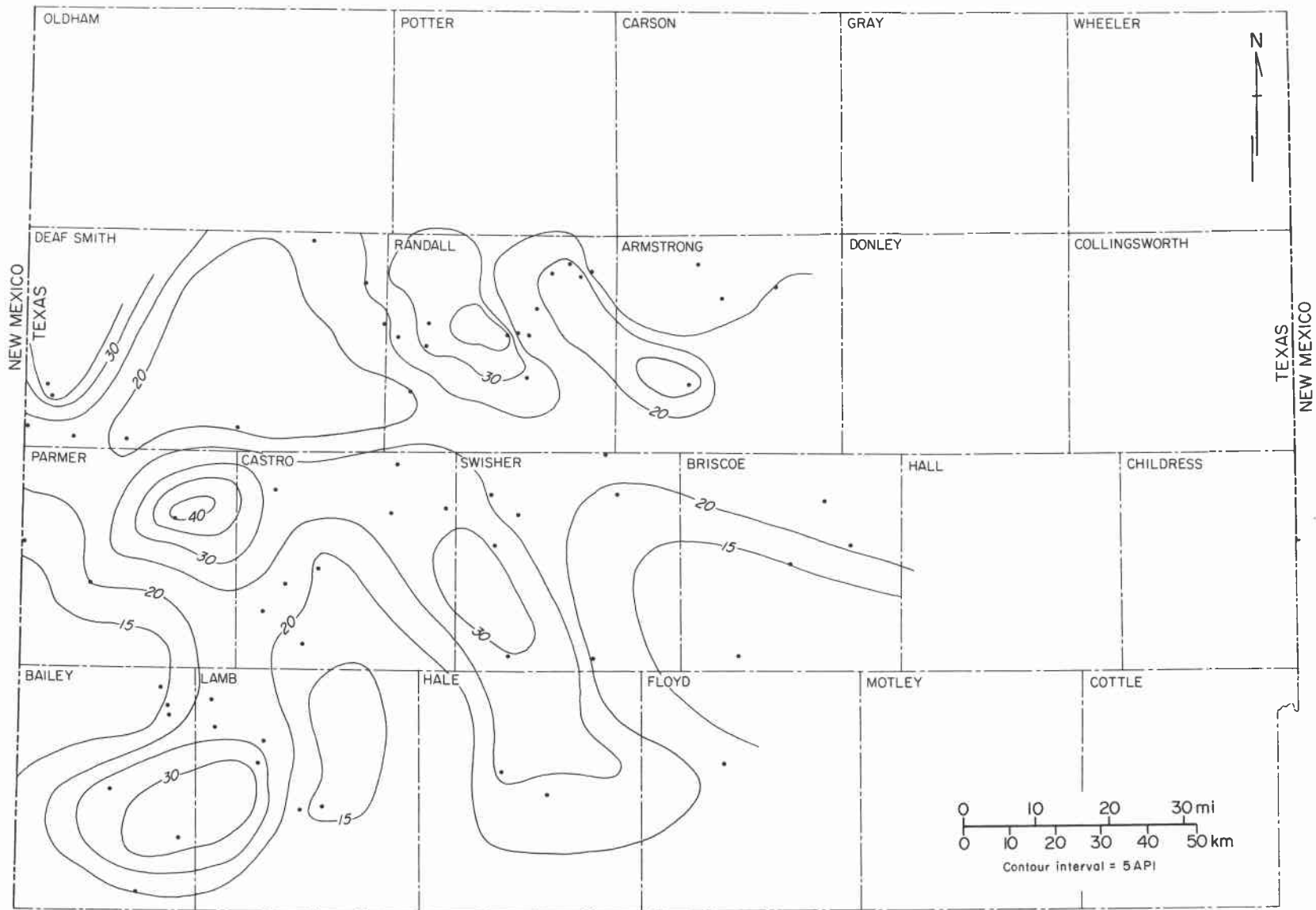


Figure 121. Contour map of average gamma-ray (API unit) values for the upper San Andres Formation salt interval. Note: Where unit is split by shale interbeds, purity values reflect thickest interval only.

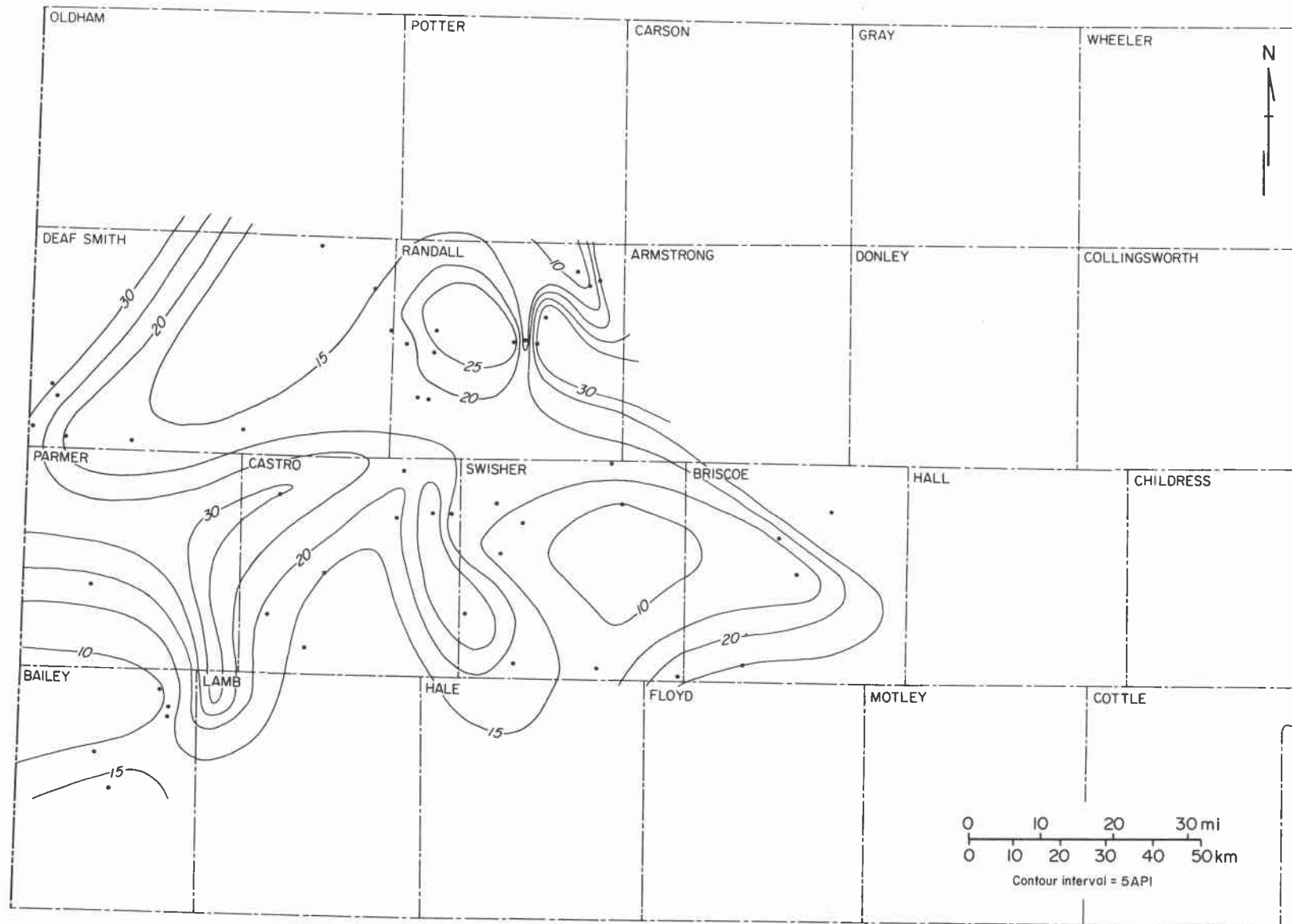


Figure 122. Contour map of average gamma-ray (API unit) values, cycle 5 salt, lower San Andres Formation.

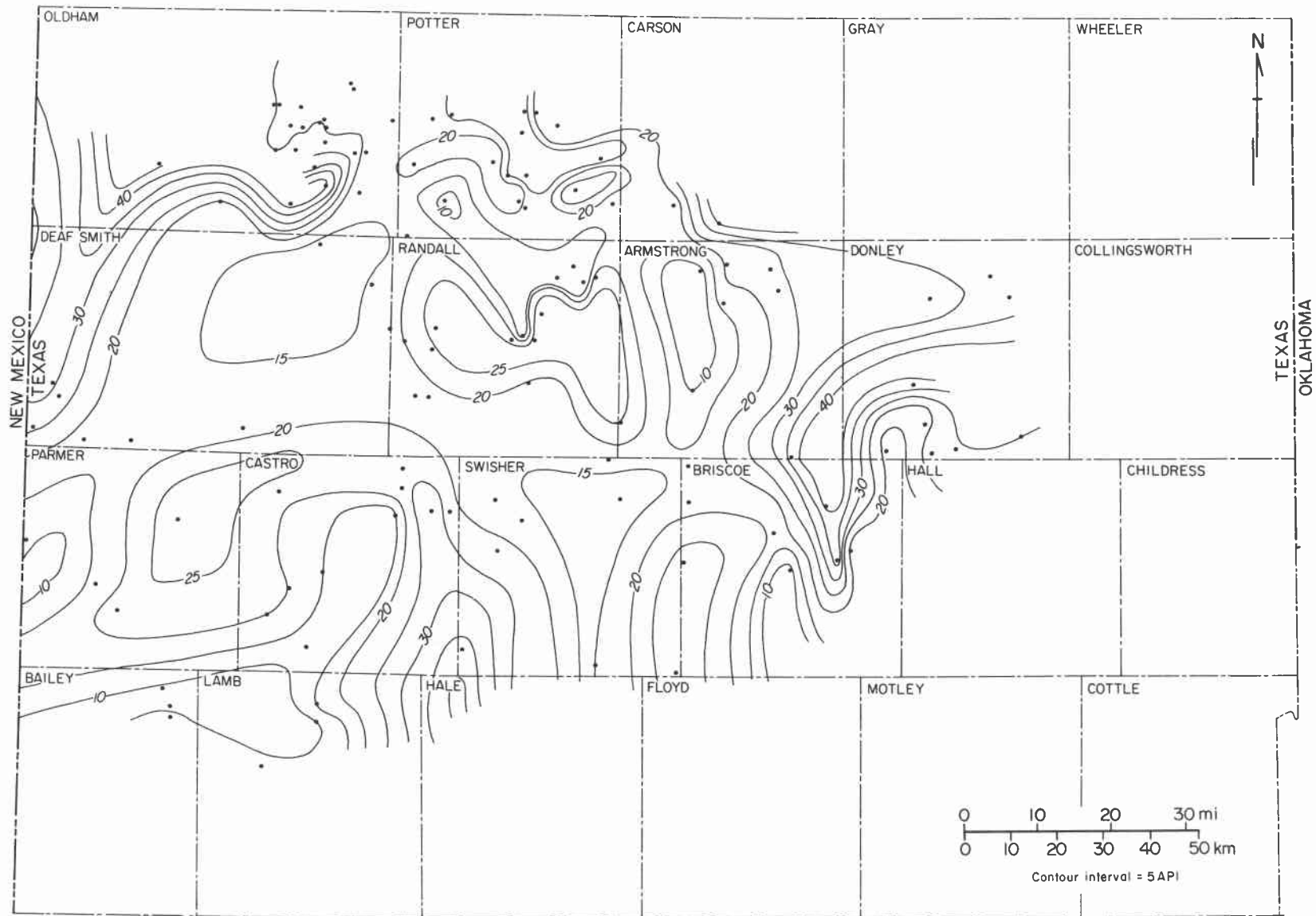


Figure 123. Contour map of average gamma-ray (API unit) values, cycle 4 salt, lower San Andres Formation.

Table 12. Point count data, cycle 4 salt, Gruy Federal, Inc.,  
Rex H. White No. 1, Randall County, Texas.

| Depth | % Halite | % Red Clay    | % Gray, Black or Green Clay | % Anhydrite | % Anhydrite/Clay? |
|-------|----------|---------------|-----------------------------|-------------|-------------------|
| 1748  | 98.8     | 1.2           |                             |             |                   |
| 1749  | 99.2     | 0.8           |                             |             |                   |
| 1750  | 99.4     | 0.6           |                             |             |                   |
| 1751  | 78.8     | 16.5          | 4.7                         |             |                   |
| 1752  | 90.0     | 10.0          |                             |             |                   |
| 1753  | 97.5     | 1.5           |                             | 1.0         |                   |
| 1754  | 96.8     | 2.3           |                             | 0.9         |                   |
| 1755  | 95.1     | 1.6           |                             | 3.3         |                   |
| 1756  | 92.8     | 1.0           | 1.7                         | 4.5         |                   |
| 1757  | 92.2     | 6.5           |                             | 1.3         |                   |
| 1758  | 53.0     | 30.8          | 14.2                        | 2.0         |                   |
| 1759  | 92.2     | 3.7           |                             | 4.1         |                   |
| 1760  | 94.4     | 0.9           |                             | 4.7         |                   |
| 1761  | 98.9     | 0.9           |                             | 0.2         |                   |
| 1762  | 98.0     | 1.2           | 0.5                         | 0.3         |                   |
| 1763  | 93.0     | 5.9           | 0.9                         | 0.2         |                   |
| 1764  | 95.9     | 1.1           | 0.5                         | 2.5         |                   |
| 1765  | 98.3     | 1.7           |                             |             |                   |
| 1766  | 98.4     | 1.6           |                             |             |                   |
| 1767  | 100.0    |               |                             |             |                   |
| 1768  | 97.8     | 2.2           |                             |             |                   |
| 1769  | 92.5     | 6.5           |                             |             |                   |
| 1770  | 82.1     | 17.9          |                             |             |                   |
| 1771  | 97.3     |               | 2.7                         |             |                   |
| 1772  | 98.0     |               | 2.0                         |             |                   |
| 1773  | 99.7     |               |                             | 0.3         |                   |
| 1774  | 99.9     |               | 0.1                         |             |                   |
| 1775  | 99.9     |               |                             | 0.1         |                   |
| 1776  | 99.7     |               |                             | 0.3         |                   |
| 1777  | 92.6     | 3.4           | 4.0                         |             |                   |
| 1778  | 74.2     | 25.4          |                             | 0.4         |                   |
| 1779  | 96.9     | 0.5           | 1.8                         | 0.2         | 0.6               |
| 1780  | 97.5     | 0.6           |                             | 1.9         |                   |
| 1781  | 95.7     | 3.9           |                             |             | 0.3               |
| 1782  | 97.4     | 2.3           | 0.3                         |             |                   |
| 1783  | 95.2     |               | 4.0                         | 0.8         |                   |
| 1784  | 61.5     | 38.5          |                             |             |                   |
| 1785  | 71.1     | 28.9          |                             |             |                   |
| 1786  | 71.0     | 0.3           |                             | 28.7        |                   |
| 1787  | 91.2     | 1.5           |                             | 7.3         |                   |
| 1788  | 99.3     | 0.3           |                             | 0.4         |                   |
| 1789  | 95.7     |               |                             | 4.3         |                   |
| 1790  |          | Not available |                             |             |                   |

Table 12. (continued)

| Depth | % Halite | % Red Clay | % Gray, Black or Green Clay | % Anhydrite | % Anhydrite/Clay? |
|-------|----------|------------|-----------------------------|-------------|-------------------|
| 1791  | 98.5     | 0.5        |                             | 0.6         | 0.4               |
| 1792  | 97.6     | 1.6        |                             | 0.8         |                   |
| 1793  | 92.6     | 2.5        |                             | 4.9         |                   |
| 1794  | 73.0     | 26.7       |                             | 0.3         |                   |
| 1795  | 97.1     | 0.2        |                             | 2.7         |                   |
| 1796  | 96.7     | 2.3        |                             | 1.0         |                   |
| 1797  | 99.5     | 0.3        |                             | 0.2         |                   |
| 1798  | 99.1     | 0.4        |                             | 0.5         |                   |
| 1799  | 99.4     |            |                             | 0.4         | 0.2               |
| 1800  | 99.1     | 0.8        |                             | 0.1         |                   |
| 1801  | 94.7     | 0.5        |                             | 4.2         | 0.6               |
| 1802  | 97.9     | 1.0        |                             | 1.1         |                   |
| 1803  | 98.2     | 1.3        |                             | 0.4         | 0.1               |
| 1804  | 99.5     | 0.05       |                             | 0.5         |                   |
| 1805  | 99.3     | 0.1        |                             | 0.6         |                   |
| 1806  | 98.4     | 0.5        |                             | 1.1         |                   |
| 1807  | 46.6     | 53.0       |                             | 0.4         |                   |
| 1808  | 49.7     | 2.3        |                             |             | 48.0              |
| 1809  | 79.3     | 18.9       |                             | 1.8         |                   |
| 1810  | 79.5     | 15.7       |                             |             | 4.8               |
| 1811  | 87.4     | 11.2       |                             | 1.4         |                   |
| 1812  | 99.0     |            |                             | 0.8         |                   |
| 1813  | 99.6     | 0.2        |                             | 0.2         |                   |
| 1814  | 98.4     |            |                             | 0.6         |                   |
| 1815  | 97.6     | 0.4        |                             | 2.0         |                   |
| 1816  | 98.8     |            |                             | 1.2         |                   |
| 1817  | 97.3     | 0.02       |                             | 2.7         |                   |
| 1818  | 85.5     | 14.5       |                             |             |                   |
| 1819  | 99.6     | 0.4        |                             |             |                   |
| 1820  | 98.9     | 0.1        |                             | 1.0         |                   |
| 1821  | 98.5     | 0.4        |                             | 1.1         |                   |
| 1822  | 95.4     | 0.03       |                             | 4.6         |                   |
| 1823  | 69.0     | 30.7       |                             |             | 1.0               |
| 1824  | 95.4     | 4.1        |                             | 0.2         | 0.3               |
| 1825  | 97.6     | 2.4        |                             |             |                   |
| 1826  | 45.5     | 54.5       |                             |             |                   |
| 1827  | 95.8     | 3.3        |                             | 0.5         | 0.4               |
| 1828  | 96.7     | 2.9        |                             | 0.4         |                   |
| 1829  | 96.4     | 2.5        |                             | 0.2         | 0.9               |
| 1830  | 96.3     | 0.3        |                             | 3.0         | 0.4               |
| 1831  | 86.7     | 1.4        | 11.9                        |             |                   |
| 1832  | 97.8     | 2.2        |                             |             |                   |
| 1833  | 46.0     | 54.0       |                             |             |                   |
| 1834  | 90.3     | 9.4        |                             | 0.3         |                   |
| 1835  | 89.3     | 10.7       |                             |             |                   |

Table 12. (continued)

| Depth | % Halite | % Red Clay    | % Gray, Black or Green Clay | % Anhydrite | % Anhydrite/Clay? |
|-------|----------|---------------|-----------------------------|-------------|-------------------|
| 1836  | 97.3     | 2.0           |                             | 0.7         |                   |
| 1837  | 97.3     | 0.5           |                             | 2.2         |                   |
| 1838  | 95.7     | 1.2           |                             | 3.1         |                   |
| 1839  | 99.2     | 0.04          |                             | 0.5         | 0.3               |
| 1840  | 91.5     | 0.4           |                             | 0.7         | 7.4               |
| 1841  | 85.4     | 3.7           |                             | 5.5         | 5.4               |
| 1842  | 94.9     | 0.2           |                             |             | 4.9               |
| 1843  | 99.2     |               |                             | 0.8         |                   |
| 1844  | 91.4     | 0.6           |                             | 1.4         | 6.6               |
| 1845  | 74.5     | 16.5          | 9.0                         |             |                   |
| 1846  | 76.3     | 23.6          |                             | 0.1         |                   |
| 1847  |          | Not available |                             |             |                   |
| 1848  |          | Not available |                             |             |                   |
| 1849  | 86.5     | 0.4           |                             | 13.1        |                   |
| 1850  | 89.7     | 9.1           |                             | 1.2         |                   |
| 1851  | 98.4     |               |                             | 1.6         |                   |
| 1852  | 97.0     |               |                             | 3.0         |                   |
| 1853  | 99.1     |               |                             | 0.9         |                   |
| 1854  | 99.5     |               | 0.4                         | 0.1         |                   |
| 1855  | 98.1     |               |                             | 1.9         |                   |
| 1856  | 93.6     |               |                             | 6.4         |                   |
| 1857  | 99.2     |               |                             | 0.8         |                   |
| 1858  | 96.7     |               |                             | 3.3         |                   |
| 1859  | 97.2     |               |                             | 2.8         |                   |
| 1860  | 94.1     | 5.6           |                             | 0.3         |                   |
| 1861  | 95.3     | 3.1           | 0.3                         | 1.3         |                   |
| 1862  | 98.2     |               |                             | 1.8         |                   |
| 1863  | 77.6     | 22.2          |                             | 0.2         |                   |
| 1864  | 75.3     | 15.0          |                             | 0.2         | 9.5               |
| 1865  | 94.4     |               |                             | 5.0         | 0.6               |
| 1866  | 95.2     |               |                             | 3.7         | 1.1               |
| 1867  | 99.9     |               |                             | 0.08        |                   |
| 1868  | 100.0    |               |                             |             |                   |
| 1869  | 97.0     |               |                             | 3.0         |                   |
| 1870  | 99.1     | 0.3           |                             | 0.6         |                   |
| 1871  | 97.2     | 0.4           |                             | 2.4         |                   |
| 1872  | 96.7     | 3.0           |                             | 0.3         |                   |
| 1873  | 88.6     | 10.4          |                             | 1.0         |                   |
| 1874  | 92.6     | 7.1           |                             | 0.3         |                   |
| 1875  | 95.0     | 2.5           |                             | 0.8         | 1.7               |
| 1876  | 97.3     | 0.1           |                             | 1.1         | 1.5               |
| 1877  | 98.0     | 0.3           |                             | 1.7         |                   |
| 1878  | 86.3     | 8.4           |                             | 3.3         | 2.0               |
| 1879  | 97.3     |               |                             | 2.7         |                   |

Table 12. (continued)

| Depth | % Halite | % Red Clay | % Gray, Black or Green Clay | % Anhydrite | % Anhydrite/Clay? |
|-------|----------|------------|-----------------------------|-------------|-------------------|
| 1880  | 88.0     |            |                             | 0.6         | 11.4              |
| 1881  | 95.6     | 2.4        |                             | 2.0         |                   |
| 1882  | 87.8     | 8.8        |                             | 1.5         | 1.9               |
| 1883  | 97.4     |            |                             | 2.6         |                   |
| 1884  | 92.3     |            |                             | 7.7         |                   |
| 1885  | 96.8     | 0.4        |                             | 2.5         | 0.3               |
| 1886  | 93.8     | 0.5        | 5.1                         | 0.6         |                   |
| 1887  | 83.6     | 12.9       | 3.2                         | 0.3         |                   |
| 1888  | 98.7     | 1.0        |                             | 0.3         |                   |
| 1889  | 99.5     | 0.3        | 0.2                         |             |                   |
| 1890  | 96.4     |            | 1.1                         | 1.0         | 1.5               |
| 1891  | 97.1     | 0.7        |                             |             | 2.2               |
| 1892  | 98.4     | 0.3        |                             |             | 1.3               |
| 1893  | 99.5     | 0.3        |                             | 0.2         |                   |
| 1894  | 91.9     | 7.0        |                             | 1.1         |                   |
| 1895  | 96.3     | 1.4        |                             | 2.3         |                   |
| 1896  | 99.0     | 0.8        |                             | 0.2         |                   |
| 1897  | 98.4     | 0.3        | 0.6                         | 0.7         |                   |
| 1898  | 98.3     | 0.2        |                             | 1.5         |                   |
| 1899  | 98.2     | 1.6        |                             | 0.2         |                   |
| 1900  | 88.5     | 11.5       |                             |             |                   |
| 1901  | 96.9     | 0.9        |                             | 2.2         |                   |
| 1902  | 94.7     | 4.0        |                             | 0.3         | 1.0               |
| 1903  | 97.6     | 1.9        |                             | 0.5         |                   |
| 1904  | 96.5     | 3.5        |                             |             |                   |
| 1905  | 97.4     | 0.6        | 1.1                         |             | 0.9               |
| 1906  | 98.1     |            |                             |             | 1.9               |
| 1907  | 89.9     | 9.0        |                             | 0.5         | 0.6               |
| 1908  | 88.0     | 8.7        |                             | 0.7         | 2.6               |
| 1909  | 90.8     | 4.9        | 1.0                         | 0.4         | 2.9               |
| 1910  | 92.3     | 3.1        | 4.6                         |             |                   |
| 1911  | 94.0     | 0.4        | 0.4                         | 5.2         |                   |
| 1912  | 98.3     |            |                             | 1.7         |                   |
| 1913  | 98.1     |            |                             | 1.9         |                   |
| 1914  | 99.4     |            |                             | 0.6         |                   |
| 1915  | 97.3     |            |                             | 2.7         |                   |
| 1916  | 94.1     |            |                             | 5.9         |                   |
| 1917  | 88.7     |            |                             | 11.3        |                   |
| 1918  | 91.9     |            |                             | 8.1         |                   |
| 1919  | 92.8     | 1.1        |                             | 6.1         |                   |
| 1920  | 94.1     |            |                             | 4.8         | 1.1               |
| 1921  | 83.9     |            |                             | 16.1        |                   |
| 1922  | 92.2     | 0.2        |                             | 7.6         |                   |
| 1923  | 88.6     |            |                             | 9.6         | 1.8               |

Table 12. (continued)

| Depth | % Halite | % Red Clay | % Gray, Black or Green Clay | % Anhydrite | % Anhydrite/Clay? |
|-------|----------|------------|-----------------------------|-------------|-------------------|
| 1924  | 90.6     | 0.5        |                             | 8.9         |                   |
| 1925  | 78.1     | 10.5       |                             | 2.6         | 8.8               |
| 1926  | 92.7     | 0.7        |                             | 5.6         |                   |
| 1927  | 97.3     |            |                             | 2.7         |                   |
| 1928  | 95.2     |            |                             | 4.8         |                   |
| 1929  | 94.6     |            |                             | 5.4         |                   |
| 1930  | 85.0     |            |                             | 15.0        |                   |
| 1931  | 79.1     | 4.1        |                             | 4.6         | 12.2              |
| 1932  | 97.9     |            |                             | 2.1         |                   |
| 1933  | 92.5     |            |                             | 6.9         | 0.6               |
| 1934  | 92.3     |            |                             | 6.6         | 1.1               |
| 1935  | 87.6     |            |                             | 12.4        |                   |
| 1936  | 93.3     |            |                             | 6.7         |                   |
| 1937  | 94.9     |            |                             | 5.1         |                   |
| 1938  | 92.3     |            |                             | 7.7         |                   |
| 1939  | 91.5     |            |                             | 8.5         |                   |
| 1940  | 89.7     |            |                             | 10.3        |                   |
| 1941  | 94.9     |            |                             | 5.1         |                   |
| 1942  | 89.0     | 0.4        |                             | 2.1         | 8.5               |
| 1943  | 95.0     |            |                             | 5.0         |                   |
| 1944  | 82.6     |            |                             | 13.9        | 3.5               |
| 1945  | 94.2     | 0.2        |                             | 5.6         |                   |
| 1946  | 95.6     | 0.4        |                             | 4.0         |                   |
| 1947  | 96.2     |            |                             | 3.8         |                   |
| 1948  | 96.5     |            |                             | 3.5         |                   |
| 1949  | 95.5     |            |                             | 4.5         |                   |
| 1950  | 76.3     |            |                             | 23.7        |                   |
| 1951  | 24.7     |            |                             | 75.3        |                   |
| 1952  | 87.2     |            |                             | 12.8        |                   |
| 1953  | 49.5     |            |                             | 50.5        |                   |
| 1954  | 65.8     |            |                             | 34.2        |                   |
| 1955  | 88.5     |            |                             | 11.5        |                   |
| 1956  | 94.0     |            |                             | 6.0         |                   |
| 1957  | 77.3     |            |                             | 22.7        |                   |
| 1958  | 77.5     |            |                             | 22.5        |                   |

Table 13. Point count data, cycle 4 salt, Gruy Federal, Inc.,  
Grabbe No. 1, Swisher County, Texas.

| Depth | % Halite | % Red Clay    | % Gray,<br>Black or<br>Green Clay | % Anhydrite | % Anhydrite/<br>Clay? |
|-------|----------|---------------|-----------------------------------|-------------|-----------------------|
| 2497  | 7.5      |               | 7.6                               | 84.9        |                       |
| 2498  | 68.5     | 14.8          | 11.5                              | 5.2         |                       |
| 2499  | 45.2     | 54.8          |                                   |             |                       |
| 2500  | 25.5     |               |                                   | 74.5        |                       |
| 2501  | 75.9     |               |                                   | 24.1        |                       |
| 2502  | 82.3     | 0.1           | 0.1                               | 17.5        |                       |
| 2503  | 29.4     |               |                                   | 70.6        |                       |
| 2504  | 23.3     |               |                                   | 76.7        |                       |
| 2505  | 20.6     |               |                                   | 79.4        |                       |
| 2506  | 22.4     |               |                                   | 77.6        |                       |
| 2507  | 22.9     |               |                                   | 77.1        |                       |
| 2508  |          | Not available |                                   |             |                       |
| 2509  | 47.8     | 0.1           |                                   | 52.1        |                       |
| 2510  | 92.4     | 3.9           | 1.8                               | 1.9         |                       |
| 2511  | 96.2     | 3.7           |                                   | 0.1         |                       |
| 2512  | 98.0     | 1.0           |                                   | 1.0         |                       |
| 2513  | 99.9     | 0.04          |                                   | 0.08        |                       |
| 2514  | 99.0     | 0.2           |                                   | 0.8         |                       |
| 2515  | 99.3     |               |                                   | 0.7         |                       |
| 2516  | 99.2     | 0.04          |                                   | 0.8         |                       |
| 2517  | 97.7     | 1.9           |                                   | 0.4         |                       |
| 2518  | 86.8     | 13.2          |                                   |             |                       |
| 2519  | 99.2     | 0.1           |                                   | 0.7         |                       |
| 2520  | 98.6     | 0.1           |                                   | 1.3         |                       |
| 2521  | 93.9     | 0.1           |                                   | 6.0         |                       |
| 2522  | 93.7     |               | 0.8                               | 5.5         |                       |
| 2523  | 95.7     | 0.8           |                                   | 3.5         |                       |
| 2524  | 97.2     | 1.3           |                                   | 1.5         |                       |
| 2525  |          | Not available |                                   |             |                       |
| 2526  | 98.2     | 1.2           |                                   | 0.6         |                       |
| 2527  | 98.2     | 1.2           |                                   | 0.6         |                       |
| 2528  | 97.6     |               |                                   | 2.4         |                       |
| 2529  | 99.0     |               |                                   | 1.0         |                       |
| 2530  | 99.4     | 0.1           | 0.05                              | 0.5         |                       |
| 2531  | 96.9     | 1.8           |                                   | 1.3         |                       |
| 2532  | 94.1     | 3.5           | 0.8                               | 1.6         |                       |
| 2533  | 94.4     | 4.9           |                                   | 0.7         |                       |
| 2534  | 99.7     |               | 0.1                               | 0.2         |                       |
| 2535  | 98.8     | 0.5           |                                   | 0.7         |                       |
| 2536  | 98.0     | 0.9           | 0.4                               | 0.7         |                       |
| 2537  | 97.0     | 0.9           | 0.2                               | 1.9         |                       |

Table 13. (continued)

| Depth | % Halite | % Red Clay | % Gray, Black or Green Clay | % Anhydrite | % Anhydrite/Clay? |
|-------|----------|------------|-----------------------------|-------------|-------------------|
| 2538  | 91.9     | 3.8        | 1.4                         | 2.2         | 0.7               |
| 2539  | 94.9     | 2.2        |                             | 2.9         |                   |
| 2540  | 97.5     | 0.8        | 0.8                         | 0.9         |                   |
| 2541  | 78.9     | 8.9        | 7.8                         | 4.4         |                   |
| 2542  | 84.9     | 0.3        | 9.2                         |             | 5.6               |
| 2543  | 83.5     | 9.6        | 1.4                         | 5.0         | 0.5               |
| 2544  | 41.2     | 6.0        | 0.2                         | 52.6        |                   |
| 2545  | 43.8     | 0.4        | 0.1                         | 55.7        |                   |
| 2546  | 47.4     |            |                             | 52.6        |                   |
| 2547  | 47.3     |            |                             | 52.7        |                   |
| 2548  | 98.6     | 0.3        | 1.1                         |             |                   |
| 2549  | 99.6     | 0.4        |                             |             |                   |
| 2550  | 99.9     | 0.1        |                             |             |                   |
| 2551  | 87.6     | 9.2        | 1.1                         | 1.1         | 1.0               |
| 2552  | 97.9     | 0.8        |                             |             | 1.3               |
| 2553  | 88.3     | 9.3        | 0.4                         | 1.3         | 0.7               |
| 2554  | 92.4     | 4.4        |                             | 3.2         |                   |
| 2555  | 46.3     | 29.9       | 6.6                         | 14.5        | 2.7               |
| 2556  | 88.9     | 2.5        |                             | 4.8         | 3.8               |
| 2557  | 92.5     | 0.7        |                             | 6.8         |                   |
| 2558  | 96.3     | 1.5        | 1.0                         | 2.2         |                   |
| 2559  | 95.3     | 1.3        |                             | 3.4         |                   |
| 2560  | 99.9     | 0.06       | 0.06                        |             |                   |
| 2561  | 96.8     |            | 3.2                         |             |                   |
| 2562  | 99.5     | 0.05       | 0.4                         | 0.05        |                   |
| 2563  | 99.0     |            | 0.3                         | 0.7         |                   |
| 2564  | 98.7     |            | 0.4                         | 0.9         |                   |
| 2565  | 99.4     |            | 0.5                         | 0.1         |                   |
| 2566  | 92.2     | 0.1        |                             | 6.7         | 1.0               |
| 2567  | 84.8     |            | 2.5                         | 12.5        | 0.2               |
| 2568  | 19.8     | 73.0       | 2.9                         | 1.5         | 2.8               |
| 2569  | 70.6     | 2.5        | 0.3                         | 6.0         | 20.6              |
| 2570  | 97.3     | 0.4        |                             |             | 2.3               |
| 2571  | 85.8     | 0.6        | 0.5                         | 1.3         | 11.8              |
| 2572  | 94.9     | 0.4        |                             | 2.9         | 1.8               |
| 2573  | 91.4     | 0.5        |                             | 6.4         | 1.7               |
| 2574  | 96.5     | 0.2        | 0.6                         | 1.1         | 1.6               |
| 2575  | 89.8     | 0.6        |                             | 2.7         | 6.9               |
| 2576  | 98.0     | 0.7        |                             | 0.5         | 0.8               |
| 2577  | 94.3     | 0.1        | 0.2                         | 5.4         |                   |
| 2578  | 61.8     | 15.2       | 20.6                        | 2.4         |                   |

Table 13. (continued)

| Depth | % Halite | % Red Clay | % Gray, Black or Green Clay | % Anhydrite | % Anhydrite/Clay? |
|-------|----------|------------|-----------------------------|-------------|-------------------|
| 2579  | 23.6     | 76.2       |                             | 0.2         |                   |
| 2580  | 95.7     | 1.9        |                             | 2.4         |                   |
| 2581  | 97.8     | 0.5        |                             | 1.7         |                   |
| 2582  | 84.8     | 0.1        |                             | 1.9         | 13.2              |
| 2583  | 37.4     | 23.3       | 4.3                         | 31.3        | 3.7               |
| 2584  | 81.4     | 5.4        |                             | 13.2        |                   |
| 2585  | 98.0     | 0.2        |                             | 1.8         |                   |
| 2586  | 98.7     | 0.1        |                             | 1.2         |                   |
| 2587  | 99.3     | 0.6        | 0.1                         |             |                   |
| 2588  | 97.3     | 1.8        |                             | 0.7         | 0.2               |
| 2589  | 96.5     | 2.6        | 0.3                         | 0.05        | 0.6               |
| 2590  | 98.0     | 1.7        |                             | 0.3         |                   |
| 2591  | 94.7     | 0.4        |                             | 4.9         |                   |
| 2592  | 87.1     | 4.8        | 6.7                         | 1.4         |                   |
| 2593  | 55.9     | 40.8       | 1.7                         | 1.5         |                   |
| 2594  | 85.5     | 13.1       |                             | 1.4         |                   |
| 2595  | 94.3     | 2.6        | 0.5                         | 1.7         | 0.9               |
| 2596  | 94.8     | 3.7        | 0.4                         | 1.1         |                   |
| 2597  | 93.5     | 4.4        |                             | 1.7         | 0.4               |
| 2598  | 99.1     | 0.5        |                             | 0.4         |                   |
| 2599  | 94.8     | 1.4        |                             | 3.8         |                   |
| 2600  | 62.7     | 13.8       | 7.5                         | 5.1         | 10.9              |
| 2601  | 12.7     |            |                             | 84.7        | 2.6               |
| 2602  | 48.9     |            | 0.5                         | 50.6        | 5.1               |
| 2603  | 93.4     | 0.6        | 0.6                         | 1.3         | 4.1               |
| 2604  | 89.8     |            |                             | 7.8         | 2.4               |
| 2605  | 96.3     | 0.5        |                             | 3.2         |                   |
| 2606  | 41.4     |            |                             | 57.3        | 1.3               |
| 2607  | 80.2     |            |                             | 14.7        | 5.1               |
| 2608  | 99.7     |            | 0.3                         |             |                   |
| 2609  | 97.6     |            | 2.4                         |             |                   |
| 2610  | 100.0    |            |                             |             |                   |
| 2611  | 97.9     |            | 2.1                         |             |                   |
| 2612  | 100.0    |            | 0.04                        |             |                   |
| 2613  | 100.0    |            |                             |             |                   |
| 2614  | 100.0    |            |                             |             |                   |
| 2615  | 100.0    |            |                             |             |                   |
| 2616  | 100.0    |            |                             |             |                   |
| 2617  | 100.0    |            | 0.03                        |             |                   |
| 2618  | 57.1     | 29.7       |                             |             | 13.2              |
| 2619  | 92.4     |            |                             |             | 7.6               |
| 2620  | 98.6     |            |                             |             | 1.4               |
| 2621  | 34.8     | 4.1        |                             |             | 61.1              |
| 2622  | 87.7     |            |                             |             | 12.3              |

Table 13. (continued)

| Depth | % Halite | % Red Clay | % Gray, Black or Green Clay | % Anhydrite | % Anhydrite/Clay? |
|-------|----------|------------|-----------------------------|-------------|-------------------|
| 2623  | 88.3     |            |                             |             | 11.7              |
| 2624  | 99.1     |            | 0.9                         |             |                   |
| 2625  | 98.1     |            | 1.3                         |             | 0.6               |
| 2626  | 98.5     |            |                             |             | 1.5               |
| 2627  | 96.2     |            |                             | 3.8         |                   |
| 2628  | 95.6     |            |                             | 4.4         |                   |
| 2629  |          |            |                             |             |                   |
| 2630  | 94.5     |            |                             | 5.5         |                   |
| 2631  | 63.2     | 11.2       | 0.7                         | 0.2         | 24.7              |
| 2632  | 97.4     |            |                             |             | 2.6               |
| 2633  | 77.5     |            |                             | 1.5         | 21.0              |
| 2634  | 94.5     |            |                             |             |                   |
| 2635  | 95.8     |            |                             | 4.2         |                   |
| 2636  | 100.0    |            |                             |             |                   |
| 2637  | 82.9     |            |                             | 17.1        |                   |
| 2638  | 61.3     |            |                             | 38.7        |                   |
| 2639  | 98.1     |            |                             | 1.9         |                   |
| 2640  | 93.6     |            |                             | 6.4         |                   |
| 2641  | 63.1     |            |                             |             | 36.9              |
| 2642  | 90.2     |            |                             |             | 9.8               |
| 2643  | 93.8     | 3.9        |                             |             | 2.3               |
| 2644  | 99.5     |            |                             |             | 0.5               |
| 2645  | 98.2     |            |                             | 1.0         | 0.8               |
| 2646  | 99.4     |            |                             |             | 0.6               |
| 2647  | 98.7     |            |                             | 1.1         | 0.2               |
| 2648  | 97.5     |            |                             | 2.5         |                   |
| 2649  | 89.7     |            |                             | 1.1         | 9.2               |
| 2650  | 77.3     | 13.2       |                             |             | 9.5               |
| 2651  | 94.9     | 0.1        |                             |             | 5.0               |
| 2652  | 98.5     |            |                             |             | 1.5               |
| 2653  | 93.2     |            |                             |             | 6.8               |
| 2654  | 95.9     |            |                             |             | 4.1               |
| 2655  | 98.7     |            |                             |             | 1.3               |
| 2656  | 93.3     |            |                             |             | 6.7               |
| 2657  | 98.8     |            |                             |             | 1.2               |
| 2658  | 99.3     |            |                             |             | 0.7               |
| 2659  | 98.9     |            |                             | 0.5         | 0.6               |
| 2660  | 95.9     |            | 0.3                         | 3.8         |                   |
| 2661  | 96.5     |            |                             | 1.5         | 2.0               |
| 2662  | 96.9     |            |                             | 3.0         | 0.1               |
| 2663  | 44.6     |            |                             | 39.3        | 16.1              |
| 2664  | 97.7     |            |                             | 1.6         | 3.7               |
| 2665  | 99.5     | 0.1        |                             | 0.4         |                   |

Table 13. (continued)

| Depth | % Halite | % Red Clay | % Gray, Black or Green Clay | % Anhydrite | % Anhydrite/Clay? |
|-------|----------|------------|-----------------------------|-------------|-------------------|
| 2666  | 98.6     |            |                             | 0.4         | 1.0               |
| 2667  | 97.4     |            |                             | 0.1         | 2.5               |
| 2668  | 99.6     |            |                             | 0.4         |                   |
| 2669  | 99.1     |            |                             |             | 0.9               |
| 2670  | 97.2     |            |                             | 2.1         | 0.7               |
| 2671  | 82.5     |            |                             | 1.1         | 16.4              |
| 2672  | 98.5     |            |                             | 0.4         | 1.1               |
| 2673  | 99.4     |            | 0.1                         |             | 0.5               |
| 2674  | 99.9     |            |                             | 0.04        | 0.1               |
| 2675  | 99.3     |            |                             |             | 0.7               |
| 2676  | 99.4     |            | 0.1                         | 0.2         | 0.3               |
| 2677  | 99.3     |            | 0.03                        | 0.2         | 0.5               |
| 2678  | 98.3     |            |                             | 0.3         | 1.4               |
| 2679  | 88.7     |            | 0.7                         |             | 10.6              |
| 2680  | 76.3     |            | 1.6                         |             | 22.1              |
| 2681  | 95.1     |            | 0.7                         | 0.3         | 3.9               |
| 2682  | 97.2     |            |                             | 1.8         | 1.0               |
| 2683  | 98.2     |            |                             | 1.8         |                   |
| 2684  | 98.5     |            |                             | 1.5         |                   |
| 2685  | 97.8     |            |                             | 2.2         |                   |
| 2686  | 96.9     |            |                             | 3.1         |                   |
| 2687  | 97.1     |            |                             | 2.9         |                   |
| 2688  | 98.8     |            |                             | 1.2         |                   |
| 2689  | 34.5     |            |                             | 65.5        |                   |
| 2690  | 89.5     |            |                             | 10.5        |                   |
| 2691  | 66.8     |            |                             | 33.2        |                   |
| 2692  | 86.5     |            |                             | 13.5        |                   |

## ACKNOWLEDGMENTS

This research was supported by the U.S. Department of Energy under contract number DE-AC97-80ET46615.

Figures for this report were prepared by John T. Ames, Robert S. Baum, Thomas M. Byrd, and Byron P. Holbert under the supervision of Dan F. Scranton. Photographic printing was by James A. Morgan. Micheline R. Davis designed the publication; Micheline R. Davis and Jamie S. Haynes assembled the report. Word processing was by Dottie C. Johnson and Margaret T. Chastain, under the supervision of Lucille C. Harrell. Editing was by Amanda R. Masterson. L. F. Brown, Jr., and E. G. Wermund reviewed this report. Michael Fracasso was the final reader.

## REFERENCES

- Adams, J. E., 1962, Foreland Pennsylvanian rocks of Texas and eastern New Mexico, in Branson, C. C., ed., Pennsylvanian System in the United States, a symposium: American Association of Petroleum Geologists, p. 372-384.
- Anderson, T., and Schmidt, V., in press, The evolution of Middle America and the Gulf of Mexico - Caribbean Sea region during Mesozoic time: Geological Society of America Bulletin.
- Arthurton, R. S., 1973, Experimentally produced halite compared with Triassic layered halite-rock from Cheshire, England: *Sedimentology*, v. 20, p. 145-160.
- Barazangi, M., and Isacks, B. L., 1976, Spatial distribution of earthquakes and subduction of the Nazca Plate beneath South America: *Geology*, v. 4, p. 686-692.
- Barnes, V. E., and Eifler, G. K., 1967, Geologic atlas of Texas, Lubbock sheet: The University of Texas at Austin, Bureau of Economic Geology, scale 1:250,000.
- \_\_\_\_\_ 1968, Geologic atlas of Texas, Plainview sheet: The University of Texas at Austin, Bureau of Economic Geology, scale 1:250,000.
- \_\_\_\_\_ 1969, Geologic atlas of Texas, Amarillo sheet: The University of Texas at Austin, Bureau of Economic Geology, scale 1:250,000.
- \_\_\_\_\_ 1970, Geologic atlas of Texas, Perryton sheet: The University of Texas at Austin, Bureau of Economic Geology, scale 1:250,000.
- Barnes, V. E., Eifler, G. K., and Reeves, C. C., Jr., 1974, Geologic atlas of Texas, Brownfield sheet: The University of Texas at Austin, Bureau of Economic Geology, scale 1:250,000.
- \_\_\_\_\_ 1978, Geologic atlas of Texas, Clovis sheet: The University of Texas at Austin, Bureau of Economic Geology, scale 1:250,000.
- Bassett, R. L., and Bentley, M. E., in press, Deep brine aquifers in the Palo Duro Basin: regional flow and geochemical constraints: The University of Texas at Austin, Bureau of Economic Geology Report of Investigations.
- Bassett, R. L., and Bentley, M. E., in press, Geochemistry and hydrodynamics of deep formation brines in the Palo Duro and Dalhart Basins, Texas: *Journal of Hydrology*.
- Bassett, R. L., and Griffin, J. A., 1981, AQ/SALT, in Gustavson, T. C., and others, Geology and geohydrology of the Palo Duro Basin, Texas Panhandle: The University of Texas at Austin, Bureau of Economic Geology Geological Circular 81-3, p. 123-129.
- Bassett, R. L., Bentley, M. E., Duncan, E. A., and Griffin, J. A., 1981, Predicting the reaction state of brines in proposed regions of nuclear waste isolation: *Scientific Basis for Nuclear Waste Management*, v. 3, p. 27-34.

- Bath, W. W., 1980, Geomorphic processes at Palo Duro Canyon, Texas Panhandle: The University of Texas at Austin, Master's thesis, 150 p.
- Bein, Amos, and Land, L. S., 1982, San Andres carbonates in the Texas Panhandle: sedimentation and diagenesis associated with magnesium-calcium-chloride brines: The University of Texas at Austin, Bureau of Economic Geology Report of Investigations No. 121, 48 p.
- Birsa, D. S., 1977, Subsurface geology of the Palo Duro Basin, Texas Panhandle: The University of Texas at Austin, Ph.D. dissertation, 360 p.
- Bradley, W. H., 1965, Vertical density currents: *Science*, v. 150, p. 1423-1428.
- Brand, J. P., 1953, Cretaceous of Llano Estacado of Texas: University of Texas, Austin, Bureau of Economic Geology Report of Investigations No. 20, 55 p.
- \_\_\_\_\_, 1956, Triassic System, in Evans, G. L. and Brand, J. P., eds., *West Texas Geological Society Guidebook*, p. 8-9.
- Bryan, R. B., 1979, The influence of slope and angle on soil entrainment by sheetwash and rainsplash: *Earth Surface Processes*, v. 4, p. 43-58.
- Carpenter, A. B., 1978, Origin and chemical evolution of brines in sedimentary basins: *Oklahoma Geological Survey Circular* 79, p. 60-77.
- Chuber, Steward, and Pusey, W. C., 1967, San Andres facies and their relationship to diagenesis, porosity, and permeability in the Reeves field, Yoakum County, Texas, in Elam, J. B., and Chuber, S., eds., *Symposium on cyclic sedimentation: West Texas Geological Society*, 232 p.
- D'Ans, J., 1933, Die Losungsgleichgewichte der Systeme der Salze Ozeanischer Salzablagerungen.
- Davis, L. V., 1955, Geology and ground-water resources of Grady and northern Stephens Counties, Oklahoma: *Oklahoma Geological Survey Bulletin* 73, p. 184.
- Dean, W. E., 1978, Trace and minor elements in evaporites: *Society of Economic Paleontologists and Mineralogists, SEPM Short Course* No. 4, p. 86-104.
- Dellwig, L. F., 1955, Origin of the Salina salt of Michigan: *Journal of Sedimentary Petrology*, v. 25, no. 2, p. 83-110.
- Dixon, G. H., 1967, Northeastern New Mexico and Texas-Oklahoma Panhandles, in McKee, E. D., and others, *Paleotectonic investigations of the Permian System in the United States: U.S. Geological Survey Professional Paper* 515, p. 65-80.
- Dobrin, M., 1960, *Introduction to geophysical prospecting*: New York, McGraw-Hill, 446 p.
- Dunbar, C. O., and others, 1960, Correlations of the Permian formations of North America: *Geological Society of America Bulletin*, v. 71, no. 12, p. 1763-1806.

- Dunlap, W. A., 1967, Deformation characteristics of granular materials subjected to rapid repetitive loading (abs.): Dissertation Abstracts International, v. 27, no. 7, p. 2344-B - 2344-B.
- Dutton, S. P., 1980, Depositional systems and hydrocarbon resource potential of the Pennsylvanian System, Palo Duro and Dalhart Basins, Texas Panhandle: The University of Texas at Austin, Bureau of Economic Geology Geological Circular 80-8, 49 p.
- Dutton, S. P., Goldstein, A. G., and Ruppel, S. C., 1982, Petroleum potential of the Palo Duro Basin, Texas Panhandle: The University of Texas at Austin, Bureau of Economic Geology Report of Investigations No. 123, 87 p.
- Ellison, W. D., 1948, Erosion by raindrop: Scientific American, v. 170, no. 5, p. 40-45.
- Emmett, W. W., 1970, The hydraulics of overland flow on hillslopes: U.S. Geological Survey Professional Paper 662-A, 69 p.
- Erxleben, A. W., 1975, Depositional systems in Canyon Group (Pennsylvanian System), North-Central Texas: The University of Texas at Austin, Bureau of Economic Geology Report of Investigations No. 82, 75 p.
- Evans, G. L., and Meade, G. E., 1944, Quaternary of the Texas High Plains: University of Texas, Austin, Bureau of Economic Geology Bulletin 4401, p. 485-507.
- Finley, R. J., and Baumgardner, R. W., Jr., 1981, Sedimentology and basin morphometry of the Little Red River basin: insights into retreat of the eastern Caprock Escarpment, in Gustavson, T. C., and others, Geology and geohydrology of the Palo Duro Basin, Texas Panhandle: The University of Texas at Austin, Bureau of Economic Geology Geological Circular 81-3, p. 148-151.
- Finley, R. J., and Gustavson, T. C., 1979, Slope erosion mechanisms, in Gustavson, T. C., and others, Geology and geohydrology of the Palo Duro Basin: The University of Texas at Austin, Bureau of Economic Geology Geological Circular 80-7, p. 58-62.
- \_\_\_\_\_ 1980, Climatic controls on erosion in the Rolling Plains and along the Caprock Escarpment of the Texas Panhandle: The University of Texas at Austin, Bureau of Economic Geology Geological Circular 80-11, 50 p.
- \_\_\_\_\_ 1981, Lineament analysis based on Landsat imagery, Texas Panhandle: The University of Texas at Austin, Bureau of Economic Geology Geological Circular 81-5, 37 p.
- Flawn, P. T., 1956, Basement rocks of Texas and southeast New Mexico: University of Texas, Austin, Bureau of Economic Geology Publication 5605, 261 p.
- Fogg, G. E., Simpson, E. S., and Neuman, S. P., 1979, Aquifer modeling by numerical methods applied to an Arizona groundwater basin: University of Arizona, Department of Hydrology and Water Resources, Reports on Natural Systems No. 32, 140 p.
- Folk, R. L., 1974, Petrology of sedimentary rocks: Austin, Texas, Hemphill Publishing Company, 182 p.

- Folk, R. L., and Land, L. S., 1975, Mg/Ca ratio and salinity: two controls over crystallization of dolomite: *American Association of Petroleum Geologists Bulletin*, v. 59, no. 1, p. 60-68.
- Forgotson, J. M., Jr., Statler, A. T., and David, M., 1966, Influence of regional tectonics and local structure on deposition of Morrow Formation in western Anadarko Basin: *American Association of Petroleum Geologists Bulletin*, v. 50, no. 3, p. 518-532.
- Foster, R. W., Frentress, R. M., and Riese, W. C., 1972, Subsurface geology of east-central New Mexico: *New Mexico Geological Society, Special Publication 4*, 22 p.
- Freeze, R. A., and Cherry, J. A., 1979, *Groundwater*: Englewood Cliffs, New Jersey, Prentice-Hall, 604 p.
- Frezon, S. F., and Dixon, G. H., 1975, Texas Panhandle and Oklahoma, in McKee, E. D., Crosby, E. J., and others, *Paleotectonic investigations of the Pennsylvanian System in the United States*: U.S. Geological Survey Professional Paper 853-J, p. 177-195.
- Friedman, G. M., 1978, Depositional environments of evaporite deposits: Oklahoma City, Society of Economic Paleontologists and Mineralogists, SEPM Short Course No. 4, p. 177-188.
- Frye, J. C., and Leonard, A. B., 1957, Studies of Cenozoic geology along eastern margin of Texas High Plains, Armstrong to Howard Counties: The University of Texas, Bureau of Economic Geology Report of Investigations No. 32, 57 p.
- \_\_\_\_\_ 1964, Relation of Ogallala Formation to the Southern High Plains in Texas: University of Texas, Austin, Bureau of Economic Geology Report of Investigations No. 51, 25 p.
- Garrison, J. R., Ramirez-Ramirez, C., and Long, L. E., 1980, Rb-Sr isotopic study of the ages and provenance of Precambrian granulite and Paleozoic greenschist near Ciudad Victoria, Mexico, in Pilger, O., ed., *The origin of the Gulf of Mexico and the early opening of the central North Atlantic Ocean*: Louisiana Geological Survey, symposium proceedings, p. 37-50.
- Geotechnical Engineers, 1978, Final report on uncertainties in the detection, measurement, and analysis of selected features pertinent to deep geologic repositories: University of California, Lawrence Livermore Laboratory, Project 77393, 96 p.
- Goldstein, A. G., 1981, Plate tectonics of the Ancestral Rocky Mountains, *Comment: Geology*, v. 9, p. 387-388.
- Gould, C. N., 1902, Oklahoma Geological Survey 2nd Biennial Report, p. 42, 47.
- \_\_\_\_\_ 1905, Geology and water resources of Oklahoma: U.S. Geological Survey Water Supply Paper 148, 178 p.
- Gustavson, T. C., Finley, R. J., and Baumgardner, R. W., Jr., 1980, Preliminary rates of slope retreat and salt dissolution along the eastern Caprock Escarpment of the Southern High Plains and in the Canadian River Valley, in Gustavson, T. C., and others, *Geology and geohydrology of the Palo Duro Basin, Texas Panhandle*: The

University of Texas at Austin, Bureau of Economic Geology Geological Circular 80-7, p. 76-82.

\_\_\_\_\_. 1981, Retreat of the Caprock Escarpment and denudation of the Rolling Plains of the Texas Panhandle: Association of Engineering Geologists Bulletin, v. 23, no. 4, p. 413-421.

Gustavson, T. C., Finley, R. J., and McGillis, K. A., 1980, Regional dissolution of Permian salt in the Anadarko, Dalhart, and Palo Duro Basins of the Texas Panhandle: The University of Texas at Austin, Bureau of Economic Geology Report of Investigations No. 106, 40 p.

Ham, W. E., and Wilson, J. L., 1967, Paleozoic epeirogeny and orogeny in the Central United States: American Journal of Science, v. 265, no. 5, p. 332-407.

Handford, C. R., 1979a, Lower Permian depositional systems, in Dutton, S. P., and others, Geology and geohydrology of the Palo Duro Basin, Texas Panhandle: The University of Texas at Austin, Bureau of Economic Geology Geological Circular 79-1, p. 26-38.

\_\_\_\_\_. 1979b, Depositional history and diagenesis of high-constructive delta systems (Wolfcampian), southeastern Palo Duro Basin, Texas: American Association of Petroleum Geologists Bulletin, v. 63, no. 11, p. 247-258.

\_\_\_\_\_. 1980, Lower Permian facies of the Palo Duro Basin, Texas: depositional systems, shelf-margin evolution, paleogeography, and petroleum potential: The University of Texas at Austin, Bureau of Economic Geology Report of Investigations No. 102, 31 p.

\_\_\_\_\_. 1981, A model of salt deposition in a coastal sabkha--an example from the Permian Lower Clear Fork Formation of the Texas Panhandle: Journal of Sedimentary Petrology, v. 51, no. 3, p. 761-778.

Handford, C. R., and Dutton, S. P., 1980, Pennsylvanian-Early Permian depositional systems and shelf-margin evolution, Palo Duro Basin, Texas: American Association of Petroleum Geologists Bulletin, v. 64, no. 1, p. 88-106.

Handford, C. R., Dutton, S. P., and Fredericks, P. E., 1981, Regional cross sections of the Texas Panhandle: Precambrian to mid-Permian: The University of Texas at Austin, Bureau of Economic Geology Cross Sections.

Handford, C. R., and Fredericks, P. E., 1980, Facies patterns and depositional history of a Permian sabkha complex: Red Cave Formation, Texas Panhandle: The University of Texas at Austin, Bureau of Economic Geology Geological Circular 80-9, 38 p.

Handford, C. R., Wiggins, W. D., Palmer, D. R., and Bassett, R. L., in press, Sedimentology, petrography, and diagenesis of Permian evaporites, Randall County, Texas: The University of Texas at Austin, Bureau of Economic Geology Report of Investigations.

Hibbard, C. W., and Dalquest, W. W., 1966, Fossils from the Seymour Formation of Knox and Baylor Counties, Texas, and their bearing on the late Kansan climate of that region: University of Michigan, Contributions from the Museum of Paleontology, v. 21, p. 1-66.

- \_\_\_\_\_ 1973, Proneofiber, a new genus of Vole (Critetidas: Rodentia) from the Pleistocene Seymour Formation of Texas, and its evolutionary and stratigraphic significance: *Quaternary Research*, v. 3, p. 264-274.
- Hills, J. M., 1972, Late Paleozoic sedimentation in West Texas Permian Basin: *American Association of Petroleum Geologists Bulletin*, v. 56, no. 12, p. 2303-2322.
- Hoffman, P., Dewey, J., and Burke, K., 1974, Aulacogens and their genetic relationship to geosynclines with a Proterozoic example from Great Slave Lake, Canada, in Dott, R. H., and Shaver, R. H., eds., Modern and ancient geosynclinal sedimentation: Society of Economic Paleontologists and Mineralogists Special Publication No. 19, p. 38-55.
- Holser, W. T., 1979, Mineralogy of evaporites, in Marine minerals: Mineralogical Society of America Short Course Notes, v. 6, p. 211-294.
- Horner, D. R., 1951, Pressure build-up in wells: *Proceedings, Third World Petroleum Congress, Leiden*, v. 2, p. 503.
- Hunt, J. M., 1979, *Petroleum geochemistry and geology*: San Francisco, W. H. Freeman, 617 p.
- Johnson, K. S., 1978, Stratigraphy and mineral resources of Guadalupian and Ochoan rocks in the Texas Panhandle and Western Oklahoma, in Geology and mineral deposits of Ochoan rocks in Delaware Basin and adjacent areas: New Mexico Bureau of Mines and Mineral Resources Circular 159, p. 57-62.
- Johnston, N., and Beeson, C. M., 1944, Water permeability of reservoir sands: *Petroleum Technology*, v. 8, no. 3, p. 43-55.
- Jones, T. S., 1953, *Stratigraphy of the Permian Basin of West Texas*: West Texas Geological Society, 63 p.
- \_\_\_\_\_ 1956, Permian System, in West Texas Geological Society Guidebook, p. 6-7.
- Keller, G. R., and Cebull, S. E., 1973, Plate tectonics and the Ouachita System in Texas, Oklahoma and Arkansas: *Geological Society of America Bulletin*, v. 84, no. 5, p. 1659-1666.
- Keyes, C. R., 1915, *Iowa Academy of Science Proceedings*, v. 22, p. 257-262, cited in Lexicon of Permian stratigraphic names of the Permian Basin of West Texas and southeastern New Mexico: West Texas Geological Society Publication No. 76-66, 341 p.
- Keys, W. S., and MacCary, L. M., 1971, Application of borehole geophysics to water-resources investigations: *U.S. Geological Survey Techniques in Water Resources Investigations, Book 2, Chapter E1*, 126 p.
- Kinsman, D. J. J., 1969, Modes of formation, sedimentary associations, and diagnostic features of shallow-water and supratidal evaporites: *American Association of Petroleum Geologists Bulletin*, v. 53, no. 4, p. 830-840.

- Kluth, C. F., and Coney, P. J., 1981, Plate tectonics of the Ancestral Rocky Mountains: *Geology*, v. 9, p. 10-15.
- Lee, W. T., 1909, The Manzano Group of the Rio Grande Valley, New Mexico: U.S. Geological Survey Bulletin 389, p. 12.
- Leopold, L. B., Emmett, W. W., and Myrick, R. M., 1966, Channel and hillslope processes in a semiarid area, New Mexico: U.S. Geological Survey Professional Paper 352-6, 253 p.
- Lewis, F. E., 1938, Stratigraphy of the Upper and Middle Permian of West Texas and southeastern New Mexico (abs.): American Association of Petroleum Geologists Bulletin, v. 22, no. 12, p. 1710-1711.
- Lochman-Balk, C., 1972, Lexicon of stratigraphic names used in East-Central New Mexico and adjacent states: New Mexico Geological Society, Guidebook of East-Central New Mexico, p. 1-11.
- McGillis, K. A., and Presley, M. W., 1981a, Tansill, Salado, and Alibates Formations: Upper Permian evaporite/carbonate strata of the Texas Panhandle: The University of Texas at Austin, Bureau of Economic Geology Geological Circular 81-8, 31 p.
- \_\_\_\_\_ 1981b, Salado-Tansill salt studies to determine original extent of youngest Permian salt and Salado potash deposits, in Gustavson, T. C., and others, *Geology and geohydrology of the Palo Duro Basin, Texas Panhandle*: The University of Texas at Austin, Bureau of Economic Geology Geological Circular 81-3, p. 41-46.
- McGookey, D., 1981, Application of Glorieta-Flowerpot facies analyses to map and distinguish between salt dissolution and facies transitions, western Amarillo Uplift and adjacent areas, in Gustavson, T. C., and others, *Geology and geohydrology of the Palo Duro Basin, Texas Panhandle*: The University of Texas at Austin, Bureau of Economic Geology Geological Circular 81-3, p. 156-165.
- McGowen, J. H., 1970, Gum Hollow fan delta, Nueces Bay, Texas: The University of Texas at Austin, Bureau of Economic Geology Report of Investigations No. 69, 91 p.
- McGowen, J. H., 1981, Depositional sequences and associated sedimentary diagenetic facies: an ongoing investigation of salt-bearing core, Swisher County, Texas, in Gustavson, T. C., and others, *Geology and geohydrology of the Palo Duro Basin, Texas Panhandle*: The University of Texas at Austin, Bureau of Economic Geology Geological Circular 81-3, p. 90-92.
- McGowen, J. H., Granata, G. E., and Seni, S. J., 1979, Depositional framework of the Lower Dockum Group (Triassic), Texas Panhandle: The University of Texas at Austin, Bureau of Economic Geology Report of Investigations No. 97, 60 p.
- McKee, E. D., and Oriel, S. S., 1967, Paleotectonic investigations of the Permian System in the United States: U.S. Geological Survey Professional Paper 515, 271 p.
- McKee, E. D., Crosby, E. J., and others, 1975, Paleotectonic investigations of the Pennsylvanian System in the United States: U.S. Geological Survey Professional Paper 853, 541 p.

- McNeal, B. L., and Coleman, N. T., 1966, Effect of solution composition on soil hydraulic conductivity: *Soil Science Society of America Proceedings*, v. 30, no. 3, p. 308-312.
- Melton, M. A., 1960, Intravalley variation in slope angles related to microclimate and erosional environment: *Geological Society of America Bulletin*, v. 71, no. 2, p. 133-144.
- Menzer, F. J., and Slaughter, B. H., 1971, Upland gravels in Dallas County, Texas, and their bearing on the former extent of the High Plains physiographic province: *The Texas Journal of Science*: v. 22, no. 2/3, p. 217-222.
- Mitchell, B. J., and Landisman, M., 1970, Interpretation of a crustal section across Oklahoma: *Geological Society of America Bulletin*, v. 81, no. 9, p. 2647-2656.
- Moore, B. J., 1976, Analyses of natural gases, 1917-1974: U.S. Bureau of Mines computer printout 1-76, NTIS PB-251 202, 532 p.
- Muehlberger, W. R., Denison, R. E., and Lidiak, E. G., 1967, Basement rock in continental interior of United States: *American Association of Petroleum Geologists Bulletin*, v. 51, no. 12, p. 2351-2380.
- Myers, B. N., 1969, Compilation of results of aquifer tests in Texas: *Texas Water Development Board Report No. 98*, 532 p.
- Naeser, C. W., Izett, G. A., and Wilcox, R. W., 1971, Zircon fission-track ages of Pearlette-like volcanic ash beds in the Great Plains: *Geological Society of America Abstracts with Programs*, v. 3, no. 7, p. 657.
- Naiman, E. R., Bein, Amos, and Folk, R. L., in press, Complex polyhedral crystals of limpid dolomite associated with halite, Permian Upper Clear Fork and Glorieta Formations, Texas.
- Narasimhan, T. N., Neuman, S. P., and Edwards, A. L., 1977, Mixed explicit-implicit iterative finite element scheme for diffusion-type problems, II, solution strategy and examples: *International Journal of Numerical Methods Engineering*, v. 4, p. 325-344.
- Narasimhan, T. N., and Witherspoon, P. A., 1977, Numerical model for saturated-unsaturated flow in deformable porous media: *Water Resources Research*, v. 13, no. 3, p. 657-664.
- Neuman, S. P., and Narasimhan, T. N., 1977, Mixed explicit-implicit iterative finite element scheme for diffusion-type problems, I, theory: *International Journal of Numerical Methods Engineering*, v. 11, p. 309-323.
- Neuman, S. P., Narasimhan, T. N., and Witherspoon, P. A., 1977, Application of mixed explicit-implicit finite element method to nonlinear diffusion type problems, in Pryden, G. F., and Gray, W. L., eds., *Proceedings of the first international conference on finite elements in water resources*, p. 1.153-1.185.
- Nicholson, J. H., 1960, Geology of the Texas Panhandle, in *Aspects of the geology of Texas, a symposium*: University of Texas, Austin, Bureau of Economic Geology Publication 6017, p. 51-64.

- Nurmi, R. D., and Friedman, G. M., 1977, Sedimentology and depositional environments of basin-center evaporites, Lower Salina Group (Upper Silurian), Michigan Basin, in Fischer, J. H., ed., Reefs and evaporites--concepts and depositional models: American Association of Petroleum Geologists Studies in Geology No. 5, p. 23-52.
- Pitt, W. D., and Scott, G. L., 1981, Porosity zones of lower part of San Andres Formation, east-central New Mexico: New Mexico Bureau of Mines and Mineral Resources Circular 179, 19 p.
- Powell, B. N., and Fischer, J. S., 1976, Plutonic igneous geology of the Wichita magmatic province, Oklahoma: Oklahoma Geological Survey Guide Book No. 2, 35 p.
- Presley, M. W., 1979a, Upper Permian evaporites and red beds, in Dutton, S. P., and others, Geology and geohydrology of the Palo Duro Basin, Texas Panhandle: The University of Texas at Austin, Bureau of Economic Geology Geological Circular 79-1, p. 39-49.
- \_\_\_\_\_ 1979b, Salt deposits, in Dutton, S. P., and others, Geology and geohydrology of the Palo Duro Basin, Texas Panhandle: The University of Texas at Austin, Bureau of Economic Geology Geological Circular 79-1, p. 50-51.
- \_\_\_\_\_ 1980a, Upper Permian salt-bearing stratigraphic units, in Gustavson, T. C., and others, Geology and geohydrology of the Palo Duro Basin, Texas Panhandle: The University of Texas at Austin, Bureau of Economic Geology Geological Circular 80-7, p. 12-23.
- \_\_\_\_\_ 1980b, Salt depositional system--an example from the Tubb Formation, in Gustavson, T. C., and others, Geology and geohydrology of the Palo Duro Basin, Texas Panhandle: The University of Texas at Austin, Bureau of Economic Geology Geological Circular 80-7, p. 24-25.
- \_\_\_\_\_ 1980c, Salt depth and thickness, in Gustavson, T. C., and others, Geology and geohydrology of the Palo Duro Basin, Texas Panhandle: The University of Texas at Austin, Bureau of Economic Geology Geological Circular 80-7, p. 33-41.
- \_\_\_\_\_ 1981a, Permeable sheet sandstones of the Glorieta Formation intertongue with salt-bearing rocks in the northwestern Texas Panhandle, in Gustavson, T. C., and others, Geology and geohydrology of the Palo Duro Basin, Texas Panhandle: The University of Texas at Austin, Bureau of Economic Geology Geological Circular 81-3, p. 10-11.
- \_\_\_\_\_ 1981b, San Andres salt stratigraphy and salt purity, in Gustavson, T. C., and others, Geology and geohydrology of the Palo Duro Basin, Texas Panhandle: The University of Texas at Austin, Bureau of Economic Geology Geological Circular 81-3, p. 33-40.
- \_\_\_\_\_ 1981c, Shelf and supratidal facies of the Permian Tubb Formation in the Texas Panhandle: The University of Texas at Austin, Bureau of Economic Geology, contract report.
- \_\_\_\_\_ 1981d, Statistical analyses of lithologic interpretations from well logs, in Gustavson, T. C., and others, Geology and geohydrology of the Palo Duro Basin,

- Texas Panhandle: The University of Texas at Austin, Bureau of Economic Geology Geological Circular 81-3, p. 19-24.
- Presley, M. W., and McGillis, K. A., 1981a, Tansill, Salado, and Alibates Formations: Upper Permian evaporite/carbonate strata of the Texas Panhandle: The University of Texas at Austin, Bureau of Economic Geology Geological Circular 81-8, 31 p.
- Presley, M. W., and McGillis, K. A., 1981b, Upper Clear Fork and Glorieta salt stratigraphy and salt purity, in Gustavson, T. C., and others, Geology and geohydrology of the Palo Duro Basin, Texas Panhandle: The University of Texas at Austin, Bureau of Economic Geology Geological Circular 81-3, p. 25-32.
- Presley, M. W., and Ramondetta, P. J., 1981, Hydrocarbon potential of San Andres carbonates in the Palo Duro Basin--stratigraphic and facies analysis, in Gustavson, T. C., and others, Geology and geohydrology of the Palo Duro Basin, Texas Panhandle: The University of Texas at Austin, Bureau of Economic Geology Geological Circular 81-3, p. 59-65.
- Quansah, C., 1981, The effect of soil type, slope, rain intensity, and their interactions on splash detachment and transport: *Journal of Soil Science*, v. 32, p. 215-224.
- Railroad Commission of Texas, 1981, 1980 annual report of the Oil and Gas Division: Austin, Railroad Commission of Texas, 666 p.
- Ramondetta, P. J., 1981, Genesis and emplacement of San Andres oil in the northern shelf of the Midland Basin, Texas, in Gustavson, T. C., and others, Geology and geohydrology of the Palo Duro Basin, Texas Panhandle: The University of Texas at Austin, Bureau of Economic Geology Geological Circular 81-3, p. 52-58.
- \_\_\_\_\_ in press, Facies and stratigraphy of the San Andres Formation, northern and northwestern shelves of the Midland Basin, Texas and New Mexico: The University of Texas at Austin, Bureau of Economic Geology Report of Investigations.
- Rascoe, B., Jr., 1962, Regional stratigraphic analysis of Pennsylvanian and Permian rocks in western mid-continent, Colorado, Kansas, Oklahoma, Texas: *American Association of Petroleum Geologists Bulletin*, v. 46, no. 8, p. 1345-1370.
- Reeve, R. C., 1953, A method for determining the stability of soil structure based upon air and water permeability measurements: *Soil Science Society of America Proceedings*, v. 17, p. 324-329.
- Robinson, R. A., and Stokes, R. H., 1965, *Electrolyte solutions*: London, Butterworths, 571 p.
- Roth, R., 1945, Permian Pease River Group of Texas: *Geological Society of America Bulletin*, v. 56, no. 10, p. 893-908.
- \_\_\_\_\_ 1960, Swisher gabbroic terrane of Texas Panhandle: *American Association of Petroleum Geologists Bulletin*, v. 44, no. 11, p. 1775-1784.
- Schlumberger, 1972, *Log interpretations: I.: principles*: New York, Schlumberger, 113 p.

- Schneider, W. T., 1943, Geology of Wasson field, Yoakum and Gaines Counties, Texas: American Association of Petroleum Geologists Bulletin, v. 27, no. 4, p. 479-523.
- Schultz, G. E., 1977, Blancan and post-Blancan faunas in Texas Panhandle, in Schultz, G. E., ed., Guidebook, field conference in Late Cenozoic biostratigraphy of the Texas Panhandle and adjacent Oklahoma: West Texas State University, Kilgon Research Center, Special Publication No. 1, p. 105-145.
- Schumm, S. A., 1965, Quaternary paleohydrology, in Wright, H. E., Jr., and Frey, D. G., eds., The Quaternary of the United States: Princeton, Princeton University Press, p. 783-794.
- Scott, G. L., and Ham, W. E., 1957, Geology and gypsum resources of the Carter area, Oklahoma: Oklahoma Geological Survey Circular 42, p. 30-33.
- Sellards, E. H., 1933, The pre-Paleozoic systems in Texas, in The geology of Texas, v. 1, stratigraphy: Austin, University of Texas Bulletin 3232, p. 15-238.
- Seni, S. J., 1980, Sand-body geometry and depositional systems, Ogallala Formation, Texas: The University of Texas at Austin, Bureau of Economic Geology Report of Investigations No. 105, 36 p.
- Shearman, D. J., 1970, Recent halite rock, Baja California, Mexico: Institute of Mining and Metallurgy Transactions, v. 79, p. 155-162.
- Silver, B. A., and Todd, R. G., 1969, Permian cyclic strata, northern Midland and Delaware Basins, West Texas and southeastern New Mexico: American Association of Petroleum Geologists Bulletin, v. 53, no. 11, p. 2223-2251.
- Stewart, S. W., and Pakiser, L. C., 1962, Crustal structure in eastern New Mexico: interpretation from the GNOME Explosion: Bulletin of the Seismological Society of America, v. 52, no. 5, p. 1017-1030.
- Tait, D. B., and others, 1962, Artesia Group of New Mexico and West Texas: American Association of Petroleum Geologists Bulletin, v. 48, no. 4, p. 504-517.
- Talwani, M., Wurzel, J. L., and Landisman, M. G., 1959, Rapid gravity computations for two-dimensional bodies with application to the Mendocino submarine fracture zone: Journal of Geophysical Research, v. 64, p. 49-59.
- Todd, R. G., 1976, Oolite bar progradation, San Andres Formation, Midland Basin: American Association of Petroleum Geologists Bulletin, v. 60, no. 6, p. 907-925.
- Totten, R. B., 1956, General geology and historical development, Texas and Oklahoma Panhandles: American Association of Petroleum Geologists Bulletin, v. 40, no. 8, p. 1945-1967.
- U.S. Army Corps of Engineers, 1976, Arkansas-Red River Basin chloride control: Design Memorandum No. 25, General Design Phase I - Plan Formulation, v. I and II.
- Walker, T. R., 1967, Formation of red beds in modern and ancient deserts: Geological Society of America Bulletin, v. 78, no. 3, p. 353-368.

Wardlaw, N. C., and Schwerdtner, W. M., 1966, Halite-anhydrite seasonal layers in the Middle Devonian Prairie Evaporite Formation, Saskatchewan, Canada: Geological Society of America Bulletin, v. 77, no. 4, p. 331-342.

West Texas Geological Society, 1953, North-south cross-section through Permian Basin of West Texas, 1 p.

Wischmeier, W. H., and Smith, D. D., 1958, Rainfall and its relationship to soil loss: EOS, v. 39, no. 2, p. 285-291.

\_\_\_\_\_ 1965, Predicting rainfall-erosion losses from cropland east of the Rocky Mountains: U.S. Department of Agriculture Handbook no. 282, 47 p.